Faculty of Science and Engineering

Department of Petroleum Engineering

Experimental Investigation of Wettability of Rock-CO_2-Brine for Improved Reservoir Characterization

Muhammad Arif

This thesis is presented for the Degree of
Doctor of Philosophy
of
Curtin University

August 2017

Declaration

To the best of my knowledge and belief this thesis contains no material previously published by any other person except where due acknowledgment has been made.

This thesis contains no material, which has been accepted for the award of any other degree or diploma in any university.

Signature: _____ (Muhammad Arif)

Date: 08/08/2017

Copyright

I warrant that I have obtained, where necessary, permission from the copyright owners to use any third-party copyright material reproduced in the thesis (e.g. questionnaires, artwork, unpublished letters), or to use any of my own published work (e.g. journal articles) in which the copyright is held by another party (e.g. publisher, co-author).

Signature: 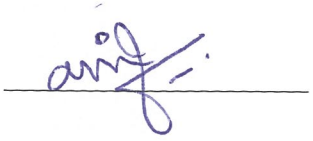 (Muhammad Arif)

Date: 08/08/2017

Dedication

I would like to dedicate my thesis to all those people who are source of my motivation!

To my parents for their enormous love and support!

To Mr. Abdus Sattar Edhi (late) the most wonderful humanitarian of Pakistan,

To the martyrs of Army Public School in Pakistan!

To them who faced hardships in life, but every time stood strong and transformed every challenge into a strength!

Acknowledgment

I would like to express the sincere gratitude to my supervisor Associate Professor Stefan Iglauer, who has the attitude of a genius: he incessantly and compellingly transferred an essence of quest to my research potential. Without his leadership and determined help, this dissertation would not have been possible. Specially, his invaluable input in executing the research plan and transforming it into a quality publication is the skill of a lift-time I learnt during this work.

I also express my deepest appreciation to the co-supervisors Associate Professor Ahmed Barifcani and Associate Professor Maxim Lebedev for their relentless motivation, and unwavering contribution towards the accomplishment of this dissertation. I am very grateful to Senior Lecturer Dr. Franca Jones from Department of Chemistry of Curtin University for very interesting technical discussions which were productive to explore the surface chemistry aspects of wettability.

A sincere vote of thanks also is devoted to the anonymous reviewers for the affirmative input and expert recommendations to enhance the quality of the publications forming this thesis. I also thank Elsevier for permission to include my published work in this dissertation.

I would like to acknowledge University of Engineering & Technology, Lahore, Pakistan, not only for the financial support granted through scholarship, but also for the cherishing moments during the tenure of my Bachelor degree as well as during my career as a faculty member. UET, you made me what I am!

My sincere appreciation to all the fellow PhD students and faculty members at the Department of Petroleum Engineering of Curtin University for being so wonderful!

Last, but not least, I express my most sincere love and thanks to my father who worked day in and day out to finance me during the early days of my education, and to my mother for her continuous prayers. My sincere appreciation goes to my wife for her love, support, trust and being on my side even at the most challenging situations during the tenure of this dissertation, which would certainly be my motivation throughout my professional life!

Abstract

Carbon capture and storage in geological formations is a promising approach to reduce anthropogenic greenhouse emissions leading to a cleaner environment. In order to ensure containment security and maximum storage capacity, a precise characterization of reservoir as well as caprock is essential. In this context, wettability of rock/CO_2/brine system is an important physicochemical aspect of reservoir characterization, which requires a comprehensive evaluation. Specifically, wettability drives the fundamental understanding of the multiphase flow in porous medium, rock/fluid interactions and microscopic fluid distribution, which in turn governs the fate of injected CO_2. Wettability also has a significant impact on the capillary pressure and relative permeability curves, which are essential input to reservoir simulators for modelling CO_2 storage performance over time. Although various studies report rock/CO_2/brine wettability, literature data lacks wettability characterization for a broad range of pressure, temperature, and salinity conditions. Moreover, there is a lack of understanding of the physical and chemical processes, which control the wettability alteration with various operating conditions.

This research is a collection of experimental measurements of wettability for various rock/CO_2/brine systems by the direct observation of water advancing and receding contact angles using the pendant drop tilted-plate technique at high pressures (up to 20 MPa) and elevated temperatures (up to 343 K) that simulates the behaviour at typical subsurface conditions. The minerals chosen for wettability investigation were calcite (a representative of carbonate rocks) and mica (a representative of caprocks). Moreover, this work reports CO_2-wettabiltiy of coals as a function of coal rank and CO_2-wettabiltiy of shales as a function of shale-TOC to determine their suitability as alternate candidates for the geological storage of CO_2 and enhanced methane recovery. The work also addresses the challenges associated with contact angle measurements such as surface chemical heterogeneity, which arises due to surface roughness and inappropriate surface cleaning methods that in turn may lead to a discrepancy in contact angle measurements. In addition, this research reports experimental data on CO_2/brine interfacial tension values at reservoir conditions, which is another important interfacial parameter relevant to CO_2 geo-storage. Both wettability and interfacial tension have a direct impact on structural and residual trapping capacities.

The results of this work demonstrate that both the water advancing and receding contact angles increased with pressure and salinity, while contact angles decreased with increasing temperature for most of the CO_2/brine/mineral systems investigated. The findings imply that the rock/fluid systems turned more CO_2-wet with increasing pressure and salinity, and more water-wet with increasing temperature. Hypothetically, under CO_2-wet conditions, an upwards directed suction force causes the buoyantly rising CO_2 plume to leak through the caprock, which leads to significant reduction in structural trapping capacities. The coals, however, when turn more CO_2-wet lead to better storage capacity owing to greater CO_2 adsorption potential under CO_2-wet conditions. Moreover, this work provides insights into solid/fluid interactions and electrochemical mechanisms responsible for wettability alteration. The results of this investigation demonstrate that the wettability significantly relates to the interplay of mineral/fluid interfacial tensions as well as the electrochemical processes at the mineral/brine interface.

The data reported in this thesis assists in evaluating the CO_2 storage potential of various rock forming minerals as well as coal seams and shales. In particular, the results are helpful to access the percolation threshold limits of capillary entry pressure for the caprock to elucidate the conditions associated with CO_2 leakage. The reported data also provides a substantial input for multiphase flow simulations, which can significantly improve the accuracy of such predictions, and thus de-risk storage projects.

Publications by the Author

(Publications forming part of thesis as standalone chapters)

1. **Arif, M.**, Al-Yaseri, A. Z., Barifcani, A., Lebedev, M., & Iglauer, S. (2016). Impact of pressure and temperature on CO_2–brine–mica contact angles and CO_2–brine interfacial tension: Implications for carbon geo-sequestration. *Journal of Colloid and Interface Science, 462,* 208-215.

2. **Arif, M.**, Barifcani, A., Lebedev, M., & Iglauer, S. (2016). CO_2-wettability of low to high rank coal seams: Implications for carbon sequestration and enhanced methane recovery, *Fuel,* 181, 680–689.

3. **Arif, M.**, Barifcani, A., & Iglauer, S. (2016). Solid/CO_2 and solid/water interfacial tensions as a function of pressure, temperature, salinity and mineral type: Implications for CO_2-wettability and CO_2 geo-storage. *International Journal of Greenhouse Gas Control,* 53, 263-273.

4. **Arif, M.**, Jones, F., Barifcani, A., & Iglauer, S. Influence of surface chemistry on interfacial properties of low to high rank coal seams, *Fuel,* 194 (2017) 211–221.

5. **Arif, M.**, Lebedev, M., Barifcani, A., & Iglauer, S. (2017) CO_2 storage in carbonates: wettability of calcite, *International Journal of Greenhouse Gas Control,* 62, 113-121.

6. **Arif, M.**, Lebedev, M., Barifcani, A., & Iglauer, S. (2017) 'Influence of shale-TOC on CO_2 storage potential' *Geophysical Research Letters,* 44, doi:10.1002/2017GL073532.

(Publications relevant to thesis but not forming part of it)

7. **Arif, M.**, Barifcani, A., Lebedev, M., & Iglauer, S. (2016). Structural trapping capacity of oil-wet caprock as a function of pressure, temperature and salinity. *International Journal of Greenhouse Gas Control,* 50, 112-120**.**

8. **Arif, M.**, Jones, F., Barifcani, A., & Iglauer, S. (2017). Electrochemical investigation of the effect of temperature, salinity and salt type on brine-mineral interfacial properties: Implications for structural trapping capacities of caprock, *International Journal of Greenhouse Gas Control*, 59 (2017) 136–147.

9. **Arif, M.**, Lebedev, M., Barifcani, A., & Iglauer, S., Influence of solid surface energy on wettability of CO_2-brine-mineral systems, *Energy Procedia*, in press.

Refereed conference presentations:

Arif, M., Lebedev, M., Barifcani, A., & Iglauer, S., Impact of solid surface energy on wettability of CO_2-brine-mineral systems, presented at *Greenhouse Gas Technology Conference* (GHGT-13) held on November 2016 at Lausanne, Switzerland (oral presentation).

Arif, M., Barifcani, A., Zubair, T. Lebedev, M., & Iglauer, S. CO_2 wettability of coals and shales, *SPE Conference at Islamabad*, Pakistan, SPE-185308-MS.

Contents

Declaration I
Copyright II
Dedication III
Acknowledgment IV
Abstract V
Publications by the Author VII
Contents IX
List of Figures XIV
List of Tables XVII

Chapter 1 Introduction 1
1.1 Background 1
1.2 Research objectives 4
1.3 Thesis organization 5

Chapter 2 Literature review 7
2.1 Introduction 7
2.2 Carbon capture and storage 7
2.3 Geological storage media 9
2.4 Trapping mechanisms for CO_2 storage 10
2.4.1 Structural trapping 10
2.4.2 Residual trapping 11
2.4.3 Solubility trapping 12
2.4.4 Mineral trapping 13
2.4.5 Adsorption trapping 14
2.5 Wettability of rock/CO_2/brine systems 15
2.5.1 Wettability characterization by contact angle measurement 16
2.5.2 Advancing and receding contact angles 17
2.5.3 Contact angle hysteresis 18
2.5.4 Equilibrium contact angle 19
2.6 Influence of CO_2-wettability on trapping potential 19
2.6.1 Influence of wettability on structural trapping 19
2.6.2 Influence of wettability on residual trapping 21

2.6.3 Influence of wettability on dissolution and mineral trapping 21
2.6.4 Influence of wettability on adsorption trapping 22
2.6.5 Assessment of trapping potential using multiphase flow observations 22
2.7 Factors influencing wettability 23
2.7.1 Pressure 24
2.7.2 Temperature 24
2.7.3 Brine composition: salinity and salt types 25
2.7.4 Surface roughness 26
2.7.5 Surface aging and hydrophobicity 26
2.8 Physics of wettability alteration 27
2.8.1 Solid surface energy concept and modelling 28
2.8.2 Surface chemistry aspects 28
2.8.2.1 Electrochemical Investigation 29
2.8.2.2 Surface functional groups 30
2.9 Interfacial tension of CO_2/brine systems 30
2.9.1 Previous studies and influencing factors 31

Chapter 3 CO_2 storage in carbonates: wettability of calcite* 32
3.1 Introduction 33
3.2 Materials and Methods 35
3.2.1 Sample and fluids used 35
3.2.2 Surface roughness 35
3.2.3 Contact angle measurements 36
3.3 Results and discussion 40
3.3.1 Effect of pressure on CO_2-wettability of calcite 40
3.3.2 Effect of temperature on CO_2-wettability of calcite 43
3.3.3 Comparison with literature 44
3.3.4 Effect of salinity on CO2-wettability of calcite 46
3.3.5 Effect of CO_2/brine equilibration on wettability 47
3.3.6 Effect of surface roughness on wettability 48
3.4 Implications 49
3.5 Conclusions 51

Chapter 4 Impact of pressure and temperature on CO_2-brine-mica contact angles and CO_2-brine interfacial tension: Implications for carbon geo-sequestration* **52**

4.1 Introduction 53

4.2 Experimental Methodology 54

4.2.1 Contact angle measurements 54

4.2.2 Interfacial tension measurements 56

4.3 Results and Discussion 57

4.3.1 Effect of pressure on contact angle 57

4.3.2 Effect of temperature on contact angle 59

4.3.3 Effect of salinity on contact angle 61

4.3.4 Comparison of Mica with Quartz 61

4.3.5 Effect of pressure and temperature on interfacial tension 63

4.3.6 Empirical correlations for contact angles and interfacial tensions 65

4.4 Implications of the results 66

4.5 Conclusions 67

Chapter 5 CO_2-wettability of low to high rank coal seams: Implications for carbon sequestration and enhanced methane recovery* **69**

5.1 Introduction 70

5.2 Materials and methods 72

5.2.1 Coal Samples 72

5.2.2 Petrology, Ultimate and Proximate Analysis 72

5.2.3 Fluids 73

5.2.4 Contact angle measurements 74

5.3 Results and Discussion 75

5.3.1 Effect of pressure on CO_2-wettability of coal 75

5.3.2 Effect of temperature on CO_2-wettability of coal 80

5.3.3 Effect of coal rank on CO_2-wettability 82

5.3.4 Effect of brine salinity on CO_2-wettability of coal 83

5.3.5 Relation between vitrinite reflectance, fixed carbon and coal wettability 84

5.4 Implications 85

5.5 Conclusions 86

Chapter 6 Influence of shale-total organic content on CO_2 geo-storage potential* 88

6.1 Introduction 88

6.2 Experimental Procedure 90

6.2.1 Materials 90

6.2.2 Contact angle measurements 91

6.3 Results and Discussion 92

6.4 Implications for CO_2 geo-storage 95

6.5 Conclusions 96

Chapter 7 Solid/CO_2 and solid/water interfacial tensions as a function of pressure, temperature, salinity and mineral type: Implications for CO_2-wettability and CO_2 geo-storage* 98

7.1 Introduction 99

7.2 Methodology 101

7.2.1 Contact angle data 101

7.2.2 Surface free energy computation 104

7.2.3 Regression fit of data 106

7.3 Results and discussion 108

7.3.1 Effect of pressure on solid/CO_2 interfacial tension 108

7.3.1.1 Case 1: quartz 108

7.3.1.2 Case 2: Mica 110

7.3.1.3 Case 3: Coals 111

7.3.2 Effect of temperature on solid/CO_2 interfacial tension 112

7.3.3 Effect of temperature on solid/water interfacial tension 114

7.3.4 Effect of salinity on solid/CO_2 interfacial tension 115

7.3.5 Effect of salinity on solid/water interfacial tension 116

7.3.6 Wettability dependence on surface energies 117

7.4 Implications 118

7.5 Conclusions 120

Chapter 8 Influence of surface chemistry on interfacial properties of low to high rank coal seams* 121

8.1 Introduction 122

8.2 Experimental Methodology 123

8.2.1 Fluid/sample preparation 123

8.2.2 Zeta potential measurements 124
8.2.3 Petrology, Ultimate and Proximate Analysis 125
8.2.4 pH measurements 125
8.2.5 Infrared spectroscopy 126
8.2.6 XRD analysis 126
8.2.7 Contact angle measurements 126
8.3 Results and discussion 127
8.3.1 Effect of temperature on zeta potential and contact angle 128
8.3.2 Effect of salinity on zeta potential and contact angle 131
8.3.3 Effect of brine composition on zeta potential and contact angle 134
8.3.4 Zeta potential and contact angles as a function of coal rank 136
8.3.5 Surface functional group and wettability 138
8.3.6 Correlation between zeta potential and wettability 141
8.4 Implications 144
8.5 Conclusions 145

Chapter 9 Conclusions, Recommendations and Outlook for Future Work. 146
9.1 Conclusions 146
9.2 Recommendations and outlook for future work 149

References 152
Appendix 171

List of Figures

Fig. 1-1 Layout of thesis objectives and structure 6

Fig. 2-1 Layout showing major steps and subsets involved in CO_2 capture and storage project (modified after Thomas and Benson, 2015) 8

Fig. 2-2 Geological storage mediums with typical depths (after Thomas and Benson, 2015) 9

Fig. 2-3 Conceptualization of in-situ trapping mechanisms (after Burnside & Naylor, 2011) 12

Fig. 2-4 Trapping mechanism efficiency over timescale (after IPCC, 2005) 13

Fig. 2-5 Force field acting on a three phase mineral/CO_2/brine system (after Iglauer et al., 2015a) 17

Fig. 2-6 Schematic of advancing and receding contacting angles using a tilting plate technique (after Attention theory note 1). 18

Fig. 3-1 Experimental setup for contact angle measurements used in this study. (a) CO_2 cylinder (b) high precision syringe pump-CO_2, (c) high precision syringe pump-water, (d) High pressure Parr reactor for fluid equilibration e) high pressure cell with substrate housed on a tilted plate inside, (f) heating unit, (g) liquid feed/drain system, (h) high resolution video camera, (i) image visualization and interpretation software, (j) pressure relief valve 37

Fig. 3-2 (a) Few example images acquired for contact angle measurements. Experimental conditions for a particular experiment are given below the image. The droplet is of DI-water, the surface on which the droplet rests is calcite, while CO_2 is in the surrounding. (b) Schematic of contact angle measurements. On the left (red) is 'advancing angle', on the right (blue) is 'receding angle'. 39

Fig. 3-3 Calcite/CO_2/DI-water contact angles measured: lines represent this work (solid: advancing, dotted: receding) at three different temperatures as a function of pressure. Open symbols represent literature measurements. *Broseta et al. (2012) analysed Rousse caprock which comprised of 70% calcite; **Yang et al. (2007) analysed limestone rock sample; Andrew et al. (2014) computed contact angles from Micro-CT image analysis. 42

Fig. 3-4 Effect of salinity on water-CO_2-calcite contact angle at 15 MPa and 323 K. 46

Fig. 3-5 AFM images of the three calcite surfaces tested: 2D deflection signal; right: 3D topography of the substrate; RMS surface roughness was a) = 7.5 nm; b) = 30 nm; c) = 140 nm. 49

Fig. 3-6 Effect of RMS surface roughness on contact angle on calcite surface. 50

Fig. 4-1 Experimental configuration for contact angle and interfacial tension measurements used in this study; (a) high P/T cell, (b) syringe pump-CO_2, (c) syringe pump-brine, (d) CO_2 source, (e) substrate housed on a tilted plate inside the

cell, (f) high resolution video camera, (g) visualization software, (h) feed/drain system, (i) three way valve, (j) flow-lines, (k) pressure relief valve, (l) data transfer module. 55

Fig. 4-2 Atomic Force Microscopy images of Muscovite surface used in the study, Left: 3D topography of the substrate; right: deflection signal (scale bar on the right represents surface heights associated with different spots on the image. 56

Fig. 4-3 Water contact angles on muscovite in CO_2 atmosphere at various operating conditions. Our measured values are shown in red (solid lines for advancing and dotted lines for receding angles), and literature values are shown in black (literature's receding angles are represented by open symbols while advancing angles by filled solid symbols). *Salinity: 0.1M NaCl, without adhesion, **Salinity: 0.1 M NaCl, with adhesion. 59

Fig. 4-4 Influence of salinity on advancing and receding contact angles (Salinity range considered from 0 wt% (DI water) to 20wt% NaCl. For all measurements, solid lines indicate advancing angles whereas dotted lines indicate receding angles.) 62

Fig. 4-5 Comparison of advancing and receding contact angles on mica and quartz surfaces. Data for quartz contact angles is taken from Sarmadivaleh et al. (2015) who used similar experimental setup. 63

Fig. 4-6 Variation of interfacial tension with pressure and temperature (20wt% NaCl brine). 64

Fig. 4-7 Values of density differences used in this study (data taken from Li et al., 2012). 65

Fig. 5-1 CO_2-DI water contact angles on high rank coal (semi-anthracite) at tested pressures (0.1 MPa-20 MPa) and temperatures (308 K-343 K). 77

Fig. 5-2 CO_2-DI water contact angles on medium rank coal (medium volatile bituminous) at tested pressures (0.1 MPa-20 MPa) and temperatures (308 K-343 K). 78

Fig. 5-3 CO_2-DI water contact angles on low rank coal (lignite) at tested pressures (0.1 MPa-20 MPa) and temperatures (308 K-343 K). 79

Fig. 5-4 Effect of temperature on CO_2-wettability for all coal samples used in the study. For simplicity measurements are shown only for 15 MPa. 81

Fig. 5-5 Effect of coal rank on CO_2-wettability 82

Fig. 5-6 Effect of salinity on CO_2-wettability of coals at 323K and 15 MPa 84

Fig. 5-7 Variation of CO_2-wettability with vitrinite reflectance and fixed carbon content 85

Fig. 6-1 Advancing and receding water contact angles of shale/CO_2/1 M NaCl systems as a function of TOC and operating pressure (at 343 K). a) 3D surface plot with a quadratic fit. 'Dark green' in the colour legend represents strongly water-wet conditions (safe structural trapping), while 'dark brown' represents strongly CO_2-wet

conditions (unsafe for structural trapping, but suitable for adsorption trapping) b) 2D plot of θ_a and θ_r as a function of temperature and showing literature data. 95

Fig. 7-1 Regression fit of experimental and model data for all minerals investigated at 343 K. 107

Fig. 7-2 Quartz/CO_2 interfacial tension as a function of pressure and temperature. 109

Fig. 7-3 Mica/CO_2 interfacial tension as function of pressure and temperature. 111

Fig. 7-4 Coal/CO_2 interfacial tension as a function of pressure, temperature and coal rank. 112

Fig. 7-5 Solid/CO_2 interfacial tension as a function of temperature at 15 MPa for various substrates. 113

Fig. 7-6 Mica/CO_2 interfacial tension as a function of pressure and temperature for two different liquids (DI-water and 20 wt% NaCl brine) 116

Fig. 7-7 Experimental and predicted water contact angles as a function of pressure at 343 K for all substrates. 119

Fig. 8-1 Zeta potential as a function of temperature and coal rank (at ambient pressure). 130

Fig. 8-2 Water contact angle as a function of temperature and coal rank (at ambient pressure). 130

Fig. 8-3 Effect of salinity on zeta potential at 323 K (and ambient pressure) as a function of coal rank. 133

Fig. 8-4 Water contact angle as a function of salinity and coal rank at 323 K (and ambient pressure). 133

Fig. 8-5 Zeta potential as a function of salt type (NaCl, $CaCl_2$, $MgCl_2$) and coal rank (at 323 K and ambient pressure). 135

Fig. 8-6 Water contact angle as a function of salt type (NaCl, $CaCl_2$, $MgCl_2$) and coal rank (at 323 K and ambient pressure). 136

Fig. 8-7 Water contact angle as a function of pressure and coal rank at 323 K (experimental data from Arif et al. 2016c). 139

Fig. 8-8 ATR-infrared spectroscopy measurements on low, medium and high rank coals 141

Fig. 8-9 Zeta potential and contact angle relationships 144

List of Tables

Table 2-1 Largest CO_2 storage projects worldwide (reproduced after IPCC, 2015)... 8

Table 2-2 Storage capacity assessment of various geological storage options (modified after, IPCC, 2005)..... 10

Table 2-3 Wettability criteria based on contact angle of rock/CO_2/brine systems (modified after Iglauer et al., 2015a) 17

Table 3-1 Review of experimental conditions and measured wettability of major studies on calcite/CO_2/water systems. 34

Table 4-1 Model parameters from simulation..... 66

Table 4-2 CO_2 column heights predicted for various storage depths 67

Table 5-1 CO_2-wettability of coals: Summary of experimental conditions used. 71

Table 5-2 Properties of coal samples used. 73

Table 6-1 Shale sample description, characterization and mineralogy. 90

Table 7-1 Contact angle data for CO_2-deionized (DI) water systems for minerals investigated in this study. 102

Table 7-2 Equilibrium contact angles for all minerals calculated using Tadmor's correlation. 102

Table 7-3 CO_2/DI-water and CO_2/brine interfacial tension data used. 103

Table 7-4 Results obtained from regression fit of the experimental and model data. 107

Table 8-1 Measured pH values of the solutions used. 125

Table 8-2 Mineral identified by XRD in the three coal samples investigated. 126

Chapter 1 Introduction

1.1 Background

Global warming which refers to the rise in average earth temperature has led to serious concerns due to its direct impact on the climate and consequently on quality of life (Dimento and Doughman, 2007; Lu et al., 2007). Carbon dioxide (CO_2) which is a critical component of the greenhouse emissions significantly contributes to the global warming (Pazhoohi, 2015; Scheffer et al., 2006). Over the past few years, the anthropogenic CO_2 emissions due to synthetic activities such as burning fossil fuels and global industrialization have led to an increase in the atmospheric CO_2 concentration from 280 ppm in 1750 to 401.5 ppm in 2017 (Buckingham and Turner, 2008; Cape Grim, 2017). Various strategies are proposed to mitigate carbon emissions such as carbon-free solar and wind power, and geological CO_2 storage (IPCC, 2005). Carbon capture and storage (CCS) is a promising method to mitigate the anthropogenic greenhouse emissions (Blunt et al., 1993; Lackner, 2003). The process involves the separation of CO_2 from large point sources such as industrial sources, or large fossil fuel, transport to a storage location and injection into deep saline aquifers or depleted oil and gas reservoirs for long-term isolation from the atmosphere (IPCC, 2005). CO_2 injection is also considerably favourable in active oil and gas reservoirs due to the associated dual advantages i.e. storage and enhanced oil recovery (EOR), while CO_2-EOR also involves CO_2-recycling (Underschultz et al., 2016). Once injected into the reservoirs, certain trapping mechanisms render CO_2 immobile within the porous space. These trapping mechanisms include structural trapping (Hesse et al., 2008, Iglauer et al. 2015a,b), capillary or residual trapping (Iglauer et al., 2011a,b; Juanes et al., 2006), dissolution trapping (Iglauer, 2011c; Lindeberg and Wessel-berg, 1997), and mineral trapping (Guas, 2010). Coal seams are another important CGS candidate where the dominant trapping mechanism is adsorption trapping (Saghafi et al., 2014; Shojaii Kaveh et al., 2012). During the first decade of a storage project, structural and residual trapping are by far the most dominant storage mechanisms. In this context, wettability of rock/CO_2/brine systems is a fundamental physicochemical parameter, which significantly controls the structural and residual trapping potential of the storage rock. A capillary force-buoyancy force balance (Iglauer et al., 2015b)

which accounts for the CO_2-column height being permanently immobilized beneath the caprock, demonstrates the structural trapping potential as follows:

$$h = \frac{2\gamma cos\theta_r}{\Delta\rho g R} \qquad \text{Eq. 1.1}$$

In Eq. 1.1, 'h' refers to height of the CO_2 column that can be permanently immobilised by the seal layer, 'γ' is the CO_2/brine interfacial tension, 'θ_r' is the water receding contact angle at the prevailing pressure and temperature, $\Delta\rho$ is the CO_2-brine density difference and 'R' is the average pore throat radius. It is quite well established from reservoir scale simulation studies and pore-scale 3D micro-CT imaging that water-wet storage reservoirs and caprocks yield better residual and structural trapping capacities (Chaudhary et al., 2013; Iglauer et al., 2015a,b; Krevor et al., 2015). In the case of a CO_2-wet caprock, an upwards directed suction force leads to the leakage of CO_2 through the caprock resulting in a dramatic reduction in storage capacity (Iglauer et al., 2015a). Moreover, CO_2/brine interfacial tension also directly affects the structural trapping and indirectly influences the residual trapping capacities (Aggelopoulos et al., 2010; Chiquet et al., 2007; Chalbaud et al., 2009; Li et al., 2012).

Coal bed formations are also highly attractive candidate for CO_2 storage, which is due in part to large surface area of coals microporous structure, which in turn significantly promotes gas adsorption capacity (Day et al., 2007), the associated drawback, however, is the permeability reduction due to coal swelling (Hol and Spiers, 2012) . Once injected, CO_2 displaces methane into the fracture network, and itself is trapped within the micropores of the coal seam via adsorption trapping. This is attributed to a preferentially higher adsorption tendency of CO_2 over CH_4 (typically CO_2/CH_4 adsorption ratio is 9:1, Clarkson and Bustin, 2000), consequently leading to dual benefits i.e. CO_2 storage and enhanced methane recovery (Durucan et al., 2014). Studies have shown that the CO_2-wettabiltiy of coals controls the ease of adsorption in micropores of the coal seam (Saghafi et al., 2014; Shojai Kaveh et al., 2012), such that in a CO_2-wet coal, CO_2 distributes more uniformly within the microporous network leading to higher CO_2 adsorption capacity.

Thus, following the above discussion, it is established that all the major CO_2 trapping mechanism are significantly influenced by the CO_2-wettabiltiy. Thus, an accurate characterization of wettability at the relevant physicochemical conditions is essential

to establish a framework of robust geological storage estimation. Many factors influence wettability of rock/fluid systems such as pressure, temperature, salinity and surface roughness and rock type itself (Iglauer et al., 2015a, 2017). In addition, the surface chemistry associated with the rock such as carbon and silanol group coverage have considerable impact on the wettability.

Wettability is typically assessed by contact angle measurement at in-situ conditions of various minerals such as calcite: a proxy for carbonates, quartz: a proxy for sandstones, mica: a constituent of caprock, shales: a naturally occurring caprock, and coals: an independent storage medium. Quartz wettability has been studied by many groups (Al-Yaser et al., 2016a; Chiquet et al., 2007; Farokhpoor et al., 2013; Saraji et al., 2013, 2014) and is not the subject of this study. Calcite and mica are important minerals and their wettability studies are required for understanding CO_2/brine interactions with these minerals and their impact on CO_2 storage. Similarly, CO_2-wettabilty characterization of coals and shales is of interest among the researchers to evaluate their feasibility as a candidate for storage. Although, a few researches evaluated CO_2-wettability of calcite, mica, coals and shales (Bikkina, 2011; Broseta et al., 2012; Chiquet et al., 2007; Espinoza and Santamarina, 2010; Farokhpoor et al., 2013; Iglauer et al., 2015a,b; Shojai Kaveh et al., 2012; Wang et al., 2012; Yang et al., 2007), but there is a general lack of understanding, summarized by following points:

1) The literature data of CO_2-wettability of calcite and mica lacks in terms of wettability characterization for a wide range of experimental conditions, and data spread is huge indicating discrepancy in the available data.
2) The so-far reported CO_2-wettability of coals are limited mainly to the medium and semi-high coals ranks, despite the fact that coal rank ranges from low to high. Wettability characterization of coals for varying rank at in-situ conditions is, nevertheless, vital for establishing the potential of CO_2 storage and enhanced methane recovery.
3) Shale-wettability is reported for only low-TOC shales, however, shale can be organic-rich. Consequently, wettability of shaly caprocks as a function of TOC is vital to help de-risk the storage projects i.e. to avoid capillary leakage.
4) The mechanistic aspects of wettability alteration (with the change in prevailing subsurface conditions) so far remain unclear. Specially, the influence of solid

surface energy and electrochemical processes at the brine/mineral interface and their control on wettability is unknown.

It is thus clear that a detailed investigation of wettability of various important rock/fluid systems (calcite, mica, coals and shales) for a wide range of operating conditions is required to establish CO_2 storage potential of caprocks and storage rocks. Furthermore, exploring the factors responsible for wettability alteration with operating conditions is essential to improve the understanding of interfacial phenomena at both the macroscopic and microscopic level.

1.2 Research objectives

This work is a collection of experimental data on CO_2-wettability of calcite, mica, coal seams of varying ranks and shales of varying TOC for a broad range of operating conditions.

The following list describes the specific objectives of this research:

1. Microscopic wettability characterization for calcite/CO_2/brine and mica/CO_2/brine systems for a broad range of influencing parameters (pressure: 0.1 MPa – 20 MPa, temperature: 308 K – 343 K, brine salinity: 0 wt% NaCl – 20 wt% NaCl) for a broad range of operating conditions and evaluating the implications of the measured data for trapping potential.

2. Investigating the CO_2-wettability for coals of low, medium and high rank to assess the CO_2-storage potential of coals.

3. Measurement of wetting behaviour of shales for a wide range of shale-TOC to determine the caprock sealing efficiency for CO_2 storage and to address the suitability of shales as a storage medium.

4. To improve the fundamental understanding of the principles responsible for wettability alteration by:

a) Utilizing the solid surface energy concept to quantify solid/fluid interfacial tensions by simulating Neumann's equation of state, which in turn governs the interplay of various interfacial tensions responsible for wettability dependency on pressure, temperature and salinity.

a) Investigation of electrochemical changes at the mineral/brine interface by measurement of zeta potential as a function of temperature, ionic strength and brine type for coal seams.
b) Analysing the surface hydrophobicity by predicting surface functional groups using advanced Fourier transform infrared (FTIR) spectroscopy for coals.

1.3 Thesis organization

The thesis includes nine chapters: Chapter 1 presents the introduction of the thesis; Chapter 2 covers the literature review relevant to the thesis, Chapters 3 – 8 cover the experimental methodology, materials, results and discussion, and implication of the measured data. Fig. 1-1 Layout of thesis objectives and structure describes the framework of the aforementioned thesis objectives covered in Chapter 3 – 8. As seen from the layout, Chapter 3 and 4 cover wettability measurement of calcite and mica respectively, while Chapter 5 and 6 describe wettability characterization of coal seams and shales respectively. Chapter 7 describes the application of surface energy concept for the characterization of various interfacial tensions responsible for wettability alteration, while Chapter 8 covers the zeta potential and wettability relationships.

Finally, Chapter 9 concludes the thesis with recommendations for future research outlook.

Note: Chapters 3 – 8 are the author's journal publications, which this work reproduced as individual chapters. Reader may like to read them separately, and the illustrations at some places in the text may appear more than once. Appendix A contains the relevant copyright forms.

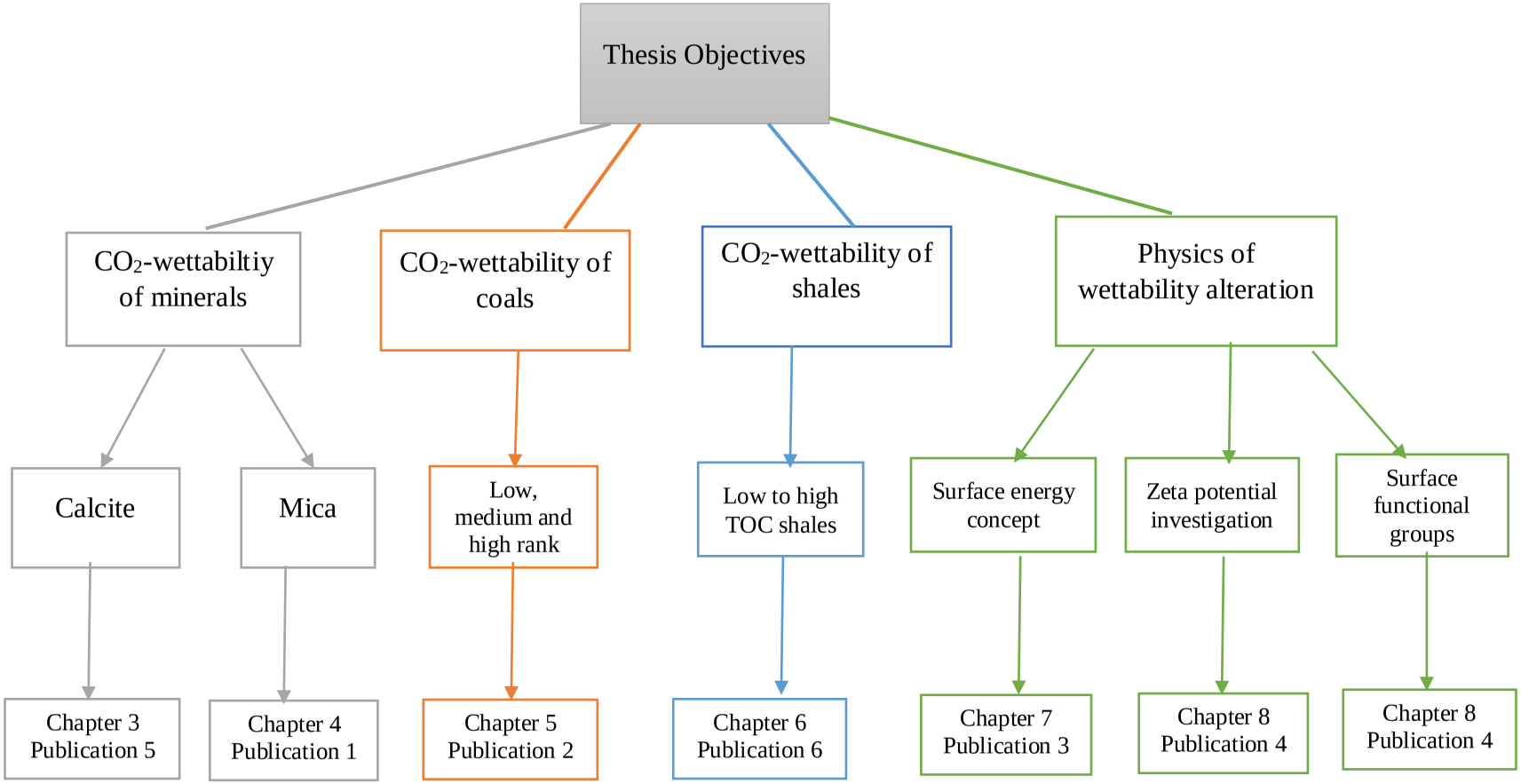

Fig. 1-1 Layout of thesis objectives and structure

Chapter 2 Literature review

2.1 Introduction

This chapter covers the literature review relevant to the CO_2-wettability of rock forming minerals and CO_2/brine interfacial tension and their implications for carbon geo-storage. CO_2 injection into deep saline aquifers and depleted oil and gas reservoirs is a promising approach to reduce anthropogenic greenhouse emissions. Moreover, CO_2 flooding in active oil reservoirs leads to a significant improvement in oil production after the completion of secondary recovery. Further, CO_2 injection into the coals seams is a viable option because of potential for coupled CO_2 storage and enhanced methane recovery leading to an improved project outlook due to the associated additional technical and economic benefits. To reduce uncertainty associated with CO_2 storage, reservoir wettability characterization of the rock forming minerals at in-situ conditions is, nevertheless, very important as it leads to optimum set of operating conditions as well as selection of formations suitable for CO_2 storage. This chapter firstly describes the significance of CO_2 geo-sequestration (CGS) followed by the illustration of trapping mechanisms. Next, the focus will shift to the CO_2 wettability of carbonates, shaly caprocks of varying TOC and coal seams of varying ranks and their relative impact on CO_2 trapping potential. Special emphasis will be devoted to the factors influencing wettability such as pressure, temperature and salinity to address the knowledge gaps and associated challenges with the current studies on CO_2 wettability of the aforementioned minerals and formations. Finally, the chapter investigates the physics of the wettability alteration.

2.2 Carbon capture and storage

Carbon capture and storage (CCS) refers to a chain of processes, which aim to reduce the carbon footprint and mitigating anthropogenic CO_2 emissions by means of underground storage, and thus ensure cleaner environment (Blunt et al., 1993; IPCC, 2005; Lackner, 2003). Fundamentally, carbon capture and storage comprises of three independent steps described in layout in Fig. 2-1. During CCS, at first, CO_2 is captured from large point sources (industrial and energy-related) using post-combustion, pre-

combustion capture and oxyfuel combustion. Next step is the CO_2 transportation to the storage site by means of for example pipelines (for example, as not all the commercial projects use pipeline transport) after compression at around 10 MPa. Finally, CO_2 flooding into the storage medium commences for a long-term isolation from the atmosphere (Gale and Davison, 2004; Marchetti, 1977; Thomas and Benson, 2015).

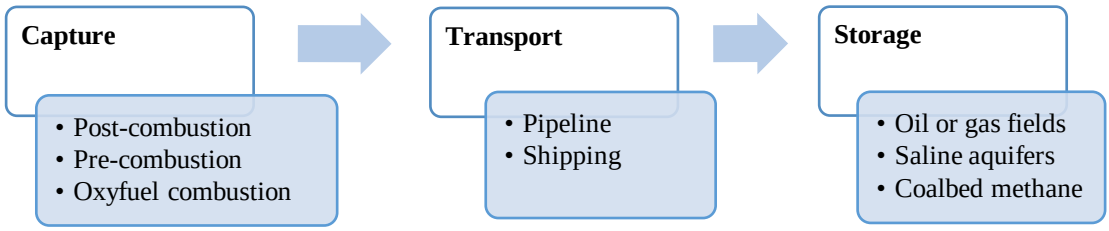

Fig. 2-1 Layout showing major steps and subsets involved in CO_2 capture and storage project (modified after Thomas and Benson, 2015)

Table 2-1 Largest CO_2 storage projects worldwide (reproduced after IPCC, 2015)

Project	**Mass of CO_2 (millions tons/year)**	**Project stage**	**Storage formation**
Sleipner, Norway	1 (since 1996)	Monitoring, modelling	Offshore saline aquifer sand formation
Weyburn, Canada	1.7 (since 2000)	Monitoring, risk assessment, performance assessment	On-shore carbonate oil reservoir
In Salah, Algeria	1 (since 2004)	Monitoring, risk assessment	On-shore sandstone gas reservoir
Gorgon, Australia	4 (up to 2006)	To be determined	Onshore saline aquifer sandstone formation
Snohvit, Norway	0.7 (up to 2006)	To be determined	Offshore saline aquifer sandstone formation

Table 2-1 presents a list of globally the largest storage projects, the Sleipner project in Norway, the Weyburn project in Canada and the In Salah project in Algeria, are a few examples (Thomas and Benson, 2015). The realization of the significance of geological CO_2 storage and the associated benefits can be assessed from the fact that around 3 – 4 million tons of CO_2 is stored in reservoirs or aquifers which would otherwise be released to the atmosphere.

2.3 Geological storage media

Geological storage media refers to the options available for underground CO_2 storage. There are three common types of storage mediums (Bachu, 2003; IPCC, 2005), which are:

1) Active and depleted oil and gas reservoirs
2) Saline aquifers
3) Coal seams

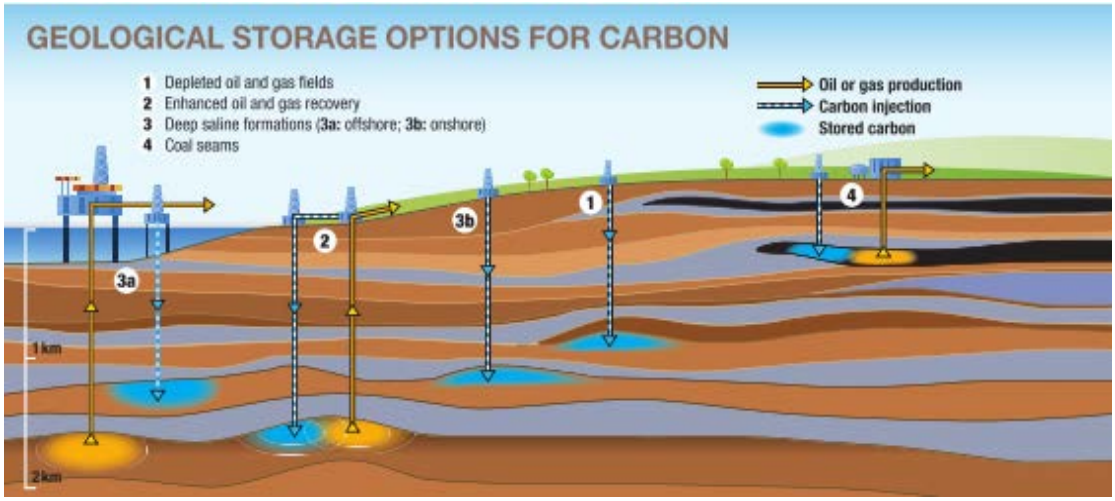

Fig. 2-2 Geological storage mediums with typical depths (after Thomas and Benson, 2015)

Oil and gas reservoirs considered for CO_2-storage, typically include carbonate and sandstone rocks. Carbonates often being highly permeable can allow greater CO_2 injection volume compared to the typically lower permeability sandstones (IPCC, 2005). The caprock/seal which prevents the upwards migration of CO_2 is usually 'shale' or salt (evaporite). The minerology of caprock reveals that mica, calcite and

quartz are significant components of the caprock (Gaus et al., 2005). In addition, over the past decade, coal seams have evolved as another substantial candidate for the geological storage (Bachu et al., 2007; IPCC, 2005; Shi and Durucan, 2005). CO_2 injection in coal seams offers dual benefits i.e. CO_2 storage and enhanced methane recovery due to preferential adsorption of CO_2 over CH_4 discussed in detail in next section. Fig. 2-2 is a schematic demonstrating the candidates for geological CO_2 storage with the typical storage depths associated with each case. It is evident from the depth scale that candidate coal seams are located much shallower, while the saline aquifers are the deepest storage medium. The estimated storage capacity of deep saline aquifers is highest among all other options (

Table 2-2).

Table 2-2 Global storage capacity assessment of various geological storage options (modified after, IPCC, 2005)

Storage formation	Lower estimate of storage capacity ($GtCO_2$)	Upper estimate of storage capacity ($GtCO_2$)
Oil and gas fields	675	900[a]
Deep saline aquifers	1,000	possibly 10^4
Unminable coal seams	3-15	200

[a] this estimate could increase by 25% if undiscovered oil and gas fields were included

2.4 Trapping mechanisms for CO_2 storage

Various physical and chemical mechanisms render CO_2 immobile in the porous medium, and these include dissolution, mineralisation, structural and stratigraphic confinement, and capillary trapping. The subsequent sections describe these mechanisms in detail.

2.4.1 Structural trapping

Once injected into the storage formation, CO_2 rises upwards due to the imbalance of buoyancy and capillary forces. In principal, capillary forces tend to retain CO_2 within

the porous medium and when buoyancy forces exceed the capillary forces, the CO_2 plume migrates up-structure within the storage formation. This rising CO_2 plume eventually encounters a thick and fine-textured rock which serves as 'caprock' or seal, which is low permeability such as shale (permeability is in the order of nano-Darcy, Neuzil, 1994). Consequently, the low permeability seal, disallows the upwards CO_2 migration, and CO_2 is structurally trapped (by capillarity or rate dependent sealing) and hence the term 'structural' trapping as depicted in **Error! Reference source not found.**.

Structural CO_2 trapping is typically the most dominant storage mechanism during the first decade of a storage project. **Error! Reference source not found.** demonstrates the relative efficiency of various trapping mechanisms over time for geological sequestration. It is evident that structural trapping can contribute to the total trapped CO_2 volume throughout the storage project life and it is most significant in first decade. In practice, however, CO_2 injection pressure must not exceed the fracture pressure of the caprock, which may otherwise lead to caprock failure, resulting in considerable reduction in caprock sealing efficiency (Chiquet et al., 2007). This can place a geo-mechanical limit on the effective storage volume in some cases (Underschultz and Strand, 2016).

In addition to geo-mechanical properties of caprocks, wettability of the caprock/CO_2/brine systems and CO_2/brine interfacial tension can significantly control the capillary sealing efficiency of caprock (Chiquet et al., 2007; Broseta et al., 2012; Iglauer et al., 2015a,b; Yang et al., 2007). Section 2.6.1 covers the influence of wettability on structural trapping potential in detail.

2.4.2 Residual trapping

Residual trapping refers to the physical immobilization of CO_2 in the pore spaces due to capillary forces, which hold the buoyant CO_2 back (Hesse et al., 2008; Juanes et al., 2006; Pentland et al., 2011). Capillary trapping is a rapid and effective mechanism, which occurs at the cessation of CO_2 injection into the targeted formation when the brine displaces and traps CO_2 as discontinuous droplets at the trailing edge of a rising CO_2 plume. In standard laboratory practice, an engineered setup involving brine injection thorough the core held in a high-pressure core holder allows the estimation

of residual CO_2 saturation which reflects the capillary trapping potential (Kumar et al., 2005; Qi et al., 2009; Saadatpoor et al., 2010). Fig. 2-3 describes the conceptualization of capillary trapping and Fig. 2-4 shows the timescale of capillary trapping. As for structural trapping, capillary trapping is significant during first few decades of a storage project.

Capillary trapping is also significantly influenced by the rock wettability (Farophpoor et al., 2013; Iglauer et al., 2013; Iglauer et al., 2015a) and interfacial tension (Chalbaud et al., 2009). Initial gas saturation, pore geometry, pore throat aspect ratio and hysteresis also influence capillary trapping effectiveness (Al-Menhali et al., 2015; Juanes et al., 2006; Suekane et al., 2010). Section 2.6.2 describes the influence of wettability on capillary trapping.

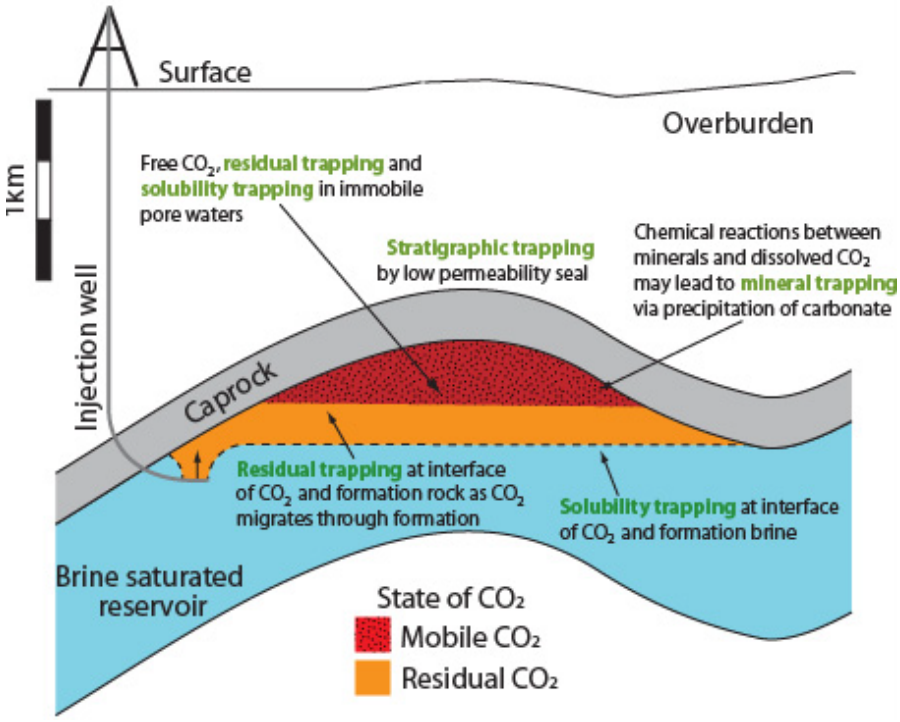

Fig. 2-3 Conceptualization of in-situ trapping mechanisms (after Burnside & Naylor, 2011)

2.4.3 Solubility trapping

Solubility trapping is a geochemical storage mechanism, which refers to the dissolution of CO_2 in the reservoir brine leading to the formation of a higher-density CO_2-enriched brine, which sinks at the bottom of the reservoir (Fig. 2-3). The pertinent

benefit associated with solubility trapping is that dissolved CO_2 does not exist as a separate phase, thereby upwards CO_2 plume migration due to buoyancy is non-existent (Iglauer, 2011c; IPCC, 2005). The quantity of CO_2 dissolved in brine i.e. solubility trapping is a direct function of the operating pressure, temperature, and brine salinity (Koschel et al., 2006; Lagneau et al., 2005). Specifically, solubility trapping is significant from mid to long-term scales (Gilfillan et al., 2009) as shown in Fig. 2-4.

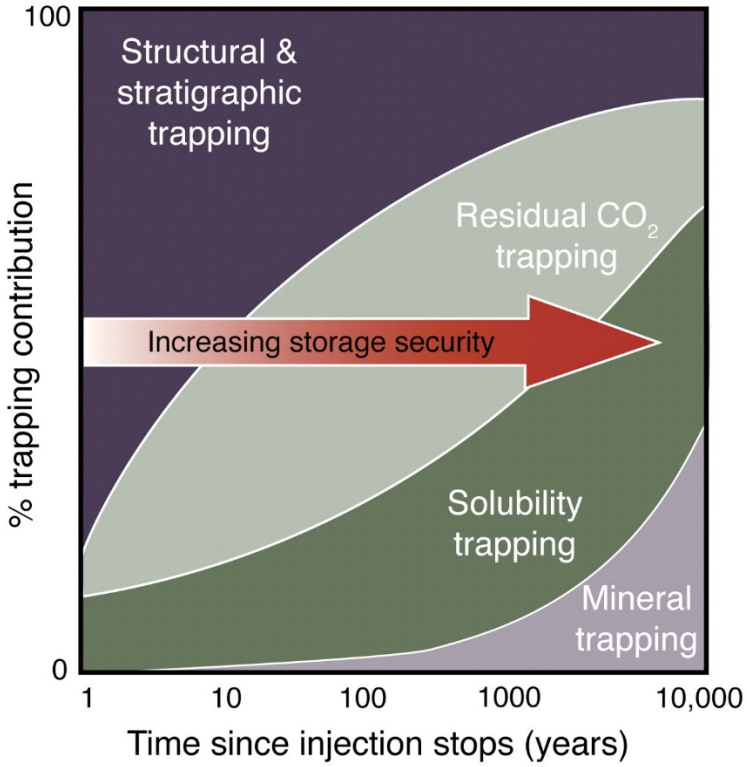

Fig. 2-4 Trapping mechanism efficiency over timescale (after IPCC, 2005)

2.4.4 Mineral trapping

Mineral trapping is the permanent trapping mechanism by which means the geochemical interactions between injected CO_2, formation fluids, and rock matrix result in the precipitation of secondary carbonate minerals (Gunter et al., 1993). This process is attractive as it can immobilize CO_2 for a long period of time (Pearce et al., 2015). CO_2 dissolved in reservoir brine results in the formation of weak acid, which can chemically react with the carbonate or silicate minerals to form insoluble bicarbonate ions. The following reactions describe the mineral trapping process (Bachu et al., 1994, Xu et al., 2001):

First, the injected CO_2 dissolves in formation brine forming carbonic acid as depicted by the following chemical reaction:

$$CO_2 + H_2O = H_2CO_3$$

Next, the carbonic acid undergoes a rapid dissociation to form the biocarboante ions as follows:

$$H_2CO_3 = H^+ + HCO_3^-$$

Then the increased acidity promotes dissolution of the primary minerals in the host rock, which results in a bicarbonate complex as follows:

$$Ca^{2+} + HCO_3^- = CaHCO_3^-$$

Finally, the dissolved bicarbonates react with the divalent mineral cations to result in carbonate precipitation e.g. formation of calcium carbonate as follows:

$$HCO_3^- + Ca^{2+} = CaCO_3 + H^+$$

The continued reaction of the bicarbonate ions with calcium, magnesium and iron from silicate minerals (such as clays, micas, chlorites and feldspars present in the rock matrix) leads to the formation of carbonate minerals (Gunter et al., 1997). Mineral trapping or precipitation is attractive in the context of carbon geo-storage as it can lead to long-term immobilization of CO_2, but due to the relevant reaction kinetics the process is often slow and the overall impact may require more than a thousand years (Fig. 2-4).

2.4.5 Adsorption trapping

The four trapping mechanisms discussed in the preceding sections apply to CO_2 storage in conventional oil and gas reservoirs i.e. carbonates and sandstones. In coal seams, however, the dominant CO_2 storage mechanism is the adsorption trapping (Golding et al., 2011; Gray, 1987; White et al., 2005). Typically, adsorption capacity of CO_2 is up to 9 times higher than that of methane (Busch et al., 2004; Clarkson and Bustin, 2000), implying that CO_2 injection in coalbeds leads to dual benefits i.e. CO_2 storage and enhanced methane recovery. Adsorption capacity is a function of pressure

(Bae and Bhatia; 2006; Busch et al., 2003; Krooss et al., 2002), temperature (Bustin and Clarkson, 1998; Perera et al., 2011), and coal rank (Clarkson and Bustin, 2000; Mastalerz et al., 2004; Siemons and Busch, 2007). The high adsorption capacity of CO_2 in coals is encouraging for CO_2 storage potential, however, the associated permeability reduction due to swelling limits the injectivity (Hol and Spiers, 2012; Reucroft and Sethuraman, 1987).

Likewise, coal seams, organic-rich shales can also store CO_2 by adsorption trapping (Busch et al., 2008; Li and Elsworth, 2015). This is currently a developing area of research (Eshkalak et al., 2014; Ferno et al., 2015), and organic-rich shale may practically evolve as a storage medium, however very low injection rate due to extremely low permeability is a pertinent limitation. Section 2.6.4 will demonstrate how CO_2-wettabiltiy of coals and organic-rich shales influences the adsorption trapping potential.

2.5 Wettability of rock/CO_2/brine systems

Wettability is the fundamental physicochemical parameter that controls the overall dynamics of multiphase flow in porous media. It is an intrinsic surface property by which one fluid preferentially remains in contact with the rock grain or matrix framework in the presence of another fluid. From the reservoir characterization perspective for multiphase fluid systems, rock wettability governs the preferential flow of one fluid within the pore space over the other, distribution of fluids in the formation, and residual saturation of fluid (Chaudhary et al., 2013; Morrow, 1990, Pentland et al., 2011). Moreover, wettability governs the capillary pressure and relative permeability curves (Jackson et al., 2005; McCaffery and Bennion, 1974, Morrow, 1990). In a microscopic sense, the ‘wetting phase’ wets the most inner pore space and occupies smallest pores, whereas the ‘non-wetting phase’ surrounds the outer pore spaces, and thus remains in the larger pores (Donaldson and Tiab, 2004).

In the context of wettability measurement methods, typically, the laboratory measurement of contact angle is regarded as the most preferable technique to assess the wettability of rock/fluid systems (Anderson, 1986; Chiquet et al., 2007; Lander et al., 1993). The next section describes the theory of contact angle measurement, and

afterwards the discussion focuses on the implications of wettability of rock/CO_2/brine for CO_2 storage.

2.5.1 Wettability characterization by contact angle measurement

The contact angle measurement is the best quantitative method to characterize wettability especially when pure fluids and proxy mineral samples are used (Giraldo et al., 2013; Mittal, 2006; Shojai Kaveh et al., 2012; 2014). This is because it facilitates sensitivity analysis of effects from pressure, temperature, brine salinity and surface roughness on wettability. Many methods of contact angle measurement have been developed, but the most widely used in the petroleum industry are captive bubble method and sessile drop method (Anderson, 1986). The sessile drop method with a tilting plate configuration (as used in this study) allows the simultaneous measurement of advancing and receding contact angles, and is regarded as the most suitable method of wettability characterization (Lander et al., 1993). There are other quantitative methods for wettability measurement, which include Amott (Amott, 1959) and USBM (Donaldson et al., 1969), while the wettability of rock/fluid systems can be predicted qualitatively by the interpretation of relative permeability and capillary pressure curves (Bryant and Blunt, 2004; Parker et al., 1987).

Theoretically, three immiscible phases (minerals, CO_2, and brine) interact with each other following CO_2 injection into the subsurface reservoir. Consequently, there are three distinct interfaces where three different interfacial force fields act on the water droplet (Fig. 2-5). These forces are solid/CO_2 interfacial tension (γ_{sc}), solid/water interfacial tension (γ_{sw}), and CO_2/brine interfacial tension (γ_{cw}). In a rock/CO_2/brine system, solid represents the carbonate or sandstones or their proxy minerals i.e. calcite and quartz respectively. The force balance of the three interfacial tensions then determines the macroscopic contact angle by Young's equation as shown below:

$$cos\theta = \frac{\gamma_{sc} - \gamma_{sw}}{\gamma_{cw}} \qquad Eq.2.1$$

Practically, the contact angle is measured through the denser phase (i.e. water). For a given set of operating conditions, the measured values of the contact angles govern the wettability and Table 2-3 lists the typical wettability state depicted by contact angle (θ) in a rock/CO_2/brine system. The system is strongly water-wet for θ less than 50°,

weakly water-wet for θ between 50-70°, intermediate-wet for the θ range 70-110°. The system turn weakly CO_2-wet for the θ range 110-130°, and strongly CO_2-wet for the θ range 130-180°. In practical rock/CO_2/brine wettability measurements, indeed, all kinds of wettability states have been reported in the literature (Iglauer et al., 2015a).

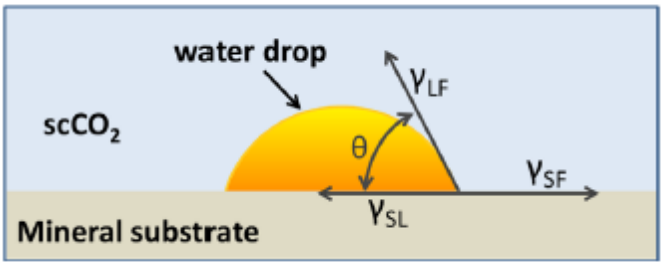

Fig. 2-5 Force field acting on a three phase mineral/CO_2/brine system (after Iglauer et al., 2015a)

Table 2-3 Wettability criteria based on contact angle of rock/CO_2/brine systems (modified after Iglauer et al., 2015a)

Wettability state	Water contact angle θ (°)
Complete wetting	0
Strongly water-wet	0 – 50
Weakly water-wet	50 – 70
Intermediate-wet	70 – 110
Weakly CO_2-wet	110 – 130
Strongly CO_2-wet	130 – 180
Complete non-wetting of water	180

2.5.2 Advancing and receding contact angles

As described in previous section, the sessile drop titled plate technique allows measurement of two distinct contact angles namely the advancing and receding contact angles. This work preferred the use of such method to measure advancing and receding contact angle over the equilibrium contact angle. This is primarily due to the pertinent relevance of water receding contact angle to structural trapping capacity, and the relevance of water advancing contact angle to the residual trapping capacity.

Chapter 3 and 4 describe the high-pressure high-temperature goniometric setup in detail. The discussion here mainly focuses on the illustration of these contact angles in the context of geological CO_2 storage.

During contact angle measurement using sessile drop titled plate, a water droplet on the surface forms two angles. Fig. 2-6 demonstrates the schematic of water advancing and receding angles. At the leading edge of the droplet, just before the droplet starts to move, the angle between rock and CO_2/brine interface is termed as water advancing contact angle (θ_a) or equivalently as CO_2-receding angle or imbibition contact angle. At the trailing edge of the droplet where CO_2 is displacing the brine phase, the angle formed at the interface is the water receding contact angle (θ_r) or CO_2 advancing angle or drainage contact angle. Water receding contact angle is relevant to the structural trapping capacity, and seen in Eq. 1.1. On the other hand, water advancing contact angle is relevant to capillary trapping mechanism, which occurs due to the imbibition of water leading to disconnection of non-wetting phase clusters (Broseta et al., 2012) i.e. when water is advancing phase and CO_2 is the receding phase. Usually advancing contact angle is higher in magnitude than its corresponding receding contact angle, the difference arises due to contact angle hysteresis, and the next section illustrates this mechanism.

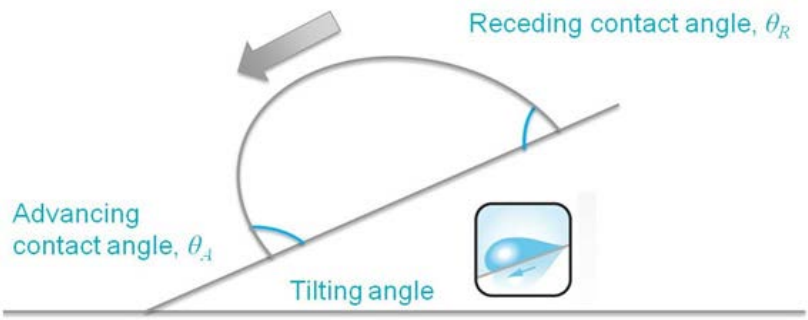

Fig. 2-6 Schematic of advancing and receding contacting angles using a tilting plate technique (after Attention theory note 1).

2.5.3 Contact angle hysteresis

The thermodynamic contact angle (θ) in Young's equation (Eq. 2.1) refers to the angle formed between a fluid on an 'ideal' or 'chemically homogenous' surface. Practically,

there exists a spectrum of contact angles (advancing and receding angles). The difference between the advancing contact angle (θ_a) and receding contact angle (θ_r) is termed as contact angle hysteresis. Typically, the hysteresis ranges from 5-20, but it can also be higher (Johnson and Dettre, 1964). From the perspective of physicochemical properties of surfaces, the factors responsible for the hysteresis phenomenon include surface roughness (Eick et al., 1975; Shuttleworth and Bailey, 1948), chemical or structural heterogeneity (Brandon and Marmur, 1996; Drelich et al., 1994, Neumann and Good, 1972), and adsorption/desorption of liquid molecules (Carre et al., 1996; Extrand, 1998).

2.5.4 Equilibrium contact angle

The equilibrium contact angle (θ) in Young's equation refers to the stable contact angle achieved after the dissipation of mass transfer effects. Mathematically, Tadmor's correlation relates the advancing and receding contact angles to their equivalent equilibrium contact angle (Tadmor, 2004), and such conversions are utilized in Chapter 7.

2.6 Influence of CO_2-wettability on trapping potential

So far, this chapter summarized the fundamental terminologies and concepts relevant to the wettability and CO_2 storage. The discussion will now shift to the significance of wettability in the context of CO_2 storage. Wettability behaviour of a rock/fluid/system strongly influences all the trapping mechanisms directly or indirectly. The sections below describe the impact of wettability on CO_2 storage potential.

2.6.1 Influence of wettability on structural trapping

Structural trapping refers to the immobilization of a rising CO_2 plume, by an overlaying caprock. The CO_2-plume migrates up-structure due to an imbalance between capillary and buoyancy forces. Once the CO_2 plume encounters the seal layer, whether or not this plume remains underneath the caprock depends on the capillary sealing efficiency of the caprock (Iglauer et al., 2015a). In addition, it also depends on the time required for leakage, which can be slow in comparison to the rate of

accumulation (Underschultz and Strand, 2016). The caprock's sealing efficiency in turn directly relates to the wettability of caprock and CO_2/brine interfacial tension as depicted by the capillary force-buoyancy force balance (Dake, 2001). Eq. 2.2 and 2.3 govern the capillary and buoyancy forces:

$$p_c = \frac{2\gamma_{cw}\cos\theta}{R} \qquad Eq.2.2$$

$$p_b = \Delta\rho g h \qquad Eq.2.3$$

Consequently, the force balance leads to an expression for storage height as was described by Eq 1.1:

$$\frac{2\gamma_{cw}\cos\theta}{R} = \Delta\rho g h$$

$$h = \frac{2\gamma_{cw}\cos\theta}{\Delta\rho g R} \qquad Eq.1.1$$

Thus, structural trapping capacity is a direct function of contact angle (i.e. wettability) and interfacial tension. Note that 'θ' in above equation is 'water receding contact angle' implying that receding contact angle is most relevant for the structural trapping capacity estimation (Broseta et al., 2012); i.e. when CO_2 is displacing the brine phase. It is quite well established that a strongly water-wet caprock i.e. $\theta < 50$, leads to better caprock sealing efficiency and a higher structural trapping potential. This is attributed to a relatively higher capillary entry pressure in water-wet caprocks. The decrease in water-wetness of the rock surface i.e. increase in θ leads to a corresponding reduction in structural trapping potential. Hypothetically, in the worst-case scenario, a CO_2-wet caprock would lead to negative storage heights due to negative capillary pressure of the caprock, and consequently CO_2 will leak through the caprock due to capillary entry pressure falling below the percolation threshold (Iglauer et al., 2015a). Such CO_2-wet situations will lead to a dramatic reduction in structural trapping potential. However, the influence of shale thickness cannot be neglected given the fact that capillary seal efficiency is a time dependent phenomena and that in thick shales the timescale of leakage could be well in excess of time required for storage (Underschultz and Strand, 2016). In summary, water-wet caprocks are desirable for higher storage potential.

2.6.2 Influence of wettability on residual trapping

Capillary trapping occurs when the capillary forces within the porous medium trap the non-wetting phase clusters. Primarily, capillary trapping takes place during the imbibition process i.e. at the trailing edge of the CO_2 plume. Capillary trapping is proportional to the product of porosity times the residual saturation. This residual CO_2 saturation is determined through laboratory measurement of relative permeability and capillary pressure curves (Krevor et al., 2012; Pini and Benson, 2013) or through pore scale models and it is a direct function of water advancing contact angle. Reservoir scale simulation and 3D micro-CT imaging reveal that water-wet rocks demonstrate better residual trapping potential, which is attributed to trapping of large residual/non-wetting phase clusters trapping by snap-off phenomenon, which occurs only in water-wet rocks (Chaudhary et al., 2013; Iglauer et al., 2013; Krevor et al., 2012; Krevor et al., 2015). In addition, it is also important to note that the water advancing contact angle is relevant to the residual trapping (Broseta et al. 2012).

2.6.3 Influence of wettability on dissolution and mineral trapping

Wettability indirectly influences the dissolution and mineral trapping. The dissolution and mineral trapping rely on the aqueous phase volumes occupied by the brine in pore space as well as pore-scale configuration of phases (Lindeberg and Wessel-Berg, 1997). Both the aforementioned parameters are dependent on the rock wettability. The pore-scale configuration directly relates to the fluid-fluid interface area, which has a direct relationship with the rate of dissolution (Iglauer, 2011; Lindeberg and Wessel-Berg, 1997). In addition, the geochemical reactions involved during mineral trapping also depend upon the fluid phase configuration in porous medium, and such configuration demonstrates the pore-scale location and amount of a particular phase, which is essential for reaction kinetics associated with mineral trapping. Establishing an accurate dependence of dissolution and mineral trapping, however, is still and active area of research (Iglauer, 2017). Note: this work does not consider the influence of wettability on dissolution and mineral trapping.

2.6.4 Influence of wettability on adsorption trapping

In coal seams, CO_2 can be stored via adsorption trapping. There is, however, only a limited evidence to establish a direct influence of CO_2-wettability on adsorption trapping in coals or likewise in organic-rich shales. Saghafi et al. (2014) demonstrated that CO_2-wettability of coals influences the storage and migration of CO_2 in micropores of the coal seam. The differential wetting of coal with CO_2 relative to water eases the CO_2 adsorption and methane desorption in coals (Saghafi et al., 2014). Moreover, influence of wettability is also evident from the fact that a water-wet coal inhibits the CO_2 injection and thus limits the diffusion and consequently the ultimate adsorption of CO_2 into the pore network of coals (Saghafi et al., 2014).

2.6.5 Assessment of trapping potential using multiphase flow observations

Earlier section (section 2.5.1) demonstrated that apart from the direct measurement of contact angle, rock wettability and CO_2 storage potential can also be assessed by multiphase flow observations such as the laboratory measurement of relative permeability and capillary pressure data. Such characteristics of the porous medium govern the movement and immobilization of the CO_2 plume (Krevor et al., 2012). For instance, Krevor et al. (2012) performed steady state CO_2/water relative permeability experiments on sandstone rocks and concluded that the residually trapped CO_2 saturations were higher in strongly water-wet systems and relatively lower in mixed-wet sandstone. Zuo et al. (2012) concluded that successive release of CO_2 from brine by pressure reduction leads to a reduction in CO_2 mobility (or relative permeability) which is favourable for CO_2 storage due to reduced migration. Pini et al. (2012) measured drainage capillary pressure curves for Berea sandstone and found that the Berea is water-wet. The relative permeability characteristics and associated residual trapping capacities are thus significantly influenced by the wettability of the CO_2/brine/rock system (Pini and Benson 2013). Li and Benson (2015) investigated the influence of rock heterogeneity on CO_2 migration in a porous medium using a pattern-free heterogeneity model and demonstrated that the small-scale heterogeneities can influence the large-scale CO_2 capillary trapping. This effect was attributed to the heterogeneities in capillary pressure-saturation relations, which give rise to the local capillary barriers that in turn lead to a significant reduction in the CO_2 frontal speed during buoyancy-driven migration (Li and Benson, 2015).

In addition, 3D micro-CT imaging is a valuable tool to characterize rock petrophysical properties such as porosity and the residual CO_2 saturation (Arns et al., 2005). For instance, Ghous et al. (2008) concluded that the traditional drainage and imbibition experiments on small cores coupled with micro-CT imaging could precisely describe the fluid distribution in the rock. Golab et al. (2013) demonstrated that 3D imaging is a unique tool to characterize the CO_2 storage potential of seal and reservoir rocks. Certain improvements in micro-CT image acquisition and analysis techniques were also proposed (Sheppard et al., 2014).

In summary, wettability measurement by contact angle is useful to observe the influence of pressure, temperature and salinity on the wetting characteristic of rock/fluid systems. However, capillary pressure and relative permeability measurements are essential to predict flow behaviour at reservoir scale.

2.7 Factors influencing wettability

There are various factors, which influence the wettability of CO_2/brine/mineral systems and the characterization of these factors is vital for understanding the wettability changes in a given rock/fluid system. Operating pressure (bottom-hole CO_2 injection pressure), reservoir temperature, brine composition (ionic strength and type of ions present in brine), surface roughness and original hydrophobicity are the major factors which influence the wettability of a given rock/CO_2/brine system (Chiquet et al., 2007; Dickson et al., 2006; Espinoza and Santamarina, 2010; Farokhpoor et al., 2013; Iglauer et al., 2015a,b). For coal seams, however, the coal rank, which can range from low-rank lignite to high-rank anthracite, also influences CO_2-wettability (Saghafi et al., 2014; Sakurovs and Lavrencic, 2011; Shojai Kaveh et al., 2012). Moreover, wettability of organic-rich shales is a function of shale-TOC (total organic carbon, Iglauer et al., 2015b). Wettability also significantly relates to the mineralogy of the rock surface. Certain experimental artefacts are also responsible for wettability alteration. For instance, Iglauer et al. (2014) established that the proper surface cleaning methods must be implemented during contact angle measurements otherwise predicted wettability maybe biased. It is important to adequately account for the aforementioned influencing factors while characterizing wettability of a given

rock/CO_2/brine system. The subsequent sections demonstrate a review of these factors and their relative impact on wettability.

2.7.1 Pressure

The CO_2 injection pressure in a storage formation relates to the storage formation depth and it is typically selected using a pore-pressure gradient of 10 MPa/km (Dake, 2001). At a pressure above 7.38 MPa and temperatures above 31.1°C, CO_2 demonstrates a supercritical phase behaviour where its properties are somewhat in between that of gaseous and liquid CO_2 (Budisa and Schulze-Makuch, 2014). During a geo-storage project, CO_2 normally exists in supercritical state in the reservoir. This is because the storage formations are often deeper than 0.738 km (note: this depth is based on pressure gradient of 10 MPa/km).

Pressure has quite a prominent effect on θ, and increase in pressure leads to increase in θ i.e. increased CO_2-wettability (Broseta et al., 2012; Chiquet et al., 2007; Farokhpoor et al., 2013; Iglauer et al., 2015a; Shojai Kaveh et al., 2012). There are studies, however, which report an insignificant change in θ with pressure (Bikkina, 2011; Espinoza and Santamarina, 2010). A few studies reported the influence of pressure on wettability of calcite and mica (e.g. Bikkina, 2011; Broseta et al., 2012). However, the reported data clearly lacks a broader range of experimental conditions. Chapters 3 to 6 cover a comprehensive review of various published data on wettability of calcite, mica, coals and shales in their 'Introduction' sections respectively.

The de-wetting of a surface with pressure i.e. increase in θ is instigated by the strong increase in CO_2-density with pressure, which in turn, leads to enhanced CO_2-mineral intermolecular interactions (Iglauer et al., 2012, 2017). Moreover, the interplay of the rock/CO_2, rock/brine and CO_2/brine interfacial tensions controls the pressure dependency of the wettability, and this work addresses this particular aspect in detail in Chapter 7.

2.7.2 Temperature

Reservoirs can be hot or cold depending on the temperature, which is typically estimated based on a geothermal gradient of 25 °C/km (Dake, 2001). There are a few studies, which report the effect of temperature on CO_2-wettabiltiy of minerals. Al-Yaseri et al., (2016a) investigated the influence of temperature on quartz wettability

and reported an increase in contact angle with increase in temperature. While most of other studies found a clear decrease in contact angle with temperature (Broseta et al., 2012; Bikkina et al., 2011; Saraji et al., 2013,2014; Wang et al., 2012; Yang et al., 2007). Moreover, Iglauer et al. (2012) performed molecular dynamics simulation to evaluate the influence of temperature on wettability of quartz, and they found a decrease in contact angle with increasing temperature, i.e. system turned more water-wet with increasing temperature. The detailed systematic influence of temperature on rock/CO_2/brine wettability is essential due to inconsistency in the so far reported temperature effect on wettability, which this study attempts to address in Chapter 3 to 6, and the factors responsible for temperature influence on wettability are addressed in Chapter 7 and 8.

2.7.3 Brine composition: salinity and salt types

Reservoir brine is composed of varying concentration of dissolved salts, and brine salinity can be typically high in storage formations e.g. saline aquifers. The brine salinity has a significant impact on wettability of rock/CO_2/brine systems; and there exists significant evidence that higher ionic strength brine leads to a corresponding increase in water contact angles i.e. the CO_2-wettability increases with brine salinity. The influence of salinity is qualitatively established in literature such that both θ_a and θ_r increase with salinity for surfaces such as quartz, calcite, mica and shales ((Al-Yaseri et al., 2016a; Arif et al., 2016a; Broseta et al., 2012; Chiquet et al., 2007; Farokhpoor et al., 2013; Iglauer et al., 2015a; Roshan et al., 2016). However, few studies found a negligible influence of salinity on wettability (Espinoza and Santamarina, 2010). Thus, there exists a discrepancy among the studies published by various groups on the influence of salinity on CO_2-wettability of minerals. Mechanistically, the alteration of wetting behaviour with salinity relates to the potential at the brine/mineral interface known as zeta potential (Mugele et al., 2016).

The type of ions comprising the formation brine also have significant effect on wettability. For instance, Al-Yaseri et al. (2016a) reported that quartz/CO_2/brine contact angles were higher for brines comprising of $MgCl_2$ than that of NaCl. The higher valence ions such as Mg^{2+}, Ca^{2+}, Al^{3+}, SO_4^{2-}) have higher charge-to-volume ratios and ionic strengths than the monovalent ions (Na^+, K^+, Cl^-), which leads to a more pronounced surface charge shielding which in turn leads to larger contact angles.

Section 2.8.2.1 covers the detail of such electrochemical changes at the brine/mineral interface and their control on rock wettability.

2.7.4 Surface roughness

In Section 2.5.3, it was discussed that surface roughness is one of the factor responsible for contact angle hysteresis. Surface roughness also influences the mean advancing and receding contact angles in the length scale of measurements. Wenzel equation (Wenzel, 1949) establishes the mathematical foundation of the roughness effect on contact angle as follows:

$$cos\theta_{app} = rcos\theta_{smooth} \qquad Eq.2.4$$

where θ_{app} is the practical contact angle, θ_{smooth} is the contact angle considering a mathematically 100% flat surface, and r is the roughness ratio (r is the measured actual surface area divided by the projected surface area; r equals unity for an ideal surface, and is always greater than unity for real surfaces). Typically, AFM (atomic force microscopy) is used to measure the RMS (root mean square) surface roughness as well as the roughness ratio (r). There are few studies that have investigated the influence of roughness on contact angle and found that contact angle decreased with the increase in surface roughness i.e. roughness prompts surface wetting. Al-Yaseri et al. (2016a) found only a minute reduction in θ (~5º) for quartz/CO_2/brine systems for surface of 560 nm RMS surface roughness versus an ultra-smooth quartz surface. However, Wang et al. (2012), reported a significantly larger difference in θ values on silica surfaces. Thus, surface effect is important to understand the surface aspects and the associated wettability changes.

2.7.5 Surface aging and hydrophobicity

The natural wettability of the storage formations varies from strongly water-wet (sandstones) to intermediate or oil-wet (i.e. carbonates). There is a common perception that caprocks too are naturally strongly water-wet i.e. hydrophilic as considered in the published data by various groups (Chiquet et al., 2007; Farokhpoor et al., 2012; Iglauer et al., 2015b; Wang et al., 2012). However, there is evidence available at the field scale

that caprocks can be intermediate-wet or even oil-wet (Broseta et al., 2012; Larter et al., 1996). Moreover, an initially water-wet seal may evolve into an oil-wet seal over time due to adsorption of a variety of compounds from crude oil, such as asphaltenes (Andersen, 1986). Literature data lacks on the influence of original hydrophobicity of caprock and storage rock on CO_2 storage potential. Such wetting behaviour, if not accounted for adequately, may lead to uncertainty in predictions.

To replicate such a wetting behaviour, surface alkylation is a standard laboratory practice that artificially tailors the wettability (Tiab and Donaldson, 2011). For this purpose, rock surfaces are aged in alkyl silane such as Dodecyltriethoxysilane, which is known for its efficient wettability alteration (Grate et al., 2012; London et al., 2013).

2.8 Physics of wettability alteration

A few previous studies reported CO_2 wettability of various rock forming minerals such as quartz, calcite, mica, and shales as well as coal seams (Broseta et al., 2012; Chiquet et al., 2007; Farokhpoor et al., 2013; Iglauer et al., 2015a; Shojai Kaveh et al., 2016; Siemens et al., 2006; Wan et al., 2014; Yang et al., 2008). However, there is no significant contribution towards understanding the physics of wettability alteration with operating conditions.

A few studies recently attempted to explain the factors accountable for wettability alteration with subsurface conditions. For instance, Al-Yaseri et al. (2016b) proposed a correlation to compute contact angles for quartz/gas/brine system from gas density as they postulated that contact angle (i.e. CO_2 wettability) is significantly controlled by the gas density. The methodology, however, was applicable to a limited range of operating conditions. Roshan et al. (2016) employed the concept of a diffuse double layer and proposed a physical model, which relates wettability to the changes in CO_2/water interfacial tensions and density. The model provides a theoretical framework to explain the wettability alteration behaviour as a function of pressure, temperature and salinity. Ameri et al. (2013) used Neumann's equation of state approach (Neumann et al., 1974) to compute sandstone/CO_2 interfacial tension, and found that the solid/CO_2 interfacial tension decreases with pressure. They concluded that the variation in the solid surface energy is responsible for pressure dependency of wettability. Nevertheless, the factors responsible for wettability variation with

pressure, temperature and salinity remain unclear and require further attention. One of the objective of this work is to evaluate the major factors controlling the physics of wettability alteration, and next section describes the theoretical basis of these factors in detail.

2.8.1 Solid surface energy concept and modelling

Theoretically, the contact angle on a solid surface is a function the three interfacial tensions, which are solid/CO_2, solid/brine and brine/CO_2 interfacial tensions described by the fundamental Young-Laplace equation (Eq. 2.1, Young, 1806). It is evident from Eq. 2.1 that the interplay of these interfacial tension controls the intrinsic wettability behaviour of given rock/fluid system. The assessment of the wettability dependence on these interfacial interactions requires quantification of the three interfacial tensions (γ_{sc}, γ_{sw} and γ_{cw}). CO_2/brine interfacial tension (γ_{cw}) data is readily available experimentally (as will be discussed below). The measurement of solid/fluid interfacial tensions is, however, an experimental constraint. An alternative is to employ empirical techniques such as Neumann's equation of state (Neumann et al., 1974). Originally, Neumann et al. (1974) applied the equation of state to compute surface energies of low energy polymers. Later, in this work, we show that Neumann equation of state is adequately applicable to mineral/CO_2/brine systems to compute mineral/CO_2 and mineral/water interfacial tensions as a function of pressure, temperature, salinity and mineral type.

2.8.2 Surface chemistry aspects

The fundamental surface chemistry of the rock/mineral is the principal factor influencing the wetting behaviour of the rock surface under investigation. Polar surfaces are generally hydrophilic i.e. more water-wet due to their natural tendency to attract water while water being highly polar (Dickson et al., 2006). Conversely, surfaces with less coverage of polar sites (or excess coverage of non-polar sites), are relatively hydrophobic i.e. CO_2-wet in nature (Dickson et al., 2006). The following two sections classify and describe the surface chemistry aspects that influence wettability.

2.8.2.1 Electrochemical Investigation

This section establishes the theoretical background of the electrochemical factors and the associated interfacial phenomena influencing wettability. The fundamental principles of surface electrochemistry reveal that a finite surface charge exists on a solid's surface when immersed in aqueous electrolyte solution due to adsorption/desorption of ions, a phenomenon referred to as cation exchange (Cavalli et al., 2016). Consequently, at the solid/fluid interface, the surface charges attract the counter ions from the solution leading to the formation of an electric double layer (EDL). The electrochemical behaviour of the interaction forces between two approaching interfaces and the resulting overlap of the electric double layers is the principal mechanism influencing wettability as well as other phenomenon associated with interfacial science such as soft matter and colloid stability (Buckley et al., 1998; Cavalli et al., 2016). In this context, zeta potential is the measure of electric potential at the diffuse edge of the electric double layer and denotes the charge at the mineral/brine interface (Erbil, 2006; Mugele et al., 2016). Experimental evidence shows that the transition of rock wettability from water-wet to CO_2-wet (or oil-wet) or converse is driven by the electrostatic charge reversal at the mineral/brine interface by adsorption of divalent cations (Erbil, 2006; Jackson et al., 2016; Lager et al., 2007). More specifically, repulsive electrostatic force generates a water-wet rock surface if the solid/water and water/oil interfaces have similar charges. Such forces arise at the mineral/brine interface, keep the disjoining pressure high, and maintains a thick water film (Erbil, 2006). For instance, Jackson et al. (2016) found that the concentration-driven adsorption of cations such as Ca^{2+} and Mg^{2+} controls the zeta potential at calcite/brine interface. Lager et al. (2007) proposed that the wettability alteration by multi-component ionic exchange between the mineral surfaces and the invading brine phase is the chief mechanism responsible for enhanced oil recovery.

The work of this thesis attempts to correlate the rock wettability to the corresponding variation of zeta potential at mineral/brine interface. In the past, only a few studies reported the zeta potential of rock forming minerals. For example, Vinogradov ad Jackson (2015) evaluated the impact of temperature on zeta potential of sandstones and found that zeta potential decreased with temperature. More recently, Al-Mahrouqi et al., (2016) experimentally measured zeta potential of calcite interfaces as a function of temperature and demonstrated that zeta potential decreases in magnitude with

temperature especially at low brine salinity. However, no study directly correlated wettability to the change in zeta potential in the context of carbon geo-sequestration and enhanced oil recovery, important for the understanding of electrochemical mechanisms occurring in the nanoscale rock/fluid interaction.

2.8.2.2 Surface functional groups

The degree of surface hydroxylation and deprotonation also significantly affects the wettability (De Gennes et al., 2013). A key mineral wettability prediction criterion is that the excess of surface hydroxyl groups imply a water-wet surface while a surface with minimal hydroxyl sites is non-wetting to water (Binks and Clint, 2002; Dickson et al., 2006). Typically, oil-wet mineral surfaces, which are CO_2-wet in a mineral/CO_2/brine environment, contain excess organic carbon (or carbon coverage) and exhibit a corresponding reduction in silanol group (SiOH) coverage (Dickson et al., 2006).

Moreover, the wetting behaviour of coals of high and medium ranks i.e. anthracite and bituminous coals and shales of high total organic carbon (TOC) relates to the surface functional groups (Curtis et al., 2012a; Hu et al., 2016; Shojai Kaveh et al., 2012). A qualitative assessment of hydrophilic vs. hydrophobic sites on sample surface reveals the functional groups responsible for a particular wetting behaviour. Advanced surface characterization tools such as Fourier transform infrared (FTIR) spectroscopy, Raman spectroscopy and X-ray photoelectron spectroscopy (XPS) can be helpful for such assessments (Chingombe et al., 2005; Hammes et al., 2008; Kundu et al., 2008; Li et al., 2006; Moreno-Castilla et al., 2000).

2.9 Interfacial tension of CO_2/brine systems

As described earlier, the storage height that can be permanently immobilized beneath the caprock, is a function of CO_2/brine interfacial tension.

CO_2/brine interfacial tension (γ) is typically measured using the same experimental setup as used for contact angle measurements by analysing the droplet shape. Principally, the method banks on the droplet shape adjustment by a static balance of gravity and surface forces (Adamson and Gast, 1997), while the liquid droplet is in

suspension from one end of the pendant cell needle and CO_2 and brine phases at the pressure, temperature and ionic strength of interest. Mathematically, the droplet shape is analysed according to the following equation to the compute CO_2/brine interfacial tension:

$$\gamma_{(CO_2-brine)} = \frac{\Delta\rho g}{\left(\beta k_{apex}\right)^2} \qquad Eq.\ 2.5$$

In Eq. 2.5 '$\Delta\rho$' is the CO_2/brine density difference, 'g' is the gravitational acceleration, 'β' is characteristic shape parameter (dimensionless), and k_{apex} is the interface curvature at the apex point of the drop. 'β' and k_{apex} relate to the associated capillary length (κ^{-1}) of the droplet where:

$$\kappa^{-1} = \sqrt{\frac{\gamma}{\Delta\rho g}} = \frac{1}{\beta k_{apex}} \qquad Eq.\ 2.6$$

2.9.1 Previous studies and influencing factors

There are studies, which report CO_2/brine interfacial tension as a function of operating pressure and temperature (Aggelopoulos et al., 2011; Hebach et al., 2002; Li et al., 2012a; Nielsen et al., 2012). However, data corresponding to higher brine salinities (upto 20 wt% brine) is missing.

Likewise, wettability, CO_2/brine interfacial tension is also influenced by factors such as pressure, temperature and salinity. There is a strong agreement found among various published studies on CO_2/brine interfacial tension about the influence of pressure, temperature and salinity (Aggelopoulos et al., 2011; Hebach et al., 2002; Li et al., 2012a; Nielsen et al., 2012). CO_2/brine interfacial tension decreases with pressure, increases with temperature, increases with ionic strength of brine and charge to surface area ratio of the ions comprising the salt (e.g. $Mg^{2+} > Ca^{2+} > Na^{+}$).

Chapter 3 CO_2 storage in carbonates: wettability of calcite*

Abstract

Limestone reservoirs are considered as potential candidates for CO_2 geo-sequestration. In order to predict structural and residual trapping capacities of CO_2 and containment security in carbonates, the wettability of the CO_2/brine/rock systems plays a vital role. Calcite is the main component in limestone and thus commonly used to characterize carbonate wettability using direct contact angle measurements. Previously, several studies determined wettability of calcite/CO_2/brine systems, but the data clearly lacks in terms of a) wettability characterization for a wide range of operating conditions, and b) published data reports contradicting results with measured wettability ranging from strongly water-wet to weakly CO_2-wet. Thus, to reduce the uncertainty in the reported measurements, we conducted an experimental study to measure advancing and receding water contact angles for calcite/CO_2/brine systems as a function of pressure (0.1 – 20 MPa), temperature (308 – 343 K) and salinity (0wt% NaCl – 20 wt% NaCl). The results indicate that calcite is strongly water-wet at ambient conditions and with the increase in pressure the surface gradually loses its water-wetness. At high-pressure storage conditions (20 MPa and 308 K), calcite surface turned weakly CO_2-wet implying that an upwards directed suction force will be created and consequently leakage may occur. Moreover, with the increase in temperature contact angle decreased implying that carbonates turn more water-wet at higher temperatures. Furthermore, contact angle increased with salinity. By comparing our results with published data, we point out that apart from pressure, temperature and salinity, the surface cleaning methods and surface roughness and nature of the sample itself can be possible sources of ambiguity in literature data. We conclude that high temperature and low salinity carbonate formations with lower injection pressures are more suitable for safe CO_2 storage.

Keywords: Contact angle; Wettability; Calcite; Structural Trapping

*Reference: Arif et al. (2017) in *International Journal of Greenhouse Gas Control*, 62, 113-121.

3.1 Introduction

Carbon capture and storage (CCS) refers to the storage of CO_2 in depleted oil/gas reservoirs and deep saline aquifers with the purpose to mitigate anthropogenic CO_2 emission (Lackner 2003; Iglauer et al., 2011a, 2013; Pentland et al., 2011). Certain trapping mechanisms render CO_2 immobile in the porous medium which are structural trapping (Arif et al., 2016a; Hesse et al., 2008, Iglauer et al. 2015a), residual trapping (Iglauer et al., 2011b; Juanes et al., 2006), mineral trapping (Gaus, 2010), dissolution trapping (Iglauer, 2011c) and adsorption trapping in coal seams (Arif et al., 2016c). Structural and residual trapping are the two most important trapping mechanisms in the first several hundred years of a storage project, and they are strongly influenced by the wettability of rock/mineral (Iglauer et al., 2015b), and CO_2/brine interfacial tension (Arif et al., 2016a). In case the storage rock is CO_2-wet, capillary forces on which these mechanisms rely are overcome by the buoyancy force resulting in an accelerated upwards directed suction force (Iglauer et al. 2015a), while residual trapping is significantly reduced, too (Al-Menhali et al., 2016; Chaudhary et al., 2013; Rahman et al. 2016). Moreover, wettability strongly influences the capillary pressure, relative permeability and fluid distribution within the reservoir (Dake, 2001; Morrow, 1990) and thus it has direct impact on enhanced oil recovery and plume migration (Krevor et al., 2015).

In this context, sandstone and carbonates are two fundamental rock candidates for CO_2 storage. For sandstones, quartz is the proxy mineral, while for carbonates, calcite is the representative mineral. Although, numerous studies confirmed that carbonates are oil-wet in water/oil systems e.g. the classical work on carbonates wettability by Treiber and Owens, (1972), and Chillingar and Yen, (1983) who analysed 151 carbonate core samples from different regions of the world (including Middle East, USA, China, Mexico Canada and India). It was found that 80% of carbonate reservoirs were oil-wet, yet it is wrong to assume that rock wettability remains unchanged when replacing hydrocarbons (oil) by CO_2 (Chiquet et al., 2007).

CO_2 wettability of calcite has been investigated previously and a summary of these studies including the associated experimental conditions and reported wettability states of calcite/CO_2/brine system are presented in Table 3-1.

Table 3-1 Review of experimental conditions and measured wettability of major studies on calcite/CO_2/water systems.

Reference	**Rock/mineral used**	**Pressure and temperature matrix**	**Pressure effect**	**Temperature effect**	**Salinity effect**	**wettability state**
Yang et al. (2007)	Weyburn limestone	up to 30 MPa at 300 K and 331 K	θ increases significantly	θ decreases	not tested	CO_2-wet
Espinoza and Santamarina, (2010)	Calcite	0-10 MPa at 296 K	θ remains constant	not tested	θ increases slightly	strongly water-wet
Bikkina, (2011)	Calcite	0-21 MPa at 298 K	θ decreases slightly	not tested	not tested	weakly water-wet
Mills et al. (2011)	Calcite	6 MPa at 295 K and 13 MPa at 313 K	θ increases slightly	not tested	not tested	strongly water-wet
Broseta et al. (2012)	Rousse caprock	0-15 MPa at 343 K	θ increases significantly	not tested	θ increases	weakly water-wet
Farokhpoor et al. (2012)	Calcite	0-30 MPa, 309 K	θ increases slightly	not tested	θ decreases	strongly water-wet
Wang et al. (2012)	Calcite	7 MPa at 303 K and 20 MPa at 323 K	θ increases slightly	not tested	θ decreases	strongly water-wet
Andrew et al. (2014)*	Ketton limestone	10 MPa, 323 K	not tested	not tested	not tested	weakly water-wet

*contact angle measured through micro-CT image analysis

Thus, the literature data on CO_2-wettability of calcite clearly lacks in terms of a) characterization of CO_2-wettability of calcite as a function of pressure, temperature and salinity for a broad range of realistic reservoir conditions, b) the data spread is high, i.e. the reported CO_2-wettability of calcite varies from strongly water-wet to weakly CO_2-wet; highest reported $\theta = 132°$; Yang et al., 2007), and c) the factors responsible for such scatter in reported calcite wettability have not been highlighted. Therefore, in this work, we measured CO_2-wettability of calcite for a broad range of operating conditions and attempt to address factors responsible for the discrepancies associated with calcite wettability which also led to a scientific debate in the CCS community (Bikkina, 2011; Bikkina, 2012; Iglauer et al., 2014; Mahadevan, 2012). To accomplish this, we measured water advancing and receding contact angles for

different pressures, temperatures and salinities (note: for CO_2 storage height estimations, only the water receding contact angles are relevant, cp. Broseta et al., 2012; Arif et al., 2016a). Our results show that the contact angle increased with pressure and decreased with temperature. The relative increase in contact angle with pressure was higher at lower temperature. Moreover, with the increase in brine salinity contact angles also increased. Thus, high pressure, low temperature and low salinity conditions are preferable for CO_2-storage. The results lead to a broad characterization and understanding of the factors responsible for wettability variation in carbonates.

3.2 Materials and Methods

3.2.1 Sample and fluids used

Pure calcite (Iceland spar, provided by Ward's Natural Science) was used in this study as it is representative of carbonate minerals (Wilson, 2012). Calcite sample have natural perfect rhombohedral cleavage in three directions not at right angles (120° and 60°; Hurlbut and Klein, 1985). The calcite sample we used was perfectly cleaved from the supplier. We did not consider the influence of cleave on contact angle in this work. Lai et al. (2015), however, reported that cleavage have significant effect on wettability of aged-calcite samples at ambient conditions (for aging time of 20 h, $\theta = 40°$ for plane 1 which was naturally cleaved calcite, and $\theta = 62°$ for plane 2 which was cleaved at an angle of 74.9° adjacent to plane 1). Acetone (99.9 mol% from Rowe Scientific) was used as cleaning agent. Deionized (DI) water (Ultrapure from David Gray; conductivity = 0.02 mS/cm) was used to prepare the NaCl (purity of salt $\geq$ 0.995 mass%, from Scharlan) brines, and CO_2 (99.9 mol%, from BOC Australia, food grade, gas code—082) was used.

3.2.2 Surface roughness

The surface roughness of the samples was measured with an AFM instrument (DS 95-20 DME NanoTechnologie GmbH). The root-mean-square (RMS) surface roughness of the sample used for testing the effects of pressure, temperature and salinity on the contact angle was 7.5 nm, which is very smooth (e.g. compare with Sarmadivaleh et al., 2015). To analyse the effect of surface roughness on contact angle, three samples

of varying surface roughness (RMS = 7.5nm, 30 nm and 140 nm, discussed in detail in Section 3.6) were tested.

3.2.3 Contact angle measurements

The contact angle measurements were conducted using a high-pressure high temperature goniometer (Arif et al., 2016a) which utilized the tilting plate method (Lander et al., 1993). The tilting plate method is considered to be the best method for contact angle measurement despite the fact that decoupling of the lateral and tangential forces on the droplet which change simultaneously for a changing angle the inclined plane (Eral and Oh, 2013), yet the reproducibility of this method is high. In addition, it allows measurement of both advancing and receding contact angles (Lander et al., 1993). The schematic of the experimental setup is shown in Fig. 3-1. A calcite sample (7.5 nm RMS surface roughness) was washed with acetone first and then cleaned with air plasma unit for 5 minutes prior to each measurement. The surface cleaning procedure is of key significance for contact angle measurements as surface contamination can generate highly biased results (Bikkina, 2012; Iglauer et al., 2014; Mahadevan, 2012).

The CO_2 and brine phases were thermodynamically equilibrated using a mixing reactor (Parr 4848 reactor, John Morris Scientific, mixing frequency = 60 hz, max. T = 350 °C, max. P = 35 MPa). The clean calcite sample was placed in the pressure cell on a metal platform (titling plate with angle of title = 15°) which was manually housed inside the pressure cell at pre-set temperatures (308 K, 323 K or 343 K. The measurements were conducted in the ascending order of temperature variation), and the reactor temperature was set equal to the cell temperature. A constant liquid volume (~ 60 ml of de-gassed brine or DI water, vacuumed for 12 h) was pumped into the reactor with a high precision syringe pump (ISCO 250D, Teledyne; pressure accuracy of 0.1% FS). Subsequently CO_2 was injected into the reactor with another high precision syringe pump (ISCO 500D, Teledyne; pressure accuracy of 0.1% FS) at prescribed pressure values (0.1 MPa, 5 MPa, 10 MPa, 15 MPa, 20 MPa). Fluids (CO_2 and water) were then mixed with an impeller in the reactor in order to eliminate/minimize dissolution effects during contact angle measurements and this equilibration lasted for ~60 min for each measurement.

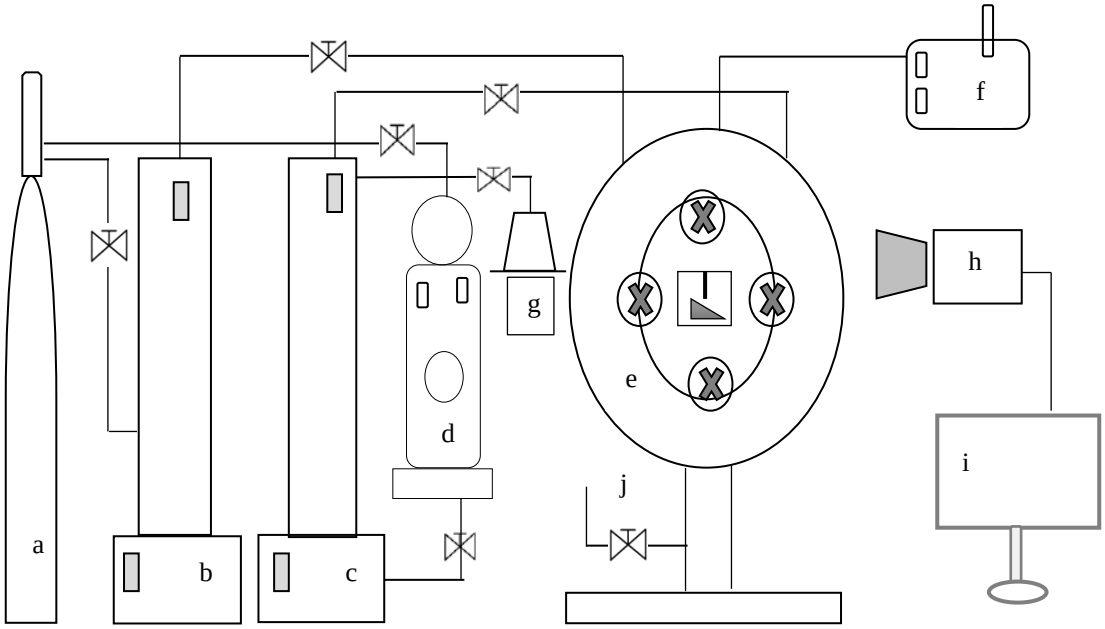

Fig. 3-1 Experimental setup for contact angle measurements used in this study. (a) CO_2 cylinder (b) high precision syringe pump-CO_2, (c) high precision syringe pump-water, (d) High pressure Parr reactor for fluid equilibration e) high pressure cell with substrate housed on a tilted plate inside, (f) heating unit, (g) liquid feed/drain system, (h) high resolution video camera, (i) image visualization and interpretation software, (j) pressure relief valve.

Subsequently CO_2 was injected into the pressure cell at the desired experimental pressure and once stabilized, a droplet of equilibrated DI-water/brine (with average volume of 6 μL ± 1 μL), was dispensed onto the tilted substrate by means of a needle. Such a tilted plate configuration is the most suitable technique to allow measurement of water advancing and receding contact angles simultaneously (Lander et al., 1993). The average droplet radius at the calcite interface was ~ (1.7 ± 0.2) mm, which is smaller than minimum capillary length of these droplets (=2.23mm; Al-Yaseri et al., 2016), and thus the influence of droplet size on contact angle is negligible (de Gennes et al., 2004). At the leading edge of the droplet, just before the droplet moved, the angle between solid surface and the water-CO_2 interface was measured as advancing contact angle (θ_a) whereas the receding contact angle (θ_r) was measured at the trailing

edge of the droplet. The entire process was recorded by a video camera (Basler scA 640–70 fm, pixel size = 7.4 μm; frame rate = 71 fps; Fujinon CCTV lens: HF35HA-1B; 1:1.6/35 mm), and contact angles were measured on images extracted from the movie files. Few of the acquired images are shown as example in Fig. 3-2a, while the advancing and receding contact angles are marked at the leading and trailing edges of an example droplet (Fig. 3-2b). The images are then visualized in the image analysis software 'ImageJ' where contact angles were measured by marking advancing and receding angles on the image using the 'angle' icon provided in the menu bar. The resulting values of angles are displayed on the analysis window.

Before every new measurement, the pressure cell was thoroughly cleaned with acetone while pump and flow lines were cleaned by circulating DI water to remove any residual contaminants. Parr reactor was cleaned after every measurement by removing the bottom cylinder out and rinsing it with acetone followed by drying for few hours. In addition, the seals were also thoroughly cleaned with acetone and DI water, and CO_2 and water were not much reactive to the seals. Sapphire glass, a transparent medium that was used to see through the cell for video recording purposes, was also washed with acetone and dried before every measurement.

The measurements were repeated thrice (each time same sample which was cleaned appropriately and a fresh batch of CO_2 and DI-water were used, while pumps and reactor were cleaned too) to ensure reproducibility of measurements and the estimated standard deviation of the measurements was ±5°. We also analysed the influence of fluid equilibration on contact angle measurements and conducted two measurements using non-equilibrated fluids and found that contact angle values were ~ 6° lower for equilibrated fluids (discussed in detail in section 3.4). Note that workflow of selected experimental matrix was such that same sample was used for all measurements, and while analysing the impact of pressure on calcite wettability, the temperature and salinity were fixed, and same was followed when effect of temperature and salinity was analysed.

20 MPa, 308 K 15 MPa, 308 K 10 MPa, 323 K

10 MPa, 343 K 5 MPa, 343 K 0.1 MPa, 343 K

(a)

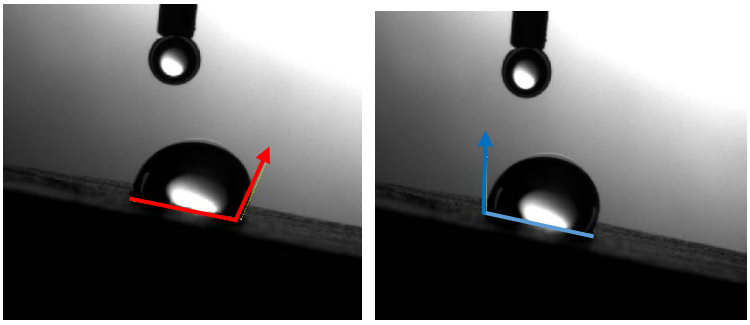

(b)

Fig. 3-2 (a) Few example images acquired for contact angle measurements. Experimental conditions for a particular experiment are given below the image. The droplet is of DI-water, the surface on which the droplet rests is calcite, while CO_2 is in the surrounding. (b) Schematic of contact angle measurements. On the left (red) is 'advancing angle', on the right (blue) is 'receding angle'.

3.3 Results and discussion

CO_2-wettability of calcite is of key significance for assessing storage potential of carbonate formations because it directly impacts structural and residual trapping capacities (Iglauer et al., 2015a) and controls the plume migration height (Iglauer et al., 2015b). It is thus important to characterize θ as a function of pressure, temperature and salinity for a wide range of conditions, as these parameters are expected to vary significantly with storage depth and formation (Tiab and Donaldson, 2011). The outcome of the study led to a broad understanding of the optimal set of conditions for efficient and safe geological CO_2 storage.

3.3.1 Effect of pressure on CO_2-wettability of calcite

The effect of pressure was tested for the pressures, 0.1 MPa, 5 MPa, 10 MPa, 15 MPa, and 20 MPa at three temperatures (308 K, 323 K, and 343 K). Both θ_a and θ_r increased with pressure throughout the experimental matrix tested (Fig. 3-3). At ambient pressure (0.1 MPa), and at all temperatures, calcite remained strongly water-wet (e.g. at 323 K and 0.1 MPa θ_a was18° and θ_r was 10°, implying that the calcite surface was strongly water-wet). The strongly water-wet nature of calcite at ambient conditions is consistent with Al-Anssari et al. (2016a). It is also consistent with other pertinent minerals such as quartz, mica and shale (e.g. reported ambient conditions contact angles were; quartz: $\theta = 0°$; Al-Yaseri et al., 2016, mica: $\theta = \sim 10°$; Arif et al., 2016b, and shale: $\theta_a = 18°$ and $\theta_r = 13°$; Roshan et al., 2016).

As pressure increased from 0.1 MPa to 5 MPa (at 323 K), θ_a increased from 25° to 52° and θ_r increased from 22° to 39° implying reduced water-wet behaviour of calcite. When pressure further increased to 10 MPa, the calcite/CO_2/water system turned intermediate-wet ($\theta_a = 85°$ and $\theta_r = 70°$). A further increase in pressure to 15 MPa at 308 K caused wettability reversal and the calcite surface showed $\theta > 90$ º, i.e. θ_a was 112° and θ_r was 102°. Further increase in pressure to 20 MPa rendered the system weakly CO_2-wet ($\theta_a = 122°$ and $\theta_r = 108°$ at 20 MPa and 308 K) implying hydrophobic nature of calcite surface at high pressure. Consequently, at these prevailing conditions (20 MPa and 308 K) in a limestone storage formation, upwards migration of CO_2 occurs due to an upwards directed suction force (in addition to the buoyancy force) leading to potential risk of CO_2 leakage through the calcite-rich caprock. This results

in reduced structural trapping capacities (Arif et al., 2016a,b; Iglauer et al., 2015a,b), and also reduced residual trapping capacities (considering calcite as a storage rock, Al-Menhali et al. 2016; Chaudhary et al. 2013; Iglauer et al., 2013; Rahman et al. 2016).

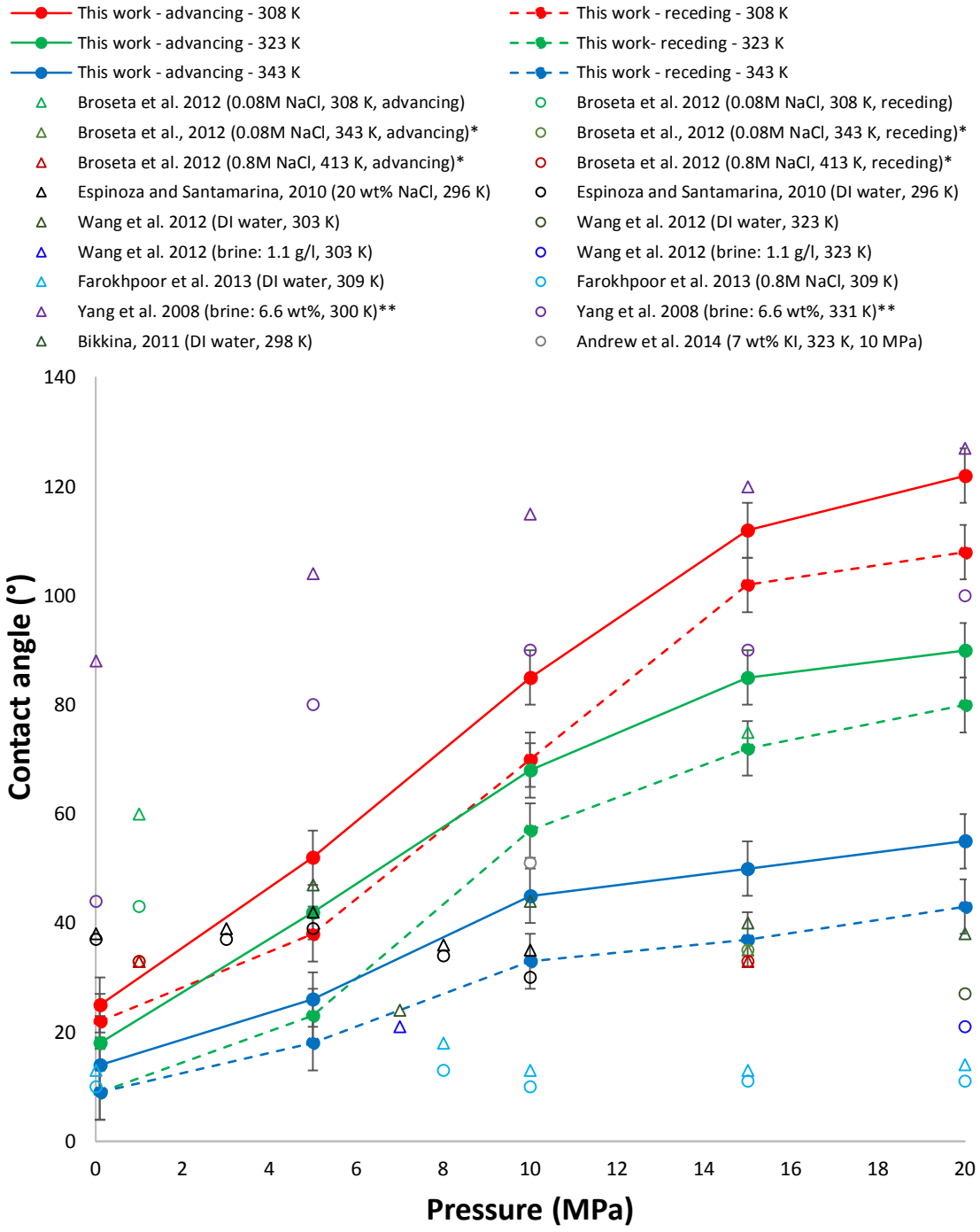

Fig. 3-3 Calcite/CO_2/DI-water contact angles measured: lines represent this work (solid: advancing, dotted: receding) at three different temperatures as a function of pressure. Open symbols represent literature measurements. *Broseta et al. (2012) analysed Rousse caprock which comprised of 70% calcite; **Yang et al. (2007) analysed limestone rock sample; Andrew et al. (2014) computed contact angles from Micro-CT image analysis.

Similar trends were observed at 323 K and 343 K, however, lower contact angles were measured due to temperature elevation (discussed in next section). The increase in contact angles with pressure was relatively smaller at higher temperatures. For instance, at 343 K, when pressure increased from 0.1 MPa to 10 MPa, θ_a increased from 13° to 44° implying a net increase of 31° which is small in comparison to the increase in contact angle for the same pressure increment at 308 K (θ_a increased from 25° to 85°; a 60° increase in θ).

Physically the contact angle (and thus wettability) of a three phase system (CO_2/brine/rock in our case), is a function of three interfacial tensions as depicted by the Young's equation below:

$$cos\theta = \frac{\gamma_{sc} - \gamma_{sw}}{\gamma_{cw}} \qquad Eq.\,3.1$$

In Eq. 3.1, γ_{sc}, γ_{sw} and γ_{cw} denote solid/CO_2, solid/water and CO_2/water interfacial tensions respectively. To assess the wettability dependence on these interfacial interactions, the quantification of the three interfacial tensions (γ_{sc}, γ_{sw} and γ_{cw}) is essential. In our previous work (Arif et al., 2016d), we used numerical techniques to quantify these interfacial tensions and evaluated their relative impact on wettability of CO_2/brine/mineral systems for various rock forming minerals. It was found that solid/CO_2 interfacial tension decreased with pressure for all minerals tested and solid/water interfacial tension was constant with pressure (Arif et al., 2016b). In addition, the CO_2/water interfacial tension decreased with pressure. Consequently, it was proved that contact angle increased with pressure due to such interplay of these three interfacial tension.

Now the question is why solid/CO_2 interfacial tension decreases with pressure? In literature, Dickson et al. (2006) reported that solid/CO_2 cohesive energy difference decreases with pressure due to increase in CO_2 cohesive energy with pressure, which is likely attributed to an increase in CO_2 density with pressure, and that in turn leads to a reduction in solid/CO_2 interfacial tension with pressure. The other factors responsible for increase in contact angle with pressure are: increase in CO_2 density with pressure and associated stronger CO_2-mineral interactions (Iglauer et al., 2012), and due to a decrease in CO_2/water interfacial tension with pressure (Shojai Kaveh et al., 2014). Indeed, the observed increase in θ is significant and calcite becomes weakly CO_2-wet at 20 MPa and 308 K. Thus, injection pressure must be carefully selected for field storage operations to avoid excessive plume migration and potentially leakage of CO_2 through the caprock (see section 4 for detail). It is also important to mention that the temperature range (308 – 343 K) selected for wettability analysis in this work is relevant to rather colder reservoirs (e.g. Deep offshore formations).

3.3.2 Effect of temperature on CO_2-wettability of calcite

Both θ_a and θ_r decreased with temperature throughout the temperature matrix tested (Fig. 3-3). At a constant pressure of 20 MPa, θ_a was 122° and θ_r was 108° for DI water at 308 K while at elevated temperature 323 K at the same pressure (20 MPa), θ_a measured 90° and θ_r measured 80° indicating that the weakly CO_2-wet state (308 K) turned intermediate-wet (323 K). When temperature was further increased to 343 K, θ_a reduced to 55° and θ_r reduced to 43°, i.e. system turned into a weakly water-wet state. Similar trends were found for other pressures. For instance, at 10 MPa and 308 K, θ_a reduced from 85° to 68° at 323K and 44° at 343 K. Thus there is a clear increase in water wettability of calcite with an increase in temperature.

The increase in water wettability with temperature is consistent with Yang et al., (2007) who found that at 20 MPa, the contact angle reduced from 127° to 100° when temperature increased from 300 K to 331 K. In addition, the decrease in CO_2/brine contact angle with temperature for calcite rich substrate (i.e. Rousse caprock) was also reported by Broseta et al. (2012) and Tonnet et al. (2010). No other study reported calcite/CO_2/water contact angles as a function of temperature. However, Bennion and Bachu (2005), tested relative permeability to CO_2 in Wabamun carbonate core samples

at different temperatures and it was found that at a constant water saturation, the CO_2 relative permeability increased with increasing temperature implying that the system shifted from weakly CO_2-wet to water-wet at higher temperatures which is thus consistent with our measurements (note: the non-wetting phase usually have higher relative permeability at most of the saturation range). The increase in water wettability with temperature is also reported by other studies on carbonate/oil/water systems (Hamouda and Rezaei Gomari, 2006; Gupta and Mohanty, 2010).

The alteration of wettability at high temperature is attributed to a) the increase in γ_{sc} (solid/CO_2 interfacial tension) with temperature due to an increase in the difference of solid/CO_2 cohesive energies with temperature [cohesive energy density of CO_2 decreases with temperature (Barton, 1991) while the cohesive energy density of the solid is expected to stay approximately constant with temperature (Kittel, 2005)], consequently, the interactions between solid and CO_2 become less favourable, which promotes water-wetting of the surface (Arif et al., 2016d), and b) due to reduction in CO_2 density with temperature (Arif et al., 2016a).

3.3.3 Comparison with literature

We compared our measurements with the major studies on calcite wettability reported in the literature (Fig. 3-3). On average, our results fall approximately into the middle of the data scatter of all studies (Fig. 3-3). Literature data spread is high and it can be distinguished into three groups: a) high θ groups, b) medium θ groups, and c) low θ groups. Broseta et al. (2012) and Yang et al. (2007) fall into the 'high θ' category, i.e. a weakly-CO_2 to strongly CO_2-wet system. Bikkina (2011), Espinoza and Santamarina (2010) and Andrew et al. (2014) groups fall into the 'medium θ group', their maximum reported wettability state was 'weakly water-wet'. However, Farokhpoor et al. (2013) and Wang et al. (2012)'s group fall into the 'low θ group' who reported essentially a strongly water-wet calcite surface even at high pressures.

In comparison with literature, our results lie somewhere in between high and medium θ groups. Our reported values are consistent with Yang et al., (2007) who measured contact angles on Weyburn limestone (limestones typically contain up to 97% calcite e.g. Indiana limestone) and found that at 300 K, the equilibrium contact angle was

122° at 15 MPa and 128° at 20 MPa which is in good agreement with our results. Our results are also consistent with Broseta et al. (2012) who measured water contact angle on Rousse caprock (70% calcite) and found that contact angle increased with pressure and θ_a measured 60° at 10 MPa and 343 K (we measured 44° at same conditions). The results are also somewhat consistent with Bikkina (2011) and Espinoza and Santamarina (2010) at low pressure and low temperatures only. But they found that θ decreased with pressure, we however found a clear increase in θ with pressure. The results show significant deviations from the reported data of Farokhpoor et al. (2013), and Wang et al. (2012) who reported very low values of water contact angles i.e. they reported calcite was strongly water-wet even at high pressure.

The possible factors responsible for discrepancy of these measurements could be the surface roughness, different types of calcite samples, and different surface cleaning methods. Higher surface roughness leads to a lower value of water contact angle (Al-Yaseri et al., 2016). Moreover, stringent cleaning methods are required to avoid highly biased contact angle values (cp. Iglauer et al., 2014), which may be a reason for the low θ observed by Bikkina, 2011 (cp. also Bikkina 2012, Mahadevan, 2012). Espinoza and Santamarina (2010) and Farokhpoor et al. (2013) reported that contact angle on calcite remained constant with pressure. We, however, found a clear increase in contact angle with pressure for calcite. Note, such an increase in contact angle is reported for various other minerals [such as quartz (Al-Yaseri et al., 2016; Saraji et al., 2014) and mica (Arif et al., 2016a,b; Chiquet et al., 2007)] too. Such de-wetting of the rock/mineral surface with increase in pressure is also found for shale (Roshan et al., 2016; Shojai Kaveh et al., 2016), coal (Arif et al., 2016c), and oil-wet sandstone (Ameri et al., 2013). For instance, Arif et al. (2016a) reported that when pressure increased from 0.1 MPa to 20 MPa at 308 K, wettability shift occurred for mica surface from strongly water-wet to weakly CO_2-wet. Theoretically θ should also increase due to increased CO_2-mineral intermolecular interactions, see also discussion above (Iglauer et al. 2012; Roshan et al. 2016, Arif et al. 2016d). In addition, surface cleavage can also be a possible factor responsible for the differences in the reported wettability of calcite, as it is reported in the literature (Lai et al., 2015) that cleavage also influences wettability. However, further investigation is required to explore this effect.

3.3.4 Effect of salinity on CO2-wettability of calcite

The salinity had two distinct effects. For low salinities (0-5 wt% NaCl), both θ_a and θ_r remained constant, while at higher salinities (5-20 wt% NaCl), θ_a and θ_r increased slightly (Fig. 3-4). For instance, at 15 MPa and 323 K, when salinity increased from 0 wt% NaCl (DI water) to 5 wt% NaCl, θ_a remained fairly constant at ~85° and θ_r also remained constant at ~72°. However, when salinity increased from 5 wt% NaCl to 20wt % NaCl, θ_a increased from ~86° to 95° within an error of ±5°. These results imply that low salinity carbonate reservoirs may turn out relatively better for CO_2 storage than high salinity reservoirs because of the more water-wet nature of the calcite at low salinities.

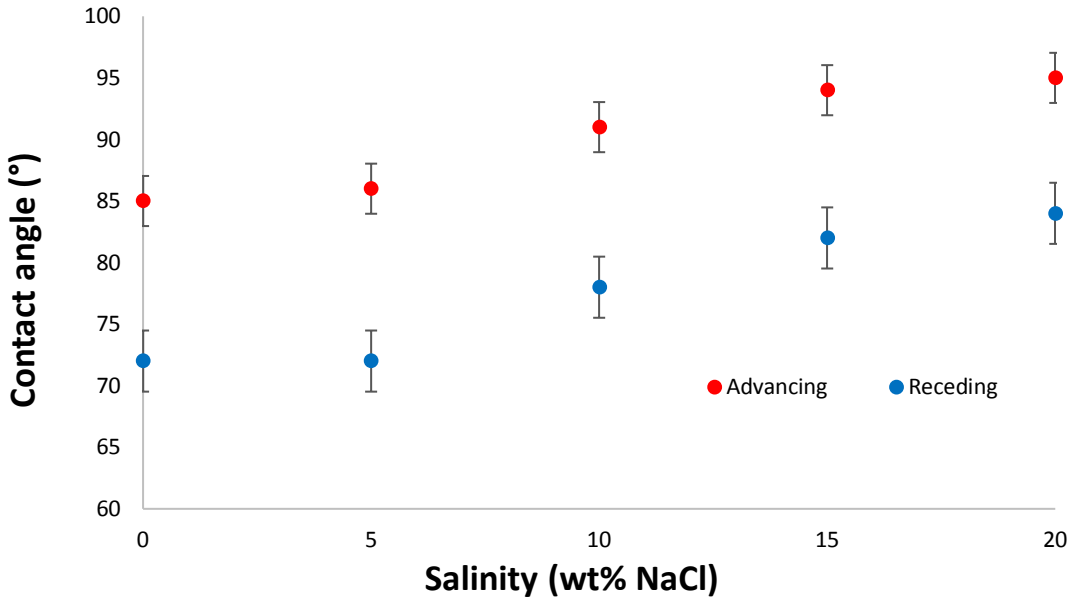

Fig. 3-4 Effect of salinity on water-CO_2-calcite contact angle at 15 MPa and 323 K.

In literature, Broseta et al. (2012) reported CO_2-brine contact angles on Rousse caprock (70% calcite, 10% quartz, illite/mica and chlorite) for low salinity brine (0.08 M NaCl) at 343 K and moderate salinity brine (0.8 M NaCl) at 413 K. The reported values were θ_a = 35° for 0.08 M NaCl brine, and θ_a = 33° for 0.8 M NaCl brine (at 5 MPa to ~15 MPa). The decrease in contact angle (from 35° to 33°) is likely due to the increase in temperature for measurements at higher salinity (0.8 M NaCl). However, θ_r was reported as constant with salinity (i.e. Broseta et al., 2012 didn't observe any hysteresis effect), which is inconsistent with our findings which may again be

attributed to change in temperature while analysing the effect of salinity. Farokhpoor et al. (2013) and Wang et al. (2012) found that contact angles decreased slightly with salinity. We point out that the differences in contact angle variation with salinity could be due to the value of salinity tested, differences in ion types or surface roughness, and the difference in mineral composition of the sample analysed. Results are also consistent with Al-Anssari, (2016), who found calcite/air/brine contact angles also increased with salinity.

For other minerals/rocks e.g. quartz, mica, coals and shales various studies reported an increase in contact angle with salinity (Arif et al., 2016a, c; Shojai Kaveh et al., 2016). The increase in contact angle with salinity is attributed to an increase in zeta potential with salinity (Arif et al., 2017a,b). As the concentration of salt increases in the solution, there are more counter ions available to neutralize the charge resulting in an increase in zeta potential with salinity which thus yields relatively less water-wet surfaces (= higher θ).

3.3.5 Effect of CO_2/brine equilibration on wettability

In this work, all experiments were conducted with thermodynamically equilibrated CO_2/brine phases, however several studies on quartz and mica demonstrated that θ is not significantly altered by equilibration during the first 60 seconds (Sarmadivaleh et al., 2015, Al-Yaseri et al. 2016; Arif et al., 2016a). Moreover, non-equilibrated fluids are most relevant at the leading edge of the CO_2 plume, i.e. when CO_2 first encounters under-saturated brine (Pentland et al. 2011). Furthermore, Shojai Kaveh et al. (2014) reported that non-equilibrated fluids can work well if contact angles are measured by releasing a droplet of brine into a CO_2 environment (as the diffusion coefficient of water in CO_2 is relatively small). However, if the contact angles are measured by using CO_2 bubbles surrounded by the water phase, fluid equilibration is necessary due to the higher diffusion coefficient of CO_2 in water.

When CO_2 is injected into a brine-saturated carbonate, carbonic acid is formed and the rock will start to dissolve; this may affect the contact angle due to mass transfer, changes in surface roughness, and changes in pH and associated possible changes in surface chemistry.

We analysed the influence of such fluid equilibration on contact angles and conducted two measurements (10 MPa and 15 MPa at 323 K) using non-equilibrated fluids and measured $\theta_a = 63°$, while $\theta_a = 68°$ for equilibrated fluids was measured at 10 MPa and 323 K. Similarly, at 15 MPa and 323 K, $\theta_a = 79°$ (within the experimental error) for non-equilibrated fluids was slightly lower than for equilibrated fluids (85°). Thus we found that contact angles with non-equilibration were ~ 6° less than that of the equilibrated measurements.

3.3.6 Effect of surface roughness on wettability

Three surfaces of varying roughness (RMS = 7.5 nm, 30 nm and 140 nm) were selected to study the influence of surface roughness on wettability. AFM images (2D and 3D) of the three surfaces are shown in Fig. 3-5. The contact angle measurements were conducted at 15 MPa and 323 K in DI water. We found that both advancing and receding contact angles decreased with the increase of surface roughness. For 7.5 nm roughness surface, θ_a was 85° and θ_r was 72°. However when surface roughness increased from 7.5 nm to 140 nm θ_a decreased to 75° and θ_r decreased to 62°; implying a reduction of 10° in contact angle with a surface roughness increase of ~132 nm. The error in these measurement was found to be ±4° represented by means of error bars in Fig. 3-6.

No study reported the influence of surface roughness on the wettability of calcite. However, our results are consistent with Al-Yaseri et al. (2016) who measured contact angles for varying roughness on quartz and found that CO_2/brine/quartz contact angles decreased with the increase in surface roughness. In summary, we establish that rougher surfaces are more water-wet than smooth surfaces and that surface roughness is one of the parameters responsible for the high literature data spread on calcite's wettability (Table 3-1 and Fig. 3-3). We, however also point out that surface roughness can change due to dissolution of calcite surface.

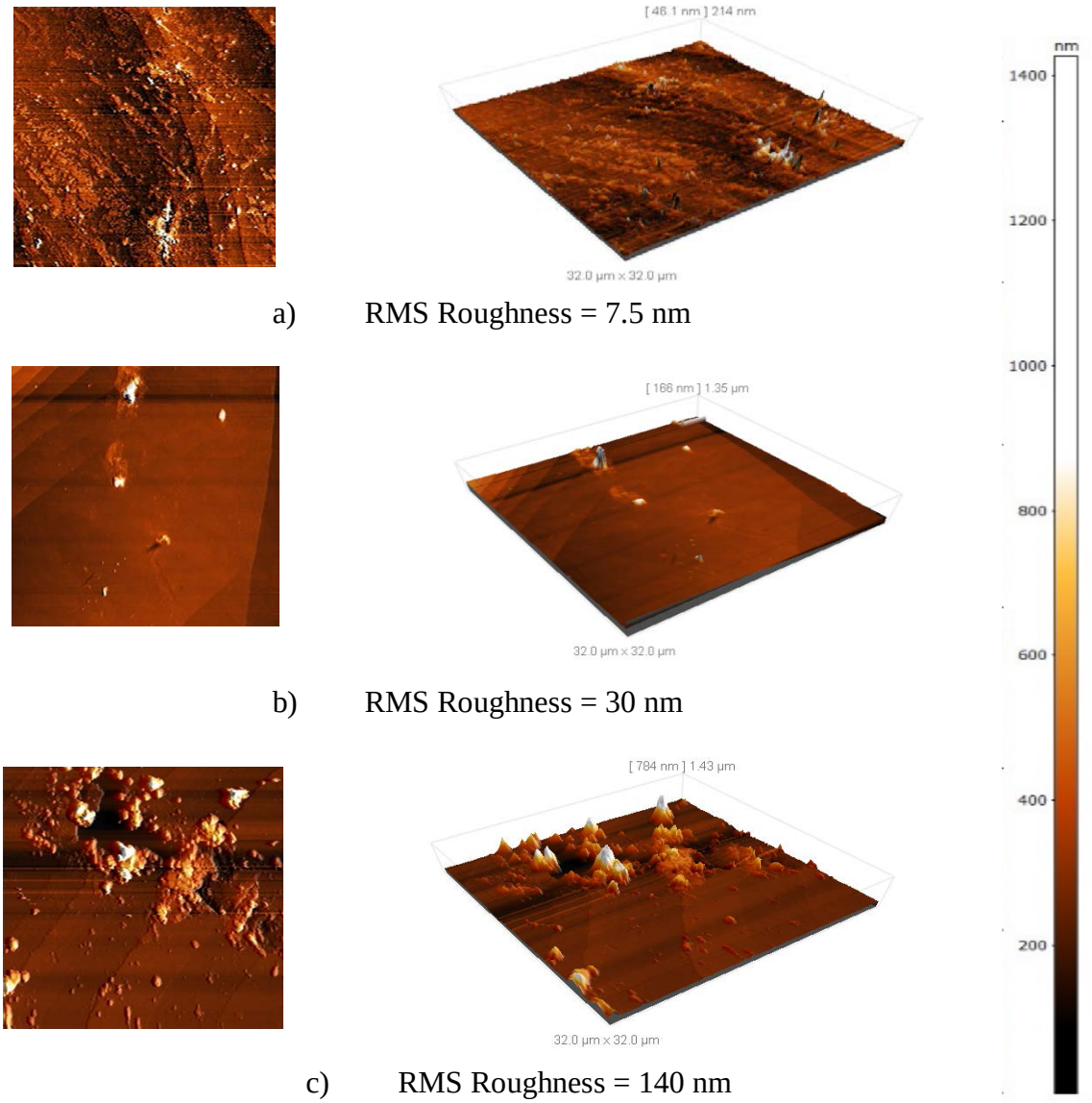

a) RMS Roughness = 7.5 nm

b) RMS Roughness = 30 nm

c) RMS Roughness = 140 nm

Fig. 3-5 AFM images of the three calcite surfaces tested: 2D deflection signal; right: 3D topography of the substrate; RMS surface roughness was a) = 7.5 nm; b) = 30 nm; c) = 140 nm.

3.4 Implications

In this work, we found that CO_2 wettability of calcite increases with pressure and salinity and decreases with temperature. Wettability characterization is essential for CO_2 storage potential assessments in carbonates. It is important to note that structural trapping is a function of caprock's wettability (Arif et al., 2016a,b; Iglauer et al., 2015a,b), and a CO_2-wet calcite-rich caprock leads to a reduction in structural trapping

capacities (Arif et al., 2016b) due to a significant reduction in capillary forces resulting in leakage through the caprock. On the other hand, the residual trapping capacity is a function of reservoir rock's wettability such that the CO_2-wet calcite-rich reservoir/storage rock (e.g. carbonate) leads to a reduction in residual trapping capacities (Al-Menhali et al., 2016; Chaudhary et al., 2013; Iglauer et al., 2013;2015a; Rahman et al. 2016) despite the larger mobile CO_2 saturation. This is due to the absence of snap-off phenomenon (a mechanism by which a large cluster of non-wetting phase is residually trapped by an advancing wetting phase) in case of CO_2-wet rocks (Krevor et al., 2015).

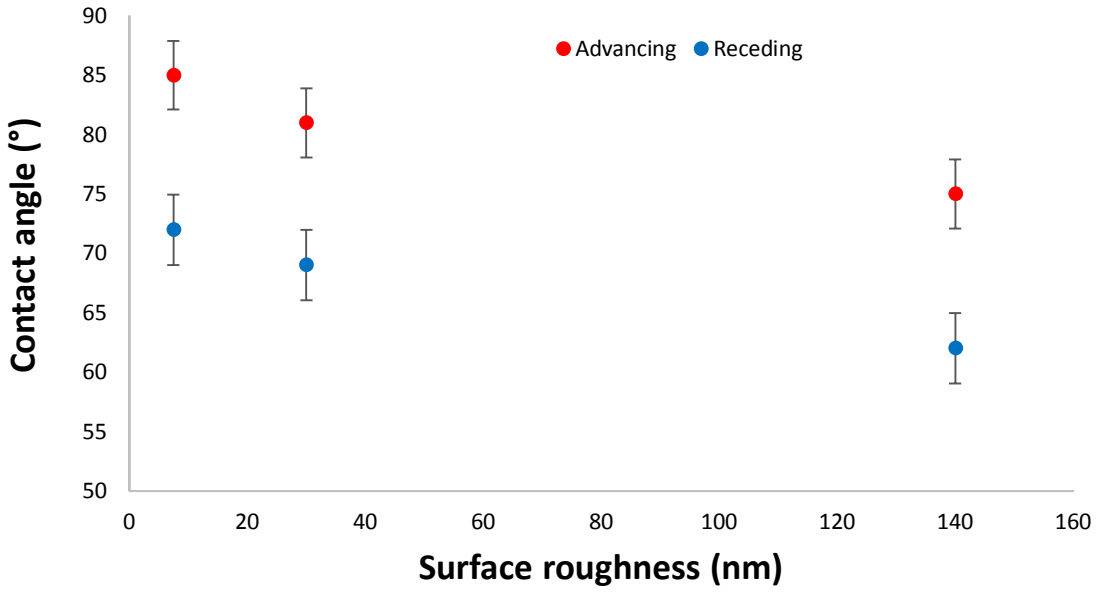

Fig. 3-6 Effect of RMS surface roughness on contact angle on calcite surface.

We, however, note that if reservoir rock is CO_2-wet, the pore volume occupied by CO_2 will be greater than in case of water-wet rock, and more lateral CO_2 spreading is expected, implying a thicker CO_2-column beneath the caprock (compared to a relatively thinner CO_2 column in water-wet rock, which would increase (the volumetric) structural storage capacity. Thus, carbonate formations must be carefully selected for CO_2 storage owing to their diverse wetting behaviour both in terms of caprock and as a storage rock at in-situ conditions. Essentially, at 20 MPa and 308 K, we found that calcite turned weakly CO_2-wet (note: water receding/drainage contact angle is considered for assessing wettability for containment security predictions;

Broseta et al., 2012). Under such conditions an upwards directed suction force is created which results in accelerated migration and capillary leakage of CO_2 causing a significant reduction in structural trapping (if calcite is considered as a caprock), and thus significantly higher CO_2 leakage risk, and reduced residual trapping (if calcite is considered as a storage rock [while volumetric structural trapping may still be high due to a thicker CO_2 column]). Therefore, operating conditions for CO_2 storage must be thoroughly investigated to undergo safe and efficient CO_2 geological storage in carbonates. Note that the temperature range (308 – 343 K) selected in this work is of interest for storage in rather colder reservoirs.

3.5 Conclusions

CO_2-wettbaility of calcite is very important for understanding the fate of injected CO_2 into the carbonates, thus, we measured advancing and receding contact angles for CO_2/water/calcite systems as a function of pressure (0.1 MPa-20 MPa), temperature (308 K-343 K) and salinity (0wt% -20wt% NaCl). It was found that both, θ_a and θ_r, increased with pressure significantly such that the system which was strongly water-wet at ambient conditions turned weakly CO_2-wet at high pressure consistent with Yang et al. (2007) and Broseta et al. (2012). We also found that θ_a and θ_r decreased with temperature implying that high temperature carbonate formations are more water-wet than low temperature formations which is consistent with Yang et al. (2007) and with other minerals such as quartz, mica and coals (Arif et al., 2016a, c). Furthermore we observed that increased salinity also caused contact angles to increase slightly; while θ decreased with increasing surface roughness consistent with Al-Yaseri et al. (2016). Our results reveals that the high data spread in the reported values of calcite wettability may be due to the difference in operating conditions (including pressure, temperature, and salinity, roughness of the substrate or surface cleaning methods). We conclude that low pressures, high temperature and low salinity conditions results in better CO_2 storage potential in carbonates due to better water-wettability of the surface. On the other hand, low temperature, high pressure and high salinity conditions should be avoided as the system then turns CO_2-wet which causes a dramatic reduction in residual trapping capacity.

Chapter 4 Impact of pressure and temperature on CO_2-brine-mica contact angles and CO_2-brine interfacial tension: Implications for carbon geo-sequestration*

Abstract

Precise characterization of wettability of CO_2-brine-rock system and CO_2-brine interfacial tension at reservoir conditions is essential as they influence capillary sealing efficiency of caprocks, which in turn, impacts the structural and residual trapping during CO_2 geo-sequestration. In this context, we have experimentally measured advancing and receding contact angles for brine-CO_2-mica system (surface roughness ~ 12nm) at different pressures (0.1 MPa, 5 MPa, 7 MPa, 10 MPa, 15 MPa, 20 MPa), temperatures (308K, 323K, and 343K), and salinities (0wt%, 5wt%, 10wt%, 20wt%). For the same experimental matrix, CO_2-brine interfacial tensions have also been measured using the pendant drop technique. The results indicate that both advancing and receding contact angles increase with pressure and salinity, but decrease with temperature. On the contrary, CO_2-brine interfacial tension decrease with pressure and increase with temperature. At 20 MPa and 308K, the advancing angle is measured to be ~110^o, indicating CO_2-wetting. The results have been compared with various published literature data and probable factors responsible for deviations have been highlighted. Finally, we demonstrate the implications of measured data by evaluating CO_2 storage heights under various operating conditions. We conclude that for a given storage depth, reservoirs with lower pressures and high temperatures can store larger volumes and thus exhibit better sealing efficiency.

Key Words: carbon geo sequestration, structural trapping, contact angle, interfacial tension, carbon dioxide, caprock, pressure, temperature, salinity

Reference: Arif et al. (2016) in *Journal of Colloid and Interface Science*, 462, 208-215

4.1 Introduction

Carbon capture and storage (CCS) in underground geological formations is considered to be a promising approach to store anthropogenic CO_2 and thus give rise to a cleaner environment (IPCC, 2005; Iglauer, 2011a; Iglauer et al., 2013; Lackner et al., 2003; Pentland et al., 2011; Sarmadivaleh et al., 2015). CO_2 is first captured at surface and then injected into depleted hydrocarbon reservoirs or deep saline aquifers where it is held trapped by means of four mechanisms which are Structural Trapping, Residual Trapping, Dissolution Trapping and Mineral Trapping (Hesse et al., 2008; Iglauer et al., 2011b,c; Juanes et al., 2006). Structural and residual trapping are the two most important storage mechanisms, and they rely on the assumption that capillary forces are of sufficient strength to hold the buoyant CO_2 back. These capillary forces are a function of CO_2-brine interfacial tension (γ), and contact angle between CO_2, brine and the rock surface (θ), equation (1) depicts the relationship:

$$p_c = p_{CO_2} - p_{water} = \frac{2\gamma cos(\theta)}{r} \qquad Eq.\,4.1$$

where p_c is the capillary pressure, 'r' is the pore throat radius corresponding to the largest pore, p_{water} is the pressure in the brine phase saturating the seal rock and p_{CO_2} is the pressure in CO_2 phase. Since during capillary leakage of CO_2, brine is displaced by CO_2, the pertinent angle 'θ' is the CO_2 advancing contact angle or equivalently the water receding contact angle (Broseta et al., 2012). Note that Eq. 4.1 assumes an ideal cylindrical capillary tube and thus only provides a first approximation as the pore geometry plays a major role, too (Iglauer et al., 2015a; Purcell, 1950). Hypothetically, CO_2-wet rock, the worst case scenario, creates an upwards directed suction force, and structural trapping is predicted to fail (Iglauer et al., 2012, 2015a; Spiteri et al., 2008), and residual trapping is significantly reduced (Iglauer et al., 2015a; Spiteri et al., 2008). We demonstrate below that this scenario can indeed occur at storage conditions (i.e. high pressure and slightly lower temperature).

In this context, we measured advancing and receding contact angles of CO_2-brine on mica (muscovite) substrates at pressures and temperatures relevant to geo-sequestration. Muscovite was selected for the analysis as it is representative of shales and has a chemical structure similar to illite, a common clay mineral (Chiquet et al., 2007; Hensen et al., 2000; McCaffery, 1972). Muscovite has the chemical formula

$KAl_2(AlSi_3O_{10})(OH)_2$ (Rickwood, 1981; Rieder et al., 1998), and it is the most common member of the mica family while other members include illite, biotite and phlogopite (Baley, 1984; Solie and Su, 1987). Moreover, muscovite is categorized as a key constituent of various rock-forming minerals present in igneous, metamorphic and sedimentary rocks, and thus muscovite wettability has an important impact on residual trapping (Iglauer et al., 2011c; Krevor et al., 2015).

For characterization of wettability of CO_2-brine-mica systems, several groups reported contact angles measurements (Broseta et al., 2012; Chiquet et al., 2007; Farokhpoor et al., 2013; Mills et al., 2011; Wan et al., 2014; Wang et al., 2012), however, data spread is high (Fig. 7-3). Furthermore the effect of temperature and salinity was not systematically tested, although it is well established that temperature and salinity can vary substantially in subsurface formations (Donaldson and Tiab, 2004). Keeping in view the implications of contact angle and interfacial tensions measurements, and the experimental complications associated with reliable contact angle measurements (Marmur, 2006) – which led to a scientific debate in the CCS community (Bikkina, 2011, 2012; Iglauer et al., 2014; Mahadevan, 2012), we measured both advancing and receding contact angles on CO_2-brine-mica systems and interfacial tensions of CO_2-brine at various pressures (0.1 MPa to 20 MPa), salinities (0wt%, 5wt%, 10wt%, 20wt% and 30wt% NaCl) and temperatures (308K, 323K and 343K) to develop better and more reliable understanding of pressure and temperature dependency of wettability. We point out that different factors such as surface roughness, chemical heterogeneity of substrate and contamination can be the possible sources of discrepancy in results reported by various groups (Butt et al., 2006; Iglauer et al., 2014). We finally provide estimates for structural CO_2 storage capacities for different storage designs with the aim to optimize and de-risk CCS projects.

4.2 Experimental Methodology

4.2.1 Contact angle measurements

The contact angle measurements were conducted with a high pressure high temperature goniometer. The schematic of the experimental setup is shown in **Error! Reference source not found.**. A muscovite sample (12 nm RMS surface roughness measured with AFM instrument DSE 95-200, Fig. 4-2) was cleaned with an air plasma

unit for at least 45 minutes before every new measurement. This cleaning procedure is of key importance as otherwise the results may be highly biased (Iglauer et al., 2014).

The clean muscovite substrate was then placed in a pressure cell at pre-set temperatures (308K, 323K or 343K), and the cell was flushed with CO_2 gas at ambient conditions for 10min. Subsequently CO_2 pressure was raised with a high precision syringe pump (ISCO 500D; pressure accuracy of 0.1% FS) to prescribed values (0.1 MPa, 5 MPa, 7 MPa, 10 MPa, 15 MPa, 20 MPa). After pressure stabilization, a droplet (with average volume of ~6μL ± 1μL) of de-gassed brine (vacuumed for more than 12 hours), was dispensed onto the tilted substrate (Lander et al., 1993) by means of a needle.

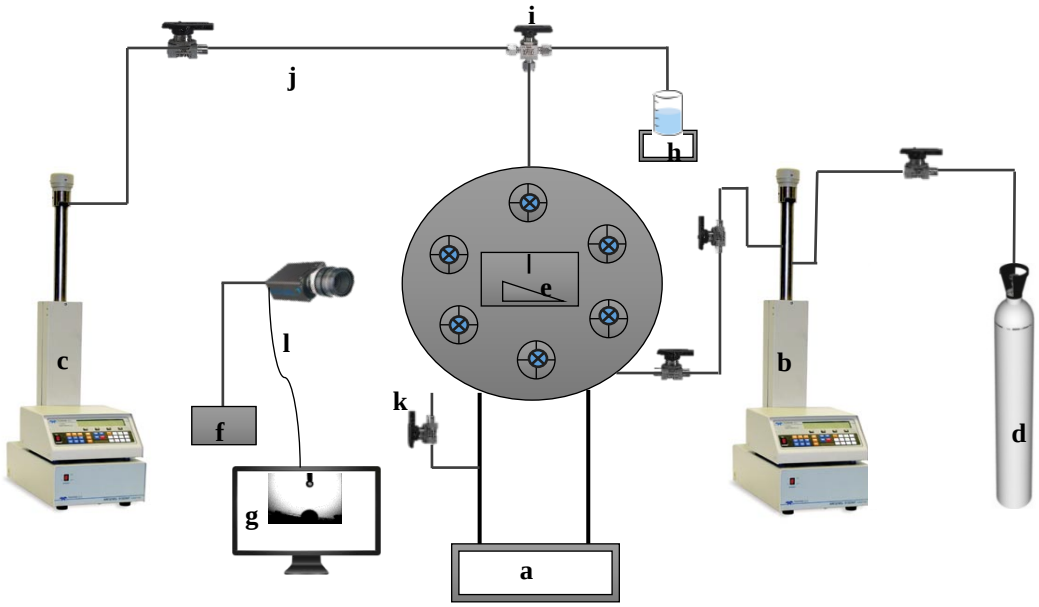

Fig. 4-1 Experimental configuration for contact angle and interfacial tension measurements used in this study; (a) high P/T cell, (b) syringe pump-CO_2, (c) syringe pump-brine, (d) CO_2 source, (e) substrate housed on a tilted plate inside the cell, (f) high resolution video camera, (g) visualization software, (h) feed/drain system, (i) three way valve, (j) flow-lines, (k) pressure relief valve, (l) data transfer module.

We note that the fluids used were not thermodynamically equilibrated, since earlier studies (Sarmadivaleh et al., 2015) demonstrated that the contact angle θ is not

significantly altered by equilibration during the first 60s, and during this time all measurements were completed. Furthermore, non-equilibrated fluids are most relevant at the leading edge of the CO_2 plume, i.e. when CO_2 first encounters undersaturated brine (Pentland et al., 2010). At the leading edge of the droplet, just before the droplet started to move, the angle between solid surface and the brine-CO_2 interface was measured as advancing contact angle (θ_a) whereas the receding contact angle (θ_r) was measured at the trailing edge of the droplet. A video camera (Basler scA 640–70 fm, pixel size = 7.4 µm; frame rate = 71 fps; Fujinon CCTV lens: HF35HA-1B; 1:1.6/35 mm) recorded the entire process, and contact angles were measured on images extracted from the movie files. The standard deviation of these measurements was ±3° based on replicate measurements.

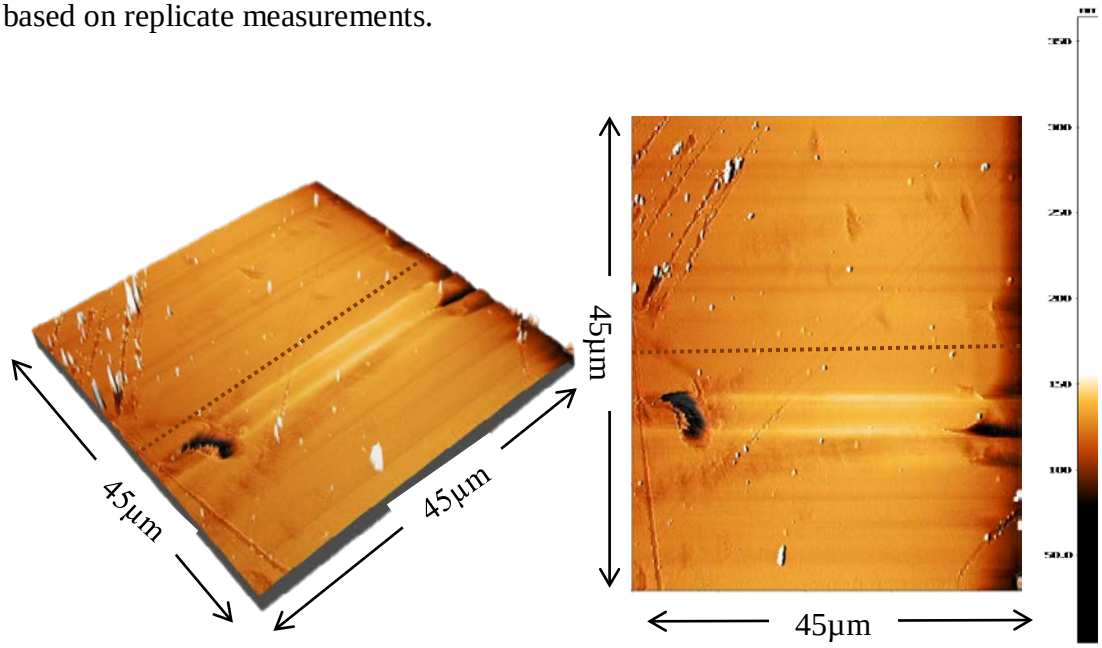

Fig. 4-2 Atomic Force Microscopy images of Muscovite surface used in the study, Left: 3D topography of the substrate; right: deflection signal (scale bar on the right represents surface heights associated with different spots on the image.

4.2.2 Interfacial tension measurements

The pendant drop technique was used to measure CO_2-brine interfacial tensions (γ) as it is convenient and flexible. In this method, a liquid droplet is allowed to hang from one end of a capillary tube (in the form of a dispensing needle) in the presence of another fluid at pressure and temperature of interest. At static conditions, the shape of

the liquid droplet is adjusted by the balance between gravity and surface forces (Adamson and Gast, 1997). This drop shape relates to the fluid-fluid interfacial tension by the Young-Laplace equation of capillarity which is:

$$\gamma_{(CO_2-brine)} = \frac{\Delta\rho g}{\left(\beta k_{apex}\right)^2} \qquad Eq.\ 4.2$$

In Eq. 4.2, $\Delta\rho$ is the density difference between CO_2 and brine, 'g' is the gravitational acceleration, 'β' is the dimensionless shape parameter, and k_{apex} denotes the interface curvature at the apex point of the drop (Georgiadis et al., 2010).

The experimental setup comprising of a high-pressure cell used for the interfacial tension measurement is the same as the one used for the contact angle measurement as shown in Fig. 4-1 The cell was again flooded with CO_2 using a high precision syringe pump at different pressures (0.1 MPa, 5 MPa, 7 MPa, 10 MPa, 15 MPa, and 20 MPa) and at different tested temperatures (308K, 323K and 343K). After pressure stabilization, a drop of brine (20 wt% NaCl) was injected at constant flow rate into the cell and was suspended at the bottom of the injection needle. A video camera connected with the experimental setup recorded the entire process. The images extracted were then analysed to determine γ (Alvarez et al., 2009; Song and Springer, 1996); the values of $\Delta\rho$ were interpolated from Li et al. (2012a) and are shown in Fig. 4-7.

4.3 Results and Discussion

CO_2-wettability of storage and seal rock is of key significance because it directly impacts the structural and residual trapping capacities (Iglauer et al., 2015a). As reservoir pressures, temperatures and salinities are expected to vary significantly between different formations and depths (Dake, 2001), it is essential to characterize 'θ' as a function of pressure and temperature.

4.3.1 Effect of pressure on contact angle

Advancing and receding water contact angles measured at different pressures are shown in **Error! Reference source not found.**. Both, θ_a and θ_r increased with the

increase of pressure for all pressures tested. At ambient conditions, both θ_a and θ_r measured ~5^o which is in agreement with literature data for ambient contact angles on quartz (Grate et al., 2012; Iglauer et al., 2014). At a temperature of 323K, θ_a increased from 0^o (complete wetting) to ~83^o (intermediate wetting) when pressure increased from 0.1 MPa to 20 MPa. At a pressure of 20 MPa and a temperature of 308K, wettability reversal occurred, as θ_a increased to ~110^o indicating a hydrophobic nature of the muscovite surface. Consequently, in a storage site where these conditions prevail, an upwards directed suction force is created, which promotes upwards migration of CO_2 (in addition to the buoyancy force). This constitutes a considerable risk as under these conditions structural trapping is predicted to fail as a first approximation (cp. Eq. 4.3 below; and Iglauer et al., 2015a).

Physically, the increase in water contact angle with pressure is related to increased intermolecular interactions between CO_2-mineral, which are enhanced by the higher CO_2 density at higher pressures (Iglauer et al., 2012). Our results are consistent with Broseta et al. (2012), who reported an increase in both receding and advancing water contact angle with pressure (θ_r increased from 40^o to 50^o and θ_a increased from 65^o to 92^o when pressure was increased from 0.5 MPa to 10 MPa at 308K for 1M NaCl), Chiquet et al.'s (2007) (θ_r measured ~60^o at 11 MPa), Farokhpoor et al. (2013) (θ increased from 16^o to 36^o as pressure increased from 1 MPa to 30 MPa), and Wan et al.'s (2014) data (θ_a increased from 35^o to 105^o when pressure increased from 6.5 MPa to 15 MPa at temperature of 318K).

Quantitatively, our results lie approximately in the average of the published data at low pressures (from 0.1 to 10 MPa), however, at high pressures (from 10 MPa to 20 MPa), significant differences exist and overall θ_a and θ_r are found to be larger in value than other published data. These differences could be caused by different surface roughness and/or salinities. Increase in surface roughness results in corresponding decrease in both θ_a and θ_r (Wang et al., 2012). Moreover, the surface cleaning methods adopted in different studies can also be potential source of ambiguities in contact angle measurements (Iglauer et al., 2014). We also note that such an increase in contact angle with pressure has been reported for quartz too (Jung and Wan, 2012; Saraji et al., 2013; Sarmadivaleh et al., 2015, Wang et al., 2012).

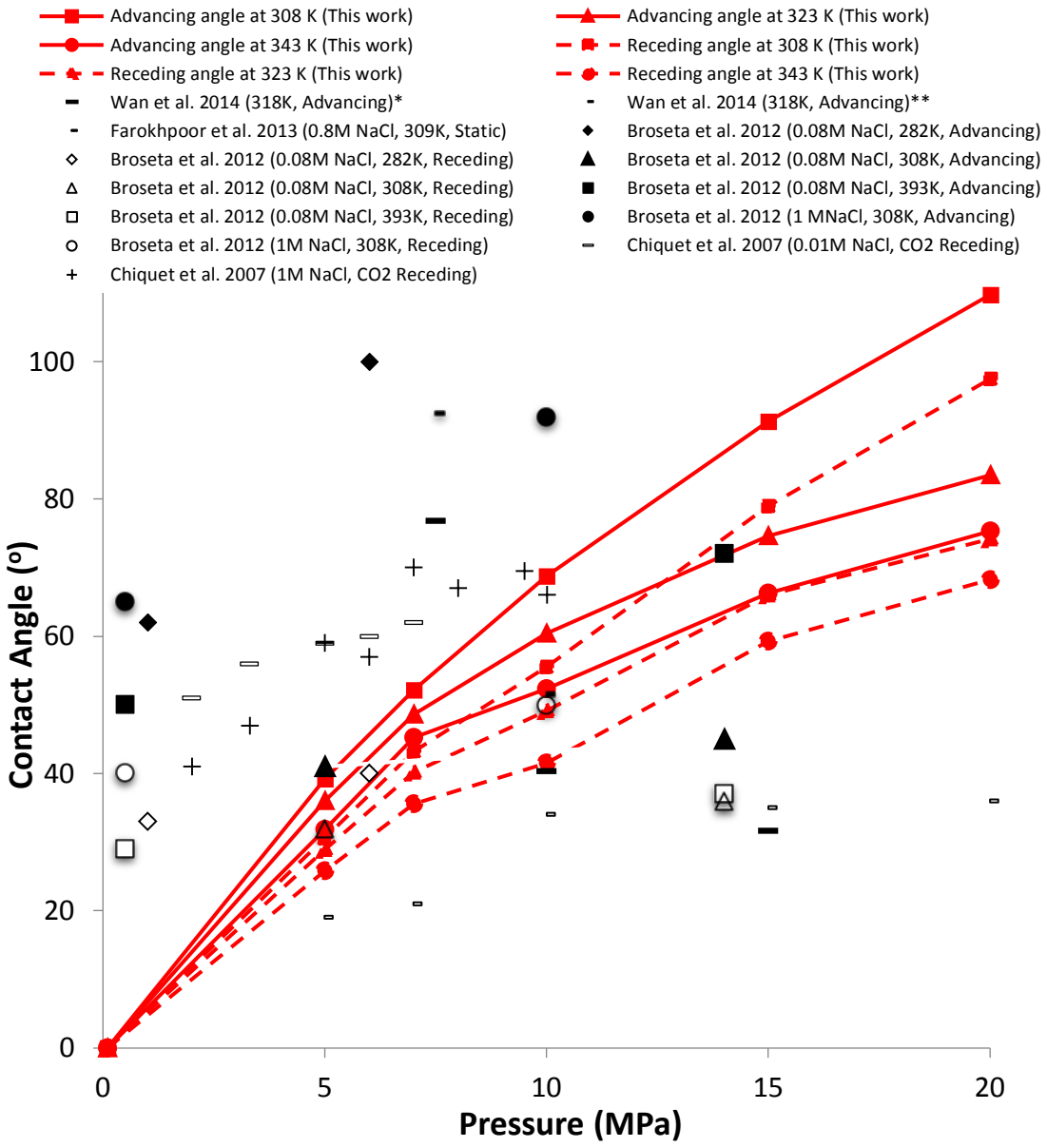

Fig. 4-3 Water contact angles on muscovite in CO_2 atmosphere at various operating conditions. Our measured values are shown in red (solid lines for advancing and dotted lines for receding angles), and literature values are shown in black (literature's receding angles are represented by open symbols while advancing angles by filled solid symbols). *Salinity: 0.1M NaCl, without adhesion, **Salinity: 0.1 M NaCl, with adhesion.

4.3.2 Effect of temperature on contact angle

Both, θ_a and θ_r decreased with temperature (Fig. 4-3). At a pressure of 15 MPa, θ_a decreased from ~91° to 75° when temperature increased from 308 K to 323 K.

Similarly, when temperature further increased to 343 K at 15 MPa, θ_a decreased to 66°. Moreover, for the lowest tested temperature 308K and highest pressure 20 MPa, wettability reversal occurred and θ_a measured to be ~110°.

The decrease in CO_2-brine-mica contact angle with temperature is consistent with Broseta et al. (2012), as they also observed a decrease in θ_a from 100° to 45° when temperature increased from 282K to 308K at a pressure of ~6 MPa for 0.08M NaCl brine. They also found that for 1M NaCl brine, θ_a and θ_r first decreased with temperature (when temperature increased from 282 K to 308 K) and then increased with temperature at 393 K; we, however, did not observe such variations throughout the selected experimental matrix.

As far as the temperature dependency of contact angle of brine-CO_2-mineral is concerned, two entirely different trends can be observed in the literature on CO_2-brine-quartz. Sarmadivaleh et al. (2015), Farokhpoor et al. (2012) and Saraji et al. (2013) observed an increase in CO_2-brine-quartz contact angle while Wang et al. (2013), Bikkina, (2012), Saraji et al. (2014) and Yang et al. (2007) measured a decrease in contact angles of CO_2-brine-quartz systems with temperature. Moreover, Iglauer et al. (2012) used molecular dynamics simulations and predicted a decrease in CO_2-brine-quartz contact angles with temperature. There are three types of interfacial tensions, which contribute to the temperature dependency of the contact angle according to the Young-Laplace equation:

$$cos\theta = \frac{\gamma_{sv} - \gamma_{sl}}{\gamma_{vl}} \qquad Eq.4.3$$

where γ_{sv} and γ_{sl} are the solid-CO_2 interfacial tension and solid-liquid interfacial tension , respectively, whereas γ_{vl} is CO_2-liquid interfacial tension. Since most of the previous studies (Chalbaud et al., 2009; Li et al., 2012; Sarmadivaleh et al., 2015) and the present work agree that CO_2-liquid interfacial tension increases with temperature, it is evident from Eq. 4.3 that the difference of solid-CO_2 interfacial tension and solid-liquid interfacial tension (numerator of equation) should increase with temperature to cause a corresponding decrease in contact angle with temperature. Consequently, we establish that hotter reservoirs exhibit relatively better water wetting state and hence better seal capacity leading to higher CO_2 storage potential than the colder reservoirs, this is further discussed below.

4.3.3 Effect of salinity on contact angle

Considering the significance of the effect of salinity on wettability of CO_2-brine-mineral systems, we measured θ_a and θ_r at two different pressures (10 MPa and 15 MPa) and two different temperatures (323K and 343K) for various brine salinities (0wt%, 5wt%, 10wt%, and 20wt% NaCl). The results are shown in Fig 4-4. At a pressure of 15 MPa and 323K, θ_a increased from 59° for 0wt% NaCl (DI water) to 74° at 20wt% NaCl brine salinity. At the same pressure and temperature, θ_r increased from 54° to 64° when salinity was increased from 0wt% to 20wt% NaCl. At higher temperature (343K), although lower values were measured for both, θ_a and θ_r, yet the trends of contact angle variations with brine salinity remained the same (θ_a measured 52° for DI water and 65° for 20wt% NaCl, and θ_r measured 48° for DI water and 51° for 20wt% NaCl). Our measurements are consistent with previous studies performed on salinity effects on mica (Broseta et al., 2012; Chiquet et al., 2007) and quartz surfaces (Bikkina, 2011; Chiquet et al., 2007; Farokhpoor et al., 2013) Similar trends are obtained for 10 MPa pressure, however, as expected, slightly lower values were obtained.

By the careful analysis of the contact angle-salinity data, we found that apart from inappropriate surface cleaning (Iglauer et al. 2014), a difference in brine salinity can also be the source of discrepancy in the published contact angle data for CO_2-brine-mica systems. The increase in contact angle with salinity can be attributed to corresponding variations in zeta potentials i.e. zeta potentials shifts from high negative values for low salinities to low negative values for high salinities (Kaya and Yukselen, 2005). Less negative zeta potentials (or higher values of zeta potential) lead to less polar surfaces and thus de-wetting of the surface (= higher water contact angles, Adamczyk et al., 2010).

4.3.4 Comparison of Mica with Quartz

In this section, we compare CO_2-brine-mica and CO_2-brine-quartz contact angles. Although numerous datasets are available in literature for CO_2-brine-quartz contact angles, we select the data from Sarmadivaleh et al. (2015), as they used same experimental setup (as shown in Fig. 4-1) and cleaning methods. Fig. 4-5 shows θ_a and θ_r for CO_2-brine systems on mica and quartz from pressure 0.1 MPa to 20 MPa and temperatures 308K, 323K and 343K for mica and 296K, 323K and 343K for quartz. Quantitatively, we find that at the same temperature and pressure (323K and

15 MPa), θ_a measured 75° for mica and 38° for quartz, which is approximately double in magnitude. Similarly, at 323K and 20 MPa, θ_a measured 83° for mica and 41° for quartz. At 323K, and at all tested pressures, θ_r also followed similar trend (double in value than that of quartz). On the contrary, at 343K, and 10 MPa, quartz and mica contact angles get relatively closer in values, θ_a measured to be 45° and 52° for quartz and mica respectively and θ_r was 26° for quartz and 40° for mica. It is important to note that θ_a and θ_r decrease with temperature for mica and increase with temperature for quartz. This different qualitative behaviour is attributed to different solid-fluid surface free energies. The results presented here are consistent with Chiquet et al. (2007).

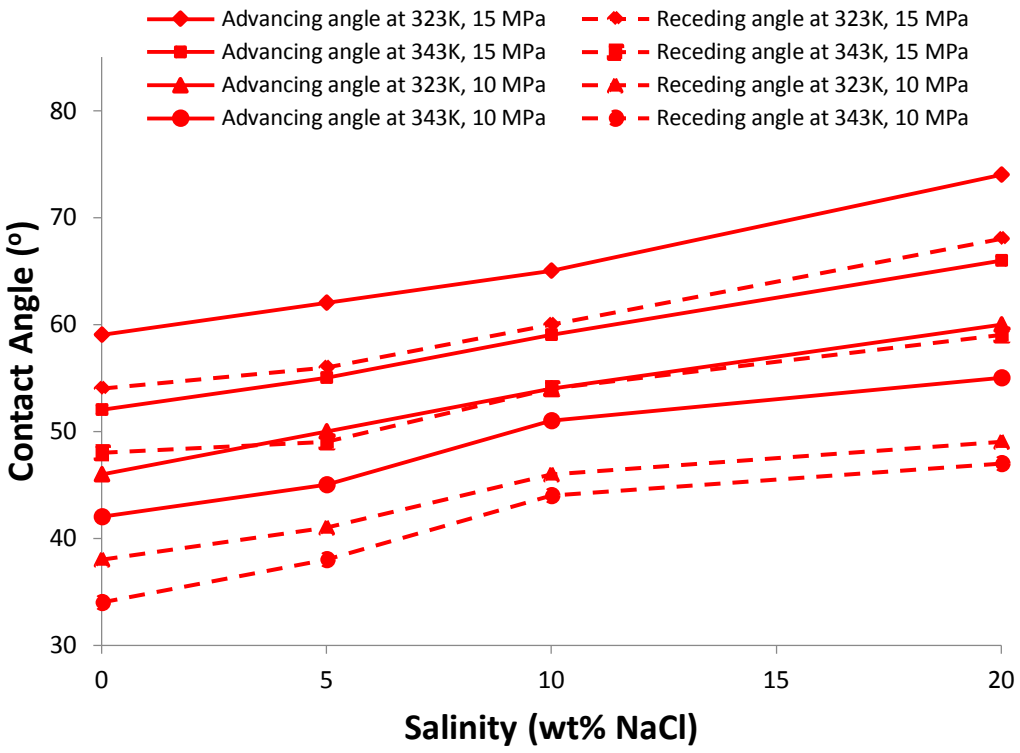

Fig. 4-4 Influence of salinity on advancing and receding contact angles (Salinity range considered from 0 wt% (DI water) to 20wt% NaCl. For all measurements, solid lines indicate advancing angles whereas dotted lines indicate receding angles.)

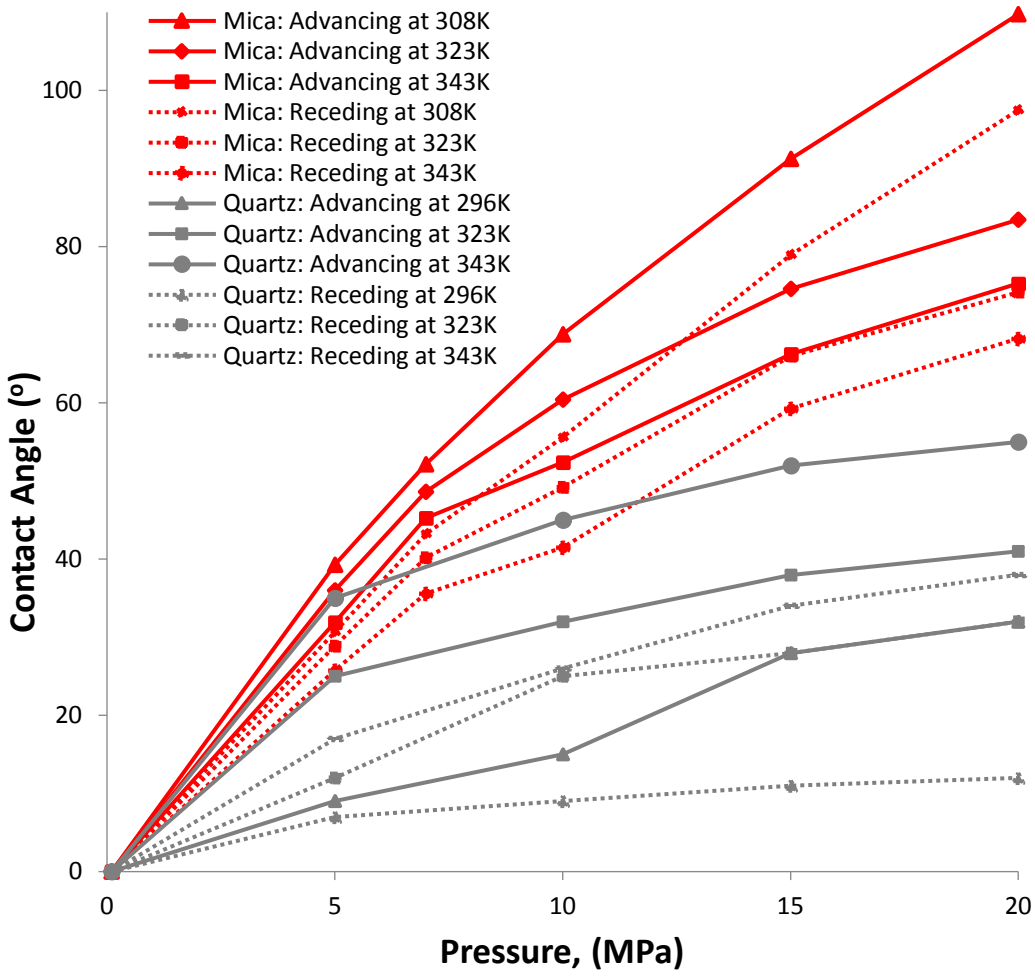

Fig. 4-5 Comparison of advancing and receding contact angles on mica and quartz surfaces. Data for quartz contact angles is taken from Sarmadivaleh et al. (2015) who used similar experimental setup.

4.3.5 Effect of pressure and temperature on interfacial tension

Many studies have reported the interfacial tension of CO_2-water systems (Sarmadivaleh et al., 2015; Akutsu et al., 2007; Hebach et al., 2002; Nielsen et al., 2012). However, data for CO_2-brine systems comprising of various salinities at relevant thermo-physical conditions are limited (Aggelopoulos et al., 2011; Bachu and Bennion, 2009; Chalbaud et al., 2009; Li et al., 2012; Lun et al., 2012; Yang et al., 2005), yet the trends of variation with pressure and temperature are reasonably consistent.

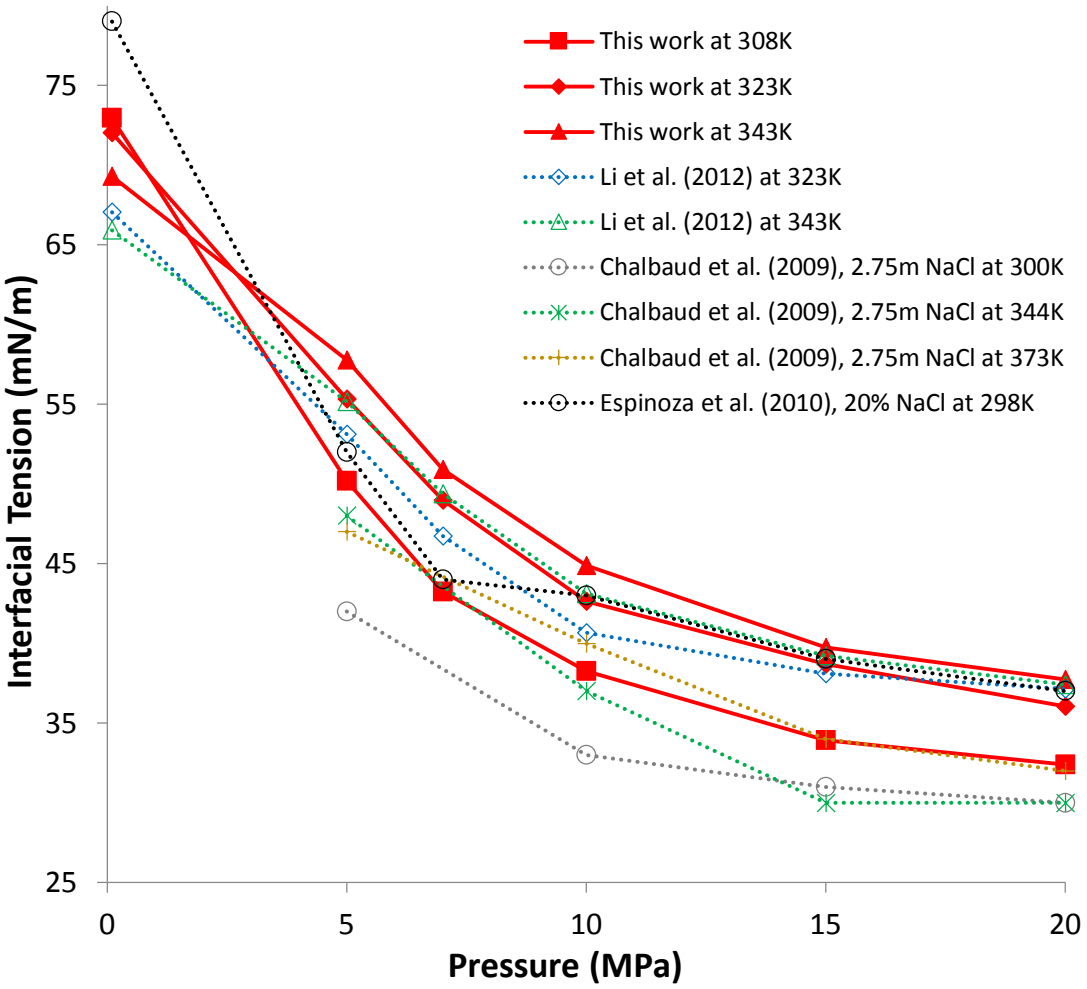

Fig. 4-6 Variation of interfacial tension with pressure and temperature (20wt% NaCl brine).

Therefore, we measured interfacial tensions between CO_2 and brine (20wt% NaCl) at different pressures and temperatures; results are plotted in Fig. 4-6; γ decreased with pressure but increased with temperature. Our measurements are consistent with Li et al. (2012), and with Espinoza and Santamarina (2010); however considerable difference exist with Chalbaud et al. (2009), which is because of the different salinities considered, Fig. 6-6. Results are also consistent with general trends reported in the literature (pressure effect: [Aggelopoulos et al., 2011; Bachu and Bennion, 2009; Li et al., 2012], temperature effect: [Li et al., 2012a; Sarmadivaleh et al 2015]). We also note that higher salinity increased γ, consistent with Chalbaud et al. (2009); however slightly different from Espinoza and Santamarina (2010) who measured slightly larger values.

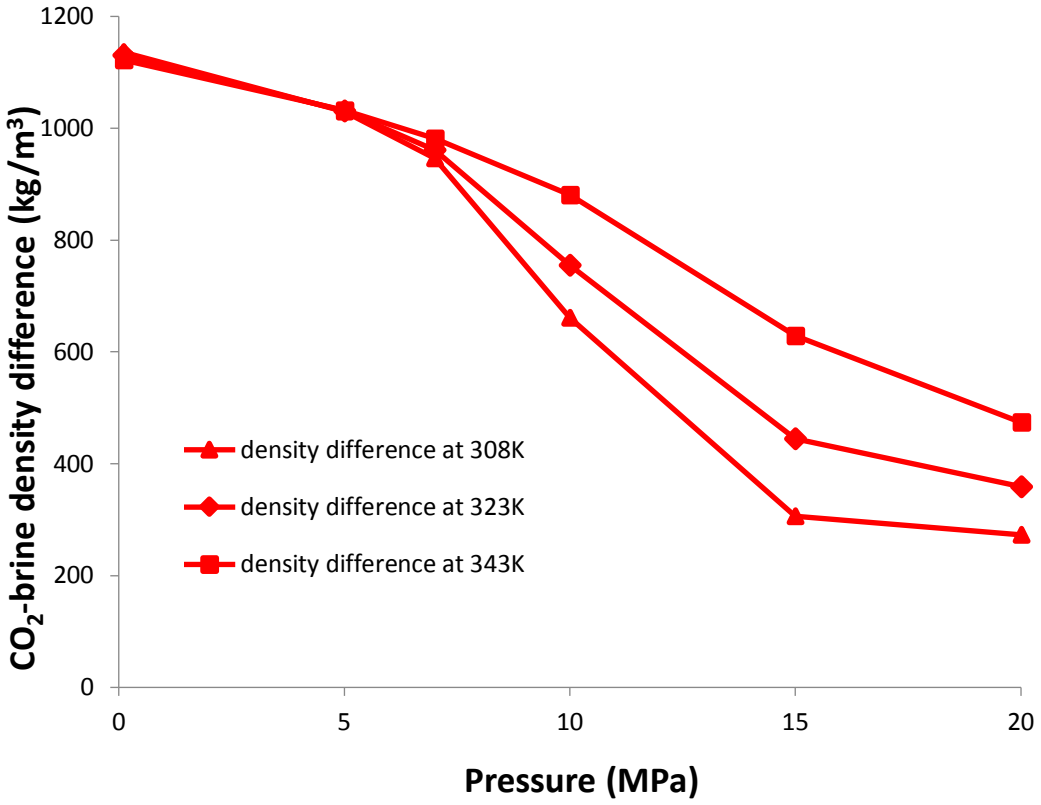

Fig. 4-7 Values of density differences used in this study (data taken from Li et al., 2012).

4.3.6 Empirical correlations for contact angles and interfacial tensions

We developed empirical correlations to describe the change in contact angle and interfacial tension with pressure and temperature for a wide range (pressures: 0.1 MPa to 20 MPa, temperatures: 308 to 343K). From simulations, we find that experimental data best fits second-degree polynomial for all the three output variables (θ_a, θ_r and γ). The relationships developed are:

$$\theta_a = a_0 + a_1P + a_2T + a_3P^2 + a_4PT + a_5T^2 \qquad Eq.4.4$$

$$\theta_r = b_0 + b_1P + b_2T + b_3P^2 + b_4PT + b_5T^2 \qquad Eq.4.5$$

$$\gamma_{(CO_2-brine)} = c_0 + c_1P + c_2T + c_3P^2 + c_4PT + c_5T^2 \qquad Eq.4.6$$

P is reservoir pressure in MPa, T is reservoir temperature in K, and the coefficients from a_0 to a_5 etc. are the model constants and are listed in Table 4-1. Eq. 4.4, 4.5 and 4.6 can determine the advancing contact angle (θ_a), receding contact angle (θ_r) and

interfacial tension (γ) at pressures ranging from 0.1 MPa to 20 MPa and temperatures ranging from 308K to 343K respectively. The selected range essentially covers the practical values encountered in reservoirs undergoing CO_2 storage. The agreement between experimental and simulated values was good with R^2-values of 0.992, 0.9917 and 0.9856 obtained from statistical fits of θ_a, θ_r and γ respectively.

Table 4-1 Model parameters from simulation

a_0	1129	b_0	877.7	c_0	-543.6
a_1	23.85	b_1	19.49	c_1	-6.683
a_2	-6.993	b_2	-5.435	c_2	3.724
a_3	-0.1712	b_3	-0.1094	c_3	0.1149
a_4	-0.04931	b_4	-0.04099	c_4	0.008005
a_5	0.0108	b_5	0.008395	c_5	-0.005623

4.4 Implications of the results

We demonstrated that both advancing and receding water contact angles on mica increase with pressure and decrease with temperature. Using a capillary force – buoyancy force equilibrium (Eq. 4.7, Iglauer et al., 2015a), we predict structural trapping capacities for different storage heights :

$$h = \frac{2\gamma cos\theta_r}{\Delta\rho g R} \qquad Eq.1.1$$

In Eq. 1.1, h is the CO_2 column height, which can be permanently immobilized by the caprock. 'θ_r' values are taken from **Error! Reference source not found.** and interfacial tension values (20wt% NaCl brine) are taken from our results (Fig. 4-6), pore throat radius (R = 0.01µm) of shale (as caprock) has been taken from (Nelson, 2009). The pressure and temperatures in Table 4-2 were selected according to the typical values of pressure and geothermal gradients (Donaldson and Tiab, 2004).

The results imply that hotter reservoirs can store larger volumes of CO_2 at the same reservoir pressure. However, at higher reservoir pressures (e.g. 20 MPa), significantly lower column heights can be achieved. This effect can be attributed to the increased de-wetting of the substrate at higher storage pressures. We therefore conclude that high pressures in colder reservoirs lead to less CO_2 storage capacity. Furthermore, we note that a temperature of 308K at ~18 MPa, θ turns > 90°, which implies that structural trapping will fail under these conditions (Iglauer et al., 2015a).

It is important to consider that these structural trapping capacities provide only a semi-quantitative guideline on the effect of pressure and temperature on CO_2 storage potential. However, in real reservoir scenarios these capacities should be evaluated based on mass of CO_2 that can be eventually stored at pressure and temperature of interest. Moreover, the influence of wetting/de-wetting behaviour on the structural trapping capacities reported in this study will vary depending upon the composition of overlaying seal layer for the case under consideration.

Table 4-2 CO_2 column heights predicted for various storage depths

Depth (m)	Pressure (MPa)	Temperature (K)	$\Delta\rho$ (kg/m^3)	IFT, γ (mN/m)	θ_r (^{o})	CO_2 column height (m)
500	5	323	1031	55	29	952
500	5	343	1032	58	26	1031
1000	10	323	755	43	50	747
1000	10	343	881	45	41	786
1500	15	323	445	38	67	681
1500	15	343	625	40	58	691
2000	20	323	359	36	74	562
2000	20	343	474	38	68	613
2500	25	323	320*	33*	79*	402
2500	25	343	380*	36*	74*	533

*values are extrapolated from our measurements

4.5 Conclusions

We conclude that precise characterization of wetting and interfacial properties of rock-fluid systems is essential for both reservoir and seal rocks as it has direct influence on structural and residual trapping (Iglauer et al., 2015a). Therefore, we measured advancing and receding contact angles for CO_2-brine-mica systems (RMS surface roughness of substrate ~12 nm) and interfacial tensions for CO_2-brine systems for a wide range of pressures, temperatures and salinities and analysed the associated trends systematically. We found that both θ_a and θ_r increased with pressure which is in agreement with most literature data; e.g. Broseta et al. (2012) and Chiquet et al.

(2007); Farookhpoor et al. (2013). The system tested was completely water wet at ambient conditions. However, with the increase in pressure, de-wetting of the substrate occurred, and at 15 MPa and 308K, the system became intermediate-wet ($\theta_a \sim 90^o$) implying considerable reduction in the residual trapping (Iglauer et al., 2015a). Moreover, at 20 MPa and 308K, wettability reversal occurred and the system turned into a CO_2-wet state ($\theta_a \sim 110^o$), which can lead to a failure of structural trapping (Iglauer et al., 2015a). We note that both θ_a and θ_r decreased with temperature, which is consistent with Broseta et al. (2012), and both θ_a and θ_r increased with salinity, which is consistent with Chiquet et al. (2007). The increase in contact angle with salinity is due to the less negative zeta potential values at higher salinities, and generally, the variation in contact angle (with temperature, pressure or salinity) is related to the interplay of solid-fluid and fluid-fluid interfacial tensions. Moreover, we found that γ decreased with pressure and increased with temperature consistent with Chalbaud et al. (2009); Espinoza et al. (2010) and Li et al. (2012). Based on experimental results, CO_2 column heights were predicted for different storage depths and geo-thermal gradients. We conclude that high temperature reservoirs have better cap-rock sealing efficiency, and thus store larger CO_2 volumes (786m at 10 MPa and 343K, Table 4-2) in comparison to colder reservoirs (747m at 10 MPa and 323K, Table 4-2). Moreover, higher reservoir pressures can lead to reduction in residual trapping because of substantial de-wetting of the rock surface, which is consistent with Iglauer et al. (2015a) and Krevor et al. (2015).

Chapter 5 CO_2-wettability of low to high rank coal seams: Implications for carbon sequestration and enhanced methane recovery*

Abstract

Coal seams offer tremendous potential for carbon geo-sequestration with the dual benefit of enhanced methane recovery. In this context, it is essential to characterize the wettability of the coal-CO_2-water system as it significantly impacts CO_2 storage capacity and methane recovery efficiency. Technically, wettability is influenced by reservoir pressure, coal seam temperature, water salinity and coal rank. Thus a comprehensive investigation of the impact of the aforementioned parameters on CO_2-wettability is crucial in terms of storage site selection and predicting the injectivity behaviour and associated fluid dynamics. To accomplish this, we measured advancing and receding water contact angles using the pendent drop tilted plate technique for coals of low, medium and high ranks as a function of pressure, temperature and salinity and systematically investigated the associated trends. We found that high rank coals are strongly CO_2-wet, medium rank coals are weakly CO_2-wet, and low rank coals are intermediate-wet at typical storage conditions. Further, we found that CO_2-wettability of coal increased with pressure and salinity and decreased with temperature irrespective of coal rank. We conclude that at a given reservoir pressure, high rank coal seams existing at low temperature are potentially more efficient with respect to CO_2-storage and enhanced methane recovery due to increased CO_2-wettability and thus increased adsorption trapping.

Keywords: Coal bed methane, Wettability, Rank, Pressure, Contact angle, CO_2-storage

*Reference: Arif et al. (2016) in *Fuel*, 181, 680-689.

5.1 Introduction

Carbon capture and storage (CCS) is the most promising approach to mitigate anthropogenic CO_2 emissions and thus ensure a cleaner environment (Blunt et al., 1993; Iglauer et al., 2013; IPCC, 2005; Lackner et al., 2003). The storage of CO_2 in depleted oil and gas reservoirs (Arts et al., 2012; Iglauer et al., 2011a) or deep saline aquifers (Andre et al., 2010; Burton et al., 2009) allows trapping of enormous volumes over a long period of time. Another option is injection of CO_2 into coal seams (Gray, 1987; Mazzotti et al., 2009; van Bergen et al., 2009] with the dual benefit of enhanced coal bed methane recovery (Busch and Gensterblum, 2011; Sams et al., 2005). In conventional reservoirs, CO_2 is held trapped by means of four mechanisms which are structural trapping (Hesse et al., 2008; Iglauer et al., 2015b), capillary or residual trapping (Iglauer 2011a,b; Juanes et al., 2006), dissolution trapping (Iglauer, 2011c; Linderberg and Wessel-Berg, 1997) and mineral trapping (Gaus, 2010). In coal seams, however, the dominant storage mechanism is adsorption trapping of CO_2 onto the coal matrix (Gray, 1987; Golding et al., 2011; White et al., 2005). Typically the adsorption capacity of CO_2 is higher than that of methane, depending on coal rank (Busch et al., 2003; Clarkson and Bustin, 2000; Krooss et al., 2002) consequently, CO_2 displaces methane towards the production well and itself gets sorbed within the micropores of the coal seam and remains trapped. CO_2 storage by means of adsorption in coal seams is strongly influenced by wettability of the CO_2-water-coal system (Gray, 1987; Saghafi et al., 2014), which in turn is generally a function of reservoir pressure (Saghafi et al., 2014; Sakurovs and Lavrencic, 2011; Shojai Kaveh et al., 2012), temperature and salinity. Moreover, in coal seams wettability is also a function of coal rank, vitrinite reflectance, fixed carbon and ash content (Crawford et al., 1994; Shojai Kaveh et al., 2012). Therefore, it is essential to describe CO_2-wettability of coals of varying ranks, and how reservoir conditions (pressure, temperature and brine salinity) influences this wettability.

In this context, several studies reported CO_2-wettability of coals at ambient conditions (Aplan, 1993; Crawford et al., 1994; Keller, 1987), but only a limited amount of literature data for the more relevant higher pressures have been reported (Chi et al., 1988; Saghafi et al., 2014; Sakurovs and Lavrencic, 2011; Shojai Kaveh et al., 2012; Siemons et al., 2006). Table 5-1 presents a summary of the major experimental variables considered in previous studies, and this work.

Table 5-1 CO_2-wettability of coals: Summary of experimental conditions used.

Reference	Pressure	Temperature	Salinity	Coal type	Overall Coal rank
Chi et al. (1988)	up to 6.2 MPa	298 K	DI water	Not mentioned	Not mentioned
Siemons et al. (2006)	up to 14 MPa	318 K	DI water	Anthracite	High
Sakurovs and Lavrencic, (2011)	up to 15 MPa	313 K	DI water	Bituminous	Medium
Shojai Kaveh et al. (2011)	up to 16 MPa	318 K	DI water	High volatile bituminous	Medium
Shojai Kaveh et al. (2012)	up to 16 MPa	318 K	DI water	Semi anthracite, High volatile bituminous	High and Medium
Saghafi et al. (2014)	up to 6 MPa	295 K	DI water	Medium volatile bituminous	Medium
This study	up to 20 MPa	308 K, 323 K and 343 K	0wt% - 10wt% NaCl	Semi-anthracite, Medium volatile bituminous, Lignite	High, Medium and Low

Therefore there is a clear lack of data available on CO_2-wettability of coals as a function of coal rank, coal formation pressure, and particularly temperature and salinity (cp. Table 5-1). Thus there exists a gap in terms of proper understanding of CO_2-wettability of coal seams of different ranks at reservoir conditions. Moreover, although it is well established that coal seams offer enormous potential for enhanced methane recovery and CO_2 sequestration, yet certain important questions need to be addressed which are: 1) Which type of coal (low rank, medium rank, or high rank) are most suitable for CO_2 storage and enhanced coalbed methane recovery under the prevailing geothermal and reservoir pressure conditions? 2) Is the suitability of CO_2 sequestration in coal seams of a particular rank valid for a wide range of reservoir pressures, temperatures and salinity conditions? 3) What mechanisms are responsible

for long term CO_2-storage in coals? To answer these questions and to generally improve the characterization of CO_2-wettability of coals, we experimentally measured water advancing and receding contact angles on three coal samples as a function of coal rank (low, medium and high ranks), vitrinite reflectance and fixed carbon at different CO_2 pressures (0.1 - 20 MPa), temperatures (ranging from 308 K to 343 K), and brine salinities (0 -10 wt% NaCl) using the pendent drop technique. The results of the study lead to a broad characterization of CO_2-wettability of coals and thus help optimize CO_2-storage and enhanced coal bed methane recovery operations. Our results indicate that CO_2-wettability of coals is strongly influenced by coal rank such that the high rank coals are more CO_2-wet and low rank coals are least CO_2-wet at a given reservoir pressure, temperature and salinity.

5.2 Materials and methods

5.2.1 Coal Samples

Three coal samples [high rank (semi anthracite; from Hazelton, Pennsylvania, USA), medium rank (medium volatile bituminous; from Morgantown, West Virginia, USA), and low rank (lignite; from North Dakota, USA; Table 5-2)] were used in this research. The samples were cut to cuboid shape (~1cm x 1cm x 0.5cm) and the surface roughness of each substrate was measured with an atomic force microscope (AFM instrument model DSE 95-200); note that typically surface roughness significantly affects contact angle measurements (Marmur, 2006; Letellier et al., 2007). The RMS surface roughness of the specific coal substrates used were 840nm, 880nm and 280nm for high, medium and low rank coals respectively.

5.2.2 Petrology, Ultimate and Proximate Analysis

The results of the proximate, ultimate and petrological analysis and the internal properties (density and volume) of the coal samples are listed in Table 5-2. Note that coal samples of different rank differ mainly in volatile matter, moisture, fixed carbon and vitrinite reflectance (Bustin et al., 1985; Butt et al., 2006). Petrology was analysed in accordance with Australian Standard AS2856 and ISO7404; proximate analysis were conducted using AS1038.3, ISO11722 and ASTM D3172-07a, and ultimate analysis were performed using AS1038.6 and ISO 609.

5.2.3 Fluids

99.9 wt% CO_2 (from BOC, gas code – 082), de-ionized water (Conductivity: 0.02 mS/cm), and 5wt% and 10wt% NaCl brine (NaCl Source: Scharlab s.l., Spain, Purity: ≥0.995mass%) were used in the study. Acetone (99.9 wt%) was used to wash the coal samples.

Table 5-2 Properties of coal samples used.

Sample	Rank	Semi-Anthracite	Medium-volatile Bituminous	Lignite
	Geological Location	Hazelton, Pennsylvania	Morgantown, West Virginia	North Dakota
	Overall rank (used in this work)	High rank	Medium rank	Low rank
Petrology	Vitrinite Reflectance (R_o, %*)	3.92	0.82	0.35
	Vitrinite (%)	89.6	73.1	83
	Liptinite (%)	0	3.4	4
	Inertinite (%)	7.6	18.8	10.8
	Minerals (%)	2.8	4.7	2.1
Proximate analysis	Moisture (air dried, %)	2.6	2	16.3
	Ash (%)	9.7	6.4	7.8
	Volatile Matter (%)	2.9	32.4	34.8
	Fixed carbon (%)	84.9	59.2	41.1
Ultimate analysis	Ash (%)	9.7	6.4	7.8
	Carbon (%)	82.6	78.6	54.6
	Total Hydrogen (%)	2.35	5.07	5.27
	Hydrogen (%)	2.06	4.85	3.45
	Nitrogen (%)	1.16	1.54	0.62
	Total Sulphur (%)	0.8	0.99	0.66
	Oxygen by difference (%)	3.68	7.62	2.87
Properties	Bulk density (g/cc)	1.30	1.28	1.44
	Dry sample volume (cc)	16.55	12.77	4.26
	Dry mass (g)	21.17	16.194	6.159
	RMS Surface Roughness (nm)	840	880	280

* All percentages in above table represent weight percent

5.2.4 Contact angle measurements

CO_2-brine wettability was measured using the pendent drop tilted plate technique (Lander et al., 1993). The experimental setup is shown in Fig. 3-1. Prior to each experiment, the coal substrates were washed with acetone and then cleaned in air plasma (Diemer Yocto instrument) for 2 min to ensure that no organic contaminants are deposited on the sample, which would introduce a significant bias (Iglauer et al., 2014). We limited plasma treatment to 2 min to avoid changes in surface chemistry, which may be induced by the plasma. We, however, note that Shojai Kaveh et al. (2011), used wet polish with a series of abrasive papers with a grid ranging from 60 to 1200, followed by polishing with 0.5 µm abrasive alumina powders and a fibrous cloth which was then terminated with ultrasonic cleaning as proposed by Drelich et al. (1997).

For each measurement, a clean and dry coal sample was placed inside the pressure cell onto the tilted plate. The temperature was set to a fixed value (308 K, 323 K, and 343 K), and CO_2 pressure in the cell was increased with a high precision syringe pump to pre-determined values (0.1 MPa, 5 MPa, 10 MPa, 15 MPa, 20 MPa) by injecting CO_2 into the cell, and samples were exposed to CO_2 until the pressure inside the cell stabilized (~20 minutes) Subsequently a droplet of de-gassed brine (average volume of ~6µL ± 1µL) was allowed to flow (at 0.4ml/min) and was dispensed onto the substrate through a needle. We note that the fluids used were not thermodynamically equilibrated, since earlier studies demonstrated that the contact angle θ is not significantly affected by mass transfer during the first 60seconds of exposure (Al-Yaseri et al., 2016a; Sarmadivaleh et al., 2015) and during this time all measurements were completed. Moreover, non-equilibrated fluids are most relevant at the leading edge of the CO_2 plume, i.e. when CO_2 first encounters under saturated brine. Furthermore, as demonstrated by Shojai Kaveh et al., (2014), non-equilibrated fluids can work well if contact angles are measured by releasing a droplet of brine into a CO_2 environment (as the diffusion coefficient of water in CO_2 is relatively small). Thus mass transfer does not affect our measurements. However, if the contact angles are measured by using CO_2 bubbles surrounded by the water phase, fluid equilibration is necessary due to the higher diffusion coefficient of CO_2 in water (Shojai Kaveh et al., 2014). Advancing (θ_a) and receding water contact angles (θ_r) were measured

simultaneously at the leading and trailing edges of the droplet, just before the droplet started to move. The standard deviation of these measurements was ±3° based on replicate measurements; however for lignite the standard deviation reached ±5°, which is due to the more complicated nature of the sample.

5.3 Results and Discussion

In order to assess CO_2-storage and methane recovery potential, CO_2-wettability of coals was characterized as a function of rank at relevant thermophysical conditions by measuring advancing and receding contact angles on coal samples of high, medium and low ranks at various reservoir conditions (pressure range: 0.1-20 MPa, temperature range: 308 K-323 K and salinity range: 0wt%-10wt% NaCl). The outcomes of the study led to a precise realisation of the relationships between coal rank and corresponding CO_2 geo-storage and ECBM potential. The subsequent sections describe the results in detail.

5.3.1 Effect of Pressure on CO_2-wettability of coal

The effect of pressure was systematically tested on the three (high, medium, low rank) samples at 0.1 MPa, 5 MPa, 10 MPa, 15 MPa and 20 MPa for three different temperatures (308 K, 323 K, and 343 K). Both, θ_a and θ_r, clearly increased with pressure at all temperatures for all coal samples (Fig. 5-1 to Fig. 5.3). High rank coal was water wet ($\theta<50°$, Iglauer et al., 2015a) at ambient pressure for all temperatures tested (308 K-343 K; Fig. 5-2). As pressure increased from 0.1 MPa to 20 MPa at 323 K, θ_a increased from 47° to 141° and θ_r increased from 42° to 129° (red lines in Fig. 5-1), and thus high rank coal became CO_2-wet at high pressure ($\theta>130°$, Iglauer et al., 2015a). Similarly, at 343K, as pressure increased from ambient to 20 MPa, θ_a increased from 32° to 118° and θ_r increased from 27° to 107°.

This increase in contact angle with pressure is consistent with independent experimental data on coal (Chi et al., 1988; Saghafi et al., 2014; Sakurovs and Lavrencic, 2011; Shojai Kaveh et al., 2012; Siemons et al., 2006). Specifically, Chi et al. (1988) measured contact angles up to 6.2 MPa at 298 K for coals of unknown ranks and found that coal hydrophobicity increased with pressure. Siemons et al. (2006)

extended the testing pressure up to 14 MPa at 318 K and analysed CO_2-water contact angle for an anthracite coal (high rank) and found that the system became CO_2-wet at 2.6 bar, however, in our case semi-anthracite became weakly CO_2-wet at around 7 MPa ($\theta_a > 110°$); this difference could be due to difference in rank of the samples (semi-anthracite in this study) and difference in experimental conditions (temperature and surface cleaning methods). Sakurovs and Lavrencic (2011) experimentally determined CO_2-water contact angles using the captive bubble technique up to 15 MPa at 313 K for low to medium rank coals (R_v% of their samples ranged from 0.62-1.4) and found an increase in CO_2-wettability with pressure for all samples. Shojai Kaveh et al. (2012) compared CO_2-wettability of high volatile bituminous (medium rank) and semi anthracite (high rank) coals up to 16 MPa and at 318 K; and reported that semi-anthracite became CO_2-wet ($\theta = 110°$) at 5.7 MPa which is close to our result (7 MPa); the slight difference could be due to different surface cleaning methods and temperature. Moreover, surface roughness of the samples (present work: RMS roughness values are 840 nm and 880 nm while Shojai Kaveh et al. (2011, 2012)'s P_a roughness values were 0.011 mm and 0.018 mm for high and medium rank coals respectively) can also be a factor responsible for this difference. We, however, note that surface roughness had a small influence on CO_2-water-quartz contact angles (cp. Al-Yaseri et al., 2016a), and higher surface roughness leads to more extreme contact angles (lower θ if $\theta < 90°$, and higher θ if $\theta > 90°$, Butt et al., 2006). Saghafi et al. (2014) also studied CO_2-wettability of high rank coal up to 6 MPa at 295 K, their sample turned CO_2-wet at 5 MPa ($\theta = 110°$).

The increase in contact angle with pressure is also consistent with experimental data on pure minerals such as mica (Arif et al., 2016a,b; Broseta et al., 2012; Chiquet et al., 2007) and quartz (Al-Yaseri et al., 2016a; Sarmadivaleh et al., 2015). This transformation of wettability from water-wet to CO_2-wet by an increase in pressure is, apart from increased intermolecular interactions of CO_2 with solid surface (Arif et al., 2016a; Iglauer et al., 2012), also related to the increased adsorption of CO_2 on the coal surface, which is evident from experimental CO_2 adsorption data on coals (Bae and Bhatia, 2006; Krooss et al., 2002; Li et al., 2010; Siemons et al., 2007). The explanation of the effect of pressure on contact angle is consistent with Shojai Kaveh et al. (2012) who reported that variations in CO_2 density, CO_2 sorption and CO_2-water interfacial tension are responsible for dependency of wettability on pressure.

Since adsorption is the dominant storage mechanism in coals, and typically accounts for 98% of the total gas stored (Gray, 1987), high pressure storage conditions are preferred as they would lead to increased storage volumes. However, further investigation is required to establish the relationship between CO_2-wettability and CO_2-adsorption. Moreover, increased CO_2-wettability of coal will lead to more uniform distribution of CO_2 within the micropores of the coal seams (since wetting phase usually occupies small pores) and thus improved displacement of methane towards the production wells. However, at high pressures coal swells (Hol and Spiers, 2012; Reucroft and Sethuraman, 1987), which leads to a significant permeability decrease, which again limits the Darcy flow (of the CO_2) and thus injectivity.

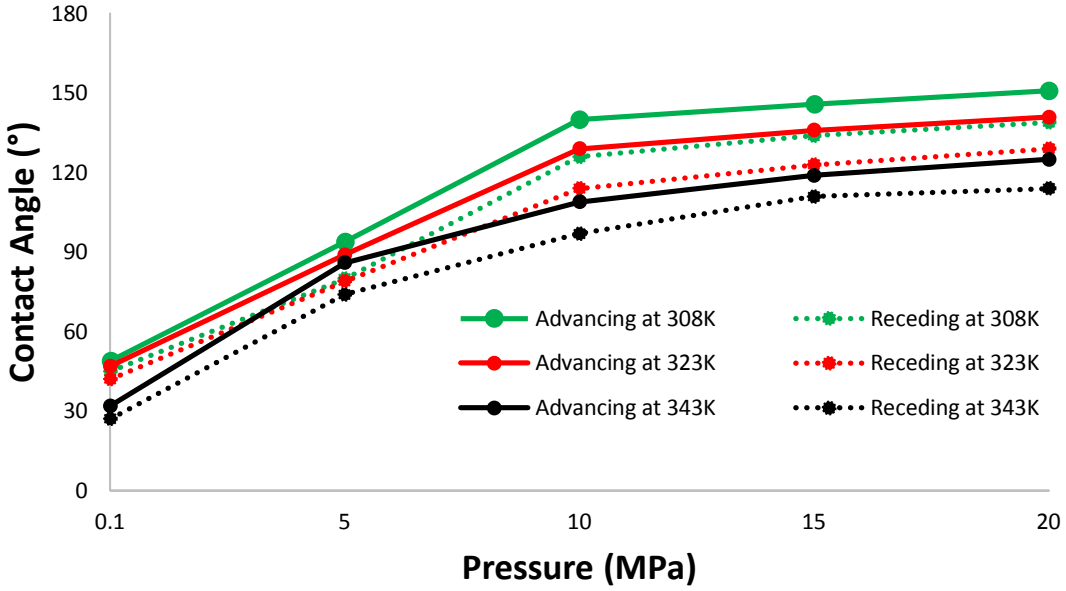

Fig. 5-1 CO_2-DI water contact angles on high rank coal (semi-anthracite) at tested pressures (0.1 MPa-20 MPa) and temperatures (308 K-343 K).

Furthermore, we found that the rate of contact angle increase with pressure is sharper for the pressure range 0.1 MPa-10 MPa (Fig. 5-1). For example, at 323K, θ_a measured 47° at 0.1 MPa and 129° at 10 MPa resulting in a net increase of 78°, whereas the net increase in θ_a for the pressure range 10 MPa-20 MPa was only 12°. Generally, the increase in contact angle with pressure flattened out for pressures between 10 MPa-20 MPa. This implies that there is only a minor increase in CO_2-wettability at high pressures. Similar trends are found in literature data on CO_2-adsorption on coals,

which report that absolute CO_2-adsorption increases steadily up to ~10 MPa and after that adsorption becomes nearly constant (Busch et al., 2003; Clarkson and Bustin, 2000). Thus we can infer from CO_2-adsorption data that injection of CO_2 in high rank coals at very high pressure may yield only marginal benefits in terms of additional volume stored. Although, there is no proof of a direct relationship between CO_2-wettability and CO_2-adsorption, yet, theoretically, it can be visualised that coals which are more CO_2-wet must adsorb more volume of CO_2 which is consistent with Saghafi et al. (2014).

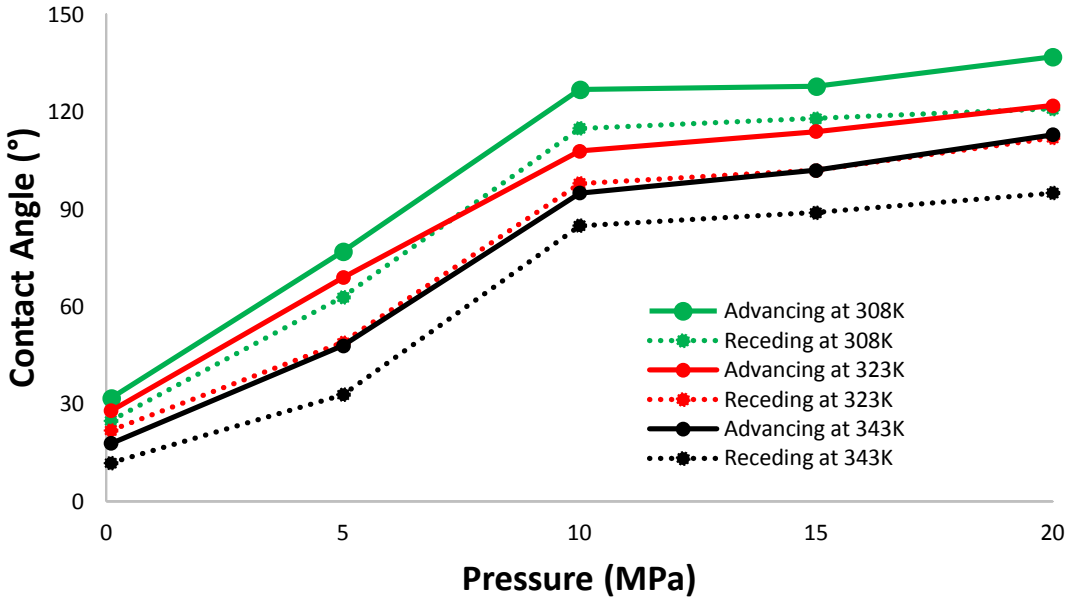

Fig. 5-2 CO_2-DI water contact angles on medium rank coal (medium volatile bituminous) at tested pressures (0.1 MPa-20 MPa) and temperatures (308 K-343 K).

The medium rank coal sample (medium volatile bituminous coal) remained water-wet (at ambient conditions) with a maximum θ_a value of 32° (Fig. 5-2). When pressure increased from 0.1 MPa to 20 MPa at 323 K, θ_a increased from 28° to 122° and θ_r increased from 18° to 113°. Consequently, the system, which was water-wet at ambient conditions, turned weakly CO_2-wet at reservoir conditions ($110° \leq \theta \leq 130°$; Iglauer et al., 2015a). Likewise high rank coal, the increase in contact angle for medium rank coal was sharp up to 10 MPa; however, the increase gradually flattened (between 10-20 MPa). The results, therefore, imply that CO_2 storage capacity in

medium rank coals increases with pressure at all temperatures owing to the increased CO_2-wetting which implies to increased adsorption trapping; however, this storage capacity increase is only marginal at higher pressures, e.g. from 15 MPa to 20 MPa. Therefore, from an economic standpoint, for practical storage purposes an optimal injection pressure must be selected.

For low rank coals, contact angles increased with pressure at all temperatures as shown in Fig. 5-3. For example, at 308 K, a sharp increase was observed for pressure 0.1 MPa to 10 MPa, and the curve flattened afterwards. However, at 323 K, the change in contact angle with pressure followed a slightly inconsistent trend such that contact angles first increased gradually up to 5 MPa (θ_a increased from 24° to 50° when pressure increased from 0.1 MPa to 5 MPa), then sharply up to 10 MPa (θ_a measured from 92°), and then a small increase was observed up to 20 MPa (θ_a increased to 116°). The maximum contact angle measured for low rank coals was 122° (at 20 MPa and 308 K) indicating that the most hydrophobic wettability regime for low rank coals is 'weakly CO_2-wet' implying reduced CO_2 trapping by means of adsorption. Similar trends were observed for higher temperature (323 K and 343 K).

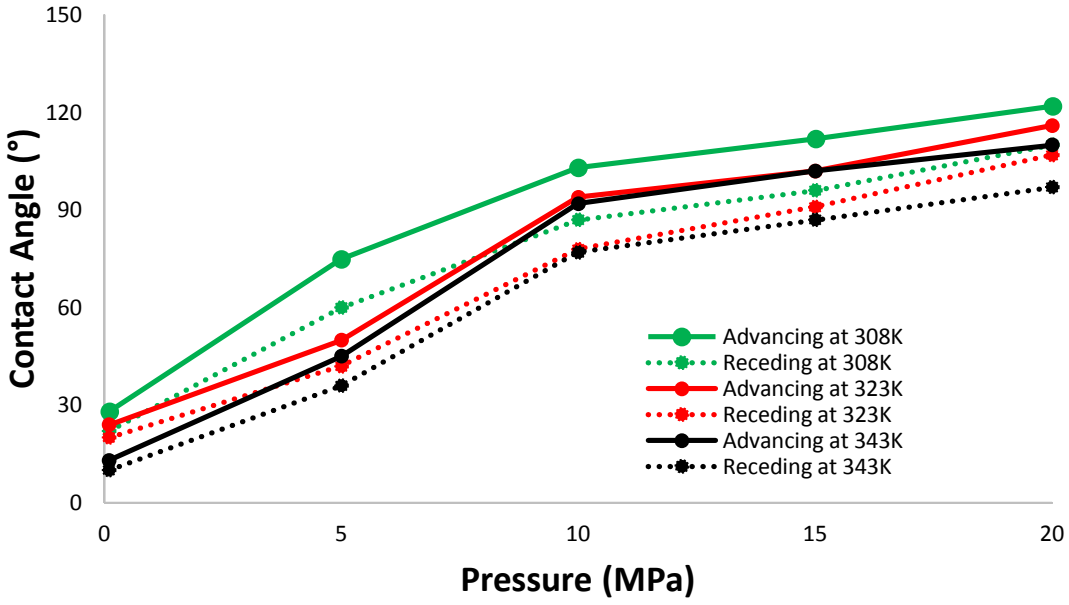

Fig. 5-3 CO_2-DI water contact angles on low rank coal (lignite) at tested pressures (0.1 MPa-20 MPa) and temperatures (308 K-343 K).

5.3.2 Effect of temperature on CO_2-wettability of coal

The trends of contact angle variation with temperature are presented in Fig. 5-1 to Fig. 5-3. For all coal samples analysed, both, θ_a and θ_r, decreased with temperature at all pressures tested. For example, when temperature increased from 308 K to 343 K at 0.1 MPa, θ_a decreased from 49° to 32° for high rank coal, while it decreased from 32° to 18° for medium rank coal and from 28° to 13° for low rank coal. At higher pressures (5 MPa-20 MPa), however, all coal types showed a clear decrease in θ_a and θ_r with temperature (Fig. 5-1 to Fig. 5-3). For simplicity, a summary of contact angle variation with temperature is shown in Fig. 5-4. At 15 MPa, for high rank coal, when temperature increased from 308 K to 323 K, θ_a decreased from 146° to 119°, implying wettability transformation from strongly CO_2-wet to weakly CO_2-wet. Similarly, for medium rank coal, θ_a decreased from 128° to 102° when temperature increased from 308 K to 343 K. However, for low rank coal, θ_a first decreased from 112° to 102° when temperature increased from 308 K to 323 K, and then became constant when temperature increased further (from 323 K to 343 K). In summary, CO_2-wettability of coal decreased with increasing temperature irrespective of the coal rank. There is no published data on the effect of temperature on CO_2-water-coal contact angles, however, the decrease in contact angle with temperature has also been reported for pure minerals such as mica (Arif et al., 2016a; Broseta et al., 2012; Chiquet et al., 2007) or quartz (Farokhpoor et al., 2013; Saraji et al., 2014).

We demonstrate that two distinct mechanisms may be held responsible for the decrease in contact angle with temperature. The first mechanism is the interplay of the three interfacial tensions (Arif et al., 2016a), which is expressed by the Young-Laplace equation as follows:

$$\cos\theta = \frac{\gamma_{sv} - \gamma_{sl}}{\gamma_{vl}} \qquad \text{Eq. 5.1}$$

In Eq. 5.1, γ_{sv} and γ_{sl} are the solid-CO_2 interfacial tension and solid-brine interfacial tension, respectively, whereas γ_{vl} is CO_2-brine interfacial tension. Since most of the previous studies (Arif et al., 2016a) agree that CO_2-brine interfacial tension increases with temperature, it is evident from Eq. 5.1 that the difference of solid-CO_2 interfacial tension and solid-brine interfacial tension (numerator of equation) should increase with temperature to cause a corresponding decrease in contact angle with temperature.

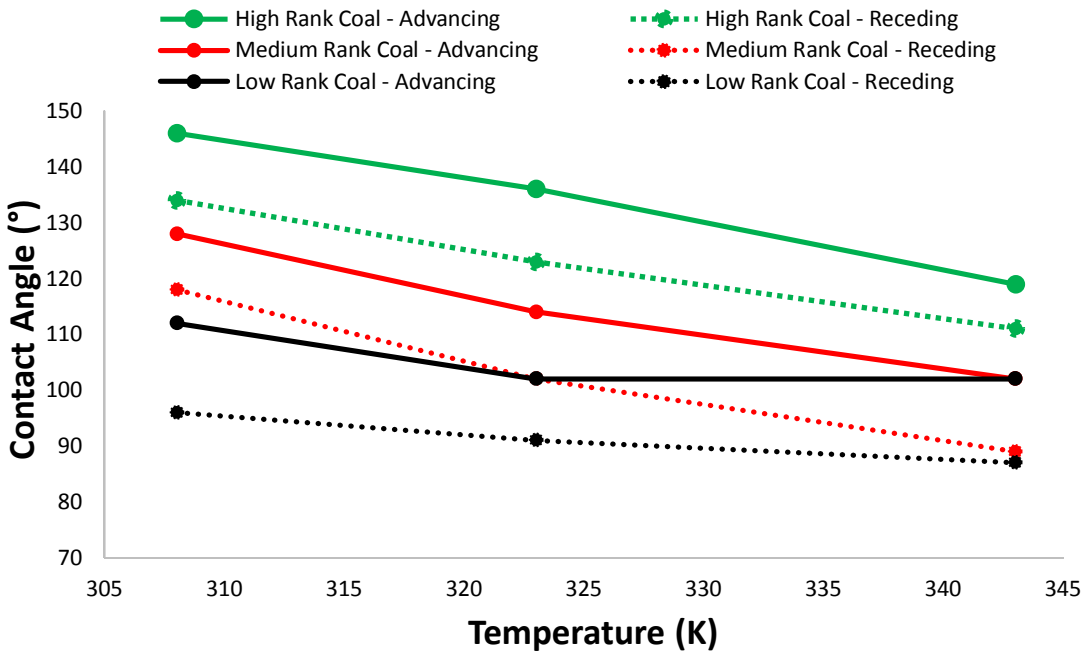

Fig. 5-4 Effect of temperature on CO_2-wettability for all coal samples used in the study. For simplicity measurements are shown only for 15 MPa.

Secondly, the decrease in the contact angle with temperature can be attributed to the CO_2 adsorption behaviour on coal. The experimental studies on the effect of temperature on CO_2 adsorption (Bustin and Clarkson, 1998; Perera et al., 2011; Sakurovs et al., 2007) report that there is a clear decrease in CO_2 adsorption on coal surfaces with temperature. This reduced CO_2-affinity is thus reflected in the contact angles. Perera et al. (2011) mentioned that the decrease in adsorption capacity with temperature is due to the increase in kinetic energy and rate of diffusion of CO_2, which tend to release gas molecules from the coal matrix resulting in a corresponding reduction in net amount of adsorbed gas. We thus conclude that low temperature coal seams have higher CO_2 storage capacities in comparison to high temperature coal seams.

5.3.3 Effect of coal rank on CO_2-wettability

In order to demonstrate the impact of coal rank on CO_2-wettability and thus on methane production and CO_2 storage potential in coals, we plotted advancing water contact angles (only for simplicity) as a function of pressure and temperature (Fig. 5-5). It is clear that at any given CO_2 pressure, apart from the ambient, high rank coal offers highest CO_2-wetting potential, and CO_2-wettability substantially decreases with rank. Low rank coals (e.g. Lignite) are least CO_2-wet and medium rank coal (e.g. Bituminous) are intermediate. These results are in agreement with Shojai Kaveh et al. (2012) who compared CO_2-wettability of semi-anthracite and high volatile bituminous coals, they measured higher contact angles for semi-anthracite coals, and thus they concluded that hydrophobicity of coals increases with coal rank. The fact that medium rank coal is less CO_2-wet as compared to high rank coal is due to the abundance of hydrophilic functional groups (such as hydroxyl or carboxylic groups) in medium rank coal. Moreover, Sakurovs and Lavrencic (2011) also concluded that high ranks coals were easier to wet with CO_2 at high pressures and that the increase in CO_2-wettability promoted the rate of penetration of CO_2 into the coals. It can therefore be established that CO_2-wettability of coals is a strong function of coal rank and that high rank coals are more CO_2-wet. We point out that this behaviour is related to the increase in CO_2 adsorption capacity with an increase in coal rank as evidenced by the literature data on adsorption isotherms of coals of varying rank (Krooss et al., 2002; Mastalerz et al., 2004).

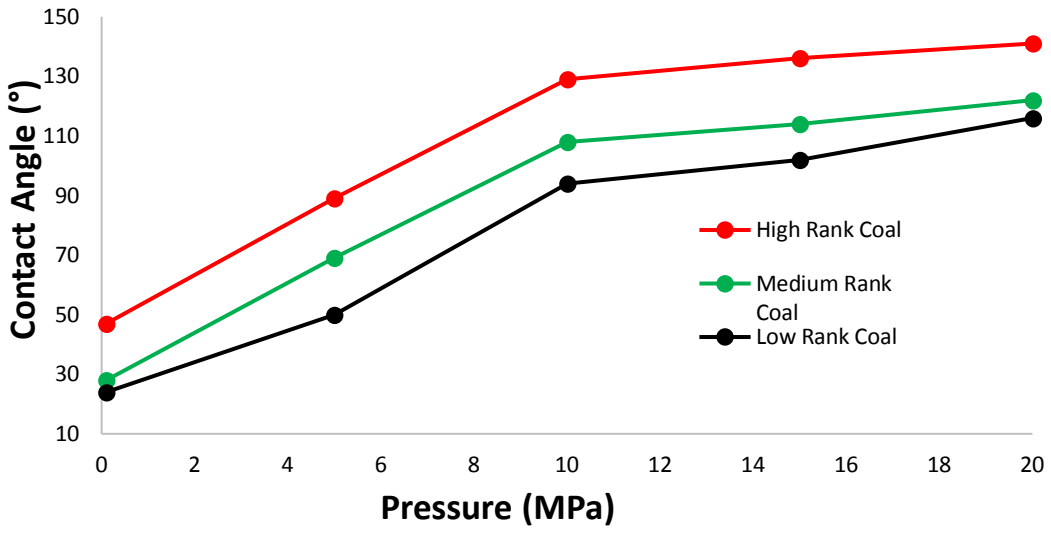

Fig. 5-5 Effect of coal rank on CO_2-wettability

5.3.4 Effect of brine salinity on CO_2-wettability of coal

Water can exist in coals seams in the form of free water in cleats, chemically bound hydration water, and water adsorbed onto the surface of the matrix blocks (Durucan et al., 2014; Zhang et al., 2015). The cleat system is initially filled with water and it provides the flow path for production by Darcy's law. We thus analysed the impact of brine salinity on CO_2-brine-coal wettability for various salinities (0wt% NaCl, 5wt%NaCl and 10wt% NaCl) at 15 MPa and 323 K on all the coal samples studied in this work; as salinity is expected to vary in subsurface coal seams (Hamawand et al., 2013).

Both, θ_a and θ_r, increased with salinity for all coal samples (Fig. 5-6). This increase was stronger for the brine salinity increase from 0 wt% NaCl to 5 wt% NaCl; e.g. for medium rank coal, θ_a increased from 114° to 127° and θ_r increased from 102° to 112° when salinity increased from 0wt% NaCl to 5wt% NaCl brine. For the salinity increase from 5 wt% NaCl to 10wt% NaCl, the increase in contact angle was very small; e.g. for medium rank coal, θ_a increased from 127° to 132° and θ_r increased from 112° to 116° when salinity increased from 5wt% NaCl to 10wt% NaCl brine. Moreover, we found similar trends for low, medium and high rank coals (Fig. 5-6). In the literature, there is a lack of data on the effect of salinity on CO_2-wettability of coal. However, our results are consistent with Ibrahim and Nasr-al-Din (2015), analysed contact angles of CO_2-brine-coal systems for brine salinities varying between 0 g/L-15 g/L NaCl), and reported that contact angles were highest for 15 g/L and lowest for DI water. Brine salinity thus does not exhibit major influence on contact angles at typical reservoir conditions. The results are consistent with Arif et al. (2016b), who found that there was only a minor increase in contact angle with salinity on CO_2-wet mica surfaces.

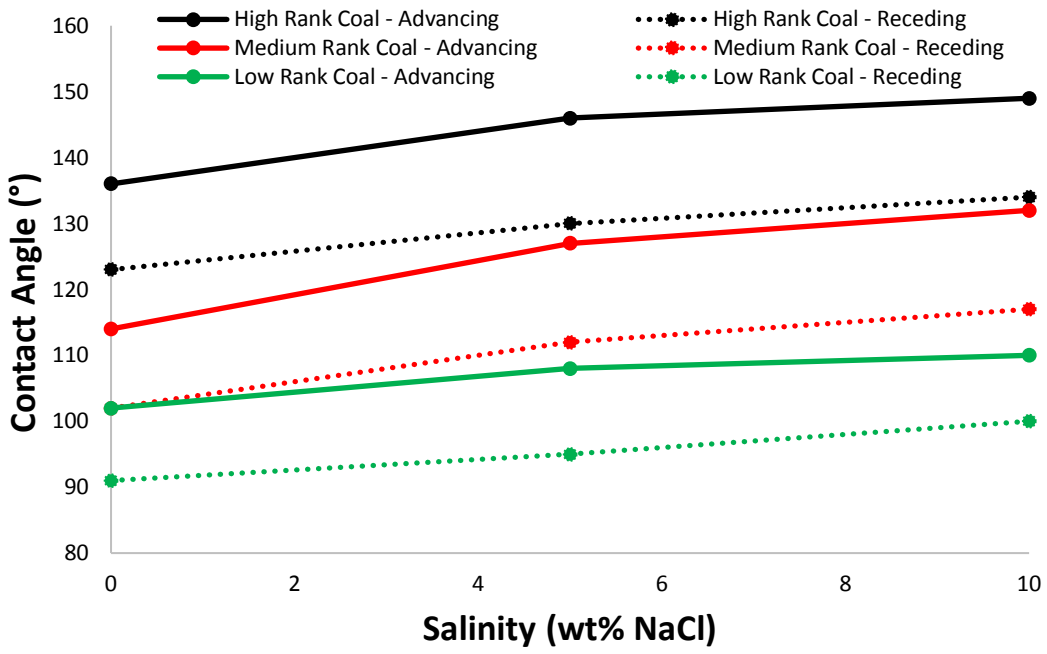

Fig. 5-6 Effect of salinity on CO_2-wettability of coals at 323K and 15 MPa

5.3.5 Relation between vitrinite reflectance, fixed carbon and coal wettability

There is a strong positive correlation between virtinite reflectance and water contact angle. Similarly, fixed carbon (which is the solid combustible residue that remains after coal is heated and volatile matter is expelled) strongly correlates with the water contact angle (Fig. 5-7). Practically, coals with higher vitrinite reflectance are more CO_2-wet and thus will store more CO_2 by means of adsorption; coals with higher fixed carbon content also have better CO_2-wetting characteristics. At 20 MPa and 323 K, coal with a vitrinite reflectance (R_o, %) of 3.8 is strongly CO_2-wet (θ_a = 140°), whereas at the same reservoir conditions medium rank coal (R_o = 0.82) is weakly CO_2-wet (θ_a = 122°) and low rank coal (R_o = 0.35) is intermediate-wet (θ_a = 116°); thus CO_2 injection into low rank coals will require higher injection pressures to completely wet the surface in comparison to medium and high rank coals. Thus we conclude that coals of higher vitrinite reflectance and fixed carbon exhibit better CO_2 adsorption storage capacity, because of their better CO_2-wettability. This effect can be attributed to the non-polar nature of vitrinite matter which promotes de-wetting of the surface.

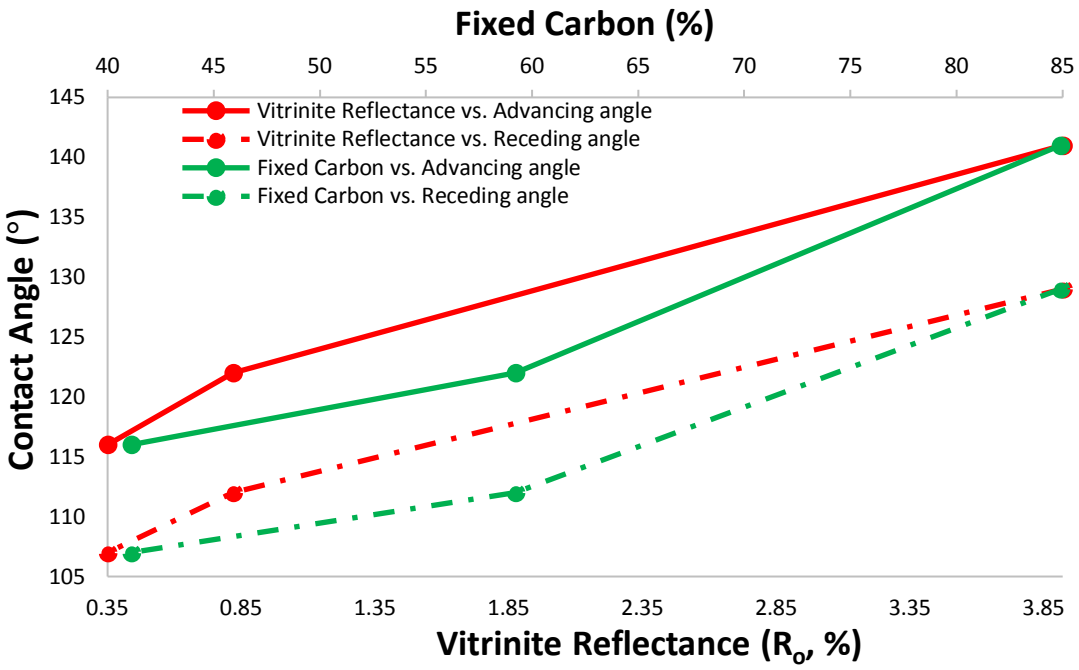

Fig. 5-7 Variation of CO_2-wettability with vitrinite reflectance and fixed carbon content

5.4 Implications

We measured CO_2-wettability of coals of varying ranks; which is essential to assess the CO_2 storage potential of coal seams, and also to assess enhanced hydrocarbon gas production from unmineable coal seams. The measured data implies that CO_2 storage in coal seams is strongly influenced by pressure, seam temperature, brine salinity, rank of the coal, vitrinite reflectance and fixed carbon. As an example, consider three potential candidate coal bed methane formations of different ranks (high, medium and low) at a depth of 1km and at temperature of 323 K. The required CO_2 injection pressure will be approximately 10 MPa (estimated using formation pressure gradient ~ 10 MPa/km). We note that at 10 MPa and 323 K, the values of the receding water contact angles for high, medium and low rank coals are 114°, 95° and 77°, respectively, implying that high rank coal is weakly CO_2-wet, medium rank coal is intermediate-wet and low rank coal is weakly water-wet at storage conditions (note: θ_r is considered here owing to the advancement of the CO_2 phase, which displaces brine; or alternatively 'drainage', Broseta et al., 2012). Considering the fact that, at any given temperature and pressure, the total amount of CO_2 adsorbed on the coal surface is higher for the high rank coal (Clarkson and Bustin, 2000; Krooss et al.,

2002), thus, the adsorption trapping capacities will be higher for high rank coal seams and least for low rank coal. It is notable that CO_2-storage potential in coal seams in primarily governed by CO_2-adsorption data, however wettability assists in these predictions (as explained in section 5.3.1). Thus, high rank coal will be more suitable for CO_2 storage considering that adsorption of CO_2 is the dominant trapping mechanism (Gray, 1987; Siemons and Busch, 2007). Moreover, CO_2 injection into high rank coal at 10 MPa and 323 K will wet the surfaces of coal with CO_2 better as compared to medium and low rank coals. Consequently, CO_2 distributes more uniformly into the micropores and thus recovery efficiency of methane will improve. It is also important to mention that with the increase in pressure and thus CO_2-wettability, coal will swell inducing a permeability reduction (Hol and Spiers, 2007) and this effect limits CO_2 storage in coal seams.

In summary, once injected, CO_2 will occupy the smallest pores (micropores of coal matrix) and brine will occupy larger pores (cleats), and as a result brine will be watered-out. In addition, it is experimentally proven that methane wettability of coal is lower than that of CO_2 (Saghafi et al., 2014), and the sorption capacities of CO_2 relative to CH_4 on the coal surface are 1.1 – 9.1 times higher depending upon the coal rank (Busch et al., 2004; Pini et al., 2010). Thus methane, which was adsorbed on the coal surfaces, will be displaced rather easily by CO_2.

5.5 Conclusions

We measured water contact angles to characterize CO_2-wettability of coals of low, medium and high rank as a function of reservoir pressure (0.1 MPa - 20MPa), temperature (308 K-343 K) and brine salinity (0wt% - 20wt%NaCl). The results demonstrate that both, θ_a and θ_r, increase with pressure, consistent with (Saghafi et al., 2014; Siemons et al., 2006; Shojai Kaveh et al., 2012) and the increase is quite rapid up to 10 MPa and it flattens if pressure is increased further (10 MPa-20 MPa, Fig. 5-1 to Fig. 5-3), implying that injection pressures must be optimized to ensure economic feasibility. The increase in contact angles with pressure is attributed to a) increased CO_2-mineral intermolecular interactions due to increased CO_2 density (Arif et al., 2016a), and b) increased CO_2 adsorption at high pressures (Krooss et al., 2002; Siemons and Busch, 2007). Further we found that θ_a and θ_r decrease with temperature

which is consistent with independent experimental CO_2-adsorption data (Bustin and Clarkson, 1998; Perera et al., 2011; Sakurovs et al., 2007). The influence of salinity was not significant, and θ_a and θ_r increased only slightly with elevated salt content. Moreover, and importantly, the CO_2-wettability increased with the increase in coal rank, which is in agreement with other studies (Shojai Kaveh et al., 2012). Specifically, we found that high rank coals (e.g. semi-anthracite) are strongly CO_2-wet at typical storage conditions, while medium rank coals (e.g. medium volatile bituminous) are weakly CO_2-wet and low rank coals (e.g. Lignite) are intermediate wet, i.e. CO_2-wettability showed a positive correlation with vitrinite reflectance and fixed carbon content. Finally, we predict that high rank coal seams existing at high temperatures and high pressures are more feasible for CO_2 storage due to increased CO_2-wettability.

Chapter 6 Influence of shale-total organic content on CO_2 geo-storage potential*

Abstract

Shale CO_2-wettability is a key factor which determines the structural trapping capacity of a caprock. However, the influence of shale-TOC on wettability (and thus on storage potential) has not been evaluated despite the fact that naturally occurring shale formations can vary dramatically in TOC, and that even minute TOC strongly affects storage capacities and containment security. Thus, there is a serious lack of understanding in terms of how shale, with varying organic content, performs in a CO_2 geo-storage context. We demonstrate here that CO_2-wettability scales with shale-TOC at storage conditions; and we propose that if TOC is low, shale is suitable as a caprock in conventional structural trapping scenarios, while if TOC is ultrahigh to medium, the shale itself is suitable as a storage medium (via adsorption trapping after CO_2 injection through fractured horizontal wells).

Key points:

- Shale total organic content (TOC) scales with CO_2-wettability
- Low TOC shales are water-wet at storage conditions (good for structural trapping)
- Organic-rich shales are CO_2-wet at storage conditions (good for adsorption trapping)

6.1 Introduction

CO_2 geo-storage (CGS) in underground geological formations is considered to be a promising approach to reduce anthropogenic CO_2 emissions (IPCC, 2005; Lackner, 2003). In CGS, structural CO_2 trapping is the principal storage mechanism whereby shale (in its classical caprock role), if strongly water-wet, provides an efficient seal to the reservoir disallowing upwards CO_2 migration (Arif et al., 2016a; Armitage et al.,

*Reference: Arif et al. (2017) in *Geophysical Research Letters*, 10.1002/2017/GL073532

2013; Chaudhary et al., 2015; Iglauer et al., 2015a). However, rock material can be even strongly CO_2-wet (Arif et al. 2016b) – which would massively reduce storage capacity (Al-Menhali et al., 2016; Chaudhary et al., 2013; Iglauer et al., 2015a,b) – and shale wettability has so far only been reported for low-TOC shales (Chaudhary et al., 2015; Iglauer et al., 2015b; Roshan et al., 2016; Shojai Kaveh et al., 2016) despite the fact that shales can be very rich in organic carbon, i.e. high-TOC (Vernik and Milovac, 2011).

Furthermore, recently there is a mounting interest in utilizing shale as a CO_2 storage medium itself (whereby CO_2 is injected through fractured horizontal wells), where CO_2 is stored by adsorption trapping (Ferno et al., 2015; Li and Elsworth, 2015; Kim et al., 2017) with the benefit of producing additional methane (Busch et al., 2008; Kang et al., 2011, Li and Elsworth, 2015)).

In both scenarios (caprock role and large CO_2 sink), shale wettability relates to CO_2 storage capacity and containment security (Arif et al., 2016b; Saghafi et al., 2014; Shojai Kaveh et al., 2012; Iglauer et al., 2015a). However, there is a serious lack of understanding in terms of how shale organic content (TOC) influences wettability, even though it has been shown that even minute TOC strongly affects storage capacities and containment security (Iglauer et al., 2015a).

Here we thus systematically analysed a broad range of shale TOC (from 0.16 wt% to 23.4 wt%) at in-situ storage conditions, and we demonstrate that shale TOC clearly scales with the CO_2-wettability: a high TOC content clearly led to strongly CO_2-wet conditions, while low TOC contents led to water-wet conditions, and medium TOC content was in between. We conclude that for the conventional caprock role, shale should have minimum TOC content to maximise storage capacity; while shale formations with a high TOC content are potentially suitable as large CO_2 sinks via CO_2 adsorption trapping.

6.2 Experimental Procedure

6.2.1 Materials

Four shale samples of low, medium, high and ultrahigh TOC content were systematically analysed, sample characteristics are summarized in Table 6-1. The samples were cut to cuboid shape (1 cm x 1 cm x 0.4 cm) with a diamond cutter. All the measurements were conducted using 1M NaCl brine which was prepared by dissolving NaCl (purity ≥ 0.995 mass %) in deionized (DI) water (Ultrapure from David Gray; electrical conductivity = 0.02 mS/cm; and de-gassed by vacuuming for 12 hours). CO_2 used was 99.9 mol% (from BOC, gas code-082). Acetone (99.9 mol%, Rowe Scientific) was used to wash the sample surfaces.

Table 6-1 Shale sample description, characterization and mineralogy.

Sample ID	Type of shale	Location	TOC* (mg/kg)	Surface roughness (nm)	Composition from XRD		Porosity range, % (from literature)
					mineral	wt %	
Shale-A	Laminated shale (Low-TOC)	Little Falls, New York, USA	1600 (0.16 wt%)	350	Quartz	37	0 – 18[a]
					Calcite	7	
					Albite	27	
					Microcline	4	
					Illite	24	
					Chlorite	1	
Shale-B	Bituminous shale (Medium-TOC)	Montana, USA	11000 (1.1 wt%)	1300	Quartz	17	3.5 – 8[b]
					Calcite	45	
					Ankerite	14	
					Albite	5	
					Pyrite	1	
					Illite	18	
Shale-C	Oil shale (High-TOC)	Garfield Co. Colorado, USA	117000 (11.7 wt%)	770	Quartz	11	4.22 – 10.77[c]
					Calcite	16	
					Ankerite	38	
					Albite	18	
					Microcline	11	
					Pyrite	1	
					Illite	5	
Shale-D	Oil Shale		234000	290	Quartz	12	8 – 19.9[d]

	Ultrahigh-TOC	Wessex Coast, Southern England	(23.4 wt%)		Calcite	28	
					Dolomite	28	
					Oligoclase	20	
					Microcline	4	
					Pyrite	1	
					Illite	7	

*TOC was measured using high temperature combustion and IR detection method at NMI, Australia

[a] David et al. (2004)

[b] Magner, (1963)

[c] Randolph, (1983)

[d] Curtis et al. (2012a)

6.2.2 Contact angle measurements

CO_2-wettability of the shale samples was measured with a pendant-drop tilted plate goniometric setup (Lander et al., 1993). The experimental configuration has been described elsewhere (Arif et al., 2017b). Prior to each measurement, the samples were washed with acetone and then cleaned for 3 minutes using air plasma (Love et al., 20005).

The samples were then positioned inside the pressure cell on the tilted plate and the cell was heated to the desired temperature (323 K, and 343 K). Subsequently, CO_2 pressure in the cell was raised to desired values (0.1 MPa, 5 MPa, 10 MPa, 15 MPa and 20 MPa). The temperature of the cell was controlled by means of a wrapped heating tape. The fluids used were thermodynamically equilibrated with an equilibrium reactor (Parr 4848 reactor controller, John Morris Scientific, (El-Maghraby et al., 2012)). Note that CO_2 was in supercritical state during the measurements at pressures 10 MPa, 15 MPa and 20 MPa, and the surface used were dry i.e. not pre-saturated with any fluid.

After pressure stabilization, a droplet of de-gassed brine was dispensed onto the substrate by a needle; and the advancing (θ_a) and receding (θ_r) water contact angles were measured simultaneously (Lander et al., 1993) at the leading and trailing edge of the droplet, just before the droplet started to move. A high-resolution video camera (Basler scA 640–70 fm, pixel size = 7.4 μm; frame rate = 71 fps; Fujinon CCTV lens: HF35HA-1B; 1:1.6/35 mm) was used to record movies of these whole processes, and

θ_a and θ_r were measured on images extracted from the movie files. The standard deviation of the angle measurements was ± 4°.

6.3 Results and Discussion

The influence of TOC on CO_2-wettability for the four shale samples (low, medium, high and ultra-high TOC shales) was comprehensively tested for a wide range of operating pressures (0.1–20 MPa) at 343 K, results are represented in Fig. 6-1a as a 3D plot with a log-linear fit (contact angle expressed as a function of TOC and pressure).

The shale/CO_2/brine system turned more CO_2-wet with increasing TOC, i.e. θ_a and θ_r, exhibited a clear increase with TOC throughout the tested experimental matrix (Fig. 6-1). A sharp increase in contact angle was observed when TOC increased from low to medium (i.e. 0.16 wt% to 1.1 wt%), however with further TOC increase from high to ultrahigh (i.e. 11.7 wt% to 23.4 wt%), the corresponding increase dampened out. For instance, at 20 MPa and 343 K, θ_a increased from 78° to 125° and θ_r increased from 71° to 109° when sample TOC increased from 0.16 wt% to 1.1 wt% (low to medium) implying that the wettability of the system shifted from weakly water-wet to weakly CO_2-wet (refer to the classification by Iglauer et al., 2015a). However, for the TOC increment from 11.7 wt% to 23.4 wt% (high to ultrahigh), at the same operating conditions (20 MPa and 343 K), θ_a only increased from 140° to 145° and θ_r increased from 130° to 134°, i.e. the system turned strongly CO_2-wet. Specifically, at any given operating pressure and temperature, the ultrahigh-TOC shale was found to be most non-wetting to water, while low-TOC shale was most water-wet. For instance, at 15 MPa and 343 K, θ_a measured 72°, 120°, 132°, and 142° and θ_r measured 63°, 104°, 123°, 131° for the low, medium, high and ultrahigh TOC shales, respectively. The results imply that low-TOC shale was weakly water-wet, medium-TOC shale was intermediate-wet, high-TOC shale was weakly CO_2-wet and ultrahigh-TOC shale was strongly CO_2-wet at typical storage conditions. Strongly CO_2-wet characteristic of ultra-high TOC shales is consistent with high rank coal (semi-anthracite) which are also strongly CO_2-wet at 20 MPa and 323 K (Arif et al., 2016c). Similarly, medium TOC shale which is intermediate-wet compares with medium rank coal which is intermediate-wet at 15 MPa and 323 K (Arif et al., 2016c). Overall, increase in CO_2-

wettability with TOC is consistent with increase in CO_2-wettability of coal with coal rank (cp. Arif et al., 2016c; Shojai Kaveh et al., 2012).

Further, an increase in pressure pronounced the effect of TOC on contact angle following a consistent trend at all pressures suggesting that the influence of organic content on wettability depends on the formation depth. Overall, the measured contact angles followed a logarithmic variation with TOC and a linear variation with pressure. Consequently, the following fits described the relationship of advancing and receding water contact angles as a function of TOC and operating pressure (P) for the data presented in Fig. 1a:

$$\theta_a = 54.33 + 3.14P + 25.4 \log TOC \qquad Eq.6.1$$

$$\theta_r = 46.025 + 2.98P + 25.67 logTOC \qquad Eq.6.2$$

In eq. 6.1 and 6.2, TOC is in wt% and 'P' is pressure in MPa, and these fits are based on data of four shales only. R^2-values for these multiple regression fits are 0.9135 for θ_a and 0.9215 for θ_r.

Shale pore network comprises of a) inorganic porosity (clay and non-clay minerals), and b) organic matter porosity where the organic pores are hydrophobic while the inorganic pores are hydrophilic (Curtis et al., 2012b). Despite the higher portion of minerals in shale, the composite wetting behaviour of shale is controlled by an overall pore network connectivity of organic matter and mineral matter porosity (Hu et al., 2016). Thus, the CO_2-wet nature of samples C and D indicates that organic matter dominates the composite wetting behaviour. In addition, shale B, which is only 1.1 wt% TOC, is intermediate-wet is also attributed to calcite dominance in the mineral percentage (45%, XRD data, Table 6-1), and pure calcite is intermediate-wet in a CO_2/brine system (Arif et al. 2017a). The increase in contact angle with TOC can be attributed to the higher organic content of the shale sample, which leads to a more hydrophobic surface and surface de-wetting (cp. Dickson et al. 2006; Arif et al., 2016c). Shale TOC can thus be regarded as a measure of the shale hydrophobicity in CO_2-water-shale systems, with high-TOC shale demonstrating more CO_2-wet

behaviour. Moreover, there is mounting evidence that shales become patchily oil-wet through in-situ maturation of organic matter or exposure to organic compounds found in formation water (Larter et al., 1996). In addition, the increase in contact angle with pressure is also evident from previous work on low-TOC shales (Iglauer et al., 2015b; Roshan et al., 2016; Shojai Kaveh et al., 2016). Physically, the increase in contact angle with pressure is attributed to a reduction in the solid/CO_2 interfacial tension with pressure which promotes de-wetting of the surface, resulting in higher water contact angles (Arif et al., 2016d) and an associated increase in CO_2-rock intermolecular interactions.

Moreover, we found two distinct trends of wettability variation with temperature (Figure 1b). θ decreased with temperature for the medium, high and ultrahigh-TOC shale samples, consistent with the reduction in CO_2-adsorption with increasing temperature [*Mosher et al.*, 2013], while θ increased with temperature for the low-TOC sample consistent with *Iglauer et al.* (2015b) and *Roshan et al.* (2016). We note that such distinct trends of shale wettability alteration with temperature is not clear so far and requires further investigation.

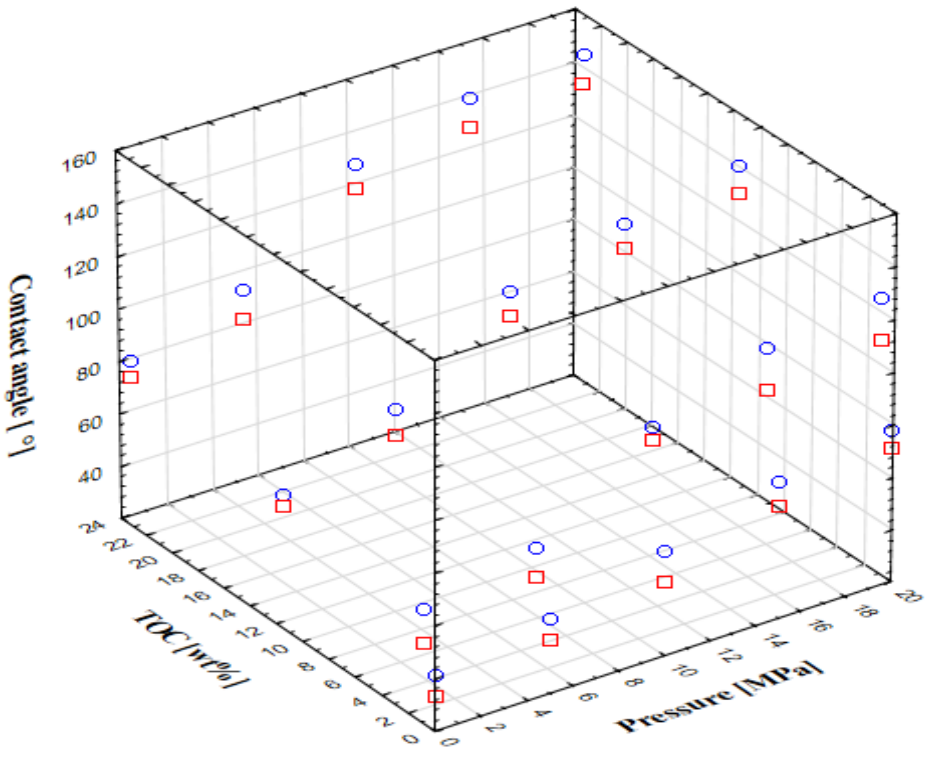

Wettability scale:
Strongly CO_2-wet (130° < θ < 180°)
Weakly CO_2-wet (110° < θ < 130°)
Intermediate-wet (70° < θ < 110°)
Weakly water-wet (50° < θ < 70°)
Strongly water-wet (0° < θ < 50°)

a)

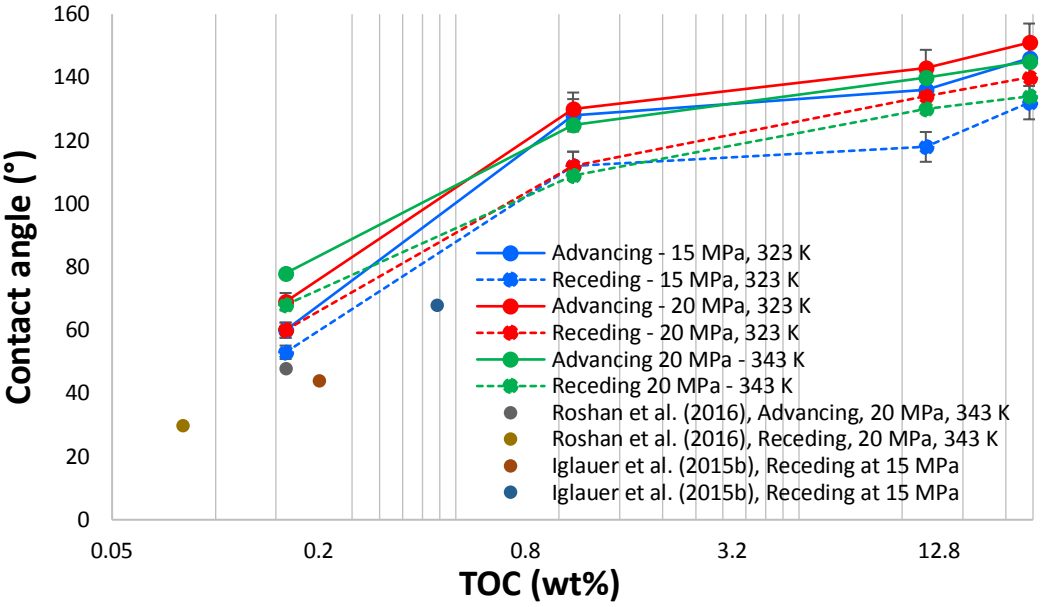

b)

Fig. 6-1 Advancing and receding water contact angles of shale/CO_2/1 M NaCl systems as a function of TOC and operating pressure (at 343 K). a) 3D plot of contact angle vs. P vs. TOC b) 2D plot of θ_a and θ_r as a function of temperature and showing literature data.

6.4 Implications for CO_2 geo-storage

The shale wetting behaviour can be related to the way shale is utilized in a storage project, as a function of shale-TOC. Low-TOC shale, which is strongly water-wet to weakly water-wet at storage conditions, is suitable for its classical caprock role as the stronger capillary forces in water-wet pores can outbalance higher CO_2 buoyancy forces (i.e. higher CO_2 column heights, Naylor et al., 2011; Iglauer, 2017). Note that the reported data also implies that the capillary sealing efficiency will be higher at lower pressure, salinity and temperature (due to lower θ cp. Arif et al., 2016a; 2017b; Iglauer et al., 2015b; Broseta et al. 2012).

On the contrary, if the caprock is an organic-rich shale (high TOC), a pertinent risk would entail to the containment security due to the CO_2-wet characteristics of these

shales i.e., negative capillary pressure will prevail under such conditions and thus leakage will occur. However, such shales (i.e. medium, high and ultrahigh TOC) can potentially be utilized as storage media themselves, i.e., they are potentially large CO_2 sinks due to their high CO_2-wettability which eases CO_2-adsorption on the organic matter in such shales (Arif et al., 2016c; Saghafi et al., 2014; Shojai Kaveh et al., 2012), and thus significant CO_2 adsorption-trapping. CO_2 injection into such organic rich shales (medium to ultrahigh TOC) is coupled with the additional benefit of enhanced methane recovery (Busch et al., 2008; Zhang et al., 2012). As soon as CO_2 wets the pore spaces, it expels methane to flow through the fracture network and get produced while CO_2 gets stored within the process (Gray, 1987; Saghafi et al., 2014). In summary, the reported data provides a guideline for the optimum caprock and shale formation selection for CO_2 storage.

From practical standpoint, however, there are certain challenges associated with CO_2 injection and subsequent storage in shales. First is the limited injectivity due to the extremely low permeability, which is currently an active area of research (Ferno et al., 2015; Kim et al., 2017). Although it has been shown that CO_2 flooding through fractured horizontal wells overcomes this limitation and is field tested as well (Eshkalak et al., 2014; Kim et al., 2017), yet the diffusion induced CO_2/CH_4 exchange and the subsequent CO_2 transport and accessibility of shale micropores which is influenced by fracture spacing (Busch et al., 2016), and constitutes a future research aspect.

Shale matrix swelling by CO_2 injection is another limiting factor, however, sorption induced shale swelling is not confirmed and not well understood as yet (Busch et al., 2016), compared to coal swelling which is well established (i.e. coal matrix permeability declines due to swelling by CO_2 (Brochard et al., 2012). There are experimental evidences that the shale swelling by CO_2 is 'reversible' i.e. permeability lost due to swelling retains its original values after sufficient interaction with CO_2 (Chareonsuppanimit et al., 2012; Kumar et al., 2016).

6.5 Conclusions

CO_2 geological sequestration (CGS) is a promising technology to reduce anthropogenic greenhouse gas emissions (IPCC, 2005). In CGS, caprock wettability

characterization is essential to elucidate the conditions that lead to safe storage conditions (Iglauer et al., 2015a). Thus shale CO_2-wettability as a function of TOC at in-situ conditions was reported here to evaluate the effective role shale can offer during CO_2 geo-sequestration. Water contact angles increased with TOC. This increase was sharp up to ~1wt% TOC and almost flattened out above ~11 wt% TOC for all conditions tested. Thus, at typical storage conditions (e.g. 20 MPa and 343 K), the higher the TOC was, the greater was the tendency of CO_2 to wet the shale, i.e. ultrahigh-TOC shale was strongly CO_2-wet, high-TOC shale was weakly CO_2-wet, medium-TOC shale was intermediate-wet and low-TOC shale was water-wet.

We thus conclude that low-TOC shale is more suitable as a classical caprock as it can render larger CO_2 columns immobile in structural trapping due to its water-wet behaviour (Iglauer et al., 2015a,b). However, if TOC is above 1.1 wt%, the shale is CO_2-wet. Although such shale may not be suitable as caprock, it may provide a large CO_2 sink via adsorption trapping (Busch et al., 2008; Chareonsuppanimit et al., 2008; Zhang et al., 2012; Kim et al., 2017).

It is clear, however, that in all cases precise knowledge of shale TOC and the associated CO_2-wettability is vital for accurate storage capacity and containment security predictions.

While the CO_2-wet behaviour of organic rich shales predicted in this work is encouraging for CO_2-adosprtion potential from geological storage prospective, the factors such as shale swelling, diffusion driven CO_2 transport, and hydraulic fracturing of shales require further investigation to develop an overall framework of CO_2 sequestration in organic-rich shales.

Chapter 7 Solid/CO_2 and solid/water interfacial tensions as a function of pressure, temperature, salinity and mineral type: Implications for CO_2-wettability and CO_2 geo-storage*

Abstract:

Wettability of CO_2/brine/mineral systems plays a significant role in the underground geological storage of CO_2 as it governs the fluid flow and distribution mechanism within the porous medium. Technically, wettability is influenced by CO_2 pressure, the temperature of the storage formation, formation water salinity and the type of mineral under investigation. Although a growing number of studies report wettability data for CO_2/water/mineral systems, yet the factors responsible for wettability variation with pressure and temperature remain unclear. In this work, we used the concept of surface energy to explain dependency of wettability on pressure, temperature and salinity. Neumann's equation of state approach was used to compute solid/CO_2 and solid/water interfacial energies using reliable contact angle and CO_2/brine interfacial tension data from the literature at a wide range of operating conditions for quartz, water-wet mica, oil-wet mica and high, medium and low-rank coals. Moreover, the all-important question that why different minerals offer different wettability to CO_2/water systems at the same pressure and temperature of investigation is addressed by comparing the interfacial energies of the minerals. We found that for all minerals solid/CO_2 interfacial energy decreased with pressure and increased with temperature, and solid/water interfacial energy decreased with temperature except for quartz for which solid/water interfacial energy increased with temperature. Furthermore, the solid/CO_2 interfacial energy was lowest for the oil-wet mica surface and highest for quartz which is due to higher hydrophobicity of oil-wet mica surface. The results of the study lead to a better understanding of the wetting phenomenon at the CO_2/brine/mineral interface and thus contribute towards the better evaluation of geological CO_2-storage processes.

Keywords: Mineral/CO_2 interfacial tension, Wettability, Contact angle, Quartz, Mica, Coal

*Reference: Arif et al. (2016) in *International Journal of Greenhouse Gas Control*, 53, 263-273

7.1 Introduction

Carbon capture and storage in depleted hydrocarbon reservoirs or deep saline aquifers contributes significantly towards the reduction of anthropogenic greenhouse gas emissions (IPCC, 2005). CO_2 is also injected into subsurface reservoirs for enhanced oil and gas recovery (e.g. Blunt et al., 1993; Iglauer et al., 2013, 2016; Lackner, 2003). In this context the wettability of CO_2-brine-mineral systems plays a crucial role in deciding the fate of the injected CO_2 within the geological formation (Iglauer et al., 2015a). The existing literature has reported experimental CO_2-wettability data as a function of pressure, temperature and salinity for rock forming minerals such as quartz (Al-Yaseri et al., 2016a; Saraji et al., 2014; Sarmadivaleh et al., 2015), mica (Arif et al., 2016a, b; Broseta et al., 2012; Chiquet et al., 2007) and coals (Arif et al., 2016c; Shojai Kaveh et al., 2012; Siemons et al., 2006). Further, molecular dynamics simulations also computed contact angles for CO_2-brine-quartz systems (Chen et al., 2015; Iglauer et al., 2012; Javanbakht et al., 2015; Liu et al., 2010; McCaughan et al., 2013). However, no significant attention has been given to evaluate the factors which are responsible for wettability variation with pressure, temperature and salinity despite the variations in trends observed in studies on CO_2 wettability of minerals (e.g. θ increased in temperature for quartz/CO_2/brine, Al-Yaseri et al., 2016a and decreased with temperature for mica/CO_2/brine and coal/CO_2/brine systems, Arif et al., 2016a,c).

Recently, a few studies attempted to explain the factors responsible for wettability variation. For instance, Al-Yaseri et al. (2016b) reported that wettability of quartz/gas/brine systems is a strong function of gas density and a mathematical correlation was developed to determine contact angles from gas densities. However, the methodology was applicable to a limited set of operating conditions only. Roshan et al. (2016) developed a physical model based the concept of the diffuse double layer to provide a theoretical framework for changes observed in wettability as a function of pressure, temperature and salinity and found that wettability is strongly related to CO_2/water interfacial tensions and density changes. Ameri et al. (2013) computed sandstone/CO_2 interfacial tension as a function of pressure using Neumann's equation of state (Neumann et al., 1974) and found that the solid/CO_2 interfacial tension decreased with pressure and they formulated that such change in solid surface energy is responsible for wettability changes. Nevertheless, the factors responsible for

wettability variation with pressure, temperature and salinity remain unclear and require further attention.

Theoretically, it is well-established that the contact angle is a function of the interplay of the three interfacial tensions (solid/CO_2, solid/brine and brine/CO_2) as related by Young-Laplace equation below:

$$cos\theta = \frac{\gamma_{sc} - \gamma_{sw}}{\gamma_{cw}} \qquad Eq.\,6.1$$

In Eq. 6.1, γ_{sc}, γ_{sw} and γ_{cw} denote solid/CO_2, solid/water and CO_2/water interfacial tensions respectively. To assess the wettability dependence on these interfacial interactions, the quantification of the three interfacial tensions (γ_{sc}, γ_{sw} and γ_{cw}) is essential. In this context, CO_2/water interfacial tensions (γ_{cw}) can be determined experimentally (many studies reported this data e.g. Li et al., 2012; Lun et al., 2012), however, an independent experimental measurement of solid/fluid interfacial tension is not possible because a solid interface is very different from a fluid-fluid interface due to absence of mobility (Li and Neumann, 1992). Consequently, the use of numerical/empirical techniques such as Neumann's equation of state becomes essential (Neumann et al., 1974). They applied this method to compute surface energies of low energy polymers (Neumann et al., 1974, Kwok and Neumann, 1999). We, thus, extend the use of Neumann's equation of state to compute mineral/CO_2 and mineral/water interfacial tensions as a function of pressure, temperature, salinity and mineral type. Essentially, three important issues are addressed in this work: 1) Computation of surface energy of solid/CO_2 and solid/brine as a function of pressure, temperature and salinity, 2) How these computed interfacial tensions explain the dependence of wettability on pressure, temperature and salinity and 3) To answer a very important question, i.e. why different minerals exhibit different wettability at the same operating conditions.

In this context, we used advancing and receding contact angle (θ_a and θ_r respectively) data for CO_2/brine systems for quartz (from Al-Yaseri et al., 2016a), water-wet mica (from Arif et al., 2016a; and the mica chosen is muscovite mica), oil-wet mica (from Arif et al., 2016b) and coal (from Arif et al., 2016c) at a wide range of operating conditions and computed mineral/CO_2 and mineral/water interfacial tensions and analysed the associated trends. Our results depict that mineral/CO_2 interfacial tension decreased with pressure and increased with temperature for all minerals. However, mineral/water interfacial tension decreased with temperature for mica and coals but

increased with temperature for quartz. The computed data in this paper can also be used to estimate contact angle from Young's equation at any pressure, temperature and salinity using known values of surface energies. Finally, we conclude that the quantification of surface energies is not only helpful in understanding the CO_2/solid interactions but also adequately explain the factors influencing wettability and thus considerably improve the understanding of geological storage processes and provide independent estimates for surface energies for various other engineering applications.

7.2 Methodology

We used the equation of state approach by Neumann (Neumann et al., 1974) to compute mineral/CO_2 and mineral/water surface energies for a wide range of operating conditions for quartz, water-wet mica, oil-wet mica, and coals of high, medium and low ranks. Following sections describe the methodology in detail.

7.2.1 Contact angle data

We selected the water advancing and receding contact angle (θ_a and θ_r) data from our previous publications (quartz: from Al-Yaseri et al., 2016a, water-wet mica from Arif et al., 2016a, and oil-wet mica from Arif et al., 2016b; high, medium and low rank coals: from Arif et al., 2016c; Table 7-1). Surface energy calculations require equilibrium contact angles (see detail below); these have been computed from Tadmor's empirical method (Tadmor, 2004, Table 7-2). Tadmor's correlation allows the calculation of equilibrium contact angles using the corresponding values of advancing and receding contact angles. The equations are as follows:

$$\theta_e = arccos\left(\frac{\Gamma_A \cos\theta_A + \Gamma_R \cos\theta_R}{\Gamma_A + \Gamma_R}\right) \qquad \text{Eq. 6.2}$$

In Eq. 6.2, θ_e is the equilibrium contact angle while θ_A and θ_R are the advancing and receding contact angles respectively, whereas, Γ_R and Γ_A are defined as follows:

$$\Gamma_R = \left(\frac{\sin^3\theta_R}{2 - 3\cos\theta_R + \cos^3\theta_R}\right)^{1/3} \qquad \text{Eq. 6.3}$$

$$\Gamma_A = \left(\frac{\sin^3\theta_A}{2 - 3\cos\theta_A + \cos^3\theta_A}\right)^{1/3} \qquad \text{Eq. 6.4}$$

Neumann et al.'s equation of state approach also requires CO_2/water interfacial tension data which was taken from Sarmadivaleh et al. (2015) and CO_2/brine interfacial tension was taken from Arif et al. (2016a), Table 7-3.

Table 7-1 Contact angle data for CO_2-deionized (DI) water systems for minerals investigated in this study.

T (K)	P (MPa)	Quartz		Water-wet mica		Oil-wet mica		High rank coal		Medium rank coal		Low rank coal	
		θ_a (°)	θ_r (°)	θ_a (°)	θ_r (°)	θ_a (°)	θ_r (°)	θ_a (°)	θ_r (°)	θ_a (°)	θ_r (°)	θ_a (°)	θ_r (°)
308*	0.1	0	0	10	5	90	65	37	30	32	25	43	32
	5	15	11	33	25	125	107	94	80	77	63	75	60
	10	23	17	55	50	148	128	140	126	127	115	103	87
	15	30	20	71	63	170	159	146	134	128	118	112	96
	20	37	23	80	72	172	160	151	139	137	121	122	110
323	0.1	0	0	4	0	74	64	51	45	28	22	38	27
	5	19	13	30	24	118	102	89	79	69	49	50	42
	10	30	25	48	40	143	125	129	114	108	98	94	78
	15	38	28	59	54	170	157	136	123	114	102	102	91
	20	42	35	70	62	170	158	141	129	122	112	116	107
343	0.1	0	0	0	0	73	65	58	53	18	12	27	18
	5	22	19	27	22	99	82	86	74	48	33	45	36
	10	42	30	43	36	108	91	109	97	95	85	92	77
	15	45	38	52	48	128	110	119	111	102	89	102	87
	20	50	42	62	53	156	134	125	114	113	95	110	97

*contact angles are interpolated at 308 K for quartz

Table 7-2 Equilibrium contact angles for all minerals calculated using Tadmor's correlation.

T (K)	P (MPa)	Equilibrium contact angle θ_e (°)					
		Quartz	Water-wet mica	Oil-wet mica	High rank coal	Medium rank coal	Low rank coal
308	0.1	0	6	74.1	33.3	28.2	36.9
	5	12.9	28.7	112.8	85.8	69	66.4
	10	19.8	52.4	131.8	130	119	93.2
	15	24.2	66.7	159.9	137	122	102

	20	29	75.7	160.5	142	126	115
323	0.1	0	2	68.49	47.8	24.8	31.9
	5	15.7	26.8	107.7	83.4	57.1	45.7
	10	27.4	43.7	129.3	119	102	84.4
	15	32.5	56.4	157.8	127	107	95.6
	20	38.3	65.7	158.8	133	116	111
343	0.1	0	0.5	68.67	55.4	14.7	22
	5	20.4	24.3	88.62	79.2	39.4	40.1
	10	35.3	39.3	97.35	102	89.3	83.1
	15	41.3	49.9	115.6	114	94.3	92.9
	20	45.7	57.1	136.6	118	101	102

Table 7-3 CO_2/DI-water and CO_2/brine interfacial tension data used.

Temperature (K)	Pressure (MPa)	CO_2/DI-water IFT[a] (mN/m)	CO_2/brine[*] IFT[b] (mN/m)
308	0.1	75.8	72.9
	5	40.2	50.1
	10	28.4	38.2
	15	22.7	33.9
	20	21.0	32.3
323	0.1	73.1	72.0
	5	49	55.3
	10	35.5	42.6
	15	29	38.7
	20	26	36.0
343	0.1	65	69.2
	5	52.18	57.7
	10	43	44.8
	15	34.5	39.7
	20	27	37.7

[a] experimental data from Sarmadivaleh et al. (2015), values interpolated at 308 K and 323 K

[b] experimental data from Arif et al. (2016a)

[*]20wt% NaCl in DI water

7.2.2 Surface free energy computation

The surface free energy of solids has been investigated by a growing number of studies (e.g. Ameri et al., 2013; Dickson et al., 2006; Kwok and Neumann, 2000; Zenkiewicz, 2007) as it is of great practical significance for many engineering applications including catalysis, coatings, flotation, printing and polymer sciences (Zenkiewicz, 2007). The most common approaches include the Zisman method (Fox and Zisman, 1952), the Fowkes method (Fowkes, 1964), the geometric-mean approach (Owens and Wendt, 1969), the harmonic-mean approach (Wu, 1971), the equation of state approach or Neumann's method (Neumann et al., 1974) and the acid-base approach or van Oss-Good method (van Oss et al., 1986). We chose Neumann's equation of state method because of convenience in its application as it requires the knowledge of experimental contact angle, θ, and CO_2/water interfacial tension (γ_{cw}) data for which reliable data is available.

Thermodynamically, solid/CO_2, solid/water and CO_2/water interfacial tensions (γ_{sc}, γ_{sw} and γ_{cw}) are interrelated by an equation of state (Neumann et al., 1974), such that:

$$\gamma_{SW} = f(\gamma_{SC}, \gamma_{CW}) \qquad \text{Eq. 6.5}$$

Neumann et al. (1974) used the hypothesis that the free energy of adhesion per unit area of a solid-liquid pair is equal to the work required to separate a unit area of solid-liquid interface and that free adhesion energy was proposed to be equal to the geometric mean of the solid cohesion work and the liquid cohesion work. These geometric means were combined so that Eq. 6.6 resulted (for a complete derivation the reader is referred to Ameri et al., 2013).

$$\gamma_{sw} = \gamma_{sc} + \gamma_{cw} - 2\sqrt{\gamma_{cw}\gamma_{sc}}[1 - \beta(\gamma_{cw} - \gamma_{sc})^2] \qquad \text{Eq. 6.6}$$

Eq. 6.7 below was then derived by Ameri et al., (2013) to find an expression for γ_{sc} instead of γ_{sw} as shown:

$$\gamma_{sc} = \gamma_{sw} + \gamma_{cw} - 2\sqrt{\gamma_{cw}\gamma_{sw}}[1 - \beta(\gamma_{cw} - \gamma_{sw})^2] \qquad \text{Eq. 6.7}$$

'β' is a constant which is related to the fit of the original experimental data (Neumann et al., 1974) to the model and in the present case it can be determined by non-linear regression of contact angle (θ) and CO_2/water interfacial tension data (γ_{cw}) as further explained below.

Combining Eq. 6.1 and 6.7, one obtains:

$$\cos\theta_e = 1 - 2\sqrt{\frac{\gamma_{sw}}{\gamma_{cw}}}[1 - \beta(\gamma_{cw} - \gamma_{sw})^2] \qquad \text{Eq. 6.8}$$

Ameri et al., (2013) applied equation 6.7 and 6.8 to determine solid/CO_2 interfacial tension of oil-wet Bentheimer sandstone as a function of pressure and they reported the corresponding values of solid/liquid interfacial tension derived by non-linear regression. To account for a systematic evaluation of wettability dependence on pressure, temperature and salinity, we express equations 6.7 and 6.8 to demonstrate that these are functions of pressure, temperature and salinity:

$$\gamma_{sc(P,T,S)} = \gamma_{sw(T,S)} + \gamma_{cw(P,T,S)} - 2\sqrt{\gamma_{cw(P,T,S)}\gamma_{sw(T,S)}}\left[1 - \beta\left(\gamma_{cw(P,T,S)} - \gamma_{sw(T,S)}\right)^2\right] \qquad \text{Eq. 6.9}$$

$$\cos\theta_{e\,(P,T,S)} = 1 - 2\sqrt{\frac{\gamma_{sw(T,S)}}{\gamma_{cw(P,T,S)}}}\left[1 - \beta\left(\gamma_{cw(P,T,S)} - \gamma_{sw(T,S)}\right)^2\right] \qquad \text{Eq. 6.10}$$

The scripts P, T and S refer to pressure, temperature and salinity, respectively, and are added to the interfacial energy terms to elucidate their dependence on them. It is notable that γ_{sw} is dependent on temperature and salinity but not on pressure (Ameri et al., 2013; Neumann et al., 1974). This is the basic assumption of the Neumann's equation of state.

Our computations begin with input data acquisition which includes a) advancing and receding contact angle data for quartz (Al-Yaseri et al., 2016a), water-wet mica (Arif et al., 2016a), oil-wet mica (Arif et al., 2016b) and coals of high medium and low ranks (Arif et al., 2016c) listed in Table 7-1, and b) CO_2/water interfacial data (Sarmadivaleh et al., 2015), listed in Table 7-3. Then, $\cos\theta_e$ (cosine of the equilibrium

contact angle) is calculated using advancing and receding contact angle data for all cases analysed (results in Table 7-2). In the next step, $\gamma_{sw(T)}$ and the constant 'β' are determined by least squares fitting of the $\cos\theta_e$ and γ_{cw} data. To accomplish this, $\cos\theta_e$ is first calculated by using equation 6.10 for any trial values of $\gamma_{sw(T)}$ and 'β' and is plotted against γ_{cw} (this data is referred as model data). Moreover, the experimental $\cos\theta_e$ (Table 7-2) is also plotted against γ_{cw} (such a plot is shown in Fig. 7-1 for all minerals analysed at 343 K), the regression analysis of these data-sets yield final values of $\gamma_{sw(T)}$ and 'β' corresponding to the best-fit (note: such plots are created at all three analysis temperatures and for all minerals, and directly provide values of $\gamma_{sw(T)}$ as a function of temperature). Finally, using these calculated values, solid/CO_2 interfacial tension is computed using equation 6.9 as a function of pressure, temperature, salinity and type of the mineral.

7.2.3 Regression fit of data

As a first step, $\cos\theta_e$ (experimental) is plotted against γ_{cw} and on the same plot $\cos\theta_e$ (calculated using equation 6.10 for arbitrary values of γ_{sw} and 'β') is also plotted againstγ_{cw}. Such plots are constructed corresponding for each temperature and for all five cases analysed. An example is shown in Fig. 7-1**Error! Reference source not found.**, where, for simplicity, only a temperature of 343 K is shown, but for all five minerals investigated. The model and experimental data are in a good agreement, however the model predictions are sensitive to CO_2/water interfacial tension values and thus reliable CO_2/interfacial tension input is required for reliable modelling of solid/fluid interfacial tensions.

The R^2-values, fitting parameters 'β' and γ_{sw} were computed for each case from the regression fits and the results are tabulated in Table 7-4. The standard deviations in experimental contact angle and interfacial tension data used were ±3° and ±3 mN/m respectively.

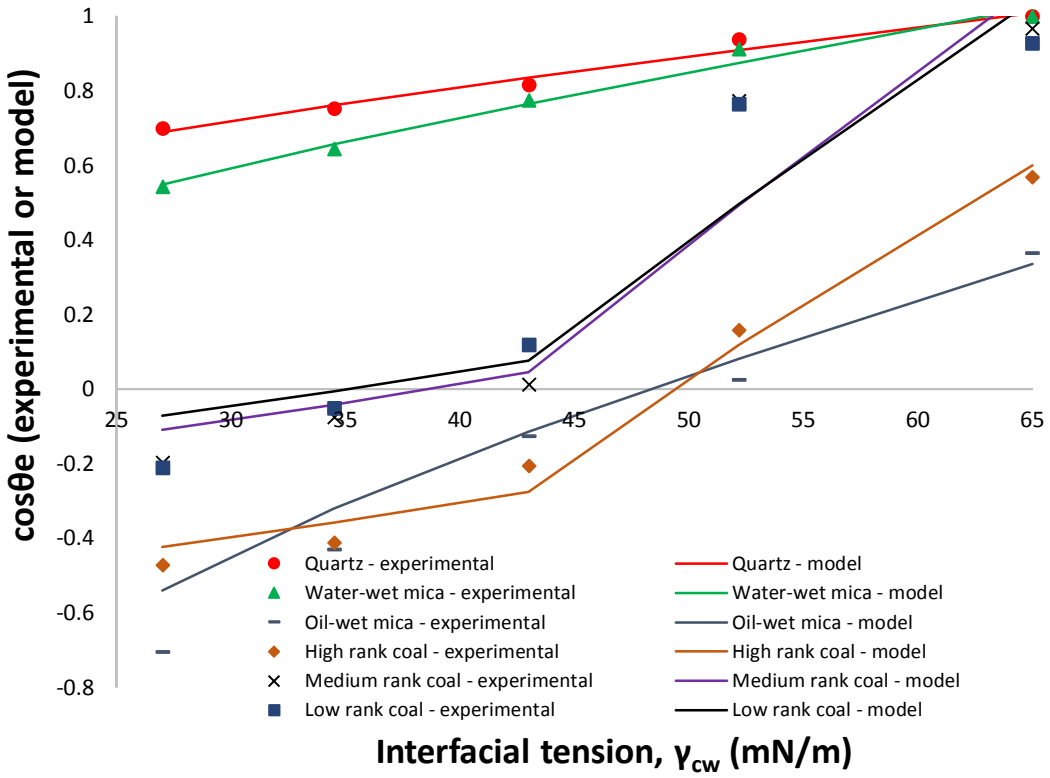

Fig. 7-1 Regression fit of experimental and model data for all minerals investigated at 343 K.

Table 7-4 Results obtained from regression fit of the experimental and model data.

Case	Temperature (K)	R^2	β	γ_{sw} (mN/m)
Quartz	308	0.898	0.000205	0.058
	323	0.943	0.000219	0.284
	343	0.988	0.0002524	0.952
Water-wet mica	308	0.899	0.00022	2.178
	323	0.935	0.00023	2.048
	343	0.992	0.00027	1.98
Oil-wet mica	308	0.9857	0.000166	20.19
	323	0.988	0.00022	25.47
	343	0.92	0.000145	16.53
High rank coal	308	0.9778	0.00033	20.25
	323	0.952	0.00028	19.23
	343	0.944	0.00021	15.37
Medium rank coal	308	0.994	0.00031	16.17
	323	0.974	0.0003	13.87
	343	0.93	0.00034	10.81

Low rank coal	308	0.989	0.00022	11.22
	323	0.954	0.0003	10.38
	343	0.946	0.00032	10.12

7.3 Results and discussion

We computed solid/CO_2 interfacial tension as a function of pressure, temperature and salinity and solid/water interfacial tension as a function of temperature and salinity via Neumann's equation of state (Neumann et al., 1974) for quartz, mica and coals using experimental contact angle data and CO_2/brine interfacial tension data. The results broaden the understanding of rock/fluid interaction properties. Specifically, the results of this study allow the understanding of the influence of surface energy on rock wettability as a function of pressure, temperature, salinity, and type of mineral. Thus, the results contribute to a better understanding of storage mechanisms which ensure containment security (Iglauer et al., 2015b; Krevor et al., 2015).

7.3.1 Effect of pressure on solid/CO_2 interfacial tension

7.3.1.1 Case 1: quartz

γ_{sc} (solid/CO_2 interfacial tension) decreased with pressure at all temperatures and for all cases analysed (Fig. 7-2). As the pressure increased from 0.1 MPa to 10 MPa, quartz/CO_2 interfacial tension decreased sharply from 75 mN/m to 31 mN/m at 323 K (Fig. 7-2). However, the decrease flattened for an additional pressure increment (from 15 MPa to 20 MPa it changed from 24.6 mN/m to 21.6 mN/m, a reduction of only 3 mN/m). A similar trend was found at elevated temperature, 343 K. Physically, as the pressure increases, the cohesive energy density of CO_2 increases and approaches to the cohesive energy of the substrate (Dickson et al., 2006). Eventually, the interactions between solid and CO_2 become more favourable and as a result, quartz/CO_2 interfacial energy decreases with pressure. Note that at pressure = 0.1 MPa, a switch in temperature occurs due to a switch in CO_2/water interfacial tensions; Table 7-3 (Arif et al., 2016a).

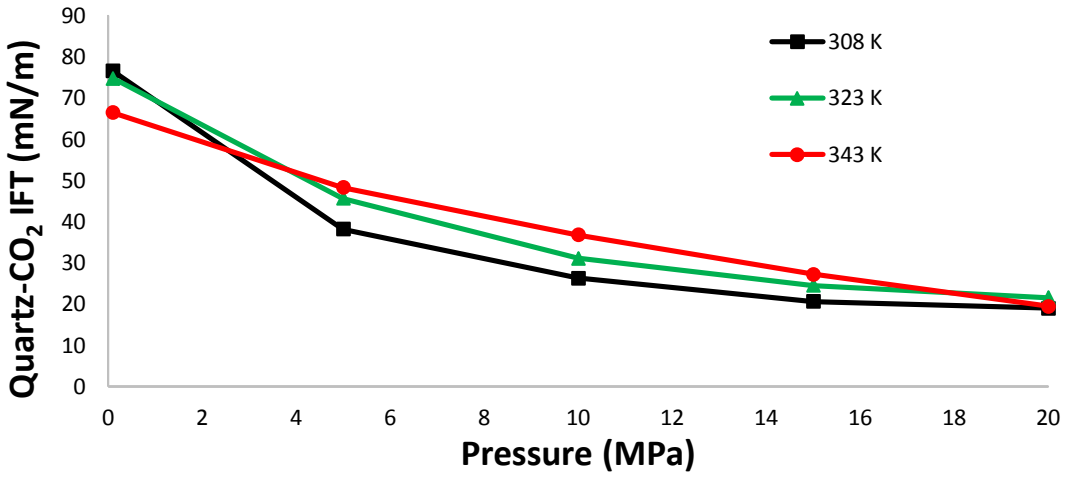

Fig. 7-2 Quartz/CO_2 interfacial tension as a function of pressure and temperature.

A few studies report surface free energies of quartz at ambient conditions. Janczuk and Zdziennicka, (1994) calculated the surface energy of quartz at ambient conditions against air using the van Oss-Good method (van Oss et al., 1986) and the values ranged from 57 mN/m to 126 mN/m, consistent with our value (~74 mN/m) estimated for a similar condition (0.1 MPa and 308 K).

Dickson et al. (2006) is the only major study which computed surface energies as a function of pressure for silica (glass)/CO_2 systems and found that for a partially methylated glass surface (63% of the surface was covered by methyl groups, the remaining 37% by SiOH groups) surface solid/CO_2 interfacial tension decreased with pressure. The values reported were 38 mN/m at a CO_2 activity of 0 (equivalent to a pressure of 0.1 MPa) and reduced to ~10 mN/m at a CO_2 activity of 1.4 (equivalent to 20 MPa) at 296 K. The decrease in quartz/CO_2 interfacial tension with pressure is thus consistent with Dickson et al. (2006), however, the difference in values is due to the fact that the surface they used had only 37% silanol group coverage (while in our case it is 100%, i.e. pure quartz). Furthermore, Dickson et al. (2006) reported solid/CO_2 interfacial tension for a 12% SiOH surface (now 88% of the surface was methylated), for which lower γ_{sc} values were reported (20 mN/m at 0.1 MPa and ~0 mN/m at 20 MPa) which is due to the higher hydrophobicity of the 12% SiOH surface (when compared with the 37% SiOH surface). Due to the limited number of silanol groups available, only a minimal amount of CO_2 is expected to cap these hydrophilic sites, thus γ_{sc} values were lower for lower silanol coverage (e.g. for our case γ_{sc} = 20 mN/m

at 20 MPa, and for Dickson et al. γ_{sc} = 10 mN/m for 37% SiOH surface, and ~0 mN/m for 12% SiOH surface).

The higher values of quartz/CO_2 interfacial tensions as compared to mica (see below) at a given pressure and temperature imply that quartz is more hydrophobic in nature.

7.3.1.2 Case 2: Mica

Two mica surfaces were analysed: a) naturally water-wet mica (Arif et al., 2016a) and b) oil-wet mica (treated with silane to achieve oil-wet conditions, ambient air/water contact angle = 120°, Arif et al., 2016b). The results indicate that, likewise quartz, mica/CO_2 interfacial tension decreased with pressure for both water-wet and oil-wet mica surfaces (Fig. 7-3). When pressure increased from 0.1 MPa to 5 MPa, mica/CO_2 interfacial tension decreased sharply from 78 mN/m to 41 mN/m, for water-mica. Gradually, the decrease flattened out with further increase in pressure (24 mN/m at 10 MPa and 16 mN/m at 20 MPa). Similar trends were found for oil-wet mica surface. However, at any given pressure, the mica/CO_2 interfacial tension was considerably higher for water-wet mica. For example, at 10 MPa and 343 K, mica/CO_2 interfacial tension was 40 mN/m for water-wet mica and only 4.6 mN/m for oil-wet mica surface. This result is quite remarkable – as it demonstrates that the hydrophobic surfaces (e.g. oil-wet mica - higher water contact angles) have considerably lower solid/CO_2 interfacial energies in comparison to the hydrophilic surfaces (e.g. water-wet mica, lower water contact angles, and quartz, even lower contact angles than water-wet mica). The permanent oil coating on the mica (to be precise: the C12 alkyl rests chemically bonded to the surface) is responsible for the low surface energy of the oil-wet mica surface. Moreover, it can also be established that the higher the solid/vapour surface energy, the higher is the tendency of the surface to wet with water (i.e. lower contact angles, e.g. Table 7-1). The results are consistent with Ameri et al. (2013) who used a similar methodology and computed interfacial interaction of CO_2 and oil-wet Bentheimer. Their results show that at any pressure, solid/CO_2 interfacial tension was lower for the more oil-wet cores. For instance, at 10 MPa and 318 K, solid/CO_2 interfacial tensions were 20 mN/m for relatively more water-wet Bentheimer (SB-1) and 1 mN/m for oil-wet Bentheimer (SB-6, Ameri et al. 2013).

These results are significant for understanding the fluid flow dynamics in oil-wet and water-wet reservoir and caprocks (Iglauer et al. 2015a), and also for material design

and development where the physicochemical surface characteristics (e.g. surface energy) play a key role for a wide range of operating conditions (Zenkiewicz, 2007).

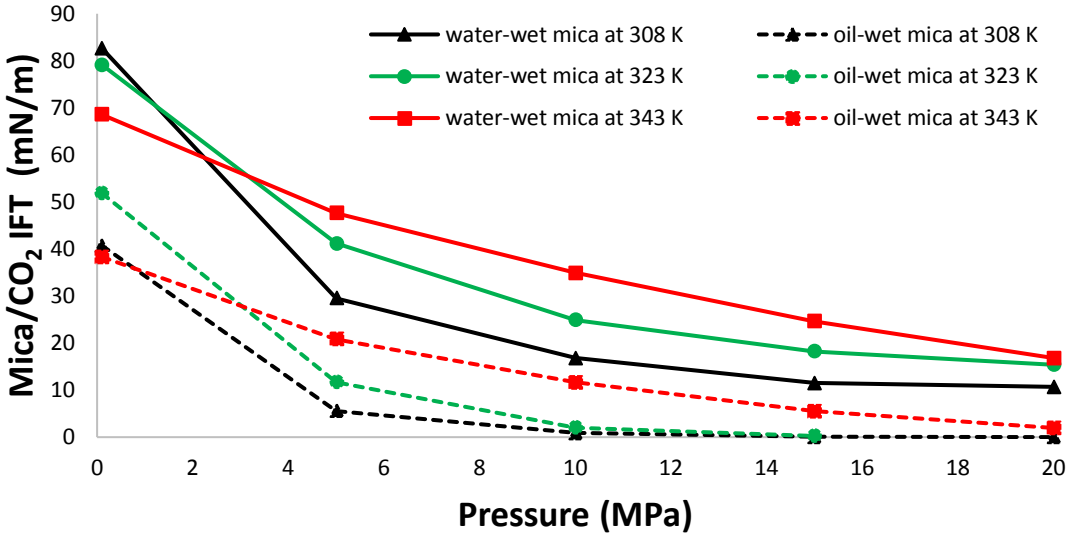

Fig. 7-3 Mica/CO_2 interfacial tension as function of pressure and temperature.

7.3.1.3 Case 3: Coals

Three coal samples [high rank (semi anthracite; from Hazelton, Pennsylvania, USA), medium rank (medium volatile bituminous; from Morgantown, West Virginia, USA), and low rank (lignite; from North Dakota, USA] were analysed for surface energy calculations. Advancing and receding contact angle data for the three coals is taken from our previous work (Arif et al., 2016c, Table 7-1). The detailed description of the properties of these coal sample can be found elsewhere (Arif et al., 2016c), however the mineral identified by XRD in the three samples revealed that the major minerals present were illite, quartz and kaolinite. We note that the measured contact angles may slightly vary with the minerology of coal; thus the results reported here must be accompanied with the minerology of the specific sample under investigation. Results showed that coal/CO_2 interfacial tension also decreased with pressure irrespective of the coal rank (Fig. 7-4). For all coals, the coal/CO_2 interfacial tension decreased sharply for the pressure interval 0.1 MPa-5 MPa, e.g. for high rank coal, at 308 K, coal/CO_2 interfacial tension decreased from 84 mN/m to ~12 mN/m when pressure increased from 0.1 MPa to 5 MPa. However, γ_{sc} turned almost constant for the pressure interval 10 MPa – 20 MPa (Fig. 7-4). Moreover, at a given pressure, the low rank coals

exhibited the highest coal/CO_2 interfacial tension values, while the high rank coal had the lowest coal/CO_2 interfacial tension, e.g. at 10 MPa and 323 K, coal/CO_2 interfacial tensions were 4.7 mN/m, 7.4 mN/m, and 10.2 mN/m for high, medium and low rank coals, respectively. At ambient conditions, Staszczuk (1989) determined surface free energy of coal, and found that the dispersion component was 45 mN/m and polar component measured 13 mN/m, thus a total surface energy of 58 mN/m comparable to our results ~ 70 mN/m for low rank coal at 308 K and 0.1 MPa.

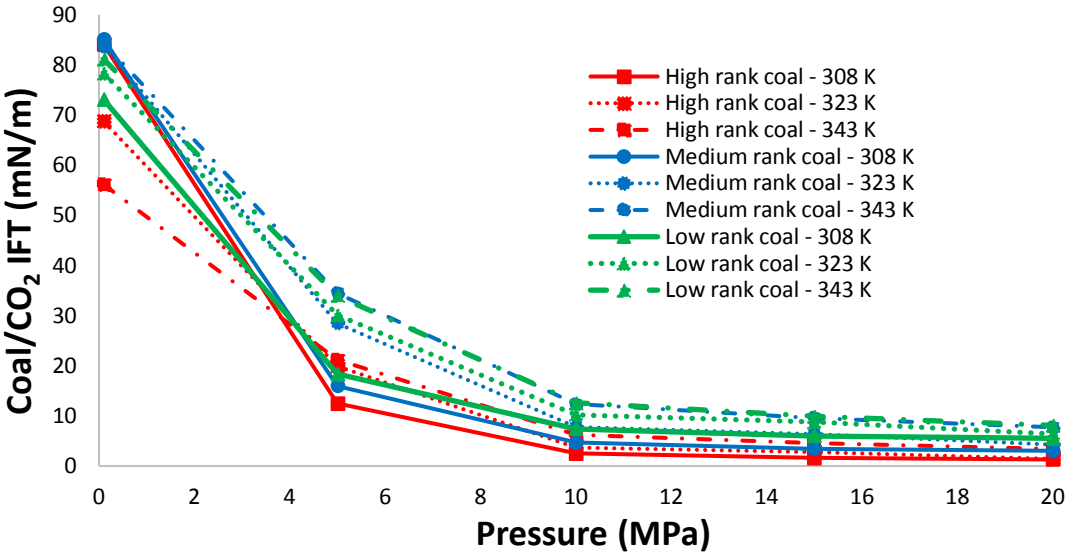

Fig. 7-4 Coal/CO_2 interfacial tension as a function of pressure, temperature and coal rank.

Note that high surface energy corresponds to strong cohesive forces and higher boiling points (Tripp and Combes, 1998). Moreover, high energy surfaces tend to reduce energy by adsorption of contaminants from the environment (Tripp and Combes, 1998).

7.3.2 Effect of temperature on solid/CO_2 interfacial tension

For all cases analysed, the solid/CO_2 interfacial tension increased with temperature (Fig. 7-5). For simplicity, a plot of solid/CO_2 interfacial tensions for the temperature range 308-343 K at 15 MPa is presented in **Error! Reference source not found.**Fig. 7-5.

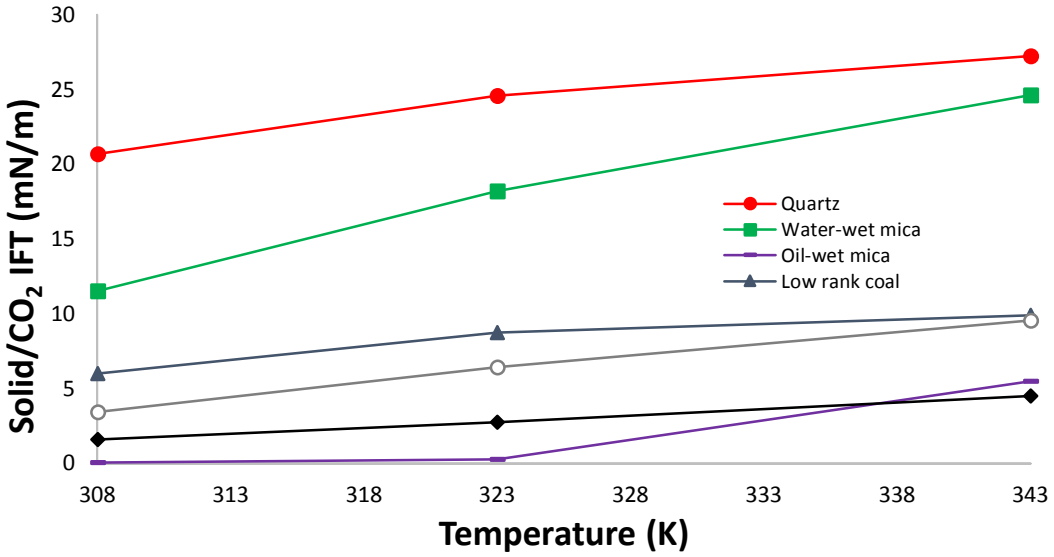

Fig. 7-5 Solid/CO_2 interfacial tension as a function of temperature at 15 MPa for various substrates.

Quartz/CO_2 interfacial tension increased from 21 mN/m to 27 mN/m when temperature increased from 308 K to 343 K (Fig. 7-5). Moreover, solid/CO_2 interfacial tension was highest for quartz, and lowest for oil-wet mica at any pressure and temperature.

Mica/CO_2 interfacial tension also followed a similar trend. For water-wet mica, mica/CO_2 interfacial tension increased from 11.5 mN/m to 24 mN/m when temperature increased from 308 K to 343 K, while for the same temperature interval, for oil-wet mica, mica/CO_2 interfacial tension increased from ~ 0 mN/m to 5 mN/m. Moreover, oil-wet mica demonstrated the lowest values of mica/CO_2 interfacial tension out of all cases at any pressure and temperature, which is again attributed to reduced number of polar sites on oil-wet mica surface.

Coal/CO_2 interfacial tension also decreased with temperature, (Fig. 7-5. For instance, for low rank coal, coal/CO_2 interfacial tension increased from 6 mN/m to ~ 9.5 mN/m when temperature increased from 308 K to 343 K. Moreover, high rank coal had the lowest coal/CO_2 interfacial tension at any temperature which is due to the lower concentration of polar surface groups on the high rank coal. Moreover, we point out that higher coal/CO_2 interfacial tensions reduces CO_2-adsorption in coals (because CO_2-adsorption in coals also decreases with temperature, Bustin and Clarkson, 1998).

For all cases analysed, the increase in γ_{sc} with temperature is attributed to a decrease in cohesive energy density of CO_2 with temperature (Barton, 1991) while the cohesive energy density of the solid is expected to stay approximately constant with temperature (Kittel, 2005), which leads to an increase in the difference of solid/CO_2 cohesive energies with temperature. Consequently, the interactions between solid and CO_2 become less favourable, thus γ_{sc} increases with temperature which promotes water-wetting of the surface. Moreover, reduction in CO_2 density with temperature leads to fewer van der Waals interactions which leads to an increase in γ_{sc} with temperature.

7.3.3 Effect of temperature on solid/water interfacial tension

Solid/water interfacial tension is directly computed from the regression fit of the experimental and model data and the results are shown in Table 7-4. For all cases, the solid/water interfacial tension decreased with increasing temperature except for quartz, for which it increased with temperature. However, the absolute quartz γ_{sw} was very low and so were the changes in γ_{sw}. When temperature increased from 308 K-343 K the quartz/water interfacial tension increased from 0.058 mN/m to 0.952 mN/m. Recently, Shojai Kaveh et al. (2016) calculated interfacial energy of shale/water systems and found that the values of shale/water interfacial tension was also quite low (0.58 mN/m at 318 K), consistent with our results. The increase in quartz/water interfacial tension with temperature is due to desorption of water molecules from the surface (Janczuk and Zdziennicka, 1994).

For mica, at any temperature, the solid/water interfacial tensions were notably higher for oil-wet mica and lower for water-wet mica (e.g. γ_{sw} = ~ 25 mN/m for oil-wet mica (21% carbon coverage, Arif et al., 2016b), and ~2 mN/m for water-wet mica (0% carbon coverage, unaltered surface, Arif et al., 2016b) at the same temperature, 323 K and pressure, 10 MPa). The larger solid/liquid interfacial tension values for the more hydrophobic surface is consistent with Dickson et al. (2006) who reported that the glass surface with higher silanol coverage had lower solid/liquid interfacial tensions (note: a higher concentration of surface silanol groups creates a more hydrophilic surface (Chen et al., 2015; McCaughan et al., 2013). Specifically, the calculated γ_{sw} values for the 37% SiOH and 12% SiOH surfaces were 13.2 and 29.2 mN/m respectively (Dickson et al., 2006), quite comparable to our results for the oil-wet mica surfaces. The results are also consistent with Ameri et al. (2013) who reported that γ_{sw}

was significantly lower for water-wet sandstones (γ_{sw} = 2.88 mN/m) as compared to oil-wet sandstones (γ_{sw} = 27.22 mN/m).

Coal surfaces also exhibited similar trends, i.e. γ_{sw} decreased with increasing temperature, and the values of coal/water interfacial tension were higher for high rank coal and lower for low rank coal (e.g. at 323 K, γ_{sw} was 19.23 mN/m for high rank coal, 13.87 mN/m for medium rank coal and 10.38 mN/m for low rank coals, Table 7-4). This effect is attributed to an abundance of hydrophilic sites (OH functional groups, typically silanol) in low rank coal and absence of hydrophilic sites in high rank coal. Essentially, presence of silanol sites leads to favourable interactions between coal surface and water, thereby resulting in a reduction of γ_{sw} for low rank coal.

Further, we point out that the proposed methodology assumes that γ_{sw} is constant versus pressure. In reality, however, the solid/water interactions are expected to change due to increase in solubility of CO_2 in water with pressure (El-Maghraby et al. 2012), and associated lower pH values (Schaeff and McGrail, 2004), which leads to increased protonation of the silanol surface groups (Brown et al., 2012).

7.3.4 Effect of salinity on solid/CO_2 interfacial tension

We compared solid/CO_2 interfacial tension (as function of pressure and temperature) for 20 wt% NaCl brine in mica/CO_2 systems and compared it with that of mica/water systems. The results showed that the mica/CO_2 interfacial tension for DI-water at a particular pressure and temperature is quite similar to the mica/CO_2 interfacial tension for 20 wt % NaCl brine case (Fig. 7-6). For instance, at 323 K, and 10 MPa, the mica/CO_2 interfacial tensions were 22.4 mN/m for liquid comprising of 20 wt% NaCl brine, and 24.8 mN/m for DI-water, thus a difference of only 2.4 mN/m (Fig. 7-6). Moreover, at the same temperature but at 15 MPa, mica/CO_2 interfacial tension for two different liquids (DI water and 20 wt % NaCl brine) is the same (~18.5 mN/m, Fig. 7-6). In summary, the R^2-values for the correlation between mica/CO_2 interfacial tensions for the two liquids were 0.997, 0.998 and 0.985 at 308 K, 323 K and 343 K, respectively, indicating a strong correlation. This implies that solid/CO_2 interfacial tension is not much changed by altering the type of the liquid in the same system. We point out that this result verifies this methodology and our predictions (of mineral/CO_2 and mineral/water interfacial tensions) to some extent.

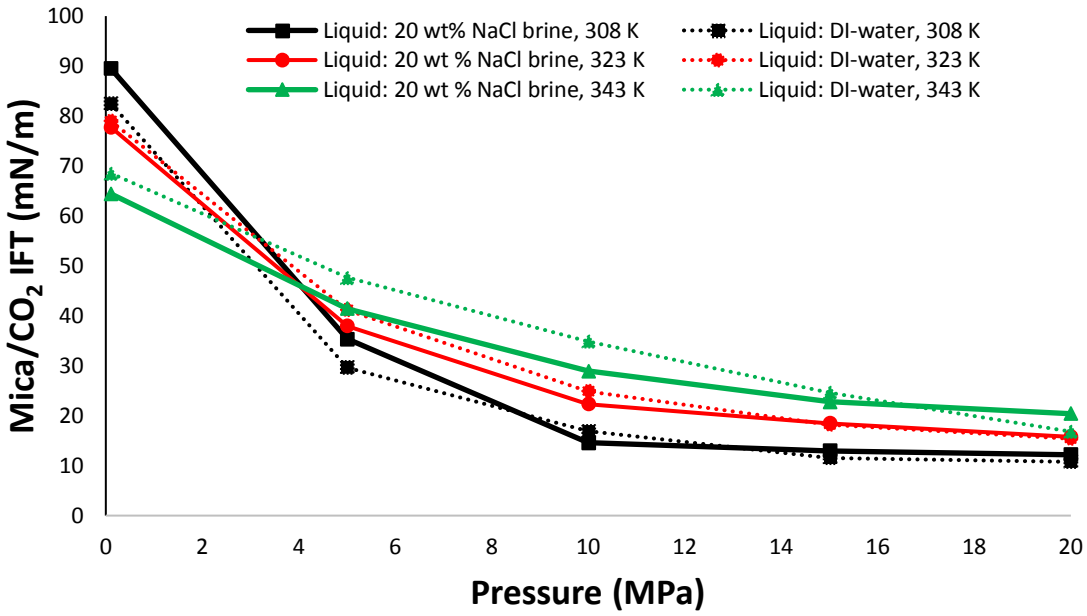

Fig. 7-6 Mica/CO_2 interfacial tension as a function of pressure and temperature for two different liquids (DI-water and 20 wt% NaCl brine)

7.3.5 Effect of salinity on solid/water interfacial tension

To analyse the effect of salinity on the solid-water interfacial energies, we compared γ_{sw} results for DI water (see above) with that of 20 wt% NaCl brine. The β values from the non-linear regression fit of cosine of the equilibrium contact angle data were 0.000267, 0.000284, and 0.00034 at 308 K, 323 K and 343 K, respectively. The Pearson coefficients were 0.846, 0.921 and 0.941, indicating good fits. The mica/brine (20wt% NaCl) interfacial tensions were 10.5 mN/m, 6.27 mN/m and 4.4 mN/m at 308 K, 323 K and 343 K, respectively implying that mica/brine interfacial tension decreased with temperature, consistent with the solid/DI-water system (discussed above). However, at any given temperature, mica/brine interfacial tension was larger than the mica/water interfacial tension. For instance, at 308 K, mica/brine (20 wt % NaCl brine) interfacial tension was 10.5 mN/m in comparison to 2.1 mN/m for mica/DI water at the same temperature (308 K). This result is consistent with Ameri et al. (2013) who found that when salinity increased from 0wt% NaCl to 3.5 wt% NaCl, γ_{sw} increased slightly. However, Shoaji Kaveh et al. (2016) found a slight reduction in γ_{sw} with salinity. The increase in solid/brine interfacial tension with

salinity is related to the intermolecular forces and the zeta potential which arises due to charged species on the surface. As salinity increases, more counter ions are available to reduce the net charge and thus reduces the polarity of the surface, which again leads to a reduction in water-surface van der Waals forces. Lower van der Waals interactions result in higher interfacial tensions. Moreover, Roshan et al. (2016), recently introduced a model to describe the physical processes for wettability variation as a function of salinity in which they related electric potential at the mineral surface to the contact angle. Their results showed that as salinity increased the surface became more hydrophobic due to a decrease in the dielectric constant of liquid with salinity.

7.3.6 Wettability dependence on surface energies

In order to evaluate the net effect of these interfacial tensions on contact angle, the right hand side (RHS) of Young's equation (the value of cosθ) was calculated for all cases analysed using the computed values of γ_{sc} , γ_{sw} and experimental values of γ_{cw}. For quartz, cosθ decreases with pressure and temperature because quartz/CO_2 interfacial tension decreases with pressure and increases with temperature, and the quartz/water interfacial tension increases with temperature. Thus the net effect of the three interfacial tension results in decrease in a cosθ with pressure and temperature and consequently θ increases with pressure and temperature for quartz (consistent with experimental data, Table 7-1). For all other cases (mica and coals), cosθ decreases with pressure and increases with temperature because solid/CO_2 interfacial tension decreases with pressure and increases with temperature and the solid/water interfacial tension also decreases with temperature (for mica and coals), thus θ increases with pressure and decreases with temperature (consistent with experimental data, Table 7-1).

Moreover, for water-wet mica, cosθ stays positive for all tested pressures and temperatures, because the mica surface remains either strongly water-wet or weakly water-wet (contact angle < 90°, cp. Iglauer et al., 2015a, Table 7-1**Error! Reference source not found.**). However, for the oil-wet mica surface, cosθ reaches negative values for a wide range of tested pressures and temperatures which indicates CO_2-wet conditions exhibited by this surface (contact angle > 90°, Iglauer et al., 2015a, Table 7-1). Moreover, θ increased more rapidly for oil-wet mica (as compared to water-wet

mica), because of the low CO_2-solid interfacial energy, which promotes de-wetting of the surface by water (Dickson et al., 2006). Because high energy fluids (e.g. water), do not tend to spread on low-energy surfaces, the presence of a low energy CO_2 layer will cause the solid/water contact angle to increase above 90° to increase the interfacial area between water and CO_2. Furthermore, for mica and coals, θ decreases with temperature because the net effect of solid/fluid and fluid/fluid interfacial tensions gives rise to an increase in the cosθ with temperature.

In summary, the increase in contact angle with pressure is due to a reduction in the difference of solid and CO_2 cohesive energies with pressure which leads to more favourable interactions between solid and CO_2. Consequently, γ_{sc} decreases with pressure and thus promotes de-wetting of the surface (i.e. higher water contact angle).

7.4 Implications

We predicted solid/CO_2 and solid/water interfacial tensions for various rock forming minerals including quartz, mica and coals for a wide range of pressure and temperature conditions. The results imply that the surfaces which are more non-wetting to water exhibit lower values of solid/CO_2 interfacial tension than the surfaces which are more water-wet (e.g. 18 mN/m for water-wet mica in comparison to ~3mN/m for oil-wet mica at 15 MPa and 323 K). Moreover, the less water-wet surfaces have higher solid/water interfacial tensions than the water-wet surfaces (24.8 mN/m for oil-wet mica and ~2 mN/m for water-wet mica, Table 7-4). Computations of these surface energies in conjunction with Young Laplace's equation enables us to predict contact angles. As an example, θ values are predicted using Young's equation (Equation 1) using the calculated values of the interfacial tensions and the results are shown at 343 K for all samples analysed (Fig. 7-7). The results show a good match between experimental contact angle and the predicted contact angles. This implies that the methodology considered in this work to compute surface energies is correct and that the predicted solid-fluid interfacial tensions correctly reproduced experimental contact angle data.

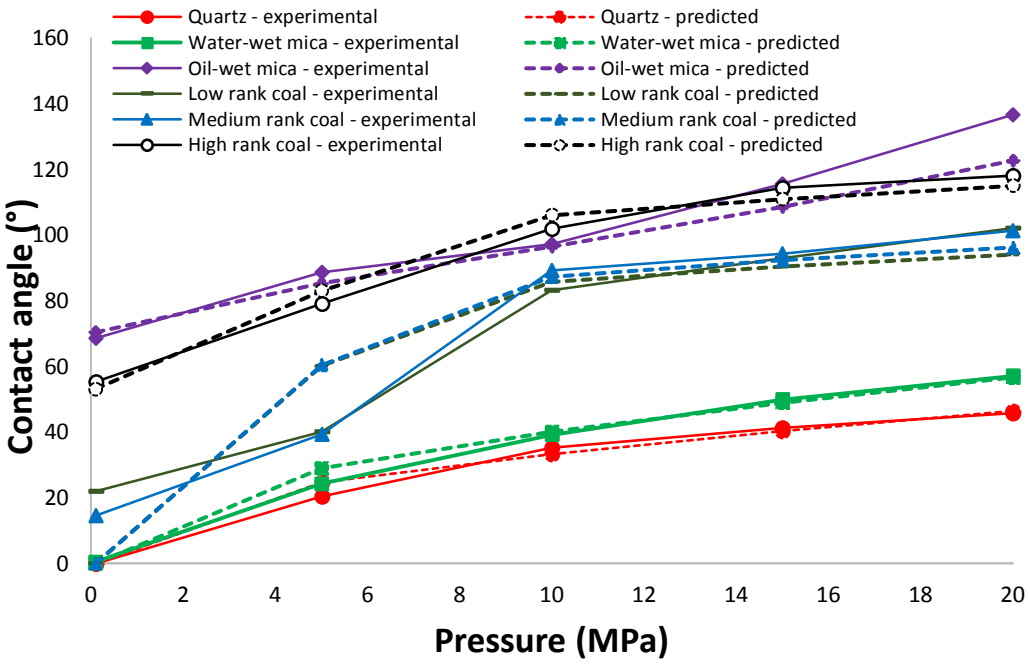

Fig. 7-7 Experimental and predicted water contact angles as a function of pressure at 343 K for all substrates.

In terms of a broader interpretation, the solid/fluid interfacial tensions reported in this study are useful for relating CO_2 storage potential to rock/fluid interfacial tension. For instance, water-wet rocks are better for CO_2 storage (Iglauer et al., 2011) because of higher solid/CO_2 (solid = rock in this case) interfacial tension and oil-wet rocks exhibit poor CO_2-storage potential in terms of structural and residual trapping (Iglauer et al., 2016) due to lower solid/CO_2 interfacial tension (e.g. pure quartz have higher solid/CO_2 interfacial tension than 37%SiOH quartz). Physically, due to higher solid/CO_2 interfacial tension for water-wet rocks, CO_2 tends to stick to the rock (rock offers more resistance to the flow/leakage of buoyant CO_2) and CO_2 is thus rendered immobile within the pores (leading to higher capillary/residual trapping in water-wet rocks; Iglauer et al., 2011). However, the detailed investigation of trapping potential must also account for solubility of CO_2 in the oil phase, sealing tendency of the caprock, and the pore geometry etc. to device suitable field scale storage plans.

7.5 Conclusions

We used Neumann's equation of state (Neumann et al., 1974) to compute the interfacial tensions of mineral/CO_2 and mineral/water systems for important rock forming minerals (quartz, water-wet mica and oil-wet mica) and for coals of high to low rank as a function of pressure, temperature and salinity. It was found that mineral/CO_2 interfacial tension decreased with pressure (consistent with Ameri et al. 2013 and Dickson et al. 2006), which is due to increased CO_2-mineral intermolecular interactions (e.g. Iglauer et al., 2012, Al-Yaseri et al. 2016b). It was also found that mineral/CO_2 interfacial tensions increased with temperature which is due to an increase in the difference of solid/CO_2 cohesive energies with temperature which thus leads to less favourable interactions between solid and CO_2 (thus higher γ_{sc}). Moreover, the more non-wetting to water the surface was, the lower were the mineral/CO_2 interfacial tensions and the higher were the mineral/water interfacial tensions, e.g. oil-wet mica showed a lower mica/CO_2 interfacial tension than water-wet mica at the same pressure and temperature. Similarly, high rank coal had a lower coal/CO_2 interfacial tension than the low rank coal, because of greater hydrophobicity of high rank coal. For all systems, solid/water interfacial tension decreased with temperature, except for quartz, where the quartz/water interfacial tension increased with temperature. The effect of salinity was also analysed and it was found that solid/water interfacial tension increased with salinity. Moreover, contact angles were predicted by Young's equation using the computed values of interfacial energies, and the predicted θ values were in good agreement with the experimental θ values.

We conclude that the Neumann equation of state is adequate to quantify the solid surface energy and that the results demonstrated significant influence of surface energy in controlling the wettability dependence on pressure, temperature and salinity.

Chapter 8 Influence of surface chemistry on interfacial properties of low to high rank coal seams*

Abstract

Wettability of CO_2/water/coal systems is a fundamental petrophysical parameter, which governs the fluid flow and distribution in coal seams and thus directly affects CO_2-storage and methane recovery from unmineable coal seams. The recognition of wettability of coal/CO_2/brine systems help to understand CO_2-storage and enhanced methane recovery potential of coal seams. To understand the factors influencing the wetting characteristics of coals, a detailed examination and characterization of coal surface chemistry is essential and literature data in this context is missing. We thus measured zeta potentials as a function of temperature (298 K-343 K), brine salinity (0 wt% NaCl – 5 wt% NaCl) and salt type (NaCl, $CaCl_2$ and $MgCl_2$) for coals of low, medium and high ranks. Further, we measured water advancing and receding contact angles as a function of temperature and salinity for the same experimental matrix in order to relate the wettability changes to the surface charge at the coal/brine interface. We found that zeta potential increased with temperature, salinity and cation valency. Both advancing and receding contact angles decreased with temperature, and increased with salinity and cation valency irrespective of the coal rank. Moreover, coal surfaces were investigated by Fourier transformed infrared (FTIR) spectroscopy and the surface functional groups responsible for a particular wetting behaviour were identified. The results revealed that the presence of polar surface functional groups (e.g. Si-OH and carboxylic acid groups) were responsible for the hydrophilic behaviour of low rank coals and the absence of these groups in high rank coal was responsible for their hydrophobic behaviour (consistent with XRD).

Keywords: Coal, Zeta potential, Wettability, Surface functional groups, CO_2-storage

*Reference: Arif et al. (2017) in *Fuel*, 194, 211-221

8.1 Introduction

The injection of CO_2 in depleted oil and gas reservoirs or deep saline aquifers is capable of trapping tremendous amounts of CO_2 and thus reduce anthropogenic CO_2 emissions (Blunt et al., 1993; Iglauer et al., 2013; IPCC, 2005). Certain trapping mechanisms render CO_2 immobile in the porous medium, and these are structural trapping (Arif et al., 2016a,b; Iglauer et al., 2015b), capillary trapping (Hesse et al., 2008; Iglauer et al., 2011a,b), dissolution or solubility trapping (Iglauer, 2011c) and mineral trapping (Gaus, 2010). Coal seams, too, offer enormous potential for CO_2 storage and enhanced methane recovery by means of preferential adsorption of CO_2 (Arif et al., 2016c; Saghafi et al., 2014). Adsorption is the major CO_2 trapping mechanism in unminable coal seams and the wettability of the specific CO_2/brine/coal system plays a significant role in this context (Shojai Kaveh et al., 2012). Typically, the adsorption capacity of CO_2 is higher than that of methane, consequently, CO_2 displaces methane towards the production well and itself gets sorbed within the micropores of the coal seam and remains trapped. Moreover, Arif et al. (2016c) pointed out that CO_2-adsorption may be higher when coals are more CO_2-wet which thus leads to larger storage volumes.

Although coal wettability has been characterized as a function of pressure, temperature, salinity and coal rank (Arif et al., 2016c; Shojai Kaveh et al., 2012), the factors responsible for a particular wetting behaviour are so far unclear. Specifically, the knowledge and characterization of coal surface chemistry is essential to understand the factors that influence its wettability (Adamson and Gast, 1997; Iglauer et al., 2015a). In this context, zeta potential is used to probe the electric double layer at the surface of the coal. The nature of the electric double layer affects the repulsion/attraction of system's components, and depends upon the physicochemical properties of all components in the overall system (Erbil, 2006). Thus, what occurs at the brine/mineral or brine/rock interface is strongly affected by the electrical double layer and studies have shown that this double layer is closely related to wettability (Alkan et al., 2005; Buckley et al., 1998; Nasralla and Nasr-El-Din, 2014).

This work, thus, examined the electrochemical behaviour of coal by measuring zeta potentials as a function of temperature (298 K-343 K), salinity (0 wt% NaCl-5 wt% NaCl), salt type (NaCl, $CaCl_2$ and $MgCl_2$) and coal rank (low, medium and high rank)

to allow surface characterization for broad range of conditions. In addition, following the same experimental matrix, advancing and receding contact angles were measured for air/coal/brine systems (at ambient pressure). The associated trends were analysed systematically and relationships were developed between zeta potential and wettability. It was found that the zeta potential increased with increasing rank and increasing salinity and contact angles also increased with increasing rank and salinity, implying a positive correlation between zeta potential and wettability. However, with increasing temperature zeta potential increased but contact angle decreased, implying that correlation with respect to temperature is inconsistent. Moreover, the zeta potential measurements were also correlated to contact angle data at high pressure, and it was hypothesized that zeta potential at high pressure may follow similar trends as those at ambient pressure.

Further, in order to evaluate the impact of coal rank on wettability of the coal/CO_2/brine systems, Fourier transformed infrared spectroscopy (FTIR) measurements were conducted on the three coal samples (low, medium and high rank) and the surface functional groups were thoroughly characterized. The results demonstrated that the abundance of OH and carboxylic acid groups on the low rank coal is responsible for the hydrophilic nature of lignite and the lack of these groups explains the hydrophobic nature of high rank coal (semi-anthracite).

8.2 Experimental Methodology

8.2.1 Fluid/sample preparation

Three coal samples of low, medium, and high rank (properties shown in Table 5-2) were used in this research. The samples were cut to cuboid shape (~1cm x 1cm x 0.5cm) or crushed into fine powder (particle size ~30 microns) using milling equipment (Labtechnics Adelaide, Model TP-4/5, and Oscillation: 50Hz). The powdered samples were then placed in an oven at 90°C for 12 hours until the weight became constant.

Coal/brine composite samples for all coal ranks were prepared by adding 2wt% coal powder to aqueous salt solutions composed of DI water (0M), 1wt% NaCl (0.17M), 5wt% NaCl (0.855M), 1wt% $CaCl_2$ (0.27M), and 1wt% $MgCl_2$ (0.305M). Note: the

numbers in brackets represent the equivalent ionic strength of electrolyte, which is typically preferred while comparing different types of salt of same strength. In this paper, we mainly used wt% to express salinity, however, for salts comparison we used ionic strength. Moreover, the alternative common units to express salinity are 'mg/L' and 'ppm'.

Materials used were de-ionized water (Conductivity: 0.02 mS/cm) and brine comprising of NaCl, $CaCl_2$ and $MgCl_2$ (Salts Source: Scharlab s.l., Spain, Purity: ≥ 0.995 mass%). The solutions were covered with parafilm and stirred for 5 hours using a magnetic stirrer at 40 °C to ensure homogenous dispersion of the solid powder within the base liquid. The dispersions were then used for the zeta potential measurements. For contact angle measurements, the cuboid samples (low, medium and high rank coal) were selected and for spectroscopic measurements, samples were used in powdered form.

8.2.2 Zeta potential measurements

Zeta potential was measured on a Zetasizer Nano ZS (Malvern instrument). The coal dispersion was placed in a folded capillary cell and sealed at the top. The zeta potential was measured for coal/DI-water for high, medium and low rank coals at 298 K, 308 K, 323 K and 343 K to investigate the effect of temperature on zeta potential. Moreover, the effect of salinity and cation type was analysed for coal dispersed in 1 wt% NaCl, 5 wt% NaCl, 1 wt% $CaCl_2$ and 1 wt% $MgCl_2$ brine. The measurements were repeated three times and the standard deviation of zeta potential measurements was 3 mV at 298 K, ~2.5 mV at 308 K and ~1.5 mV at 323 K and 343 K. Moreover, for higher salinities (5wt% NaCl), standard deviation was also high (3 mV). We used error bars to graphically represent the standard deviation in our results. We observed that the sources of error in zeta potential measurements are evaporation, time lapse between sample preparations to actual measurement, degree of homogeneity of mixing, size of coal particle and electrolyte strength. If these factors are not properly addressed the Zetasizer Nano ZS may give different quality of measurements. We here reported the best three set of measurements which we observed.

8.2.3 Petrology, Ultimate and Proximate Analysis

The results of the proximate, ultimate and petrological analysis and the internal properties (density and volume) of the coal samples were the same as listed in Table 5-2. Note that coal samples of different rank differ mainly in volatile matter, moisture, fixed carbon and vitrinite reflectance (Bustin et al., 1985). Petrology was analysed in accordance with Australian Standard AS2856 and ISO7404; proximate analysis was conducted using standards AS1038.3, ISO11722 and ASTM D3172-07a, and ultimate analysis was performed using standards AS1038.6 and ISO 609.

8.2.4 pH measurements

The pH values of the solutions were measured at 298 K using a pH meter (model: Orion 420+ and a Thermofisher pH probe, accuracy: ±0.005 pH), the results of which are tabulated in Table 8-1. These pH measurements are helpful for a) explanation of zeta potential results as a function of coal rank and brine salinity, and b) precise comparison with zeta potential literature data. The solutions were equilibrated for 72 hours before the pH measurements, and such equilibration is important to establish as slight changes in pH can result in corresponding changes in zeta potential measurements (Alroudhan and Vinogradov, 2016). The measured pH values demonstrate an appropriate trend whereby the low rank coals that have more hydrophilic groups (in particular –COOH) have the lower pH values. As the coals increase in rank and have fewer COOH groups, the pH measured is higher.

Table 8-1 Measured pH values of the solutions used.

Electrolyte	pH values		
	Anthracite*	Bituminous*	Lignite*
DI-water	7.09	6.78	6.78
1wt% NaCl	8.13	7.37	6.42
5wt% NaCl	7.97	7.05	6.03
1wt% $CaCl_2$	7.57	6.96	5.48
1wt% $MgCl_2$	8.21	8	5.86

*All solutions contained 2 wt% coal powder.

8.2.5 Infrared spectroscopy

Fourier Transformed Infrared spectroscopy was performed using a Nicolet iS50-FTIR instrument (from Thermo Scientific) at 4 cm^{-1} resolution. The powdered sample was placed on a diamond attenuated total reflection (ATR) crystal and pressed into contact. A total of 64 scans were added to generate the final infrared spectrum and the internally available ATR correction was applied to each spectrum with the software (which was supplied by the manufacturer with the instrument).

8.2.6 XRD analysis

XRD analysis was carried out on the three coal samples and minerals were detected in each sample (Table 8-2). It is evident that the coal mainly comprised of quartz and kaolinite, however, overall mineralogy of these coals is different.

Table 8-2 Mineral identified by XRD in the three coal samples investigated.

Mineral name	Chemical formula	High rank coal	Medium rank coal	Low rank coal
Illite	$(K,H_3O)Al_2Si_3AlO_{10}(OH)_2$	34	17	_
Quartz	SiO_2	21	41	76
Kaolinite	$Al_2Si_2O_5(OH)_4$	24	30	24
Anatase	TiO_2	21	_	_
Montmorillonite	$HAl_2CaO.5O_{12}Si_4$	_	6	_
Illite-montmorillonite	$KAl_4(Si,Al)_8O_{10}(OH)_4.4H_2O$	_	6	_

8.2.7 Contact angle measurements

Contact angles were measured using the pendant drop titled plate technique (Lander et al., 1993), the schematic of the experimental apparatus has been published previously (Arif et al., 2016c). The coal substrates were placed in the cell and temperature was set to a desired value (298 K, 308 K, 323 K or 343 K within ± 1 K). Coal surfaces were washed with acetone and then cleaned with air plasma for 2 min. Within this selected time the error in contact angle measurements was minimum) and

this selected time was neither too short to compromise the surface contaminants, (Iglauer et al., 2014), and neither too intense to allow the removal of natural particles from the coal surfaces (Arif et al., 2016c). A few studies, however, report different coal-surface cleaning methods, e.g. the use of wet polish with abrasive papers, which were then removed by ultrasonic cleaning (Drelich et al., 1997).

Subsequently brine was pumped with a high precision syringe pump (ISCO Teledyne 500D) resulting in a droplet of de-gassed brine (vacuumed for 12 h) being dispensed onto the substrate (in air, at ambient pressure and the pre-set temperature) by means of a needle. At the leading edge of the droplet, just before the droplet started to move, the angle between coal surface and the brine interface was measured as the advancing contact angle (θ_a) whereas the receding contact angle (θ_r) was measured at the trailing edge of the droplet. A high performance video camera (Basler scA 640–70 fm, pixel size = 7.4 lm; frame rate = 71 fps; Fujinon CCTV lens: HF35HA-1B; 1:1.6/35 mm) recorded the entire process, and contact angles were measured on images extracted from the movie files. The standard deviation of these measurements was ±4° based on measurements repeated thrice and is shown by error bars in the results. The measurements were done on one sample each of low, medium and high rank. The coal samples may vary in terms of composition, thus the conclusions drawn in the study may vary depending upon the composition of the coal samples under investigation. In fact, our results revealed that difference in coal rank (e.g. low, medium and high rank, which are obviously different in composition) leads to different zeta potential (at the same operating conditions) which leads to different wettability (discussed in detail in section 3.4).

8.3 Results and discussion

In order to understand the factors influencing wettability of coal seams, we examined the surface properties of coals. The results lead to a broad understanding of the factors responsible for the distinct wetting characteristics of coals as a function of coal rank, pressure, temperature and brine salinity and thus the results help to precisely understand fluid flow and distribution in coal seams. This information can be used to optimize CO_2-storage and (enhanced) methane recovery projects. Below the influence of each individual parameter is discussed in detail.

8.3.1 Effect of temperature on zeta potential and contact angle

We found a clear and consistent temperature dependence trend of contact angle and zeta potential for coal/DI water systems. Zeta potentials of these systems increased with increasing temperature within the experimental error (at constant ambient pressure, Fig. 8-1), irrespective of coal rank. Moreover, the advancing and receding water contact angles decreased with temperature for all coal ranks (Fig. 8-2, consistent with (Arif et al., 2016c). The increase in zeta potential with increasing temperature implies a surface with more screening ions within the electric double layer at higher temperatures which in turn gives a more water-wet coal surface, i.e. the observed behaviour is different than previously reported behaviour (Rodriguez and Araujo, 2006).

Specifically, for the high rank coal (semi-anthracite), the zeta potential increased from -23.1 mV to 2.63 mV when temperature increased from 298 K to 343 K (Fig. 8-1). For the same temperature increase, θ_a decreased from 59° to 32° and θ_r decreased from 52° to 27° (Fig. 8-2). Similar trends were found for medium and low rank coals i.e. the zeta potentials of coal/DI water increased with temperature (Fig. 8-1) and corresponding θ_a and θ_r decreased with temperature. For instance, for the medium rank coal (medium volatile bituminous), the zeta potential increased from -24.8 mV to 0.236 mV when temperature increased from 298 K to 343 K, and correspondingly, θ_a decreased from 40° to 18° and θ_r decreased from 33° to 12° (Fig. 8-2).

On the coal surface, ionisable groups are present (e.g. phenolic and carboxylic groups, (Laskowski, 2001), thus, as temperature increases and the pH decreases (pH decreases with temperature due to reduction in pK values of water and also due to a reduction in hydrogen bonding leading to increased number of protons (H^+); Akiva and Savage, 2002), the released protons (H^+) interact with the surface functional groups and ionize them, e.g. C=O reacts to C-OH^+ or C-OH^+ reacts to C-OH_2^{2+} (Laskowski, 2001). Therefore the surface of the coal becomes more positive with an increase in temperature, and consequently the zeta potential increases. Moreover, it is also reported that with increase in temperature, surface oxidation is accelerated and hydrophilic groups are formed on the coal surface at high temperature (Ding, 2009; Ramesh and Somasundaran, 1989; Somasundaran et al., 1991) which may lead to

lower water contact angles with increasing temperature. However, we believe that oxidation of coal surfaces require sufficient exposure time, which is likely to be well beyond the timescale of surface exposure to high temperature during our contact angle measurements (Calemma et al., 1988). Thus, we point out that oxidation may not be a governing factor for the decrease in contact angle with temperature despite a corresponding increase in zeta potential. We believe that further research is required to explore this effect.

Somasundaran et al. (1991) found that for high volatile bituminous coal (from Pennsylvania), the magnitude of zeta potential decreased with temperature (at a pH of 6.78, zeta potential measured -26 mV at 300 K and reduced to -20 mV at 363 K). At the same pH (6.78, Table 8-1), the zeta potential of our medium rank coal (medium volatile bituminous) measured -24.8 mV at 298 K in good agreement with Somasundaran et al. (1991). The slight difference is probably due to the slightly different coal and associated differences in coal surface chemistry. Because of the limited literature data on zeta potential of coals, we compared our data with coals of similar ranks (if not exactly the same) despite their origin from a different basin (e.g. Somasundaran's coal from Pennsylvania is compared to our coal sample from West Virginia).

The observed increase in zeta potential with increasing temperature is attributed to the reduction in pH (with increasing temperature), consistent with Vinogradov and Jackson (2015), who reported that zeta potentials of sandstones decreased in magnitude with increasing temperature for low salinity brine (0.6 wt% NaCl to 3 wt% NaCl), and they concluded that pH reduction with increasing temperature was responsible for the zeta potential variation. Note: The coals are compared with quartz (Vinogradov and Jackson's (2015) work) because mineralogy of these coals revealed that quartz is a significant component of these coals (XRD results, Table 8-2).

To further explain the charge reversal behaviour, we conducted pH measurements of the solutions at high temperatures and found that pH dropped only slightly (e.g. for lignite/water solution pH = 6.5 at 323 K and pH = 6.32 at 343 K), thus zeta potentials are only slightly impacted by pH changes. Therefore, divalent ions could possibly be acting as potential determining ions.

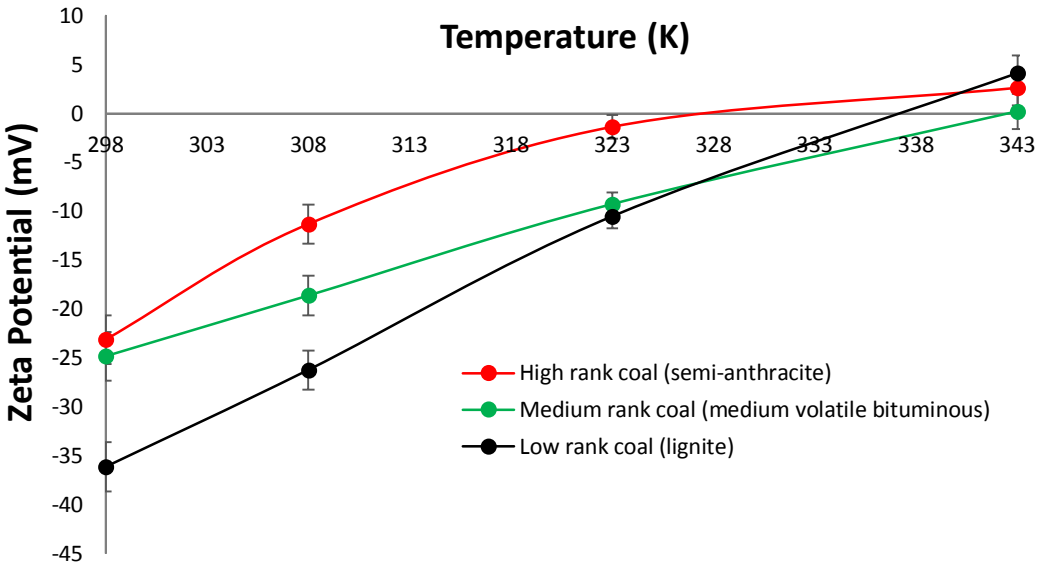

Fig. 8-1 Zeta potential as a function of temperature and coal rank (at ambient pressure).

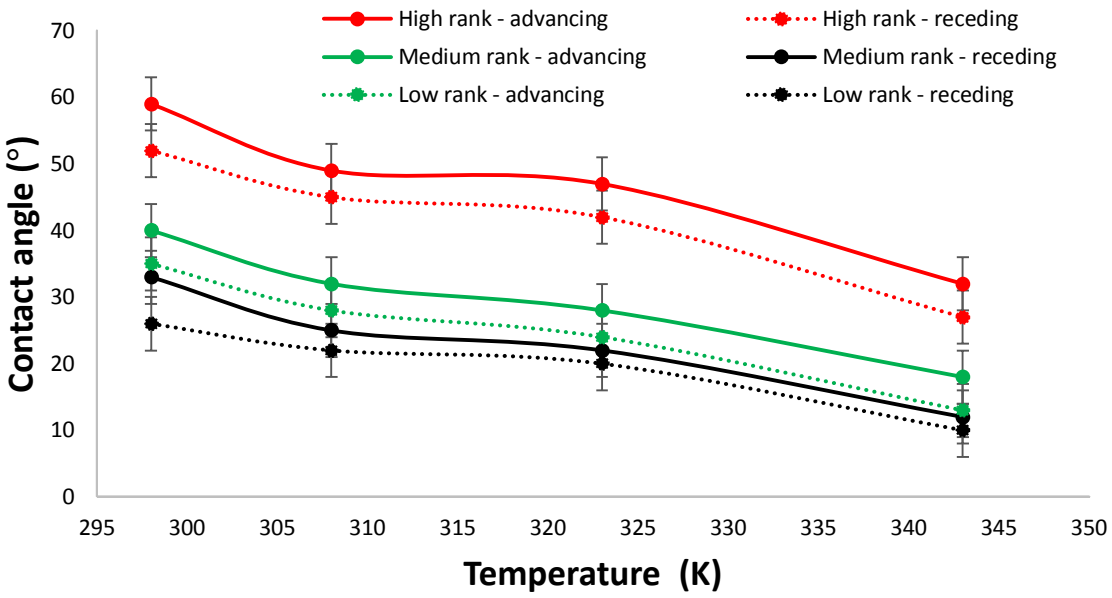

Fig. 8-2 Water contact angle as a function of temperature and coal rank (at ambient pressure).

We further found that at any given temperature, high rank coal exhibited higher values of zeta potential and higher water contact angles than low rank coals. For instance, at

323 K, the zeta potential measured -1.36 mV for the high rank coal, -9.25 mV for medium rank coal, and 10.5 mV for low rank coal (Fig. 8-1), while the associated contact angles were (θ_a = 47°, 28° and 24° and θ_r = 42°, 23° and 20° for high, medium and low rank coals respectively). This behaviour is attributed to the lack of hydrophilic function groups (OH groups) in high rank coals (further discussed in Section 3.5).

Considering the above electrochemical behaviour of coals at ambient pressure, we now consider CO_2/brine/coal contact angle data at high pressure (15 MPa) from our previous work (Arif et al., 2016c). It was found that at 15 MPa, for high rank coal, when temperature increased from 308 K to 323 K, θ_a decreased from 146° to 119°, implying a wettability transformation from strongly CO_2-wet to weakly CO_2-wet. Similarly, for medium rank coal, θ_a decreased from 128° to 102° when temperature increased from 308 K to 343K. However, for low rank coal, θ_a first decreased from 112° to 102° when temperature increased from 308 K to 323 K, and then became constant when temperature increased further (from 323 K to 343 K; Arif et al., 2016c). In summary, water-wettability of coal increased with increasing temperature irrespective of the coal rank. Thus, the effect of temperature on wettability is similar at high pressure as that found at ambient pressure (i.e. air/brine contact angles at low pressure and CO_2/brine contact angles at high pressure followed similar trend). It can therefore be concluded that the temperature dependence of CO_2-wettability of coals is considerably controlled by electrochemical changes at the water/coal interface and that increase in temperature render the coal surface more water-wet due to formation of ionized surface functional groups.

8.3.2 Effect of salinity on zeta potential and contact angle

The effect of salinity on zeta potential and contact angle was studied as a function of brine salinity (0 wt% NaCl, 1 wt% NaCl and 5 wt% NaCl) at constant temperature (323 K). It was found that zeta potential increased with an increase in salinity for all coal ranks (Fig. 8-3). Moreover, both θ_a and θ_r increased with salinity for all coal samples (Fig. 8-4). Specifically, for the high rank coal, when salinity increased from 0 wt% NaCl to 5 wt% NaCl (or equivalently from 0M to 0.855M), zeta potential increased from -1.63 mV to 2.63 mV. For the same salinity increase, θ_a increased from 47° to 60° and θ_r increased from 42° to 53° (Fig. 8-4). Similarly, for medium rank

coal, the zeta potential increased from -9.25 mV to 0.263 mV when salinity increased from 0 wt% NaCl to 5 wt% NaCl, indicating a clear increase in zeta potentials with increasing salinity, and the corresponding values of θ_a increased from 28° to 41° and θ_r increased from 22° to 35° (Fig. 8-4). Generally, for any solid/brine system, the composition of solid and the concentration and valency of ions in the solution are responsible for the sign and value of the zeta potential (Butt et al., 2006). Physically, the coal surface exhibits negative charges due to the presence of polar functional entities, which partially dissociate, e.g. carboxylic or phenolic groups (Sarwar et sl., 2012); the concentration of these functional groups depends on the coal rank (Wu et al., 2014), see also FTIR discussion below. The results found here are consistent with Ibrahim and Nasr-El-Din (2015) who reported that both zeta potentials and contact angles on coals increased with salinity. Fuerstenau et al. (1983) reported that for low ash anthracite coal, the zeta potential was measured to be -25 mV at 0.01 M NaCl (pH = 7) at room temperature. We found that for high rank coal (semi-anthracite) at (almost) the same pH (7.09, Table 8-1), the zeta potential was measured to be -23 mV (Fig. 8-1) indicating consistent results. Harvey et al. (2002) also found an increase in zeta potential of coal with salinity. They reported that for sub-bituminous (medium rank) coal, at a pH of 8, zeta potential increased from -32 mV to -25 mV when salinity changed from 0 wt% NaCl (DI-water) to 0.5 wt% NaCl at room temperature. For a similar bituminous coal we also measured an increase in zeta potential at 323K (-9.25 mV for DI-water decreased to -8.5 mV for 0.5 wt% NaCl brine, Fig. 8-3). Roshan et al. (2016) recently introduced a model to describe the physical processes for wettability variation as a function of salinity and they related the contact angle to the electric potential at the mineral surface. According to their explanation, the dielectric constant of the fluid decreases with increasing salinity, which leads to an increased contact angle. The decrease in zeta potential correlates with the charge on the surface being more screened as more ions are present in the electric double layer, this leads to an increased water contact angle (Mugele and Baret, 2005).

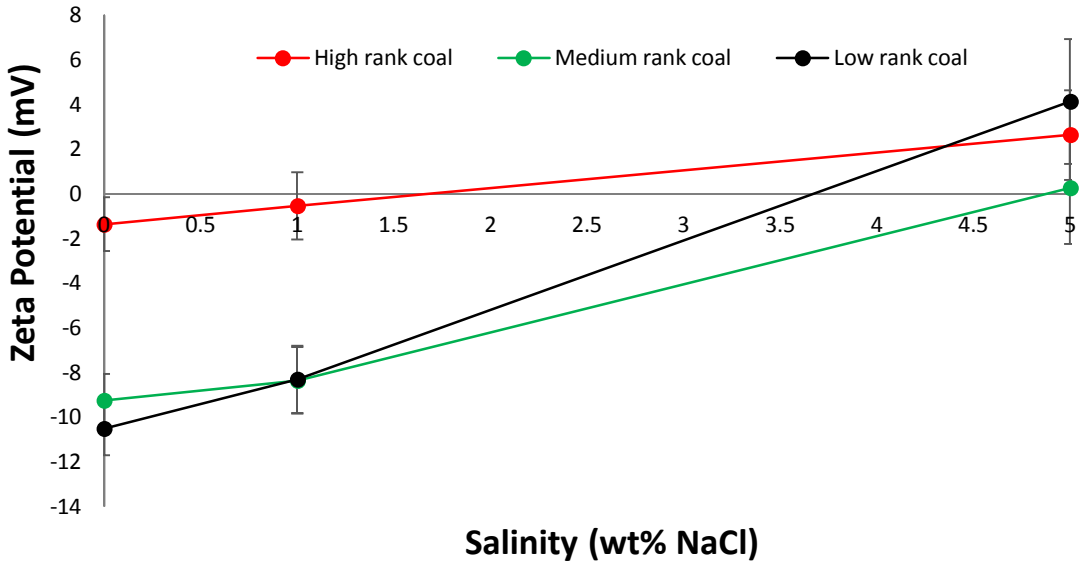

Fig. 8-3 Effect of salinity on zeta potential at 323 K (and ambient pressure) as a function of coal rank.

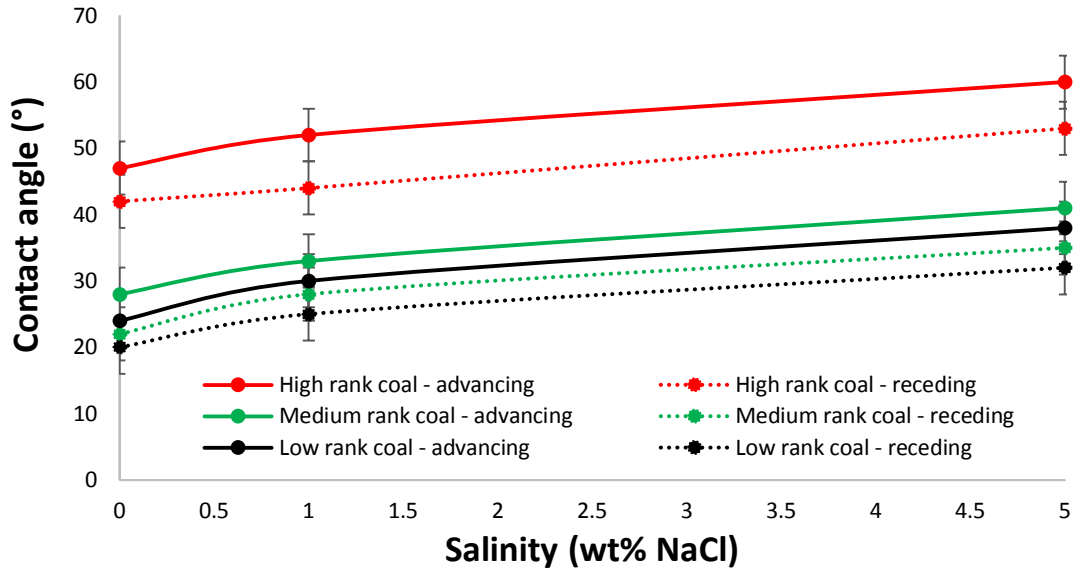

Fig. 8-4 Water contact angle as a function of salinity and coal rank at 323 K (and ambient pressure).

Mechanistically, with the increase in ionic strength, the number of counter ions on the surface increases, which screens the surface charge (and thus results in a reduction of the thickness of the Debye layer). This means that the zeta potential decreases with increasing salt concentration. It is also notable that for the high rank coal, at a salinity

of approximately 1.8 wt% NaCl the zeta potential is zero, while for low rank coal 3.7 wt% NaCl (Fig. 8-3) is required to reach the point of zero zeta potential. The shift in salinity at which a zero charge is obtained varies between high, medium and low rank coal and is associated with the relative affinity of the respective coal surface for H^+ and OH^- ions (which varies with coal rank; Sarwar et al., 2012), and again is related to the concentration of surface functional groups, see FTIR discussion in Section 3.5). The salt content for achieving a zero charge as reported here is also of important consideration for processes that involve colloidal dispersion and coagulation (Butt et al., 2005), e.g. in coal processing (Chi et al., 1988).

Further, we compared zeta potentials to advancing and receding contact angles measured at high pressure (15 MPa and 323 K, Arif et al., 2016c). For all coal ranks, both, θ_a and θ_r, increased with salinity at high pressures (Arif et al., 2016c). For medium rank coal, at 15 MPa and 323 K, θ_a increased from 114° to 127° and θ_r increased from 102° to 112° when salinity increased from 0 wt% NaCl to 5 wt% NaCl brine. For a salinity increase from 5 wt% NaCl to 10 wt% NaCl, θ_a increased from 127° to 132° and θ_r increased from 112° to 116°. Moreover, we found similar trends for low and high rank coals. Considering the fact that the trends of contact angle variation with temperature, salinity, and rank at high pressures were same as those at ambient conditions, it can be hypothesized that zeta potentials might also follow similar trends at high pressures (in a coal/CO_2/brine system) as we showed in this work at ambient pressure (in a coal/air/brine system).

8.3.3 Effect of brine composition on zeta potential and contact angle

The effect of salt type on zeta potential and contact angles was analysed by measuring zeta potentials and contact angles for coal/brine systems at 323 K and ambient pressure for three brines 0.27M (1.6 wt%) NaCl, 0.27M (1 wt%) $CaCl_2$ and 0.305M (1 wt%) $MgCl_2$ for all coal ranks investigated (Fig. 8-5). Note: ionic strength (M) of electrolyte is preferred over mass concentration for comparison among different type of salts. For the ionic strength of 0.27M (1.6 wt%) NaCl, the zeta potential and contact angle values are interpolated from Fig. 8-3 and Fig. 8-4 respectively.

We found that from Na to Ca to Mg brine types, at the same salinity and temperature, the zeta potential increased (Fig. 8-5) and contact angle also increased for all coal

ranks (Fig. 8-6). Specifically, for instance, for medium rank coal the zeta potential at the interface of coal/NaCl-brine measured -6.2 mV, while at the coal/$CaCl_2$-brine interface it measured -3.09 mV, and at coal/$MgCl_2$-brine interface it measured -2.65 mV indicating an increase in zeta potential with increasing cation charge-to-volume ratio (which is 2.61 x 10^{-7} C.pm^{-3} for Na^+, 4.92 x 10^{-7} C.pm^{-3} for Ca^+ and 1.66 x 10^{-6} C.pm^{-3} for Mg^+, Al-Yaseri et al., 2016a).

The negative values of the coal zeta potentials can be attributed to dissociation of surface functional groups (e.g. –COOH) (Crawford and Mainwaring, 2001). The positive zeta potential values obtained are attributed to the surface charge screening effect due to counter ions provided by the cations of the salt as discussed above. Moreover, θ_a increased from 52° to 60° and θ_r increased from 44° to 53° when brine composition changed from NaCl to $MgCl_2$ brines (Fig. 8-6). The results are consistent with (Ibrahim and Nasr-El-Din, 2015) who also reported that coal/brine zeta potentials increased for divalent cations (Ca^{2+} and Mg^{2+}). Harvey et al. (2002) also found that $MgCl_2$ brine resulted in an increase in zeta potential.

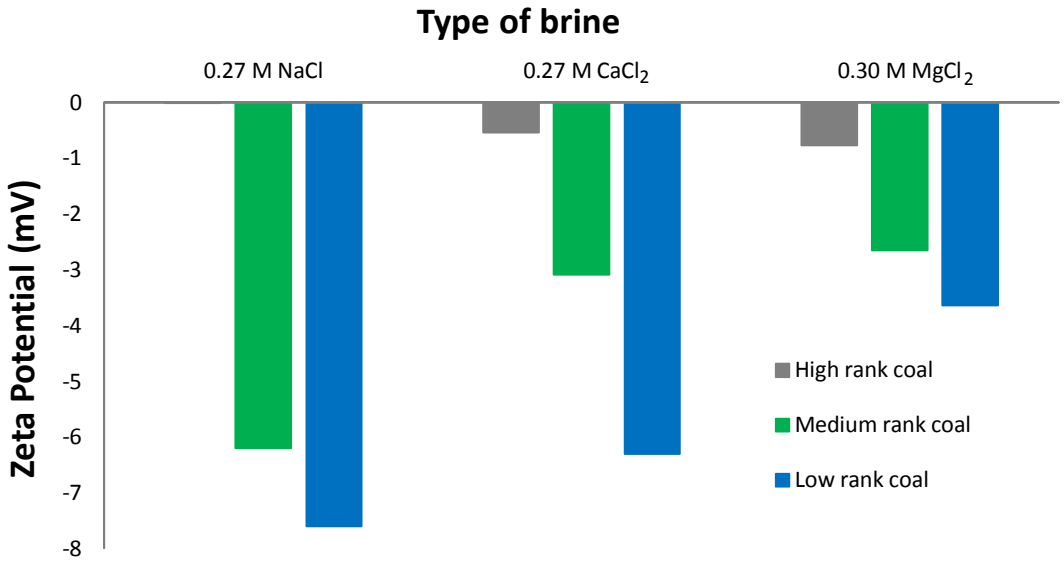

Fig. 8-5 Zeta potential as a function of salt type (NaCl, $CaCl_2$, $MgCl_2$) and coal rank (at 323 K and ambient pressure).

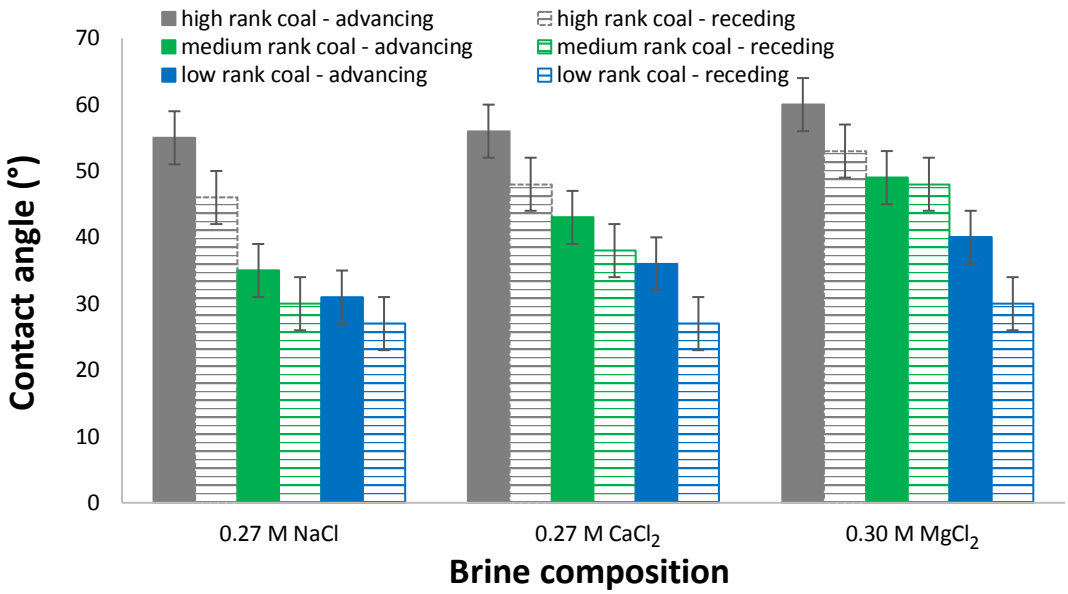

Fig. 8-6 Water contact angle as a function of salt type (NaCl, $CaCl_2$, $MgCl_2$) and coal rank (at 323 K and ambient pressure).

8.3.4 Zeta potential and contact angles as a function of coal rank

To investigate the impact of coal rank on zeta potential and wettability, the results shown in Fig. 8-1 through Fig. 8-6 are reconsidered briefly. At any temperature (except 343 K), the zeta potential of the coal/water system increased with increasing rank (Fig. 8-1). For instance, at 308 K, the zeta potential was -26.2 mV for low rank coal (lignite, R_o = 0.35%), -18.6 mV for medium rank coal (medium volatile bituminous, R_o = 0.82%) and -11.3 mV for high rank coal (semi-anthracite, R_o = 3.92%). This is consistent with Abotsi et al. (1992) who found that at a pH > 5.5 low rank coal had more negative zeta potential values in DI water at room temperature. For instance, they reported that at a pH = 6.5, zeta potentials of lignite (North Dakota) were -40 mV, ~ -30 mV for sub-bituminous and ~ -20 mV for bituminous coals which is quite comparable to our results (at 298 K, zeta potentials measured -36 mV and -25 mV for low and medium rank coals, respectively).

As the coal rank increases, the zeta potential increases, indicating a diminishing number of polar surface sites (a proportion of which are negatively charged due to dissociation, Chi et al., 1988). This results in a strong dependence of the isoelectric

point (the pH at which the surface carries no net charge) and the sign of the zeta potential on the carbon content (i.e. the coal rank, Crawford and Mainwaring, 2001).

In addition, aqueous cationic ion concentrations increase due to dissociation of groups capable of forming ions or decrease by re-adsorption of some dissolved ions on the solid particle surface (Xu et al., 2006). Consequently the electrical double layer on the particle becomes thinner or thicker, which induces a change in zeta potential. In the case of coal, the high mineral content and dissociation of ionogenic groups on the (complex) coal surface (Doymus, 2007) leads to different charges on coals of different ranks (low zeta potentials for low rank coal and high zeta potentials for high rank coal).

We relate the variation in zeta potential as a function of coal rank to the mineralogy of coal. In this context, we note that the major components of the coals are quartz and kaolinite (XRD results, Table 8-2). The low rank coal contains 76% quartz and 24% kaolinite. At room temperature, we find from Kaya and Yukselen (2005) that zeta potential of quartz/water and kaolinite/water were both negative for a wide range of tested pH and that quartz/water zeta potential was much lower than that of the kaolinite/water (e.g. at pH of 6.8, zeta potentials were -52 mV for quartz and -34 mV for kaolinite). Thus our measured value of zeta potential of lignite which was -36.1 mV at room temperature is in accordance to the mineralogy of lignite i.e. the zeta potential of lignite is comparable to individual mineral's zeta potentials. Moreover the percentages of quartz and kaolinite were 41 wt% and 30 wt% in medium rank coals, and 21 wt% and 24 wt% in high rank coals (Table 8-2). The measured values of zeta potential of medium and high rank coal at 298 K were -24.8 mV and -23.1 mV. The impact of minerology is thus clear in the sense that the increase in percentage of quartz and kaolinite in coal leads to a reduction in zeta potential (low rank coal has lower zeta potential because of higher quartz and kaolinite content).

The decrease in negative charge density on the coal surface with increasing coal rank is attributed to the increase in fixed carbon (%) and a decrease in oxygen content with rank (Fuerstenau et al., 1988), Table 5-2. We note that high and medium rank coal demonstrated similar trend of zeta potential variation as a function of salinity but low rank coal showed slightly inconsistent behaviour as a function of salinity at higher

salinity (5wt% NaCl) which can be attributed to the presence of more hydrophilic groups (OH groups) in low rank coals, Fig. 8-3).

The surface charge on coal in the presence of electrolytes is induced by ionization or protonation of the surface carboxylic and hydroxyl groups; note that the dissociation of carboxylic groups is enhanced in the presence of OH^- (Puri, 1970).

$$-COOH_2^+ \overset{H^+}{\leftarrow} -COOH \overset{OH^-}{\longrightarrow} -COO^- + H_2O$$

$$-COH_2^+ \overset{H^+}{\leftarrow} -COH \overset{OH^-}{\longrightarrow} -CO^- + H_2O$$

8.3.5 Surface functional group and wettability

In order to assess the factors responsible for the wetting behaviour of the coal/CO_2/brine systems, we consider experimental data for water advancing and receding contact angle from our previous work (Arif et al. 2016c), Fig. 8-7. It can be seen that water wettability of coals decreases with increasing pressure and increasing rank. At any given CO_2 pressure, the high rank coal had the highest water contact angle which means that these coals are less water-wet. Low rank coals (e.g. lignite) are more water-wet and medium rank coal (e.g. bituminous) are intermediate-wet. These results are in agreement with Shojai Kaveh et al. (2012) who compared CO_2-wettability of semi-anthracite and high volatile bituminous coals, and they measured higher contact angles for semi-anthracite coals, and thus they concluded that hydrophobicity of coals increases with coal rank. However, the surface functional groups responsible for such wetting behaviour were unclear. We thus conducted FTIR (Fourier transformed infrared) spectroscopy measurements on the three coal samples, the results are presented in Fig. 8-8.

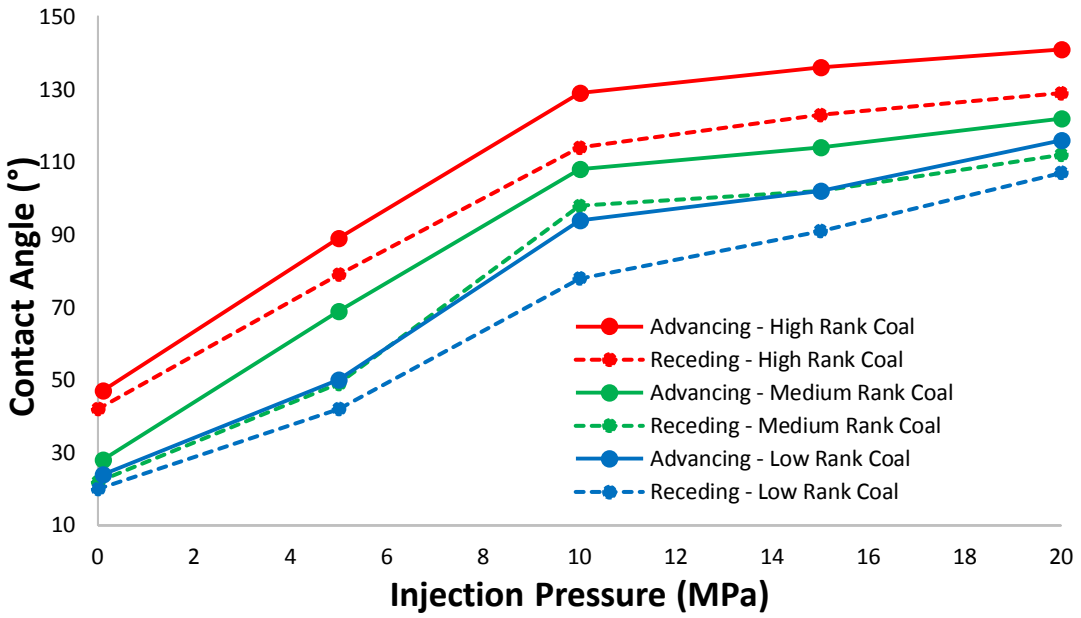

Fig. 8-7 Water contact angle as a function of pressure and coal rank at 323 K (experimental data from Arif et al. 2016c).

High rank coal (semi-anthracite) demonstrated a rather smooth FTIR intensity response throughout the observed wavenumber spectrum, with only small bands observed at a wavenumber range of at 600-800 cm^{-1} due to a possible C-S stretching vibration, the 1000-1100 cm^{-1} due to C-H out of plane bending and Si-O-H asymmetric stretch vibrations and a minute band at ~ 3800 cm^{-1} due to –OH and N-H bond stretching vibrations (Griffiths and De Haseth, 2007; Socrates, 2004); considering the fact that XRD confirmed the presence of Si (Table 8-2) and elemental analysis confirmed the presence of sulphur and nitrogen (Table 5-2). The rough part of the spectra for 2000-2400 cm^{-1} should be ignored as this is where the ATR crystal is absorbing itself (diamond) and the bands don't always perfectly cancel out. From the stand point of surface functional groups and associated wetting behaviour, the absence (or only minute presence) of hydrophilic sites e.g. OH groups in high rank coal is responsible for its hydrophobic behaviour (θ>130°, Fig. 8-7).

On the contrary, medium rank coal (medium volatile bituminous) exhibited significantly stronger bands (in comparison to high rank coal) at wave numbers from 600-800 cm^{-1} and 1000-1100 cm^{-1} indicating the presence of more C-S stretching vibrations and C-H out of plane bending. Moreover, medium rank coal also exhibited

larger bands at ~3600-3700 cm^{-1} which is attributed to O-H and N-H stretch vibrations. Furthermore, distinct bands were observed at 2800-2900, and 1500-1700 cm^{-1} which are due to C=C and C=O stretch vibrations respectively (Socrates, 2004). Thus, the presence of more hydrophilic sites (OH groups) in medium rank coal renders it relatively less CO_2-wet in comparison to high rank coal (e.g. for instance at 10 MPa, θ_a = 108° for medium rank coal in comparison to 129° for high rank coal, Fig. 8-7).

Low rank coal demonstrated the largest peak beginning at about 2800 cm^{-1} and ending at 3800 cm^{-1} which is attributed to the O-H and N-H stretch vibrations and this largest peak is responsible for the hydrophilic nature of lignite coal even at high pressures (Fig. 8-7). The band at ~2900 cm^{-1} observed for low rank coal is due to the presence of aliphatic C-H stretching vibrations (Wu et al., 2014); however, its absence in high rank coal is unusual and is perhaps due to C-H stretching where the carbon is in a C=C bond. Moreover, the sharp band observed at 1500-1800 cm^{-1} for low rank coal is attributed to aromatic ring vibrations, which are enhanced by oxygen groups (Sarwar et al., 2012). The corresponding shoulder peaks at 1600 cm^{-1} is attributed to C=O stretching vibrations and these represent all C=O functionalities, e.g. carboxylic acids or phenolic esters (Manoj et al., 2009; Tsai, 1982). Chemically, the presence of such polar functional groups leads to an increase in hydrophilicity of the coals' surface and that is evident from the contact angle data (e.g. lignite is relatively more water-wet as compared to bituminous and anthracite coals).

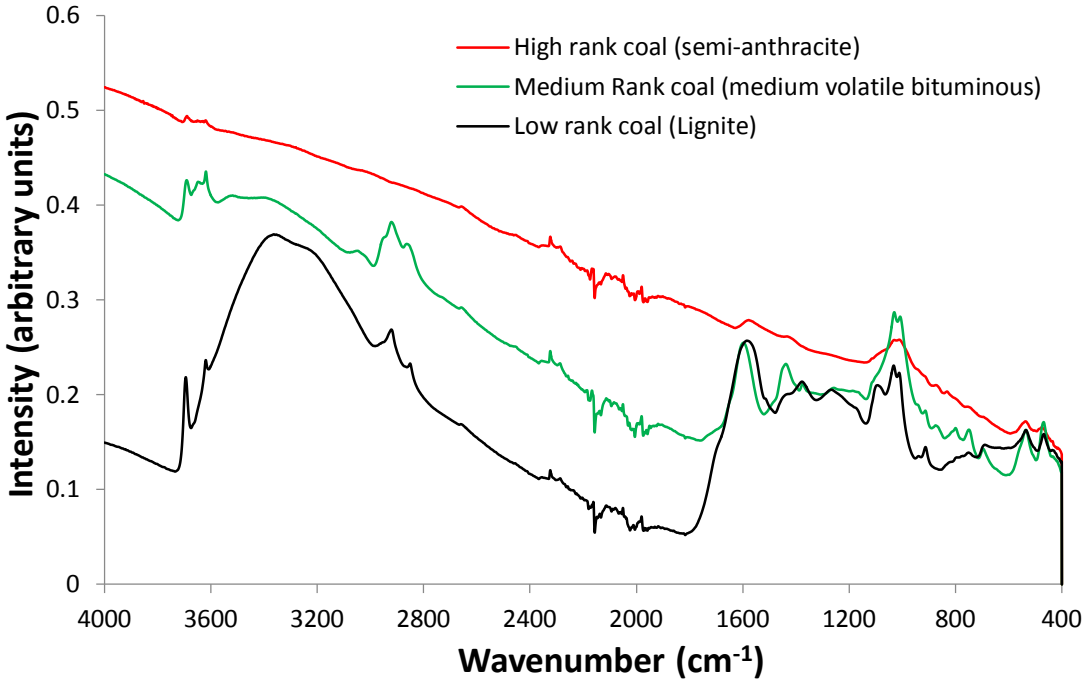

Fig. 8-8 ATR-infrared spectroscopy measurements on low, medium and high rank coals

In summary, the much lower number of Si-OH, hydroxyl, ester, and carboxylic groups in high rank coal is responsible for its hydrophobic behaviour. On the contrary, the abundance of these groups (especially OH) is responsible for the hydrophilic nature of low rank coal. Medium rank coal stands somewhere in the middle (consistent with contact angle data; Fig. 8-7). Thus, the increase in contact angle (at typical operating conditions) with coal rank (Fig. 8-7, Arif et al., 2016c) is adequately explained by surface functional groups.

8.3.6 Correlation between zeta potential and wettability

Our results showed that zeta potential increased with increasing rank and salinity, and contact angle also increased with increasing rank and salinity, implying a positive correlation between zeta potential and coal-wettability, i.e. higher zeta potential correspond to a less water-wet surface (= higher θ). In order to demonstrate this relation, we developed a cross plot between water advancing contact angle and zeta potential as a function of rank (Fig. 8-9a) and as a function of salinity (Fig. 8-9b).

Specifically, for any given temperature (298 K-343 K), advancing contact angle increased with the increase in zeta potential (all solid coloured trend lines in Fig. 8-9a) for all coals. Moreover, as salinity increased, zeta potential increased and contact angle also increased (Fig. 8-9b). The overall correlation between zeta potential and wettability is also positive (Fig. 8-9b).

However, with respect to temperature, a contradictory trend is found such that as temperature increased zeta potential increased but contact angle decreased (this can be visualized by joining the points of the same symbol in Fig. 8-9a by means of a trend line). The reason for this contradiction is not clearly known, yet the possible factors responsible for this deviation could be evaporation at high temperature, and/or the experimental error associated with equipment at high temperatures (which we found was relatively high).

On a whole, it is reasonable to establish that zeta potential has significant control on coal-wettability consistent with Jackson et al. (2016) who reported that in a carbonate/oil/brine system, the zeta potential was a primary driver of wettability. Thus, we here also establish that zeta potential provides a primary control on the coal-wettability variation. Moreover, as shown in our previous work (Arif et al., 2016d), the pressure and temperature dependency of wettability of rock forming minerals and coals is also governed by the interfacial interactions of fluids with solid surface.

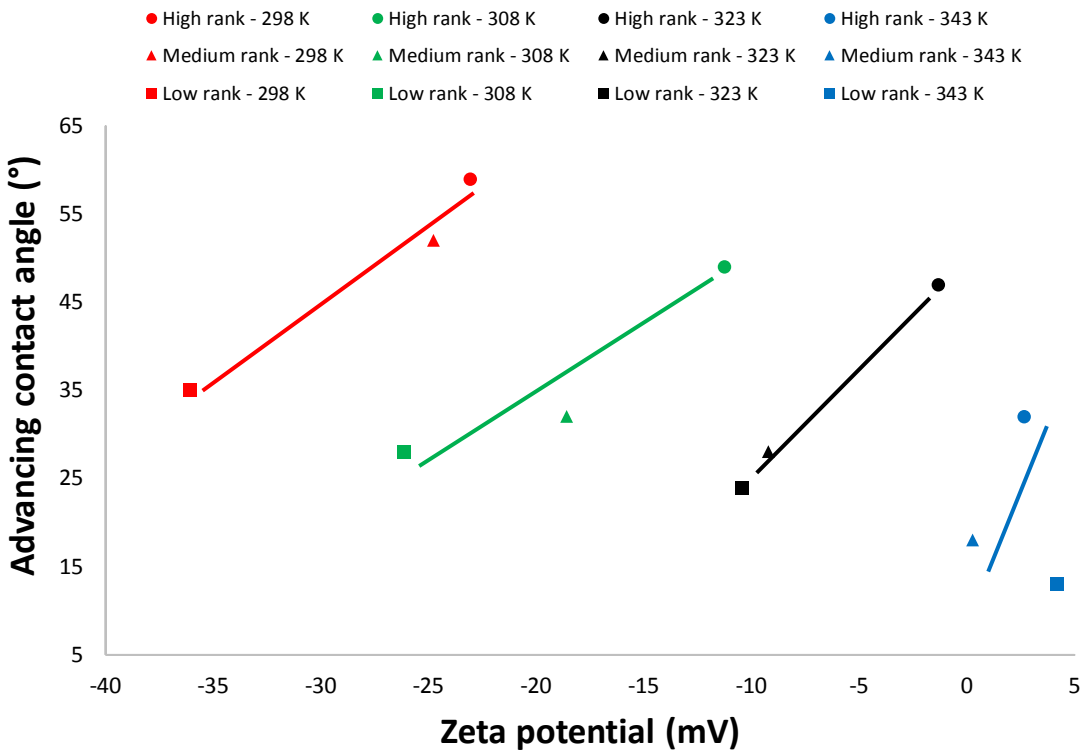

a) Contact angle-zeta potential cross plot at all temperatures as a function of coal rank. Circle = high rank, triangle = medium rank, square = low rank coal. The colour differentiates the measurements as a function of temperature (red, green, black and blue). The solid lines are the trend lines for relation between zeta potential and wettability as a function of coal rank at isothermal and iso-saline conditions.

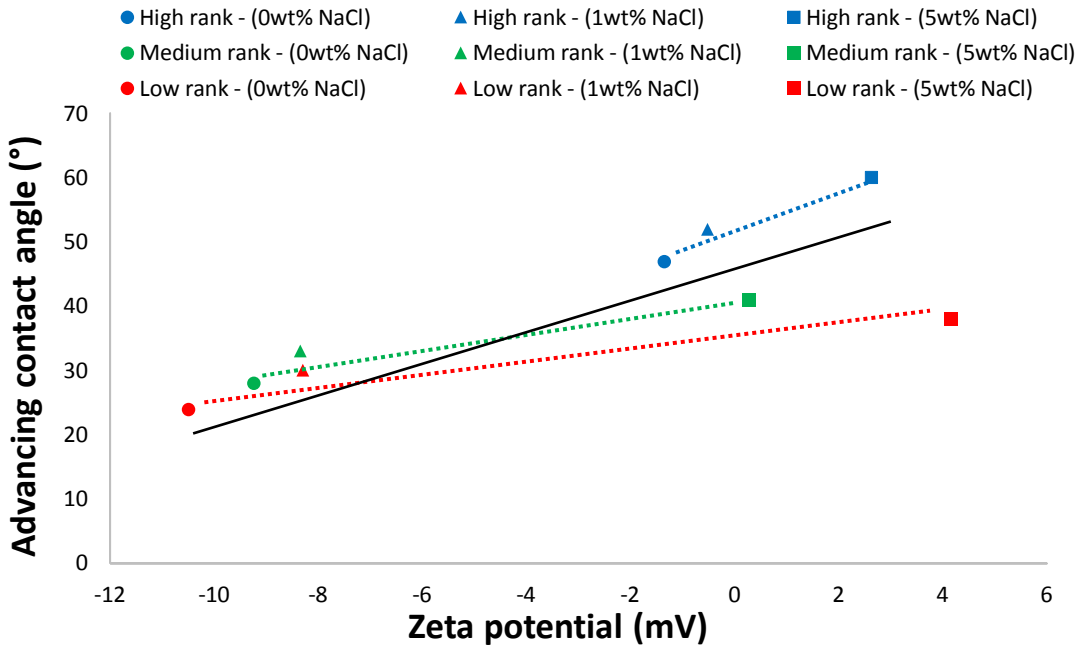

b) Contact angle-zeta potential cross plot as a function of salinity for all coal ranks at 323 K. The symbol differentiates the measurements as a function of salinity (Circle: DI-water, triangle: 1wt% NaCl, square: 5wt% NaCl). The dotted lines are the trend lines for relation between zeta potential and wettability as a function of salinity for all ranks at isothermal conditions. The solid black line represent the overall trend.

Fig. 8-9 Zeta potential and contact angle relationships

8.4 Implications

In order to assess the factors affecting wetting behaviour of coals, which is of immense importance in terms of understanding micro- and nano-scale fluid dynamics in coal seams, we provided insight into the fluid interactions at the coal/brine interface and their relation with wetting behaviour as a function of temperature, salinity and coal rank. The measured data essentially leads to a better understanding of the mechanism occurring at the pore scale and is, therefore, useful for understanding CO_2 storage and (enhanced) methane recovery in coal beds. Zeta potential measurements provide a better understanding of the effect of salinity and rank on wettability, however trend of zeta potential with temperature needs further investigation. Moreover, the presence of typical surface functional groups (e.g. OH and carboxylic groups) is responsible for the specific wettability of coals (Fig. 8-7), and this data can thus be used to assess the storage potential of coal seams.

Specifically, we observed that high rank coal was CO_2-wet (at reservoir conditions), and thus once injected, CO_2 occupies the smallest pores (nano- and micropores in the coal seams) due to its larger affinity to adsorb onto the coal surface (Busch et al., 2003; Clarkson and Bustin, 2000). As a result, methane is displaced towards the production wells and thus leads to improved methane production. However, the lower coal ranks are relatively less suitable for enhanced methane recovery and CO_2-storage due to their more water-wet characteristics, which implies poorer adsorption of CO_2 onto the coal micro surface (Mastalerz et al., 2004). We also point out that with the increase in pressure coal swelling occurs which leads to a reduction in permeability; and this effect limits CO_2 injection into coal seams (Reucroft and Sethuraman, 1987).

8.5 Conclusions

We measured zeta potentials as a function of temperature and salinity for low, medium and high rank coals. It was found that zeta potential increased with temperature and the water contact angle decreased with temperature. Zeta potentials increased with increasing salinity due to reduction in the thickness of the Debye layer, which occurred because of the surface charge screening by the counter ions. The coal/brine/CO_2 water contact angle also increased with increasing salinity. Furthermore Mg^{2+} brine demonstrated higher contact angles and higher zeta potentials than those of Ca^{2+} and Na^{+} brines, and, at any temperature or salinity, high rank coals exhibited high zeta potentials, which is due to their higher carbon content and associated lower surface charge (due to absence of polar functional groups). Zeta potential increased with salinity and rank, and contact angles also increased with salinity and rank, implying a positive relation between zeta potential and wettability. Thus, it can be concluded that zeta potential have a significant control on coal-wettability.

The contact angle trends with temperature and salinity at ambient conditions were similar to those at high pressures and thus we hypothesized that zeta potential measurements at ambient conditions should follow similar trends at high pressure conditions. Furthermore, we conducted ATR-FTIR spectroscopy measurements on the coal substrates, and we measured an abundance of OH groups on the low rank coal, which is responsible for their hydrophilic nature, while high rank coals exhibited minimal OH peaks (and thus absence of OH groups), which explains their hydrophobic nature.

We furthermore provided implications of the measured data for CO_2-storage and enhanced methane recovery and it can be concluded that high rank coal seams (at low temperature and high pressure) are most feasible for CO_2-storage and enhanced methane recovery due to better CO_2-wettability and thus improved CO_2-adsoprtion capacity.

Chapter 9 Conclusions, Recommendations and Outlook for Future Work

9.1 Conclusions

This thesis reported experimental wettability data of rock/CO_2/brine systems by means of advancing and receding contact angle measurements as a function of pressure, temperature, salinity and surface roughness for rock forming minerals, and coal seams and shales. A broad range of experimental conditions were covered (pressure: 0.1 MPa – 20 MPa, temperature: 298 K – 343 K, brine salinity: 0 wt% NaCl to 20 wt% NaCl). The associated implications of wettability and interfacial tension on principle trapping mechanisms were also analysed. In general, the results of the study lead to a better understanding of wettability and realization of its impact on CO_2 storage capacity and containment security predictions. The following points summarize the most significant findings of this work:

1. Wettability of rock/CO_2/brine systems:

- Both advancing and receding contact angles increased with increasing pressure and salinity throughout the experimental matrix, and this trend was consistent for all the samples tested. The observed behaviour was consistent with most of the published data on CO_2-wettabiltiy. The results were also consistent with molecular dynamics simulations, capillary pressure-saturation relationships, and 3D microCT imaging of CO_2 cluster distribution in water-wet and oil-wet formations. Thus, the research concludes that increasing pressure causes significant de-wetting of the rock surface (i.e. surface turns less water-wet with increasing pressure), while increasing salinity only slightly de-wets it. Increase in temperature, however, makes the rock more water-wet. The magnitude of contact angle increase with pressure is more than its decrease with temperature implying that system is expected to be more non-wetting with the increase in depth.

- Both calcite and mica were strongly water-wet at ambient conditions. However, at 20 MPa and 308 K, calcite is weakly CO_2-wet while mica is intermediate-wet. Such conditions may lead to a significant reduction in the storage capacity of caprocks and storage rocks (comprising of these minerals). However, a detailed storage capacity estimate would involve storable CO_2 mass computation, and rock minerology consideration. Wettability measurements on rock forming minerals revealed that low pressure, high temperature and low salinity conditions favour the CO_2 trapping potential due to water-wet behaviour of rock under these conditions.

- CO_2-wettability of coals increased consistently with coal rank. Under in-situ conditions, high rank coal was strongly CO_2-wet (maximum θ = 150^o), medium rank coal was weakly CO_2-wet (maximum θ = 140^o), and low rank coal was weakly water-wet to intermediate-wet (maximum θ = ~110^o). Such wetting characteristics of coals suggest that all other factors being equal, high rank coals are more suitable for CO_2 storage and enhanced methane recovery due to their CO_2-wet behaviour, which in turn promotes CO_2 adsorption onto the coal micropores.

- Shale CO_2-wettability scaled with shale-TOC. More specifically, low-TOC shale was water-wet, high-TOC shale was weakly CO_2-wet and ultrahigh-TOC shale was strongly CO_2-wet. It was deduced from such wetting behaviour that for all other factors being equal, storage capacity is higher for the low-TOC shales, while storage capacity is reduced for high-TOC shales. However, suitability of CO_2 storage in scenarios where caprock is a high-TOC shale is also strongly dependent on the hydrocarbon saturation of the shale, the bulk permeability and thickness of the shale and the carbon storage scenario (saline aquifer, depleted hydrocarbon field or other storage scenario). In addition, high-TOC shales may also be suitable as independent CO_2 sinks for CO_2 storage by adsorption trapping.

2. CO_2/brine interfacial tension:

- CO_2/brine interfacial tension decreased with increasing pressure, and it increased with increasing temperature and increasing brine salinity. The results were consistent with previous studies on CO_2/brine interfacial tension.

3. Factors controlling the wettability alteration:

a. Solid surface energy analysis:

- Rock/fluid interfacial tensions were simulated using the Neumann's equation of state approach to quantify the mineral/CO_2 and mineral/brine interfacial tensions. Mineral/CO_2 interfacial tension decreased with increasing pressure, which favours the interaction of CO_2 with the rock surface, hence a higher contact angle with pressure is justified– i.e. a more CO_2-wet surface. Similarly, the increase in mineral/CO_2 interfacial tension with temperature was consist with the observed wettability alteration with temperature.
- At the same pressure and temperature of investigation, the mineral/CO_2 interfacial tensions were highest for the more water-wet surface. For instance, mica/CO_2 interfacial tension was lower than that of quartz, which is consistent with the hydrophobic nature of the mica surface at high pressures. Similarly, high rank coal demonstrated lower coal/CO_2 interfacial tensions as compared to low rank coal, which implied that high rank coal is more hydrophobic than low rank coal.

b. Surface chemistry aspects:

- This thesis directly correlated rock wettability to the electrochemical changes at the mineral/brine interface. A systematic comparison of zeta potentials and contact angles at coal/brine interface and their associated trends demonstrated a positive correlation between zeta potential and wettability. Both contact angles and zeta potential increased with ionic strength. In addition, zeta potentials were higher in magnitude for the coal/brine interfaces when brines were comprised of divalent (rather than monovalent) cations, and the corresponding contact angles demonstrated the same trend. This led to the conclusion that the electrochemical changes at the mineral/brine interface have a significant control over the wettability alteration due to salinity where the

higher salinities and higher concentration of divalent cations in the brines increased the contact angle at coal/brine interfaces.

- Zeta potential at the coal/brine interface increased with temperature, however the corresponding contact angles decreased with temperature i.e. an indirect proportionality. This led to a conclusion that temperature dependent zeta potential is a secondary factor controlling the temperature dependency of wettability.
- Abundance of hydrophilic groups i.e. OH groups on the low rank coal were held responsible for water-wet behaviour of such coals, while high rank coals demonstrated minimal OH peaks, which elucidated their hydrophobic nature.

9.2 Recommendations and outlook for future work

Despite a broader range of wettability data collection for various important rock/CO_2/brine systems, and the in-depth analysis of the associated wettability alteration mechanisms, there are certain gaps and limitations which this work did not address, and thus define the outlook for future work as follows:

- The surface roughness modification due to chemical interaction of CO_2 and brine, especially on an electrochemically active surface such as calcite, is still an open research area and requires further investigation.

- The composite influence of surface chemical heterogeneity is still not well established. Such characterization must first involve fractional characterization of wettability for individual minerals, and subsequently sum these up to govern the true picture of overall rock wettability using the following relation (Iglauer et al., 2015a):

$$\gamma_{i,cw} cos\theta^* = \sum_{n=1}^{N} f_i(\gamma_{i,sc} - \gamma_{i,sw}) \qquad Eq.\ 9.1$$

In Eq. 9.1, '*i*' is the number of surface components, θ^* is the contact angle on heterogeneous surface, '*f*' is the fraction of material on the substrate; $\gamma_{i,sc}$, $\gamma_{i,sw}$ and $\gamma_{i,cw}$ are the solid/CO_2, solid/water and CO_2/brine interfacial tensions of the i^{th} components respectively.

- CO_2-wettability of coals and shales revealed that high rank coals and high-TOC shale, which were CO_2-wet, have the potential for CO_2 storage and enhanced methane recovery via 'adsorption trapping' based on other supplementary evidence. However, wettability studies alone may not fully draw such conclusions. Instead, a wettability/adsorption coupled study will establish a more realistic outlook of CO_2 storage potential of coals and shales by microscopic adsorption.

- The influence of a new parameter i.e. shale-TOC on shale CO_2-wettabiltiy where the samples of different TOCs were from distinct basins/origin was investigated. It is, however, also important to analyse the impact of TOC variation on wettability of shale within a single shale formation, as TOC within a shale formation varies across the depth and lateral extent of the reservoir.

- CO_2-wettability and CO_2/brine interfacial tension have implications for characterizing structural trapping capacity. However, prediction of structural trapping by Eq. 1.1 provides only a first approximation of the storage heights with the assumption of the rock being a cylindrical capillary, whereas realistically rock pore morphology is considerably more complex. A direct estimation of capillary entry pressure of CO_2 (P_c) via a sophisticated coreflooding setup can overcome this limitation. In summary, practical storage capacity estimates should involve a) the influence of caprock composition and the associated wettability of real caprock samples, b) consideration of pore geometry, and c) caprock permeability characterization to establish the rate of CO_2 leakage through the caprock.

- Although there is a great deal of consensus among various pore scale experimental studies and reservoir scale simulations that residual trapping capacity is higher when the rock in question is water-wet, one mechanism, needs further investigation. It is the 'lateral coverage of CO_2' in the storage rock, which is actually higher when the rock is more CO_2-wet. Essentially, a thicker CO_2 plume exists in CO_2-wet storage rocks compared to a relatively

thin plume in water-wet rocks. Thus, the more realistic estimate of overall storage capacity must account for this effect.

- Neumann's equation of state was reasonably good in terms of its predictive ability for solid/CO_2 interfacial tensions, however there is one limitation concerning the prediction of 'solid/brine' interfacial tension, which is that solid/brine interfacial tension is only dependent on temperature and brine salinity but not on 'pressure'. However, solid/brine interfacial tension may change due to increased CO_2/brine dissolution resulting in solution pH reduction, which in turn may lead to increased protonation of surface silanol groups. Therefore, future studies must account for this effect.

- Zeta potentials measurements in this study were limited to ambient pressure primarily due to the limitation associated with the commercially available zeta potential measurement instruments. The development of a sophisticated facility that allows zeta potential measurements for a true rock/CO_2/brine system at high CO_2 pressures will lead to a broader experimental matrix for studies on wettability alteration mechanisms.

- Advanced characterization tools such as FTIR spectroscopy qualitatively explained the functional groups controlling the absolute wetting behaviour; however, such characterization at high CO_2 pressure is still a challenge and will certainly improve the outlook of wettability studies in future.

References

Abotsi, G. M., Bota, K. B., & Saha, G. (1992). Interfacial phenomena in coal impregnation with catalysts. *Energy & Fuels*, 6(6), 779-782.

Adamczyk, Z., Zaucha, M., & Zembala, M. (2010). Zeta potential of mica covered by colloid particles: a streaming potential study. *Langmuir*, *26*(12), 9368-9377.

Adamson, A. W., & Gast, A. P. (1997). The solid–liquid interface-contact angle. *Physical chemistry of surfaces*, *4*, 333-361.

Aggelopoulos, C. A., Robin, M., Perfetti, E., & Vizika, O. (2010). $CO_2/CaCl_2$ solution interfacial tensions under CO_2 geological storage conditions: influence of cation valence on interfacial tension. *Advances in Water Resources*, *33*(6), 691-697.

Aggelopoulos, C. A., Robin, M., & Vizika, O. (2011). Interfacial tension between CO_2 and brine (NaCl+ $CaCl_2$) at elevated pressures and temperatures: The additive effect of different salts. *Advances in Water Resources*, *34*(4), 505-511.

Al-Anssari, S., Barifcani, A., Wang, S., & Iglauer, S. (2016). Wettability alteration of oil-wet carbonate by silica nanofluid. *Journal of Colloid and Interface Science*, *461*, 435-442.

Al Mahrouqi, D., Vinogradov, J., & Jackson, M. D. (2016). Temperature dependence of the zeta potential in intact natural carbonates. *Geophysical Research Letters*, *43*(22).

Al-Menhali, A., Niu, B., & Krevor, S. (2015). Capillarity and wetting of carbon dioxide and brine during drainage in Berea sandstone at reservoir conditions. *Water Resources Research*, 51(10), 7895-7914.

Al-Menhali, A. S., Menke, H. P., Blunt, M. J., & Krevor, S. C. (2016). Pore Scale Observations of Trapped CO_2 in Mixed-Wet Carbonate Rock: Applications to Storage in Oil Fields. *Environmental Science & Technology*, *50*(18), 10282-10290.

Alroudhan, A., Vinogradov, J., & Jackson, M. D. (2016). Zeta potential of intact natural limestone: Impact of potential-determining ions Ca, Mg and SO_4. *Colloids and Surfaces A: Physicochemical and Engineering Aspects*, *493*, 83-98.

Alvarez, N. J., Walker, L. M., & Anna, S. L. (2009). A non-gradient based algorithm for the determination of surface tension from a pendant drop: Application to low Bond number drop shapes. *Journal of Colloid and Interface Science*, *333*(2), 557-562.

Al-Yaseri, A. Z., Lebedev, M., Barifcani, A., & Iglauer, S. (2016a). Receding and advancing (CO_2+ brine+ quartz) contact angles as a function of pressure, temperature, surface roughness, salt type and salinity. *The Journal of Chemical Thermodynamics*, *93*, 416-423.

Al-Yaseri, A. Z., Roshan, H., Lebedev, M., Barifcani, A., & Iglauer, S. (2016b). Dependence of quartz wettability on fluid density. *Geophysical Research Letters*, *43*(8), 3771-3776.

Akutsu, T., Yamaji, Y., Yamaguchi, H., Watanabe, M., Smith, R. L., & Inomata, H. (2007). Interfacial tension between water and high pressure CO_2 in the presence of hydrocarbon surfactants. *Fluid Phase Equilibria*, *257*(2), 163-168.

Alkan, M., Demirbaş, Ö., & Doğan, M. (2005). Electrokinetic properties of kaolinite in mono-and multivalent electrolyte solutions. *Microporous and Mesoporous Materials*, 83(1), 51-59.

Akiya, N. and P. E. Savage (2002). Roles of Water for Chemical Reactions in High-Temperature Water. *Chemical Reviews*, 102(8), 2725-2750.

Ameri, A., Kaveh, N. S., Rudolph, E. S. J., Wolf, K. H., Farajzadeh, R., & Bruining, J. (2013). Investigation on Interfacial Interactions among Crude Oil–Brine–Sandstone Rock–CO_2 by Contact Angle Measurements. *Energy & Fuels*, 27(2), 1015-1025.

Amott, E. (1959). Observations relating to the wettability of porous rock.

Anderson, W. (1986). Wettability literature survey-part 2: Wettability measurement. *Journal of petroleum technology*, *38*(11), 1-246.

André, L., Azaroual, M., & Menjoz, A. (2010). Numerical simulations of the thermal impact of supercritical CO_2 injection on chemical reactivity in a carbonate saline reservoir. *Transport in Porous Media*, 82(1), 247-274.

Andrew, M., Bijeljic, B., & Blunt, M. J. (2014). Pore-scale contact angle measurements at reservoir conditions using X-ray microtomography. *Advances in Water Resources*, 68, 24-31.

Aplan, F. F. (1993). Coal properties dictate coal flotation strategies. *Mining engineering*, *45*(1), 83-96.

Arif, M., Al-Yaseri, A. Z., Barifcani, A., Lebedev, M., & Iglauer, S. (2016a). Impact of pressure and temperature on CO_2–brine–mica contact angles and CO_2–brine interfacial tension: Implications for carbon geo-sequestration. *Journal of Colloid and Interface Science*, 462, 208-215.

Arif, M., Barifcani, A., Lebedev, M., & Iglauer, S. (2016b). Structural trapping capacity of oil-wet caprock as a function of pressure, temperature and salinity. *International Journal of Greenhouse Gas Control*, 50, 112-120.

Arif, M., Barifcani, A., Lebedev, M., & Iglauer, S. (2016c). CO_2-wettability of low to high rank coal seams: Implications for carbon sequestration and enhanced methane recovery. *Fuel*, 181, 680-689.

Arif, M., Barifcani, A., & Iglauer, S. (2016d). Solid/CO_2 and solid/water interfacial tensions as a function of pressure, temperature, salinity and mineral type: Implications for CO_2-wettability and CO_2 geo-storage. *International Journal of Greenhouse Gas Control*, 53, 263-273.

Arif, M., Jones, F., Barifcani, A., & Iglauer, S. (2017a). Influence of surface chemistry on interfacial properties of low to high rank coal seams. *Fuel*, 194, 211-221.

Arif, M., Jones, F., Barifcani, A., & Iglauer, S. (2017b). Electrochemical investigation of the effect of temperature, salinity and salt type on brine/mineral interfacial properties. *International Journal of Greenhouse Gas Control*, 59, 136-147.

Arns, C. H., Bauget, F., Limaye, A., Sakellariou, A., Senden, T., Sheppard, A., ... & Oren, P. E. (2005). Pore scale characterization of carbonates using X-ray microtomography. *SPE Journal*, 10(04), 475-484.

Armitage, P. J., Faulkner, D. R., & Worden, R. H. (2013). Caprock corrosion. *Nature Geoscience*, *6*(2), 79-80.

Arts, R. J., Vandeweijer, V. P., Hofstee, C., Pluymaekers, M. P. D., Loeve, D., Kopp, A., & Plug, W. J. (2012). The feasibility of CO_2 storage in the depleted P18-4 gas field offshore the Netherlands (the ROAD project). *International Journal of Greenhouse Gas Control*, *11*, S10-S20.

Attention theory note 1, Static and dynamic contact angles and their measurement techniques, www.bioscientific.com

Bachu, S., Gunter, W. D., & Perkins, E. H. (1994). Aquifer disposal of CO_2: hydrodynamic and mineral trapping. *Energy Conversion and Management*, 35(4), 269-279.

Bachu, S. (2003). Screening and ranking of sedimentary basins for sequestration of CO_2 in geological media in response to climate change. *Environmental Geology*, 44(3), 277-289.

Bachu, S., Bonijoly, D., Bradshaw, J., Burruss, R., Holloway, S., Christensen, N. P., & Mathiassen, O. M. (2007). CO_2 storage capacity estimation: methodology and gaps. *International Journal of Greenhouse Gas Control*, 1(4), 430-443.

Bachu, S., & Bennion, D. B. (2008). Interfacial tension between CO_2, freshwater, and brine in the range of pressure from (2 to 27) MPa, temperature from (20 to 125) °C, and water salinity from (0 to 334 000) mg· L^{-1}. *Journal of Chemical & Engineering Data*, *54*(3), 765-775.

Bae, J. S., & Bhatia, S. K. (2006). High-pressure adsorption of methane and carbon dioxide on coal. *Energy & Fuels*, 20(6), 2599-2607.

Bailey, S. W. (1984). Crystal chemistry of the true micas. Reviews in Mineralogy and Geochemistry, 13(1), 13-60.

Barton, A. F. (1991). *CRC handbook of solubility parameters and other cohesion parameters*. CRC press.

Bennion, B., & Bachu, S. (2005, January). Relative permeability characteristics for supercritical CO_2 displacing water in a variety of potential sequestration zones. In *SPE Annual Technical Conference and Exhibition*. Society of Petroleum Engineers.

Blunt, M., Fayers, F. J., & Orr, F. M. (1993). Carbon dioxide in enhanced oil recovery. *Energy Conversion and Management*, *34*(9), 1197-1204.

Bikkina, P.K., 2011. Contact angle measurements of CO_2–water–quartz/calcite systems in the perspective of carbon sequestration. International Journal of Greenhouse Gas Control 5 (5), 1259-1271.

Bikkina, P. K. (2012). Reply to the comments on "Contact angle measurements of CO_2–water–quartz/calcite systems in the perspective of carbon sequestration". *International Journal of Greenhouse Gas Control*, *7*, 263-264.

Binks, B. P., & Clint, J. H. (2002). Solid wettability from surface energy components: relevance to Pickering emulsions. *Langmuir*, 18(4), 1270-1273.

Brandon, S., & Marmur, A. (1996). Simulation of contact angle hysteresis on chemically heterogeneous surfaces. *Journal of Colloid and Interface Science, 183*(2), 351-355.

Broseta, D., Tonnet, N., & Shah, V. (2012). Are rocks still water-wet in the presence of dense CO_2 or H_2S? *Geofluids*, 12(4), 280-294.

Brown, M. A., Huthwelker, T., Beloqui Redondo, A., Janousch, M., Faubel, M., Arrell, C. A., ... & van Bokhoven, J. A. (2012). Changes in the silanol protonation state measured in situ at the silica–aqueous interface. *The Journal of Physical Chemistry Letters*, 3(2), 231-235.

Bryant, S., & Blunt, M. (1992). Prediction of relative permeability in simple porous media. *Physical Review A*, 46(4), 2004.

Buckingham, S., & Turner, M. (Eds.). (2008). Understanding environmental issues. Sage.

Buckley, J. S., Liu, Y., & Monsterleet, S. (1998). Mechanisms of wetting alteration by crude oils. *SPE Journal*, *3*(01), 54-61.

Budisa, N., & Schulze-Makuch, D. (2014). Supercritical carbon dioxide and its potential as a life-sustaining solvent in a planetary environment. *Life*, *4*(3), 331-340.

Burnside, N., & Naylor, M. (2011) Evaluation of CO_2 storage actuarial risk: defining an evidence base. DEVEX, 12th May, *School of Geoscience, University of Edinburgh*, Aberdeen.

Burton, M., Kumar, N., & Bryant, S. L. (2009). CO_2 injectivity into brine aquifers: Why relative permeability matters as much as absolute permeability. *Energy Procedia*, 1(1), 3091-3098.

Busch, A., & Gensterblum, Y. (2011). CBM and CO_2-ECBM related sorption processes in coal: a review. *International Journal of Coal Geology*, *87*(2), 49-71.

Busch, A., Gensterblum, Y., & Krooss, B. M. (2003). Methane and CO_2 sorption and desorption measurements on dry Argonne premium coals: pure components and mixtures. *International Journal of Coal Geology*, 55(2), 205-224.

Busch, A., Gensterblum, Y., Krooss, B. M., & Littke, R. (2004). Methane and carbon dioxide adsorption–diffusion experiments on coal: upscaling and modelling. *International Journal of Coal Geology*, 60(2), 151-168.

Busch, A., Alles, S., Gensterblum, Y., Prinz, D., Dewhurst, D. N., Raven, M. D., ... & Krooss, B. M. (2008). Carbon dioxide storage potential of shales. *International Journal of Greenhouse Gas Control*, 2(3), 297-308.

Bustin, R. M., Barnes, M. A., & Barnes, W. C. (1985). Diagenesis 10. Quantification and modelling of organic diagenesis. *Geoscience Canada*, *12*(1).

Bustin, R. M., & Clarkson, C. R. (1998). Geological controls on coalbed methane reservoir capacity and gas content. *International Journal of Coal Geology*, 38(1), 3-26.

Butt, H. J., Graf, K., & Kappl, M. (2006). *Physics and chemistry of interfaces*. John Wiley & Sons.

Calemma, V., Rausa, R., Margarit, R., & Girardi, E. (1988). FT-ir study of coal oxidation at low temperature. *Fuel*, 67(6), 764-770.

Cape Grim (2017). Cape Grim Greenhouse Gas Web Data. http://www.csiro.au/greenhouse-gases/.

Carre, A., Gastel, J. C., & Shanahan, M. E. (1996). Viscoelastic effects in the spreading of liquids. *Nature*, *379*(6564), 432.

Cavalli, A., Bera, B., van den Ende, D., & Mugele, F. (2016). Analytic model for the electrowetting properties of oil-water-solid systems. *Physical Review E*, 93(4), 042606.

Chalbaud, C., Robin, M., Lombard, J. M., Martin, F., Egermann, P., & Bertin, H. (2009). Interfacial tension measurements and wettability evaluation for geological CO_2 storage. *Advances in Water Resources*, 32(1), 98-109.

Chaudhary, K., Bayani Cardenas, M., Wolfe, W. W., Maisano, J. A., Ketcham, R. A., & Bennett, P. C. (2013). Pore-scale trapping of supercritical CO_2 and the role of grain wettability and shape. *Geophysical Research Letters*, *40*(15), 3878-3882.

Chaudhary, K., Bayani Cardenas, M., Wolfe, W. W., Maisano, J. A., Ketcham, R. A., & Bennett, P. C. (2013). Pore-scale trapping of supercritical CO_2 and the role of grain wettability and shape. *Geophysical Research Letters*, *40*(15), 3878-3882.

Chen, C., Wan, J., Li, W., & Song, Y. (2015). Water contact angles on quartz surfaces under supercritical CO_2 sequestration conditions: Experimental and molecular dynamics simulation studies. *International Journal of Greenhouse Gas Control*, 42, 655-665.

Chi, S. M., Morsi, B. I., Klinzing, G. E., & Chiang, S. H. (1988). Study of interfacial properties in the liquid carbon dioxide-water-coal system. *Energy & Fuels*, *2*(2), 141-145.

Chilingar, G. V., & Yen, T. F. (1983). Some notes on wettability and relative permeabilities of carbonate reservoir rocks, II. *Energy Sources*, 7(1), 67-75.

Chingombe, P., Saha, B., & Wakeman, R. J. (2005). Surface modification and characterisation of a coal-based activated carbon. *Carbon*, 43(15), 3132-3143.

Chiquet, P., Broseta, D., & Thibeau, S. (2007). Wettability alteration of caprock minerals by carbon dioxide. *Geofluids*, 7(2), 112-122.

Clarkson, C. R., & Bustin, R. M. (2000). Binary gas adsorption/desorption isotherms: effect of moisture and coal composition upon carbon dioxide selectivity over methane. *International Journal of Coal Geology*, 42(4), 241-271.

Crawford, R. J., & Mainwaring, D. E. (2001). The influence of surfactant adsorption on the surface characterisation of Australian coals. *Fuel*, 80(3), 313-320.

Crawford, R. J., Guy, D. W., & Mainwaring, D. E. (1994). The influence of coal rank and mineral matter content on contact angle hysteresis. *Fuel*, *73*(5), 742-746.

Curtis, M. E., Cardott, B. J., Sondergeld, C. H., & Rai, C. S. (2012a). Development of organic porosity in the Woodford Shale with increasing thermal maturity. *International Journal of Coal Geology*, 103, 26-31.

Curtis, M. E., Sondergeld, C. H., Ambrose, R. J., & Rai, C. S. (2012). Microstructural investigation of gas shales in two and three dimensions using nanometer-scale resolution imaging. *AAPG bulletin*, *96*(4), 665-677.

Dake, L. P. (2001). *The practice of reservoir engineering (revised edition)* (Vol. 36). Elsevier.

David, G., Lombardi, T. E., & Martin, J. P. (2004). Fractured shale gas potential in New York. *Northeastern Geology and Environmental Sciences*, *26*(1/2), 57-78.

Day, S., Sakurovs, R., & Weir, S. (2008). Supercritical gas sorption on moist coals. *International Journal of Coal Geology*, 74(3), 203-214.

de Gennes, P. G., Brochard-Wyart, F., & Quéré, D. (2004). Capillarity and Gravity. In *Capillarity and Wetting Phenomena* (pp. 33-67). Springer New York.

De Gennes, P. G., Brochard-Wyart, F., & Quéré, D. (2013). Capillarity and wetting phenomena: drops, bubbles, pearls, waves. *Springer Science & Business Media*.

Dickson, J. L., Gupta, G., Horozov, T. S., Binks, B. P., & Johnston, K. P. (2006). Wetting phenomena at the CO_2/water/glass interface. *Langmuir*, *22*(5), 2161-2170.

DiMento, J. F., & Doughman, P. (2014). Climate change: what it means for our children, our grandchildren, and us. MIT Press.

Ding, L. P. (2009). Investigation of bituminous coal hydrophobicity and its influence on flotation. *Energy & Fuels*, 23(11), 5536-5543.

Donaldson, E. C., Thomas, R. D., & Lorenz, P. B. (1969). Wettability determination and its effect on recovery efficiency. *Society of Petroleum Engineers Journal*, *9*(01), 13-20.

Donaldson, E. C., & Tiab, D. (2004). Petrophysics: Theory and Practice of measuring reservoir rock and fluid transport properties. *Gulf Professional Publishing*.

Doymus, K. (2007). The effect of ionic electrolytes and pH on the zeta potential of fine coal particles. *Turkish Journal of Chemistry*, 31(6), 589-597.

Drelich, J., Miller, J. D., Kumar, A., & Whitesides, G. M. (1994). Wetting characteristics of liquid drops at heterogeneous surfaces. *Colloids and Surfaces A: Physicochemical and Engineering Aspects*, *93*, 1-13.

Drelich, J., Laskowski, J. S., Pawlik, M., & Veeramasuneni, S. (1997). Preparation of a coal surface for contact angle measurements. *Journal of Adhesion Science and Technology*, *11*(11), 1399-1431.

Durucan, S., Ahsan, M., Shi, J. Q., Syed, A., & Korre, A. (2014). Two phase relative permeabilities for gas and water in selected European coals. *Fuel*, *134*, 226-236.

Eick, J. D., Good, R. J., & Neumann, A. W. (1975). Thermodynamics of contact angles. II. Rough solid surfaces. *Journal of Colloid and Interface Science*, 53(2), 235-248.

El-Maghraby, R. M., Pentland, C. H., Iglauer, S., & Blunt, M. J. (2012). A fast method to equilibrate carbon dioxide with brine at high pressure and elevated temperature including solubility measurements. *The Journal of Supercritical Fluids*, *62*, 55-59.

Eral, H. B., & Oh, J. M. (2013). Contact angle hysteresis: a review of fundamentals and applications. *Colloid and polymer science*, *291*(2), 247-260.

Erbil, H. Y. (2006). *Solid and Liquid Interfaces*. Blackwell Publishing, Oxford.

Eshkalak, M. O., E. W. Al-Shalabi, A. Sanaei, U. Aybar, and K. Sepehrnoori (2014), Simulation study on the CO_2-driven enhanced gas recovery with sequestration versus the re-fracturing treatment of horizontal wells in the US unconventional shale reservoirs, *Journal of Natural Gas Science and Engineering, 21*, 1015-1024.

Espinoza, D. N., & Santamarina, J. C. (2010). Water-CO_2-mineral systems: Interfacial tension, contact angle, and diffusion—Implications to CO_2 geological storage. *Water Resources Research*, *46*(7).

Extrand, C. W. (1998). A thermodynamic model for contact angle hysteresis. *Journal of Colloid and interface Science*, *207*(1), 11-19.

Farokhpoor, R., Bjørkvik, B. J., Lindeberg, E., & Torsæter, O. (2013). Wettability behaviour of CO_2 at storage conditions. *International Journal of Greenhouse Gas Control*, *12*, 18-25.

Gale, J., & Davison, J. (2004). Transmission of CO_2—safety and economic considerations. *Energy*, 29(9), 1319-1328.

Fernø, M. A., L. P. Hauge, A. Uno Rognmo, J. Gauteplass, and A. Graue (2015), Flow visualization of CO_2 in tight shale formations at reservoir conditions, *Geophysical Research Letters, 42*(18), 7414-7419.

Fowkes, F. M. (1964). Attractive forces at interfaces. *Industrial & Engineering Chemistry*, 56(12), 40-52.

Fox, H. W., & Zisman, W. A. (1952). The spreading of liquids on low-energy surfaces. III. Hydrocarbon surfaces. *Journal of Colloid Science*, 7(4), 428-442.

Fuerstenau, D. W., Rosenbaum, J. M., & Laskowski, J. (1983). Effect of surface functional groups on the flotation of coal. *Colloids and Surfaces*, *8*(2), 153-173.

Fuerstenau, D. W., Rosenbaum, J. M., & You, Y. S. (1988). Electrokinetic behavior of coal. *Energy & Fuels*, 2(3), 241-245.

Gaus, I., Azaroual, M., & Czernichowski-Lauriol, I. (2005). Reactive transport modelling of the impact of CO_2 injection on the clayey cap rock at Sleipner (North Sea). *Chemical Geology*, 217(3), 319-337.

Georgiadis, A., Maitland, G., Trusler, J. M., & Bismarck, A. (2010). Interfacial tension measurements of the (H_2O+ CO_2) system at elevated pressures and temperatures. *Journal of Chemical & Engineering Data*, *55*(10), 4168-4175.

Ghous, A., Knackstedt, M. A., Arns, C. H., Sheppard, A., Kumar, M., Sok, R., ... & Pinczewski, W. V. (2008, January). 3D Imaging of Reservoir Core at Multiple Scales; Correlations to Petrophysical Properties and Pore Scale Fluid Distributions. *In International Petroleum Technology Conference*. IPTC – 12767.

Gilfillan, S. M., Lollar, B. S., Holland, G., Blagburn, D., Stevens, S., Schoell, M., ... & Ballentine, C. J. (2009). Solubility trapping in formation water as dominant CO_2 sink in natural gas fields. *Nature*, 458(7238), 614-618.

Giraldo, J., Benjumea, P., Lopera, S., Cortés, F. B., & Ruiz, M. A. (2013). Wettability alteration of sandstone cores by alumina-based nanofluids. *Energy & Fuels*, 27(7), 3659-3665.

Golab, A., Romeyn, R., Averdunk, H., Knackstedt, M., & Senden, T. J. (2013). 3D characterisation of potential CO_2 reservoir and seal rocks. *Australian Journal of Earth Sciences*, *60*(1), 111-123.

Golding, S. D., Uysal, I. T., Boreham, C. J., Kirste, D., Baublys, K. A., & Esterle, J. S. (2011). Adsorption and mineral trapping dominate CO_2 storage in coal systems. *Energy Procedia*, 4, 3131-3138.

Grate, J. W., Dehoff, K. J., Warner, M. G., Pittman, J. W., Wietsma, T. W., Zhang, C., & Oostrom, M. (2012). Correlation of oil–water and air–water contact angles of diverse silanized surfaces and relationship to fluid interfacial tensions. *Langmuir*, 28(18), 7182-7188.

Gray, I. (1987). Reservoir engineering in coal seams: Part 1-The physical process of gas storage and movement in coal seams. *SPE Reservoir Engineering*, *2*(01), 28-34.

Griffiths, P. R., & De Haseth, J. A. (2007). *Fourier transform infrared spectrometry* (Vol. 171). John Wiley & Sons.

Gunter, W. D., Perkins, E. H., & McCann, T. J. (1993). Aquifer disposal of CO_2-rich gases: reaction design for added capacity. *Energy Conversion and Management*, 34(9), 941-948.

Gunter, W. D., Wiwehar, B., & Perkins, E. H. (1997). Aquifer disposal of CO_2-rich greenhouse gases: extension of the time scale of experiment for CO_2-sequestering reactions by geochemical modelling. *Mineralogy and Petrology*, 59(1-2), 121-140.

Gupta, R., & Mohanty, K. (2010). Temperature effects on surfactant-aided imbibition into fractured carbonates. *SPE Journal*, *15*(03), 588-597.

Hamawand, I., Yusaf, T., & Hamawand, S. G. (2013). Coal seam gas and associated water: a review paper. *Renewable and Sustainable Energy Reviews*, *22*, 550-560.

Hammes, K., Smernik, R. J., Skjemstad, J. O., & Schmidt, M. W. (2008). Characterisation and evaluation of reference materials for black carbon analysis using elemental composition colour, BET surface area and 13 C NMR spectroscopy. *Applied Geochemistry*, 23(8), 2113-2122.

Hamouda, A. A., & Rezaei Gomari, K. A. (2006, January). Influence of temperature on wettability alteration of carbonate reservoirs. In *SPE/DOE Symposium on Improved Oil Recovery*. Society of Petroleum Engineers.

Hansen, G., Hamouda, A. A., & Denoyel, R. (2000). The effect of pressure on contact angles and wettability in the mica/water/n-decane system and the calcite+ stearic acid/water/n-decane system. *Colloids and Surfaces A: Physicochemical and Engineering Aspects*, *172*(1), 7-16.

Harvey, P. A., Nguyen, A. V., & Evans, G. M. (2002). Influence of electrical double-layer interaction on coal flotation. *Journal of Colloid and Interface Science*, *250*(2), 337-343.

Hebach, A., Oberhof, A., Dahmen, N., Kögel, A., Ederer, H., & Dinjus, E. (2002). Interfacial tension at elevated pressures measurements and correlations in the water+ carbon dioxide system. *Journal of Chemical & Engineering Data*, *47*(6), 1540-1546.

Hesse, M. A., Orr, F. M., & Tchelepi, H. A. (2008). Gravity currents with residual trapping. *Journal of Fluid Mechanics*, *611*, 35-60.

Hol, S., & Spiers, C. J. (2012). Competition between adsorption-induced swelling and elastic compression of coal at CO_2 pressures up to 100MPa. *Journal of the Mechanics and Physics of Solids*, *60*(11), 1862-1882.

Hu, Y., Devegowda, D., & Sigal, R. (2016). A microscopic characterization of wettability in shale kerogen with varying maturity levels. *Journal of Natural Gas Science and Engineering*, 33, 1078-1086.

Hurlbut, C.S., Klein, C., 1985, *Manual of Mineralogy*, 20th ed., Wiley, ISBN 0-471-80580-7

Ibrahim, A. F., & Nasr-El-Din, H. A. (2015). Effects of water salinity, CO_2 solubility, and gas composition on coal wettability. In *EUROPEC 2015*. Society of Petroleum Engineers.

Iglauer, S., Paluszny, A., Pentland, C. H., Blunt, M. J. (2011a). Residual CO_2 imaged with X-ray micro-tomography. *Geophysical Research Letters*, 38 (21).

Iglauer, S., Wülling, W., Pentland, C. H., Al-Mansoori, S. K., Blunt, M. J. (2011b). Capillary-trapping capacity of sandstones and sandpacks. *SPE Journal* 16 (4), 778-783.

Iglauer, S. (2011c). Dissolution trapping of carbon dioxide in reservoir formation brine-a carbon storage mechanism. INTECH Open Access Publisher.

Iglauer, S., Mathew, M. S., & Bresme, F. (2012). Molecular dynamics computations of brine–CO_2 interfacial tensions and brine–CO_2–quartz contact angles and their effects on structural and residual trapping mechanisms in carbon geo-sequestration. *Journal of Colloid and Interface Science*, 386(1), 405-414.

Iglauer, S., Paluszny, A., & Blunt, M. J. (2013). Simultaneous oil recovery and residual gas storage: A pore-level analysis using in situ X-ray micro-tomography. *Fuel*, 103, 905-914.

Iglauer, S., Salamah, A., Sarmadivaleh, M., Liu, K., & Phan, C. (2014). Contamination of silica surfaces: impact on water–CO_2–quartz and glass contact angle measurements. *International Journal of Greenhouse Gas Control*, *22*, 325-328.

Iglauer, S., Pentland, C. H., & Busch, A. (2015a). CO_2 wettability of seal and reservoir rocks and the implications for carbon geo-sequestration. *Water Resources Research*, 51(1), 729-774.

Iglauer, S., Al-Yaseri, A. Z., Rezaee, R., & Lebedev, M. (2015b). CO_2 wettability of caprocks: Implications for structural storage capacity and containment security. *Geophysical Research Letters*, 42(21), 9279-9284.

Iglauer, S. (2017). CO_2–Water–Rock Wettability: Variability, Influencing Factors, and Implications for CO_2 geo-storage. *Accounts of Chemical Research*.

IPCC, Carbon Dioxide Capture and Storage in: B. Metz, O. Davidson, H.d. Coninck, M. Loos, L. Meyer (Eds.) IPCC, 2005.

Jackson, M. D., Valvatne, P. H., & Blunt, M. J. (2005). Prediction of wettability variation within an oil/water transition zone and its impact on production. *SPE Journal*, *10*(02), 185-195.

Jackson, M. D., Al-Mahrouqi, D., & Vinogradov, J. (2016). Zeta potential in oil-water-carbonate systems and its impact on oil recovery during controlled salinity water-flooding. *Scientific Reports*, 6.

Janczuk, B., & Zdziennicka, A. (1994). A study on the components of surface free energy of quartz from contact angle measurements. *Journal of Materials Science*, 29(13), 3559-3564.

Javanbakht, G., Sedghi, M., Welch, W., & Goual, L. (2015). Molecular Dynamics Simulations of CO_2/Water/Quartz Interfacial Properties: Impact of CO_2 Dissolution in Water. *Langmuir*, 31(21), 5812-5819.

Johnson Jr, R. E., & Dettre, R. H. (1964). *Contact angle hysteresis*.

Juanes, R., Spiteri, E. J., Orr, F. M., & Blunt, M. J. (2006). Impact of relative permeability hysteresis on geological CO_2 storage. *Water Resources Research*, 42(12).

Jung, J. W., & Wan, J. (2012). Supercritical CO*2* and ionic strength effects on wettability of silica surfaces: Equilibrium contact angle measurements. *Energy & Fuels*, *26*(9), 6053-6059.

Kang, S. M., Fathi, E., Ambrose, R. J., Akkutlu, I. Y., & Sigal, R. F. (2011). Carbon dioxide storage capacity of organic-rich shales. *SPE Journal*, *16*(04), 842-855.

Kaya, A., & Yukselen, Y. (2005). Zeta potential of clay minerals and quartz contaminated by heavy metals. *Canadian Geotechnical Journal*, *42*(5), 1280-1289.

Keller, D. V. (1987). The contact angle of water on coal. *Colloids and surfaces*, *22*(1), 21-35.

Kim, T. H., Cho, J., & Lee, K. S. (2017). Evaluation of CO_2 injection in shale gas reservoirs with multi-component transport and geomechanical effects. *Applied Energy*, *190*, 1195-1206.

Kittel, C. (2005). *Introduction to solid state physics*. Wiley.

Koschel, D., Coxam, J. Y., Rodier, L., & Majer, V. (2006). Enthalpy and solubility data of CO_2 in water and NaCl (aq) at conditions of interest for geological sequestration. *Fluid Phase Equilibria*, 247(1), 107-120.

Krevor, S., Pini, R., Zuo, L., & Benson, S. M. (2012). Relative permeability and trapping of CO_2 and water in sandstone rocks at reservoir conditions. *Water Resources Research*, 48(2).

Krevor, S., Blunt, M. J., Benson, S. M., Pentland, C. H., Reynolds, C., Al-Menhali, A., & Niu, B. (2015). Capillary trapping for geologic carbon dioxide storage–From pore scale physics to field scale implications. *International Journal of Greenhouse Gas Control*, *40*, 221-237.

Krooss, B. M., Van Bergen, F., Gensterblum, Y., Siemons, N., Pagnier, H. J. M., & David, P. (2002). High-pressure methane and carbon dioxide adsorption on dry and moisture-equilibrated Pennsylvanian coals. *International Journal of Coal Geology*, 51(2), 69-92.

Kumar, A., Noh, M. H., Ozah, R. C., Pope, G. A., Bryant, S. L., Sepehrnoori, K., & Lake, L. W. (2005). Reservoir simulation of CO_2 storage in aquifers. *SPE Journal*, *10*(03), 336-348.

Kundu, S., Wang, Y., Xia, W., & Muhler, M. (2008). Thermal stability and reducibility of oxygen-containing functional groups on multiwalled carbon nanotube surfaces: a quantitative high-resolution XPS and TPD/TPR study. *The Journal of Physical Chemistry C*, 112(43), 16869-16878.

Kwok, D. Y., & Neumann, A. W. (1999). Contact angle measurement and contact angle interpretation. *Advances in Colloid and Interface Science*, 81(3), 167-249.

Kwok, D. Y., & Neumann, A. W. (2000). Contact angle interpretation in terms of solid surface tension. *Colloids and Surfaces A: Physicochemical and Engineering Aspects*, 161(1), 31-48.

Lackner, K. S. (2003). A guide to CO_2 sequestration. *Science*, 300(5626), 1677.

Lager, A., Webb, K. J., & Black, C. J. J. (2007). Impact of brine chemistry on oil recovery. In *IOR 2007-14th European Symposium on Improved Oil Recovery*.

Lagneau, V., Pipart, A., & Catalette, H. (2005). Reactive Transportmodelling and Long Term Behaviour of CO_2 Sequestration in Saline Aquifers. *Oil & Gas Science and Technology*, 60(2), 231-247.

Lai, C.Y., Cozzolino, M., Diamanti, M.V., Al Hassan, S., Chiesa, M., 2015. Underlying Mechanism of Time Dependent Surface Properties of Calcite ($CaCO_3$): A Baseline for Investigations of Reservoirs Wettability. *The Journal of Physical Chemistry C*, 119(52), 29038-29043.

Lander, L. M., Siewierski, L. M., Brittain, W. J., & Vogler, E. A. (1993). A systematic comparison of contact angle methods. *Langmuir*, *9*, 2237-2237.

Larter, S. R., Bowler, B. F. J., Li, M., Chen, M., Brincat, D., Bennett, B., & Horstad, I. (1996). Molecular indicators of secondary oil migration distances. *Nature*, 383(6601), 593-597.

Laskowski, J. (2001). *Coal flotation and fine coal utilization* (Vol. 14). Gulf Professional Publishing.

Letellier, P., Mayaffre, A., & Turmine, M. (2007). Drop size effect on contact angle explained by nonextensive thermodynamics. Young's equation revisited. *Journal of colloid and interface science*, *314*(2), 604-614.

Li, X., Hayashi, J. I., & Li, C. Z. (2006). FT-Raman spectroscopic study of the evolution of char structure during the pyrolysis of a Victorian brown coal. *Fuel*, 85(12), 1700-1707.

Li, D., & Neumann, A. W. (1992). Equation of state for interfacial tensions of solid-liquid systems. *Advances in Colloid and Interface Science*, 39, 299-345.

Li, D., Liu, Q., Weniger, P., Gensterblum, Y., Busch, A., & Krooss, B. M. (2010). High-pressure sorption isotherms and sorption kinetics of CH_4 and CO_2 on coals. *Fuel*, *89*(3), 569-580.

Li, X., Boek, E., Maitland, G. C., & Trusler, J. M. (2012a). Interfacial tension of (Brines + CO_2) : (0.864 NaCl + 0.136 KCl) at temperatures between (298 and 448) K, pressures between (2 and 50) MPa, and total molalities of (1 to 5) mol·kg^{-1}. *Journal of Chemical & Engineering Data*, 57(4), 1078-1088.

Li, B., & Benson, S. M. (2015). Influence of small-scale heterogeneity on upward CO_2 plume migration in storage aquifers. *Advances in Water Resources*, 83, 389-404.

Li, X., and D. Elsworth, (2015), Geomechanics of CO_2 enhanced shale gas recovery, *Journal of Natural Gas Science and Engineering., 26*, 1607-1619.

Lindeberg, E., & Wessel-Berg, D. (1997). Vertical convection in an aquifer column under a gas cap of CO_2. *Energy Conversion and Management*, *38*, S229-S234.

Liu, S., Yang, X., & Qin, Y. (2010). Molecular dynamics simulation of wetting behavior at CO_2/water/solid interfaces. *Chinese Science Bulletin*, 55(21), 2252-2257.

London, G., Carroll, G. T., & Feringa, B. L. (2013). Silanization of quartz, silicon and mica surfaces with light-driven molecular motors: construction of surface-bound photo-active nanolayers. *Organic & Biomolecular Chemistry*, 11(21), 3477-3483.

Love, J. C., Estroff, L. A., Kriebel, J. K., Nuzzo, R. G., & Whitesides, G. M. (2005). Self-assembled monolayers of thiolates on metals as a form of nanotechnology. *Chemical reviews*, *105*(4), 1103-1170.

Lu, J., Vecchi, G. A., & Reichler, T. (2007). Expansion of the Hadley cell under global warming. *Geophysical Research Letters*, *34*(6).

Lun, Z., Fan, H., Wang, H., Luo, M., Pan, W., & Wang, R. (2012). Interfacial Tensions between Reservoir Brine and CO_2 at High Pressures for Different Salinity. *Energy & Fuels*, *26*(6), 3958-3962.

Mahadevan, J. (2012). Comments on the paper titled “Contact angle measurements of CO_2–water-quartz/calcite systems in the perspective of carbon sequestration”: A case of contamination? *International Journal of Greenhouse Gas Control*, *7*, 261-262.

Manger, G. E. (1963). Porosity and bulk density of sedimentary rocks (No. 1144-E). USGPO.

Manoj, B., Kunjomana, A. G., & Chandrasekharan, K. A. (2009). Chemical leaching of low rank coal and its characterization using SEM/EDAX and FTIR. *Journal of Minerals and Materials Characterization and Engineering*, *8*(10), 821.

Marchetti, C. (1977). On geoengineering and the CO_2 problem. *Climatic Change*, 1(1), 59-68.

Marmur, A. (2006). Soft contact: measurement and interpretation of contact angles. *Soft Matter*, *2*(1), 12-17.

Mastalerz, M., Gluskoter, H., & Rupp, J. (2004). Carbon dioxide and methane sorption in high volatile bituminous coals from Indiana, USA. *International Journal of Coal Geology*, 60(1), 43-55.

Mazzotti, M., Pini, R., & Storti, G. (2009). Enhanced coalbed methane recovery. *The Journal of Supercritical Fluids*, *47*(3), 619-627.

McCaffery, F. G. (1972). Measurement of interfacial tensions and contact angles at high temperature and pressure. *Journal of Canadian Petroleum Technology*, *11*(03).

McCaffery, F. G., & Bennion, D. W. (1974). The effect of wettability on two-phase relative permeabilities. *Journal of Canadian Petroleum Technology*, *13*(04).

McCaughan, J., Iglauer, S., & Bresme, F. (2013). Molecular dynamics simulation of water/CO_2-quartz interfacial properties: application to subsurface gas injection. *Energy Procedia*, 37, 5387-5402.

Mills, J., Riazi, M., & Sohrabi, M. (2011, September). Wettability of common rock-forming minerals in a CO_2-brine system at reservoir conditions. In *International Symposium of the Society of Core Analysts* (pp. 19-21). Fredericton, Canada: Society of Core Analysts.

Mittal, K. L. (Ed.). (2006). *Contact angle, wettability and adhesion* (Vol. 4). CRC Press.

Moreno-Castilla, C., Lopez-Ramon, M. V., & Carrasco-Marın, F. (2000). Changes in surface chemistry of activated carbons by wet oxidation. *Carbon*, 38(14), 1995-2001.

Morrow, N. R. (1990). Wettability and its effect on oil recovery. *Journal of Petroleum Technology*, *42*(12), 1-476.

Mugele, F., & Baret, J. C. (2005). Electrowetting: from basics to applications. *Journal of Physics: Condensed Matter*, 17(28), R705.

Mugele, F., Siretanu, I., Kumar, N., Bera, B., Wang, L., de Ruiter, R., ... & Collins, I. (2016). Insights From Ion Adsorption and Contact-Angle Alteration at Mineral Surfaces for Low-Salinity Waterflooding. *SPE Journal*.

Nasralla, R. A., & Nasr-El-Din, H. A. (2014). Double-layer expansion: is it a primary mechanism of improved oil recovery by low-salinity waterflooding? *SPE Reservoir Evaluation & Engineering*, 17(01), 49-59.

Nelson, P. H. (2009). Pore-throat sizes in sandstones, tight sandstones, and shales. *AAPG bulletin*, *93*(3), 329-340.

Neumann, A. W., & Good, R. J. (1972). Thermodynamics of contact angles. I. Heterogeneous solid surfaces. *Journal of Colloid and Interface Science*, *38*(2), 341-358.

Neumann, A. W., Good, R. J., Hope, C. J., & Sejpal, M. (1974). An equation-of-state approach to determine surface tensions of low-energy solids from contact angles. *Journal of Colloid and Interface Scienc*e, 49(2), 291-304.

Neuzil, C. E. (1994). How permeable are clays and shales? *Water Resources Research*, 30(2), 145-150.

Nielsen, L. C., Bourg, I. C., & Sposito, G. (2012). Predicting CO_2–water interfacial tension under pressure and temperature conditions of geologic CO_2 storage. *Geochimica et Cosmochimica Acta*, *81*, 28-38.

Owens, D. K., & Wendt, R. C. (1969). Estimation of the surface free energy of polymers. *Journal of Applied Polymer Science*, 13(8), 1741-1747.

Parker, J. C., Lenhard, R. J., & Kuppusamy, T. (1987). A parametric model for constitutive properties governing multiphase flow in porous media. *Water Resources Research*, *23*(4), 618-624.

Pazhoohi, F. (2015). Climate Change: What It Means for Us, Our Children, and Our Grandchildren. *Electronic Green Journal*, (38), 1.

Pearce, J. K., Kirste, D. M., Dawson, G. K., Farquhar, S. M., Biddle, D., Golding, S. D., & Rudolph, V. (2015). SO_2 impurity impacts on experimental and simulated CO_2–water–reservoir rock reactions at carbon storage conditions. *Chemical Geology*, 399, 65-86.

Pentland, C. H., Itsekiri, E., Al-Mansoori, S., Iglauer, S., Bijeljic, B., & Blunt, M. J. (2010). Measurement of nonwetting-phase trapping in sandpacks. *SPE Journal*, *15*(02), 274-281.

Pentland, C. H., El-Maghraby, R., Iglauer, S., & Blunt, M. J. (2011). Measurements of the capillary trapping of super-critical carbon dioxide in Berea sandstone. *Geophysical Research Letters*, 38(6).

Perera, M. S. A., Ranjith, P. G., Choi, S. K., Bouazza, A., Kodikara, J., & Airey, D. (2011). A review of coal properties pertinent to carbon dioxide sequestration in coal seams: with special reference to Victorian brown coals. *Environmental Earth Sciences*, 64(1), 223-235.

Pini, R., Ottiger, S., Storti, G., & Mazzotti, M. (2010). Prediction of competitive adsorption on coal by a lattice DFT model. *Adsorption*, *16*(1-2), 37-46.

Pini, R., Krevor, S. C., & Benson, S. M. (2012). Capillary pressure and heterogeneity for the CO_2/water system in sandstone rocks at reservoir conditions. *Advances in Water Resources*, 38, 48-59.

Pini, R., & Benson, S. M. (2013). Simultaneous determination of capillary pressure and relative permeability curves from core-flooding experiments with various fluid pairs. *Water Resources Research*, 49(6), 3516-3530.

Purcell, W. R. (1950). Interpretation of capillary pressure data. *Journal of Petroleum Technology*, *2*(08), 11-12.

Puri, B. R. (1970). Surface complexes on carbons. *Chemistry and Physics of Carbon*, 6, 191-282.

Qi, R., LaForce, T. C., & Blunt, M. J. (2009). Design of carbon dioxide storage in aquifers. *International Journal of Greenhouse Gas Control*, *3*(2), 195-205.

Rahman, T., Lebedev, M., Barifcani, A., & Iglauer, S. (2016). Residual trapping of supercritical CO_2 in oil-wet sandstone. *Journal of Colloid and Interface Science*, *469*, 63-68.

Ramesh, R., & Somasundaran, P. (1989). Chemical and wettability studies on coal, humic acid and cyclized humic acid. *Fuel*, 68(4), 533-535.

Randolph, P. L. (1983). Porosity and permeability of Mesaverde sandstone core from the US DOE Multiwell Experiment, Garfield County, Colorado. *In SPE/DOE Low Permeability Gas Reservoirs Symposium*. Society of Petroleum Engineers.

Rickwood, P. C. (1981). The largest crystals. *American Mineralogist*, *66*(9-10), 885-907.

Rieder, M., Cavazzini, G., D'yakonov Y. S., V. Kamenetskii A. F., Gottardi, G., S. Guggenheim (1998). Nomenclature of the Micas. *The Canadian Mineralogist*, 36, 10-20.

Roshan, H., Al-Yaseri, A. Z., Sarmadivaleh, M., & Iglauer, S. (2016). On wettability of shale rocks. *Journal of Colloid and Interface Science*, *475*, 104-111.

Reucroft, P. J., & Sethuraman, A. R. (1987). Effect of pressure on carbon dioxide induced coal swelling. *Energy & Fuels*, *1*(1), 72-75.

Saadatpoor, E., Bryant, S. L., & Sepehrnoori, K. (2010). New trapping mechanism in carbon sequestration. *Transport in Porous Media*, *82*(1), 3-17.

Saghafi, A., Javanmard, H., & Pinetown, K. (2014). Study of coal gas wettability for CO_2 storage and CH_4 recovery. *Geofluids*, *14*(3), 310-325.

Sakurovs, R., Day, S., Weir, S., & Duffy, G. (2007). Application of a modified Dubinin− Radushkevich equation to adsorption of gases by coals under supercritical conditions. *Energy & fuels*, *21*(2), 992-997.

Sakurovs, R., & Lavrencic, S. (2011). Contact angles in CO_2-water-coal systems at elevated pressures. *International Journal of Coal Geology*, *87*(1), 26-32.

Sams, W. N., Bromhal, G., Jikich, S., Ertekin, T., & Smith, D. H. (2005). Field-project designs for carbon dioxide sequestration and enhanced coalbed methane production. *Energy & fuels*, *19*(6), 2287-2297.

Saraji, S., L. Goual, M. Piri, and H. Plancher (2013), Wettability of supercritical carbon dioxide/water/quartz systems: Simultaneous measurement of contact angle and interfacial tension at reservoir conditions, *Langmuir*, 29, 6856–6866.

Saraji, S., Piri, M., & Goual, L. (2014). The effects of SO_2 contamination, brine salinity, pressure, and temperature on dynamic contact angles and interfacial tension of supercritical CO_2/brine/quartz systems. *International Journal of Greenhouse Gas Control*, *28*, 147-155.

Sarmadivaleh, M., Al-Yaseri, A. Z., & Iglauer, S. (2015). Influence of temperature and pressure on quartz–water–CO_2 contact angle and CO_2–water interfacial tension. *Journal of Colloid and Interface Science*, 441, 59-64.

Sarwar, A., Khan, M. N., & Azhar, K. F. (2012). Coal chemistry and morphology of thar reserves, Pakistan. *Journal of Minerals and Materials Characterization and Engineering*, 11(08), 817.

Schaeff, H. T., & McGrail, B. P. (2004). Direct measurements of pH in H_2O-CO_2 brine mixtures to supercritical conditions. *In Proceedings of the 7th International Conference on Greenhouse Gas Control Technologies* (GHGT-7).

Scheffer, M., Brovkin, V., & Cox, P. M. (2006). Positive feedback between global warming and atmospheric CO_2 concentration inferred from past climate change. *Geophysical Research Letters*, *33*(10).

Shi, J. Q., & Durucan, S. (2005). CO_2 storage in deep unminable coal seams. *Oil and Gas Science and Technology*, 60(3), 547-558.

Sheppard, A., Latham, S., Middleton, J., Kingston, A., Myers, G., Varslot, T., ... & Francois, N. (2014). Techniques in helical scanning, dynamic imaging and image segmentation for improved quantitative analysis with X-ray micro-CT. *Nuclear Instruments and Methods in Physics Research Section B: Beam Interactions with Materials and Atoms*, 324, 49-56.

Shojai Kaveh, N., Rudolph, E. S. J., Wolf, K. H. A., & Ashrafizadeh, S. N. (2011). Wettability determination by contact angle measurements: hvBb coal–water system with injection of synthetic flue gas and CO_2. *Journal of Colloid and Interface Science*, 364(1), 237-247.

Shojai Kaveh, N., Wolf, K. H., Ashrafizadeh, S. N., & Rudolph, E. S. J. (2012). Effect of coal petrology and pressure on wetting properties of wet coal for CO_2 and flue gas storage. *International Journal of Greenhouse Gas Control*, *11*, S91-S101.

Shojai Kaveh, N., Rudolph, E. S. J., Van Hemert, P., Rossen, W. R., & Wolf, K. H. (2014). Wettability evaluation of a CO_2/water/bentheimer sandstone system: contact angle, dissolution, and bubble size. *Energy & Fuels*, 28(6), 4002-4020.

Shojai Kaveh, N., Barnhoorn, A., & Wolf, K. H. (2016). Wettability evaluation of silty shale caprocks for CO_2 storage. *International Journal of Greenhouse Gas Control*, 49, 425-435.

Shuttleworth, R., & Bailey, G. L. J. (1948). The spreading of a liquid over a rough solid. *Discussions of the Faraday Society*, *3*, 16-22.

Siemons, N., Bruining, H., Castelijns, H., & Wolf, K. H. (2006). Pressure dependence of the contact angle in a CO_2–H_2O–coal system. *Journal of Colloid and Interface Science*, *297*(2), 755-761.

Siemons, N., & Busch, A. (2007). Measurement and interpretation of supercritical CO_2 sorption on various coals. *International Journal of Coal Geology*, 69(4), 229-242.

Socrates, G. (2004). *Infrared and Raman characteristic group frequencies: tables and charts*. John Wiley & Sons.

Solie, D. N., & Su, S. C. (1987). An occurrence of Ba-rich micas from the Alaska Range. *American Mineralogist*, *72*(9-10), 995-999.

Somasundaran, P., Roberts, C. E., & Ramesh, R. (1991). Effects of oxidizing methods on the flotation of coal. *Minerals Engineering*, 4(1), 43-48.

Song, B., & Springer, J. (1996). Determination of interfacial tension from the profile of a pendant drop using computer-aided image processing: 1. Theoretical. *Journal of Colloid and Interface Science*, *184*(1), 64-76.

Spiteri, E. J., Juanes, R., Blunt, M. J., & Orr, F. M. (2008). A new model of trapping and relative permeability hysteresis for all wettability characteristics. *SPE Journal*, *13*(03), 277-288.

Staszczuk, P. (1989). On the determination of surface free energy of coal by means of the derivatograph. *Fuel Science and Technology International*, 7(1), 89-101.

Suekane, T., Zhou, N., Hosokawa, T., & Matsumoto, T. (2010). Direct observation of trapped gas bubbles by capillarity in sandy porous media. *Transport in Porous Media*, 82(1), 111-122.

Tiab, D., & Donaldson, E. C. (2011). Petrophysics: theory and practice of measuring reservoir rock and fluid transport properties. Gulf professional publishing.

Tadmor, R. (2004). Line energy and the relation between advancing, receding, and young contact angles. *Langmuir*, *20*(18), 7659-7664.

Thomas, D. C., & Benson, S. M. (Eds.). (2015). Carbon dioxide capture for storage in deep geologic formations-results from the CO_2 Capture Project: Vol 2. *Geologic Storage of Carbon Dioxide with Monitoring and Verification*. Elsevier.

Tonnet, N., Broseta, D. F., & Mouronval, G. (2010, January). Evaluation of petrophysical properties of a carbonate-rich caprock for CO_2 geological storage purposes. In *SPE EUROPEC/EAGE Annual Conference and Exhibition*. Society of Petroleum Engineers.

Treiber, L. E., & Owens, W. W. (1972). A laboratory evaluation of the wettability of fifty oil-producing reservoirs. *SPE Journal*, 12(06), 531-540.

Tripp, C. P., & Combes, J. R. (1998). Chemical modification of metal oxide surfaces in supercritical CO_2: The interaction of supercritical CO_2 with the adsorbed water layer and the surface hydroxyl groups of a silica surface. *Langmuir*, 14(26), 7348-7352.

Tsai, S. C. (1982). *Fundamentals of coal beneficiation and utilization* (Vol. 2). Elsevier Science & Technology.

Underschultz, J., & Strand, J. (2016). Capillary seal capacity of faults under hydrodynamic conditions. Geofluids, 16(3), 464-475.

Underschultz, J., Dodds, K., Michael, K, Sharma, S., Wall, T., & Whittaker, S. (2016). Chapter 23 Carbon Capture and Storage, in ed. Sheila Devasahayam, Kim Dowling, and Manoj Mahapatra. Sustainability in the Mineral/Energy Sectors. CRC press. 730 p.

van Bergen, F., Krzystolik, P., van Wageningen, N., Pagnier, H., Jura, B., Skiba, J., ... & Kobiela, Z. (2009). Production of gas from coal seams in the Upper Silesian

Coal Basin in Poland in the post-injection period of an ECBM pilot site. *International Journal of Coal Geology,* 77(1), 175-187.

Van Oss, C. J., Good, R. J., & Chaudhury, M. K. (1986). The role of van der Waals forces and hydrogen bonds in "hydrophobic interactions" between biopolymers and low energy surfaces. *Journal of Colloid and Interface Science*, 111(2), 378-390.

Vernik, L., & Milovac, J. (2011). Rock physics of organic shales. *The Leading Edge*, *30*(3), 318-323.

Vinogradov, J., & Jackson, M. D. (2015). Zeta potential in intact natural sandstones at elevated temperatures. *Geophysical Research Letters*, *42*(15), 6287-6294.

Wan, J., Kim, Y., & Tokunaga, T. K. (2014). Contact angle measurement ambiguity in supercritical CO_2–water–mineral systems: Mica as an example. *International Journal of Greenhouse Gas Control*, 31, 128-137.

Wang, S., Edwards, I. M., & Clarens, A. F. (2012). Wettability phenomena at the CO_2–brine–mineral interface: implications for geologic carbon sequestration. *Environmental science & technology*, *47*(1), 234-241.

Wenzel, R. N. (1949). Surface Roughness and Contact Angle. *The Journal of Physical Chemistry*, *53*(9), 1466-1467.

White, C. M., Smith, D. H., Jones, K. L., Goodman, A. L., Jikich, S. A., LaCount, R. B., ... & Schroeder, K. T. (2005). Sequestration of carbon dioxide in coal with enhanced coalbed methane recovery a review. *Energy & Fuels*, 19(3), 659-724.

Wilson, J. L. (2012). Carbonate facies in geologic history. *Springer Science & Business Media*.

Wu, S. (1971). Calculation of interfacial tension in polymer systems. *Journal of Polymer Science Part C: Polymer Symposia*, 34(1) 19-30.

Wu, D., Liu, G., & Sun, R. (2014). Investigation on structural and thermodynamic characteristics of perhydrous bituminous coal by fourier transform infrared spectroscopy and thermogravimetry/mass spectrometry. *Energy & Fuels*, 28(5), 3024-3035.

Xu, T., Apps, J. A., & Pruess, K. (2001). Analysis of mineral trapping for CO_2 disposal in deep aquifers. *Lawrence Berkeley National Laboratory*.

Xu, R., Hu, B., He, Q., Cai, J., Pan, Y., & Shen, J. (2006). Effect of compound inorganic nano-stabilizer on the stability of high concentration coal water mixtures. *Fuel*, 85(17), 2524-2529.

Yang, D., Tontiwachwuthikul, P., & Gu, Y. (2005). Interfacial tensions of the crude oil+ reservoir brine + CO_2 systems at pressures up to 31 MPa and temperatures of 27 C and 58 C. *Journal of Chemical & Engineering Data*, *50*(4), 1242-1249.

Yang, D., Gu, Y., & Tontiwachwuthikul, P. (2007). Wettability determination of the reservoir brine− reservoir rock system with dissolution of CO_2 at high pressures and elevated temperatures. *Energy & Fuels*, 22(1), 504-509.

Young, T., (1805). An essay on the cohesion of fluids. *Philosophical Transactions of the Royal Society of London*, 95, 65–87.

Zhang, J., Feng, Q., Zhang, X., Wen, S., & Zhai, Y. (2015). Relative permeability of coal: a review. *Transport in Porous Media*, *106*(3), 563-594.

Żenkiewicz, M. (2007). Methods for the calculation of surface free energy of solids. *Journal of Achievements in Materials and Manufacturing Engineering*, 24(1), 137-145.

Zuo, L., Krevor, S., Falta, R. W., & Benson, S. M. (2012). An experimental study of CO_2 exsolution and relative permeability measurements during CO_2 saturated water depressurization. *Transport in Porous Media*, 91(2), 459-478.

Appendix

This appendix contains the copyright agreements between the author and Journals to reuse the author's own published material in this thesis.

Chapter 3, Article: "CO_2 storage in carbonates: Wettability of calcite in *International Journal of Greenhouse Gas Control*"

ELSEVIER LICENSE
TERMS AND CONDITIONS

May 22, 2017

This Agreement between Muhammad Arif ("You") and Elsevier ("Elsevier") consists of your license details and the terms and conditions provided by Elsevier and Copyright Clearance Center.

License Number	4114030472020
License date	May 22, 2017
Licensed Content Publisher	Elsevier
Licensed Content Publication	International Journal of Greenhouse Gas Control
Licensed Content Title	CO2 storage in carbonates: Wettability of calcite
Licensed Content Author	Muhammad Arif,Maxim Lebedev,Ahmed Barifcani,Stefan Iglauer
Licensed Content Date	Jul 1, 2017
Licensed Content Volume	62
Licensed Content Issue	n/a
Licensed Content Pages	9
Start Page	113
End Page	121
Type of Use	reuse in a thesis/dissertation
Portion	full article
Format	both print and electronic
Are you the author of this Elsevier article?	Yes
Will you be translating?	No
Order reference number	
Title of your thesis/dissertation	Experimental Investigation of Wettability of Rock-CO2-Brine for Improved Reservoir Characterization
Expected completion date	Sep 2017
Estimated size (number of pages)	220
Elsevier VAT number	GB 494 6272 12
Requestor Location	Muhammad Arif 46 Gillon Street Karawara Perth, WA 6152 Australia Attn: Muhammad Arif
Total	0.00 USD
Terms and Conditions	

Chapter 4, Article: “Impact of pressure and temperataure on CO_2-brine-mica contact angles and CO_2-brine-interfacial tension: Implications for carbon geo-sequestration” in *Journal of Colloid and Interface Science*

ELSEVIER LICENSE
TERMS AND CONDITIONS

Apr 30, 2017

This Agreement between Muhammad Arif ("You") and Elsevier ("Elsevier") consists of your license details and the terms and conditions provided by Elsevier and Copyright Clearance Center.

License Number	4099090996523
License date	Apr 30, 2017
Licensed Content Publisher	Elsevier
Licensed Content Publication	Journal of Colloid and Interface Science
Licensed Content Title	Impact of pressure and temperature on CO2–brine–mica contact angles and CO2–brine interfacial tension: Implications for carbon geo-sequestration
Licensed Content Author	Muhammad Arif,Ahmed Z. Al-Yaseri,Ahmed Barifcani,Maxim Lebedev,Stefan Iglauer
Licensed Content Date	15 January 2016
Licensed Content Volume	462
Licensed Content Issue	n/a
Licensed Content Pages	8
Start Page	208
End Page	215
Type of Use	reuse in a thesis/dissertation
Intended publisher of new work	other
Portion	full article
Format	both print and electronic
Are you the author of this Elsevier article?	Yes
Will you be translating?	No
Order reference number	
Title of your thesis/dissertation	Experimental Investigation of Wettability of Rock-CO2-Brine for Improved Reservoir Characterization
Expected completion date	Sep 2017
Estimated size (number of pages)	220
Elsevier VAT number	GB 494 6272 12
Requestor Location	Muhammad Arif 46 Gillon Street Karawara Perth, WA 6152 Australia Attn: Muhammad Arif
Total	0.00 USD
Terms and Conditions	

Chapter 5, Article: "CO_2-wettability of low to high rank coal seams: Implications for carbon sequestration and enhanced methane recovery", in *Fuel*

ELSEVIER LICENSE
TERMS AND CONDITIONS

Apr 28, 2017

This Agreement between Muhammad Arif ("You") and Elsevier ("Elsevier") consists of your license details and the terms and conditions provided by Elsevier and Copyright Clearance Center.

License Number	4097631206083
License date	Apr 28, 2017
Licensed Content Publisher	Elsevier
Licensed Content Publication	Fuel
Licensed Content Title	CO2-wettability of low to high rank coal seams: Implications for carbon sequestration and enhanced methane recovery
Licensed Content Author	Muhammad Arif,Ahmed Barifcani,Maxim Lebedev,Stefan Iglauer
Licensed Content Date	1 October 2016
Licensed Content Volume	181
Licensed Content Issue	n/a
Licensed Content Pages	10
Start Page	680
End Page	689
Type of Use	reuse in a thesis/dissertation
Portion	full article
Format	both print and electronic
Are you the author of this Elsevier article?	Yes
Will you be translating?	No
Order reference number	
Title of your thesis/dissertation	Experimental Investigation of Wettability of Rock-CO2-Brine for Improved Reservoir Characterization
Expected completion date	Sep 2017
Estimated size (number of pages)	220
Elsevier VAT number	GB 494 6272 12
Requestor Location	Muhammad Arif 46 Gillon Street Karawara Perth, WA 6152 Australia Attn: Muhammad Arif
Total	0.00 USD
Terms and Conditions	

Chapter 6, Article: “Influence of shale-TOC on CO_2 storage potential’ in *Geophysical Research Letters*

Permissions

***PLEASE NOTE: If the links highlighted here do not take you to those web sites, please copy and paste address in your browser.**

Permission to reproduce AGU journal Content:

Requests to reproduce material from American Geophysical Union publications are being handled through the RightsLink® automated permissions service.

Simply follow the steps below to obtain permission via the Rightslink® system:

- Locate the article you wish to reproduce on Wiley Online Library (http://agupubs.onlinelibrary.wiley.com)
- Click on the ‘Request Permissions’ link, under 'INFORMATION' on the navigational menu of the article
- Follow the online instructions and select your requirements from the drop down options and click on ‘quick price’ to get a quote
- Create a RightsLink® account to complete your transaction (and pay, where applicable)
- Read and accept our Terms & Conditions and download your license
- For any technical queries please contact customercare@copyright.com
- For further information and to view a Rightslink® demo please visit www.wiley.com and select Rights & Permissions.

AUTHORS - If you wish to reuse your own article (or an amended version of it) in a new publication of which you are the author, editor or co-editor, prior permission is not required (with the usual acknowledgements). However, a formal grant of license can be downloaded free of charge from RightsLink if required.

Chapter 7, Article: "Solid/CO_2 and solid/water interfacial tensions as a function of pressure, temperature, salinity and mineral type: Implications for CO_2-wettability and CO_2 geo-storage", in *International Journal of Greenhouse Gas Control*

ELSEVIER LICENSE
TERMS AND CONDITIONS

May 22, 2017

This Agreement between Muhammad Arif ("You") and Elsevier ("Elsevier") consists of your license details and the terms and conditions provided by Elsevier and Copyright Clearance Center.

License Number	4114031375149
License date	May 22, 2017
Licensed Content Publisher	Elsevier
Licensed Content Publication	International Journal of Greenhouse Gas Control
Licensed Content Title	Solid/CO2 and solid/water interfacial tensions as a function of pressure, temperature, salinity and mineral type: Implications for CO2-wettability and CO2 geo-storage
Licensed Content Author	Muhammad Arif,Ahmed Barifcani,Stefan Iglauer
Licensed Content Date	Oct 1, 2016
Licensed Content Volume	53
Licensed Content Issue	n/a
Licensed Content Pages	11
Start Page	263
End Page	273
Type of Use	reuse in a thesis/dissertation
Intended publisher of new work	other
Portion	full article
Format	both print and electronic
Are you the author of this Elsevier article?	Yes
Will you be translating?	No
Order reference number	
Title of your thesis/dissertation	Experimental Investigation of Wettability of Rock-CO2-Brine for Improved Reservoir Characterization
Expected completion date	Sep 2017
Estimated size (number of pages)	220
Elsevier VAT number	GB 494 6272 12
Requestor Location	Muhammad Arif 46 Gillon Street Karawara Perth, WA 6152 Australia Attn: Muhammad Arif
Total	0.00 USD
Terms and Conditions	

Chapter 8, Article: **“**Influence of surface chemistry on interfacial properties of low to high rank coal seams”, in *Fuel*

ELSEVIER LICENSE
TERMS AND CONDITIONS

May 22, 2017

This Agreement between Muhammad Arif ("You") and Elsevier ("Elsevier") consists of your license details and the terms and conditions provided by Elsevier and Copyright Clearance Center.

License Number	4114040269479
License date	May 22, 2017
Licensed Content Publisher	Elsevier
Licensed Content Publication	Fuel
Licensed Content Title	Influence of surface chemistry on interfacial properties of low to high rank coal seams
Licensed Content Author	Muhammad Arif,Franca Jones,Ahmed Barifcani,Stefan Iglauer
Licensed Content Date	Apr 15, 2017
Licensed Content Volume	194
Licensed Content Issue	n/a
Licensed Content Pages	11
Start Page	211
End Page	221
Type of Use	reuse in a thesis/dissertation
Intended publisher of new work	other
Portion	full article
Format	both print and electronic
Are you the author of this Elsevier article?	Yes
Will you be translating?	No
Order reference number	
Title of your thesis/dissertation	Experimental Investigation of Wettability of Rock-CO2-Brine for Improved Reservoir Characterization
Expected completion date	Sep 2017
Estimated size (number of pages)	220
Elsevier VAT number	GB 494 6272 12
Requestor Location	Muhammad Arif 46 Gillon Street Karawara Perth, WA 6152 Australia Attn: Muhammad Arif
Total	0.00 USD
Terms and Conditions	